# Design of a Versatile Monitoring System for Measuring Near-Airport Aircraft Pollution

# Final Report

Report Version No. 1.1

June 21, 2022- Delft, The Netherlands


Group 04 – Under supervision of Dr. I.C. Dedoussi, Prof.dr.ir. M. Snellen, Ir. G. Dacome and Ir. G. Kus

| | | | |
|---|---|---|---|
| Adriano Casablanca | 5056926 | Erin Lucassen | 4683293 |
| Mihai Constantinov | 5007445 | Vaclav Marek | 4592425 |
| Bahier Khan | 5051908 | Yaro Oei | 4662245 |
| Stein Köbben | 4886488 | Alec Pietersz | 5020328 |
| Ahmed Kubba | 4785584 | Jort Simons | 5056462 |

Delft University of Technology


This page intentionally left blank

# Design of a Versatile Monitoring System for Measuring Near-Airport Aircraft Pollution

## Final Report

Report Version No. 1.1
June 21, 2022- Delft, The Netherlands

by


Group 04 – Under supervision of Dr. I.C. Dedoussi, Prof.dr.ir. M. Snellen, Ir. G. Dacome and Ir. G. Kus

| | | | |
|---|---|---|---|
| Adriano Casablanca | 5056926 | Erin Lucassen | 4683293 |
| Mihai Constantinov | 5007445 | Vaclav Marek | 4592425 |
| Bahier Khan | 5051908 | Yaro Oei | 4662245 |
| Stein Köbben | 4886488 | Alec Pietersz | 5020328 |
| Ahmed Kubba | 4785584 | Jort Simons | 5056462 |



Course Code: AE3200
Project Duration: April 19, 2022 – June 24, 2022
Faculty: Aerospace Engineering, Delft University of Technology

# Preface

This report represents the effort of 10 students working for their Design Synthesis Exercise (DSE), the final component of the Bachelor of Science program offered by the Aerospace Engineering faculty of Delft University of Technology. This document presents the results of ten weeks of full-time research, design, and development.

While writing this report, a basic knowledge of the underlying mathematics was assumed, as well as familiarity with the chemical and engineering nomenclature. All abbreviations are explained in the nomenclature section to ensure understanding. For readers interested in the total environmental metric, refer to Chapter 3, for the optimisation model used to create the data, Chapter 9, and for the overview of sustainability, Chapter 14.

We would like to express our gratitude to our tutors, Dr. I.C. Dedoussi and Prof.dr.ir. M. Snellen, and our coaches Ir. G. Kus and Ir. G. Dacome. Their guidance, advice, and technical knowledge has been invaluable to deepen our knowledge, expand our horizons and to complete this DSE project. Furthermore, we would like to thank Mr. N. van Oosten for providing insight on the practical application of noise and emissions measurement systems and models and for taking time to attend our presentations. Lastly, we are grateful for all the resources offered to us by the DSE team, as well as the guidance the teaching assistants and specifically Yasser Elnily provided throughout the project.

June 21, 2022

| | |
|---|---|
| Adriano Casablanca | Erin Lucassen |
| Mihai Constantinov | Vaclav Marek |
| Bahier Khan | Yaro Oei |
| Stein Köbben | Alec Pietersz |
| Ahmed Kubba | Jort Simons |

# Executive Summary

As a fundamental pillar of global socio-economic growth, the aviation industry has asserted itself as a key instrument for the improvement of quality of life for people across the world. Aviation facilitates trade, generates economic growth, and helps alleviate poverty, all while providing the social inter-connectivity offered by enabling tourism and exchange of culture. However, these benefits come at a cost: aircraft air and noise pollution negatively impact the well-being of near-airport communities, with local residents experiencing an increased risk of respiratory and cardiovascular diseases. To help mitigate the impact of airports on their local community, policy makers require comprehensive models of aviation based pollution. While models for the spread of both noise and emission concentrations exist and are used, these are often either classified, inaccurate, or not available for all airports; thus, there is a need for a measurement system which can be deployed anywhere to provide accurate measurements available to anyone. With the objective of improving current understanding of aviation pollution, the following mission need statement was established:

| Mission Need Statement |
| --- |
| *"The distribution of individual aircraft events' noise and air pollution concentrations from aircraft paths to near airport communities is not sufficiently understood."* |

The Autonomous Lab for Environmental Computation (ALEC) is a heterogeneous system designed to track aircraft-based pollution by deploying a network of emission drones, noise drones, ground level sensors, and a central ground station. The system can be split into the runway and the near-airport community components. The runway components consist of four emission measuring drones and two drones specialised in noise measurements. The drones are employed at airport runways to accurately map aircraft events during the landing and-take off phase. Additionally, 40 ground level sensors will be located in neighbouring communities impacted by aircraft operations, where the noise experienced by local residents will be accurately tracked using microphones. ALEC is rounded off by a ground station responsible for facilitating the operation of the flying components. The ALEC ground station is capable of sending commands to the drones, providing platforms for safe landing and take-off operations, charging of drone batteries, providing processing power and communicating with air traffic control. Overall, ALEC has two main objectives which are summarised by the project objective statement:

| Project Objective Statement |
| --- |
| *"To accurately measure noise and air pollution to calculate a metric for tracking the environmental impact of aviation on near-airport communities."* |

The first goal is to provide a total environmental metric which can be used to attribute, in near-real time, the environmental impact a specific aircraft event has on the local community. The goal of the metric is to analyse the total amount of air pollutants and noise emitted by a specific aircraft during its operation, to obtain a way to quantify its impacts compared to the average aircraft event. In the short term, this metric can help local residents and airport operators by providing a simplified view on the aircraft types which are more harmful to near-airport communities. This is done by employing a machine learning technique based on Gaussian Processes Regression and Bayesian Optimisation, which helps develop a preliminary model of the distribution of pollutants based on a specific aircraft event, while also determining the optimal location to place the sensors. Models for the emission and noise have been developed and used to verify the feasibility of approach, and the results showed promise for future developments. A visualisation on the performance of the algorithm for a simple pollution model is shown in Figure 1, where on the left side the concentration of a pollutant modelled using an emissions model is plotted, while on the right the functions fitted

using the modelling algorithm with a different number of samples is shown. Moreover, the sampling locations chosen by the algorithm are highlighted in red in the figures.

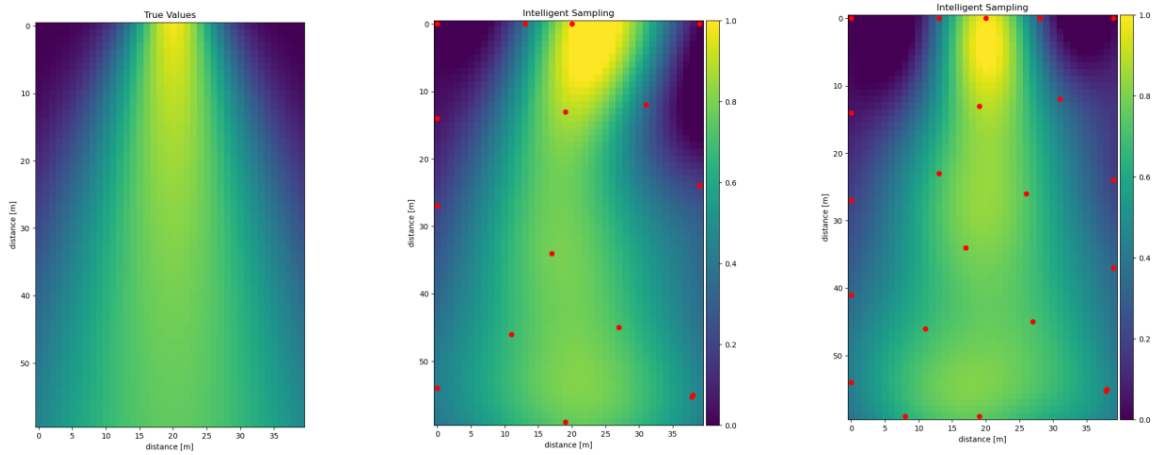


**Figure 1:** *Model improvement by intelligently selecting sample location using Gaussian Processes with Bayesian Optimisation for the 2D model of normalised concentrations of a pollutant in a 2D Gaussian Plume with the sampling locations highlighted, for $n = 9$ and $n = 21$ samples*

The second goal is focused on the long term aggregation of measured data, for the use of scientists and policy makers to develop a more sophisticated understanding of the sources and impacts of aviation based pollution. A critical design component of ALEC is that all collected data could be made open-source if desired by the client, such that the environmental footprint of different aircraft can be transparently estimated by anyone. It is planned that the databases can be accessed through a website, allowing visitors to access both the raw database for research purposes, as well as to view the total environmental footprint metric of a single aircraft event landing or taking-off from a certain runway, similarly with Figure 5. This availability of the raw data to the public is an option which can be enabled or disabled by the customer. As the database is expanded, it is planned to add the option to assess the effect of a certain aircraft type or compare certain airliners. An additional objective of ALEC is to serve as a noise and emissions mapping to service airports in assessing their own environmental impact.

A rendering of an emissions drone is shown in Figure 2. The drone is a quad-copter with a chopped carbon fibre reinforced polymer structure and equipped with seven sensors capable of measuring different gases, integrated through a sensor airflow system capable of providing the necessary flow conditions for the measurements. Furthermore, the system includes two cameras which are used for the autonomous collision avoidance and autonomous take-off and landing of the flying vehicle. The drone has a hover time of 25 minutes, which means that during mission operations only three will be carrying out measurements at any time, with one drone returning to the ground station to recharge. During an aircraft event each emission drone will hover around a selected location and height such that it is able to attribute its measurements to a specific space in the airport, which is then used to estimate the total amount of air pollutants emitted by the aircraft engines during take-off and landing. These measurements are then stored and used for the calculation of the total environmental metric.

The noise drone is designed to take acoustic measurements at an airport, requiring it to capture noise at higher frequencies than the ground level sensors. Its rendering is shown in Figure 3. Furthermore, a high degree of flexibility in operation is achieved by relocating the microphone to different measuring locations due to use of a quad-copter: at the beginning of each operational day, the system will select an ideal location for the flying vehicle, where it will then land and measure

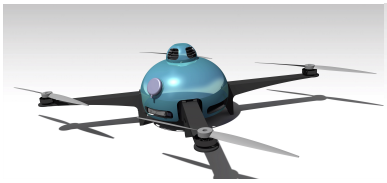

**Figure 2:** *Render of ALEC's emission drone subsystem*

**Figure 3:** *Render of ALEC's noise drone subsystem*

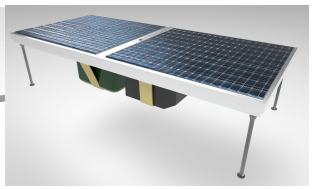

**Figure 4:** *Render of ALEC's ground level sensors*

until it has to return to the ground station. This allows the system to completely focus on the noise of specific aircraft events as the measurements are not affected by the ego-noise of the propellers. In addition to two cameras incorporated for autonomous flight, the drone includes a daisy shaped plate to reduce the distortion due to the ground effect as experienced by the microphone. The data collected by the noise drones is used for calculating the total environmental metric, and it is important for estimating the thrust levels of each aircraft which is valuable for predicting the total air pollutants emitted. As the measurements are distinctly accurate and include higher frequencies, which are otherwise attenuated over large distances, the collected information is invaluable for researchers interested in aviation-based noise.

| Aircraft | Time | Flight Nr. | Noise Score | Emission Score | Combined Metric |
|---|---|---|---|---|---|
| Type A | 03:07:46 UTC | AE4431 | 0.64 | 0.83 | 0.72 |
| Type B | 03:09:12 UTC | EE4685 | 1.32 | 1.11 | 1.23 |
| Type C | 03:11:32 UTC | AE2223 | 3.04 | 3.47 | 3.13 |

**Figure 5:** *Example of data displayed on the website, including scores awarded on the noise and emissions impact*

The development of technology over the past decades has seen monitoring networks stray away from expensive, professional equipment and towards low-cost sensor units that are easily deployable. As current noise models are insufficient at predicting the true impact of aviation on local communities, the ground level sensors of the ALEC system will be placed across affected areas to help develop a better understanding of the true impact of aircraft noise at a local level. Project ALEC builds upon the pioneering work performed by eco-acoustic projects and uses a system that has been proven in the harsh climates of Borneo and in the bustling metropolis of central London. Containing a flexible and robust audio sensing system, the ground level sensors are capable of being deployed in a multitude of locations, such as on buildings and on street lamps. Its configuration consists of a solar panel which acts as independent energy source, a microphone, and an electronics configuration capable of storing, processing, and transmitting audio data - an indicative rendering can be seen in Figure 4. The ground level sensors are capable of transmitting full, uncompressed spectral data, with the obtained measurements being used within the total environmental metric to estimate the noise associated with an aircraft event experienced by local communities.

Ground level operations are complemented by the use of a ground station responsible for determining the measurement location of the drone. Through the use of ADS-B data in combination with the acquisition function of the algorithm, the ground station is capable of calculating the optimal location to infer information of a certain aircraft event. In addition, for safety, the ground station can command any of the drones to land or to return to the base during emergencies. Additionally, the ground station provides a landing pad for the drones to take-off and land, and a means to swap and recharge the batteries of the drones when electric charge needs to be replenished.

In total, ALEC's hardware costs of emission drones, noise drones, ground level sensors, and ground station are estimated to cost €22,500. The hardware cost is part of the one-time cost which includes

manufacturing costs (€31,000), development costs (€750,000), drones certification costs (€15,200), and the acquisition of two vans (€117,500). The total one-time cost is about €1,035,500. Furthermore, the total monthly operational cost is €19,350 which includes installation cost (€4,000), employees (€8,100), Transportation Cost (€2,200), and miscellaneous cost (€5,050). Miscellaneous cost consist of manufacturing, power, data transmission, and insurance/certification costs. These costs will be covered by providing a noise and emissions environmental mapping to airports and/or local authorities, as ALEC is the only available system capable of offering complete aircraft-based noise and emissions mapping services for near-airport communities. The subscription cost for ALEC will be a monthly cost of €39,995. This will result in a break-even point of maximum three years in the case when one system is operating at a time.

Operations of the system have been designed such that the system is fully operational by only two operators. The system only needs two operators because an autonomous take-off, collision avoidance, sampling, and landing system reduces the need of specifically controlling the individual drones; allowing the user to actively manage near-runway operations as a whole. Additionally, near-runway operations can be set up in less than an hour and require two vans for moving the components.

An essential aspect of the design process is ensuring the sustainability of the designed system. As an instrument employed to realise sustainable development and help people affected by aviation noise and emissions, the system has been created while considering its own impact on the environment. ALEC has been developed to produce no harmful emissions during its operation and to be as sustainable as possible. To achieve sustainable design a sustainable development strategy was used in the design process. The main objectives of this strategy were; 'Choosing low-impact materials', 'Minimising amount of materials used', 'Sustainable production and manufacturing', 'Optimising operations and logistics', 'Minimising impact during operation', 'Optimising the lifetime of the product', and 'Optimising the end of life plan'. The strategy was used to include sustainability in the trade-off for the main concepts and in the design of the mission configuration. The mission was designed in a way that no drones have to fly over communities, as to remove the potential nuisance caused by drone noise to the people the system is meant to help. In the detailed design phase the strategy was used to make proper decisions on components and designs. This has resulted in the system consisting of 89 % recyclable components. The main materials used for the drones, apart from the batteries, are chopped carbon fibre reinforced nylon, high-density polyethylene, and carbon fibre sandwich sheets. The chopped carbon fibre reinforced nylon and high-density polyethylene are fully recyclable and have a very small negative impact on environmental, social, and economic sustainability, and the batteries can be recycled as well. The carbon footprint of the operation of the system is 2,44 kg of $CO_2$ per day and an end-of-life plan was made to ensure recyclable materials and components will be recycled.

To conclude, the ultimate goal of ALEC is to contribute to reducing the impact of aviation on near-airport communities. This has been done by designing a system which provides information on the impact of aircraft events using an environmental footprint metric for each aircraft event while also allowing researchers to access the raw data as measured by the various measuring systems. However, the design of the system is not finished after this phase. Further research should focus on improving the environmental footprint metric, the sensor payload of the emissions drone, implementing the software for the sampling and modelling algorithm, and the structure of the drone.

# Contents

# Nomenclature

| Abbreviation | Definition | Abbreviation | Definition |
|---|---|---|---|
| ADS-B | Automatic Dependent Surveillance Broadcast | MEMS | Micro-electromechanical System |
| AE | Aerodynamics | MLL | Mean Log Loss |
| AEMS | Autonomous Environmental Monitoring System | MR | Mission Requirement |
| ALEC | Autonomous Lab for Environmental Computation | MTOW | Maximum Take Off Weight |
| ATC | Air Traffic Control | NMVOC | Non-Methane Volatile Organic Compounds |
| AUT | Autonomy | NN | Neural Network |
| BLDC | Brushless DC Motor | NOMOS | Noise Monitoring System |
| BMS | Battery Management System | NPD | Noise Power Distance |
| CA & S | Control, Autonomy & Stability | OAT | One at A Time |
| CAGR | Compound Annual Growth Year | OC | Organic Carbon |
| CDHS | Command Data & Handling System | OECD | Organization for Economic Cooperation and Development |
| CF | Carbon Fiber | OPER | Operations |
| CFD | Computational Fluid Dynamics | PEM | Proton Exchange Membrane |
| CON | Control | PERF | Performance |
| CPI | Consumer Price Index | PM10 | Particulate Matter 10 |
| CPU | Central Processing Unit | PM2.5 | Particulate Matter 2.5 |
| CS | Control, Autonomy & Stability | PMSM | Permanent Magnet Synchronous Motor |
| DC | Direct Current | PMU | Power Management Unit |
| DIMS | Dimensions | ppb | Parts per Billion |
| DOT | Design Option Tree | ppm | Parts per Million |
| DSE | Design Synthesis Exercise | ppmv | Parts per Million per Volume |
| ECM | Electret Condenser Microphone | PROP | Propulsion |
| EOL | End of Life | QALY | Quality Adjusted Life Years |
| EPA | Environmental Protection Agency | RAMS | Reliability, Availability, Maintainability, Safety |
| EPN | Effective Perceived Noise | RDT | Requirements Discovery Tree |
| EPS | Electrical Power System | RDTE | Research, Development, Test & Evaluation |
| ESA | European Space Agency | RMSE | Root Mean Square Error |
| ESC | Electronic Speed Controller | ROI | Return on Investment |
| ESRS | Environmental Science and Remote Sensing | RPA-L | Remotely Piloted Aircraft License |
| FBS | Function Breakdown Structure | RQ | Rational Quadratic |
| FC | Flight Controller | S-BvL | Special Certificate of Airworthiness |
| FEM | Federal Equivalent Methods | SAF | Safety |
| FFD | Functional Flow Diagram | SAR | Safety & Reliability |
| FRC | Farthest Reachable Corner | SCM | Superconducting Motors |
| FRM | Federal Reference Method | SEN | Sensors |
| FRM | Federal Reference Methods | SGD | Stochastic Gradient Descent |
| FTP | File Transfer Protocol | SM | Structures, Manufacturing & Aerospace Materials |
| FWeV | Fixed Wing eVTOL | SNR | Signal to Noise Ratio |
| FY | Fiscal Year | SPL | Sound Pressure Level |
| GDP | Gross Domestic Product | SR | System Requirement |
| GLS | Ground Level Sensor | SUST | Sustainability |
| GP | Gaussian Process | SWOT | Strengths, Weaknesses, Opportunities, and Threats |
| GPS | Global Positioning System | synTS | Synchronous Thompson Sampling |
| GS | Ground Station | TBD | To Be Determined |
| ICAO | International Civil Aviation Organization | TC | Telecommunication |
| ID | Identifier | UAV | Unmanned Aerial Vehicle |
| ILT | Human Environment Transportation Inspectorate | UR | User Requirement |
| IOT | Internet of Things | US | United States |
| IP | Ingress Protection | USD | US Dollar |
| ISA | International Standard Atmosphere | UV | Ultra Violet |
| KLM | Koninklijke Luchtvaart Maatschappij | V&V | Verification & Validation |
| L | Lift | VOC | Volatile Organic Compound |
| LML | Log Marginal Likelihood | VSL | Value of Statistical Life |
| LTE | Long-Term Evolution | VTOL | Vertical Take-Off and Landing |
| LTO | Landing and Take-Off | WASN | Wireless Acoustic Sensor Network |
| MAI | Manufacturing, Assembly & Integration | WRMSE | Weighted Root Mean Square Error |

# 1

# Introduction

Aviation, as an industry, provides significant socio-economic benefits and is fundamental to the development of the modern world [1]. However, the way the world is currently powering aircraft comes at a unsustainable cost: aviation is a heavily polluting industry and contributes to approximately 3.5 % of the total anthropogenic effective radiative forcing for 2018 [1]. Additionally, communities living in close proximity to airports are disproportionately affected by the negative health effects related to pollution from aviation. The noise and emissions created by aircraft can have detrimental effects on human health, with approximately 16,000 people dying prematurely every year due to aircraft emissions [2]. Furthermore, prolonged exposure to noise and emissions from aircraft has been associated with multiple negative health effects such as an increased risk of respiratory diseases [3] and cardiovascular diseases [4]. To ensure a sustainable future growth for this sector, significant efforts have to be put into mitigating its negative effects, such as the noise and emission pollution, both by the scientific community as well as authorities.

A thorough understanding of these effects represents the first step in the long-term promotion of sustainable growth within the aviation industry. Currently, there is a lack of accurate data necessary for the development of accurate models. The current project represents the contribution to this goal by ten Aerospace Engineering students who, for their Design Synthesis Exercise, have designed a complex system able to create an accurate map of emissions and noise data near airports, with the final goal of reducing the negative effects that near-airport communities disproportionately experience from aviation.

The project is structured in four phases, the current report presents the work of phase IV, during which a detailed design of the system is presented, along with some guidelines concerning the future development of the project. The description of the system as a whole and the mission profile & logistics are presented in Chapter 2. The main goal of the project is to provide a total environmental footprint metric, the details of its calculations of this metric from the various measured quantities are the subject of Chapter 3.

Furthermore, the detailed design for each subsystem of ALEC is presented in the subsequent chapters: Chapter 4 elaborates on the emission drone and its various components, while Chapter 5 is concerned with the noise drone's design. Chapter 6 presents the propulsion subsystem, which is identical for both drones and thus afforded its own chapter. The ground station design can be found in Chapter 7, Chapter 8 describes the ground level sensors. The theory of the algorithm developed for model generation, as well as some results, are described in detail in Chapter 9. Afterwards, the report is concerned with describing the overall system, such as the manufacturing, assembly, and integration plan (MAI) which is presented in Chapter 10, and the verification & validation procedures which are found in Chapter 11. Furthermore, the financial aspects of the project are covered in Chapter 12. Chapter 13 provides information on the risks associated with design. The report concludes with a sustainability analysis, in Chapter 14, a design and development logic analysis in Chapter 15, and conclusions and recommendations in Chapter 16.

[1] https://www.atag.org/our-activities/social-and-economic-benefits-of-aviation.html#:~:text=It%20facilitates%20tourism%2C%20trade%2C%20connectivity,development%20of%20the%20modern%20world. [Cited 11-06-2022]

# 2

# Conceptual Design

The conceptual design phase takes place before the final design phase of the project. This phase involves designing a mission and a system which could optimally comply with and achieve the user requirements and desires, and is summarised in this chapter in order to provide the required context for the remainder of the report.
Section 2.1 covers the overall objective of this project and the purpose of this project. Then, Section 2.2 presents the mission and system which is designed in detail in this report. After this, the operation of the system is documented in Section 2.3. Finally, the trade-off used to select the best concept for the flying vehicle component of the mission is summarised in Section 2.4.

## 2.1. Project Objectives

The impact of aviation on society is significant, as discussed in Chapter 1. The quantifying the impact is not an easy task as there is not publicly available data about the noise and emissions related to aviation, leading to the mission need statement:

*"The distribution of individual aircraft events' noise and air pollution concentrations from aircraft paths to near airport communities is not sufficiently understood."*

The following objective of the project is defined as to address the mission need statement:

*"To accurately measure noise and air pollution to calculate a metric for tracking the environmental impact of aviation on near-airport communities."*

That is, to address the aforementioned problems, an understanding of them must first be developed. Decision makers such as regulatory bodies, governments, and corporations, can not make optimal decisions if the necessary data to thoroughly assess the problem is not available. Having access to accurate data on the impact of individual aircraft the decision makers can create specific, localised, and effective methodologies to alleviate these issues.
For example, Schiphol airport actively manages their runway usage based on weather conditions as to reduce noise nuisance, and several departure routes are promoted to reduce the total amount of time an aircraft spends over inhabited areas. In addition, noisier and more polluting aircraft have to pay higher fees for operating at Schiphol [1]. However, not all airports are capable of tracking the pollution generated by individual aircraft event. ALEC has been designed to provide airport stakeholders the necessary data about specific aircraft operations to identify the most effective strategies for the promotion and advancement of sustainable aviation. This system has been designed to be versatile enough to be applied to any airport or region and only requires sufficient access to the airport and communities which have to be mapped. Depending on the customer who commissions the mission to determine the environmental metric, there is an option to make the environmental metric and raw data available to the public.

## 2.2. Measurement Philosophy

Based on the demand of the client who commissioned the design of this system, a list of user requirements is compiled: the starting point for the conceptual design phase. The requirements are presented in Table 2.1. Along with the requirements, the compliance matrix indicating whether

[1] https://www.schiphol.nl/en/schiphol-as-a-neighbour/page/noise-and-runway-combinations/ [20 June 2022]

the final design meets the requirement is provided in parts with the relevant sections of the report which document the compliance. A ✓ indicates that the requirement has been met, ~ indicates partial compliance and × shows that the requirement has not been met. Furthermore, key requirements are shown using the indicator **requirement (key)**.

**Table 2.1:** *User requirements and compliance*

| Requirement ID | Requirement | Compliance | Comments |
|---|---|---|---|
| ALEC-UR-PERF-01 | The monitoring system shall have an operational set-up time shorter than an hour. | ✓ | Presented in Chapter 7 |
| ALEC-UR-PERF-02 | The monitoring system shall produce individual noise metrics. | ✓ | Presented in Chapter 3 |
| ALEC-UR-PERF-03 | The monitoring system shall produce individual emission metrics. | ✓ | Presented in Chapter 3 |
| **ALEC-UR-PERF-04 (key)** | The monitoring system shall produce a total environmental metric near airports. | ✓ | Presented in Chapter 3 |
| ALEC-UR-PERF-05 | The monitoring system shall display background noise levels. | ✓ | Presented in Chapter 8 |
| ALEC-UR-PERF-06 | The monitoring system shall display aviation attributable metrics. | ✓ | Presented in Chapter 3 |
| ALEC-UR-PERF-07 | The monitoring system shall be able to store and/or transmit one day's worth of measurement. | ✓ | Presented in Chapter 4, Chapter 5, and Chapter 8 |
| ALEC-UR-SAR-01 | The monitoring system shall be able to operate at wind conditions up to and including Beaufort 4. | ✓ | Presented in Chapter 4, and Chapter 5 |
| **ALEC-UR-SAR-02 (key)** | The monitoring system shall not intervene with aircraft operations. | ✓ | Presented in Chapter 4, and Chapter 5 |
| ALEC-UR-SAR-03 | The monitoring system shall be capable of operating under dry weather conditions. | ✓ | Presented in Chapter 4, and Chapter 5 |
| **ALEC-UR-SUST-01 (key)** | The monitoring system shall consist of at least 70% recyclable or re-processable system parts. | ✓ | Presented in Chapter 14 |
| ALEC-UR-SUST-02 | The operations of the monitoring system shall be emission-free. | ✓ | Presented in Chapter 6 |
| ALEC-UR-SUST-03 | The monitoring system shall make as less noise as possible. | ✓ | Presented in Chapter 8 |
| ALEC-UR-DIMS-01 | The monitoring system shall have a maximum length of 2 meters in all directions. | ✓ | Presented in Chapter 4, and Chapter 5 |
| **ALEC-UR-COST-01 (key)** | The monitoring system shall have a hardware cost less than 25000 Euro (2022) excluding VAT. | ✓ | Presented in Chapter 12 |
| **ALEC-UR-AUT-01 (key)** | The monitoring system shall be as autonomous as possible. | ✓ | Presented in Chapter 9 |

To fulfill the project objective, the ALEC system will measure noise and air pollution caused by specific aircraft events. A suitable measurement system must be designed to achieve this goal. The aim of the system is to quantify the effect of single aviation events in their entirety on the community. The process of devising a measurement philosophy to achieve this is documented in the midterm report [5]. In summary, four subsystems are deemed to be necessary to optimally meet the requirements of the system and the desires of the customer, namely emission drones, noise drones, ground level sensors and a ground station.

The emission drones have to capture data which allows for the total mass of the relevant polluting species emitted during an LTO operation to be modelled as accurately as possible. These drones will operate next to the runway to allow for the slow and unpredictably diffusing emissions to be directly captured. The noise drones will also operate in vicinity of the runway in order to provide accurate and high quality data on the noise produced by the aircraft during the LTO operation.

The first two subsystems aid in capturing measurements used to produce the desired metrics near

the runway, but the objective of the project is to map the entire effect of an aviation event on the community. For this, the aircraft's pollution must be tracked for a larger portion of the flight than just the LTO phase. However, for emissions this is deemed infeasible due to the aforementioned characteristics of emissions. With noise, it is more realistic to capture the pollution of the aircraft beyond the LTO phases. This is where the GLS kits come into effect, as they are deployed in communities to directly measure the noise produced by an aircraft at larger distances from the airport. The final subsystem is the ground station (GS), which is responsible for facilitating the operation of the drones at the airport and providing an interface for the operator to view the data collected and control the operation.

Selecting the number of components within the system is a result of a trade off between cost, performance, and operational risk between the various sub-systems. A priority within the selection is maximising the number of GLS, due to the wide coverage area required. This leads to a bottleneck within the duration of the mission which is that the number of emission drones employed within the system would have been considerably lower than the total noise sensors, such as noise drones and GLS. First, an operational analysis of the emission drones is conducted to show that the maximum number of emission drones which could be employed within the system is four as operators need to manually swap the batteries. Next, a mission duration analysis is conducted in Chapter 9 to show that maximising the number of drones helps reduce mission duration leading to four emission drones being selected. Next, a trade-off between the number of noise drones and GLS is undertaken: as a goal of the ALEC system is measuring the noise experienced by near-airport communities, the minimum number of noise drones employable in the system selected is two. The noise drones are needed to measure aircraft noise near airports and are used to estimate the total thrust generated during aircraft events, which means that only two components are required for redundancy. After considering the cost of the ground station, the remainder of the budget is allocated to the remaining 40 GLS.

The subsystems are capable of sending the data which is collected in real time to an FTP server through the internet. The GS is then able to download and present this data to the operator if desired. A total environmental metric must be derived to quantify the effect of a single aircraft event on near-airports communities. The derivation of this metric is discussed in Chapter 3. As the system is based on uploading data to an internet FTP server, this metric can be easily accessed by any interested party through a website interface. Besides the metric, the raw data used to construct this metric can also be downloaded through the website if this option is enabled by the customer.

## 2.3. System Operations and Logistics

The system is applicable to any airport and is delivered as a service not meant to be permanently installed. The system is thus deployed to a specific airport and the surrounding community temporarily. A single mission is defined as all operations required to generate the environmental metric for flight events originating or departing from a single runway in a single direction. In order to do so, GLS kits are distributed along the relevant approach or departure paths of the chosen runway direction. These temporary kits will be distributed and left in their location for a duration a month or more. The mission starts when the kits are deployed and ends when they are picked up again. This is the mission on the larger time scale. The deployment of the GLS kits takes 3-5 working days. Once the GLS kits have been installed, the segment of the mission involving drones can commence. The operation of the drones is performed on a day-to-day scale. Every day, the operators transport the drones and ground station to the airport and operate at the specific runway for a working day of eight hours. At the end of the day, the operators pack up the drones and ground station and return to their home base. As a note, two operators are required to operate the system, both in the GLS deployment phase and the day-today operations.

Each subsystem's specific operations and mission is further elaborated on in their respective chapters. The mission requirements are derived from the description of the mission and are included in Table 2.2 below. An overview of how the subsystems communicate with each other is provided in Figure 2.1.

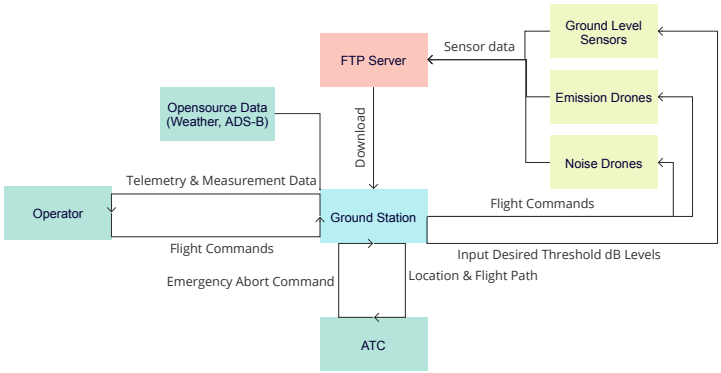


**Figure 2.1:** *Global communications diagram of ALEC system*

**Table 2.2:** *Mission requirements and constraints*

| Requirement ID | Requirement | Compliance | Comments | Verification |
|---|---|---|---|---|
| ALEC-MR-01 | The system shall be able to attribute a measurement to a location within a volume of $5m^3$ | ✓ | Presented in Chapter 4, and Chapter 5 | Test - show accuracy in test conditions |
| **ALEC-MR-03 (key)** | The system shall not hinder the operation of any taxiing, taking-off, or landing aircraft. | ✓ | Presented in Chapter 4, and Chapter 5 | Analysis - review mission operations |
| ALEC-MR-04 | The system shall be able to store an operational days worth of data. | ✓ | Presented in Chapter 4, Chapter 5, and Chapter 8 | Demonstrate- verify under test conditions |
| **ALEC-MR-05 (key)** | The system hardware shall cost less than 25000 Euro (2022) excluding VAT. | ✓ | Presented in Chapter 12 | Analysis - add cost of system components |
| ALEC-MR-06 | The system shall consist of at least 70% recyclable or re-processable parts. | ✓ | Presented in Chapter 14 | Analysis - conduct sustainability analysis |
| ALEC-MR-07 | The system shall be operable in wind speeds up to 7.9 m/s. | ✓ | Presented in Chapter 4 and Chapter 6 | Test - test in windtunnel |
| **ALEC-MR-08 (key)** | The system shall derive the total environmental footprint. | ✓ | Presented in Chapter 3 | Test - show accuracy of metric in test conditions |
| ALEC-MR-09 | The system shall not use radio frequencies which are used by airport operations. | ✓ | Presented in Chapter 4 | Analysis - review mission operations |
| ALEC-MR-10 | The system and ground station shall be transportable in a volume of 2.1x1.7x1.4m. | ~ | Partially covered in Chapter 4, but requires further analysis | Demonstrate - show packing scheme |
| ALEC-MR-11 | The system shall operate below 100 meters from the ground | ✓ | Presented in Chapter 4 | Analysis - review mission operations |
| ALEC-MS-12 | The system shall not operate within 20 meters of airplane flight paths. | ✓ | Presented in Chapter 4 | Analysis - review mission operations |

## 2.4. Trade-Off Flying Vehicle

One of the steps taken in the conceptual design phase is to decide on the optimal flying vehicle to serve as the platform for the emission and noise measurement subsystems. This section presents a summary of the trade-off performed. The full trade-off is presented in the midterm report [5].

Two main trade-offs are performed for the type of flying vehicle: one trade-off for the vehicle measuring emissions and one for the vehicle measuring noise near the runway, respectively. Separate trade-offs for the emissions and noise vehicles are performed as they have different missions and therefore could score differently on certain criteria in the trade-off table. After analysing the possible solutions in phase II of the project, three feasible options are selected. These are a dirigible

balloon, fixed wing eVTOL (electric vertical take-off and landing), and an N-copter. The dirigible balloon consists of an inflatable container filled with a lighter-than-air gas to provide lift. To this container the components required for its mission are attached, such as the measuring instruments, the propulsion system, and the flight controller, among others. The fixed wing eVTOL is a combination of a fixed wing aircraft and an N-copter. It has a conventional fixed wing to provide lift during horizontal flight. Propellers are placed both vertically and horizontally. The vertically placed propellers provide thrust during horizontal flight, whereas the propellers in horizontal position generate the lift required during hovering. The N-copter is a drone equipped with multiple propellers in horizontal direction such that it can hover and fly horizontally. All the lift required to keep it in the air is provided by these propellers, also during horizontal flight.

The trade-offs are performed using trade-off tables. The scoring system of the trade-off is provided in Table 2.3. Furthermore, each criteria is assigned a weight. The weighting is based on the importance that criteria have for the design of the system.

**Table 2.3:** *Scoring system for the trade-off [5]*

| Concept | Criterion |
|---|---|
| 1 | Excellent (Green) |
| 2 | Good (Blue) |
| 3 | Correctable Deficiencies (Orange) |
| 4 | Unacceptable (Red) |
| Weighting Factor | 1-5 |

The main trade-off tables for the emission measuring vehicle and noise measuring vehicle can be found in Table 2.4 and Table 2.5 respectively [5]. Sub-trade-offs are performed for various trade-off criteria too. For example, the values for the control, autonomy, and stability (CA&S) criteria are obtained by performing a trade-off with the criteria controllability, stability, and mission autonomy. The sub-trade-offs can be found in the midterm report [5].

**Table 2.4:** *Main trade-off table emissions vehicle [5]*

| Concepts | Suitability | Sustainability | Complexity | CA & S | RAMS | Flight Performance | Total score |
|---|---|---|---|---|---|---|---|
| Dirgible balloon | 2.0 (Orange) | 2.8 (Blue) | 2.5 (Blue) | 2.2 (Orange) | 3.0 (Blue) | 2.3 (Orange) | **2.4** |
| Fixed Wing eVTOL | 2.0 (Orange) | 2.4 (Orange) | 2.0 (Orange) | 3.3 (Blue) | 2.8 (Blue) | 3.0 (Blue) | **2.5** |
| N-copter | 3.0 (Blue) | 2.8 (Blue) | 3.0 (Blue) | 3.7 (Green) | 2.7 (Blue) | 2.5 (Blue) | **2.9** |
| Weights | 5 | 5 | 5 | 4 | 3 | 4 | |

**Table 2.5:** *Main trade-off table noise vehicle [5]*

| Concepts | Suitability | Sustainability | Complexity | CA & S | RAMS | Flight Performance | Total score |
|---|---|---|---|---|---|---|---|
| Dirgible balloon | 2.0 (Orange) | 2.8 (Blue) | 2.5 (Blue) | 2.2 (Orange) | 3.0 (Blue) | 2.3 (Orange) | **2.4** |
| Fixed Wing eVTOL | 1.0 (Red) | 2.4 (Orange) | 2.0 (Orange) | 3.3 (Blue) | 2.8 (Blue) | 3.0 (Blue) | **2.3** |
| N-copter | 4.0 (Green) | 2.8 (Blue) | 3.0 (Blue) | 3.7 (Green) | 2.7 (Blue) | 2.5 (Blue) | **3.1** |
| Weights | 5 | 5 | 5 | 4 | 3 | 4 | |

As one can conclude from Table 2.4 and Table 2.5, the N-copter turned out to be the best option for

both the vehicle measuring noise and the vehicle measuring emissions. The main benefits of the N-copter compared to the fixed wing eVTOL and dirigible balloon are its good control, autonomy and stability. Furthermore, the N-copter has a high score for suitability for the noise vehicle as the N-copter is very reliable in vertical landing and take-off, which is an important requirement for the noise vehicle. Contrary, the dirigible balloon is susceptible to being displaced by strong winds when stationary on the ground performing measurements and the fixed wing eVTOL is unstable during the transition between vertical and horizontal flight (and vice versa).
A sensitivity analysis is performed to analyse what the effect would be when changing a certain score on the final outcome. It served as a measure to check the robustness of the decision a N-copter for the noise and emissions vehicles. Two types of methods for the sensitivity analyses are used, namely the 'One At a Time" (OAT) and 'Monte Carlo' methods. The outcomes of the sensitivity analyses using the Monte Carlo method proved that the trade-off is robust and only 5% of the experiments would output different results when allowing changes up to 2 standard deviations. Moreover, for more realistic values of the standard deviation, the experiments are consistently more robust.

# 3

# Total Environmental Footprint Metric

The environmental footprint metric is defined as a measure for the impact of a single aircraft event on the near-airport communities. This metric is one of the outputs of the ALEC system. This chapter first discusses how the environmental footprint metric is calculated in Section 3.1. Thereafter, the weights of noise and emissions within the equation for the environmental footprint are discussed in Section 3.2. The weights for the specific emission species are analysed in Section 3.3. Section 3.4 discusses how the data from the total environmental footprint is presented. Finally, recommendations for future development are discussed in Section 3.5.

## 3.1. Calculation of Environmental Footprint

The goal of a total environmental metric is to derive an estimate of the impact of a specific aircraft event on the nearby community. The goal is to obtain a score capable of incorporating both the air and noise pollution within this metric to allow the direct comparison of the environmental metric of different aircraft events. The standard environmental footprint is calculated using Equation 3.1 solely based on estimates of aviation emissions, but there will be several options which can be used to compare the score with respect to further metrics, such as population and the number of passengers in the aircraft. The additional options are discussed in Section 3.4.

$$E = w_1 \frac{L}{\tilde{L}} + w_2 \sum_{i=1}^{N} \frac{u_i C_i}{\tilde{C}_i}, \tag{3.1}$$

where $E$ is the total environmental footprint metric. $E$ represents the impact of a certain aircraft event relative to the median of aircraft events better, where the lower this value is, the smaller the impact of a certain aircraft event was on the near-airport communities. $L$ is the noise level created by the aircraft, as experienced by people on the ground. $C_i$ is the parameter that represents an estimate of the total emissions of a a specific emission species $i$ during an aircraft event. The noise level and emissions values are normalized using the median pollution measured at a certain airport. The median values, $\tilde{L}$ and $\tilde{C}_i$, are used as it reduces the impact of outliers compared to when the mean were to be used. That means that in the beginning the footprint metric will be less indicative of the relative impact of a single aircraft event, as the median value shows high variance, but over time the metric will become more accurate. For the noise level measurements normalizing happens in Equation 3.1. The noise level and species concentration measurements are normalized in the environmental footprint metric because they have different units, and are possible to add directly due to this process. $w_1$ and $w_2$ are the weights assigned to noise pollution and emissions pollution, respectively, and further described in Section 3.2. $u_i$ is the weight of the specific species of emissions. The values for $u_i$ are discussed in Section 3.3.

**Sound Level** $L$

The noise level is calculated using data measured by the GLS and noise drones together with noise models. It was decided to use the noise levels as this is a measure for the amount of noise experienced by people on the ground, contrary to the sound pressure level which is dependent on the noise produced by a source and not the distance is between the source and the observer. This distance is an important factor for near-airport communities as the higher an aircraft flies, the less noise is experienced by people on the ground. Using the noise measured by the ground level sensors and noise drones together with noise models, a map of noise levels can be created with the

Gaussian Processes as explained in Chapter 9. The noise level will be integrated over area and time to come to a total metric throughout a certain aircraft event. The area over which it is integrated is a square of 20 km by 20 km in the direction that the aircraft flies over the near-airport communities measured from the end of the runway. A distance of 20 km was chosen "For airports with a significant number of operations, populations living along radials aligned with runways or flight paths may be exposed predominantly to damages from noise as much as 20 km further away from the airport." [6]. When an aircraft enters the runway, noise levels will be measured by the various microphones which serve as input data for the noise models. Until the the aircraft leaves the 20 km by 20 km region, the models will keep estimating the noise levels on the ground using data from the noise drones and GLS kits once a second. Once the aircraft leaves the bounded area, the noise levels within that region for the time that the aircraft produced within that frame are summed up to get a total value for the noise impact a single aircraft event had on the near-airport communities.

**Emissions Concentrations** $C$
$C$ represents the total emission of five types of species measured by the emissions drones and estimated through a model. Despite the emissions drones measuring NO and $O_3$, they will not be taken into account in the environmental footprint calculation. The majority of $NO_x$ emitted is $NO_2$, and therefore this measurement is used to estimate the total $NO_x$. Ozone ($O_3$) is not taken into account in the total environmental footprint metric as it is a secondary emission, which is produced by a reaction of $NO_x$ in air in the presence of VOCs and UV-light. Nonetheless, the value is important in the long-term to estimate the distribution of gasses in the atmosphere, and can be used by researchers for further analysis. $C$ will be calculated using Equation 3.2;

$$C = \sum_{i=1}^{5} u_i \cdot \frac{C_i}{\bar{C}_i}. \tag{3.2}$$

In Equation 3.2, $u_i$ is the weight assigned to each type of species, based on its effect on human health and explained below. As mentioned above, the concentration measurements are normalised by dividing the concentration for a certain species for a certain aircraft event by the median of all aircraft events. The total emissions will be calculated by modeling the amount of emissions produced by the aircraft from when it enters the runway to when it leaves the runway (take-off for departing aircraft, taxiing off the runway for arriving aircraft). This is done using measurements from the emission drones in combination with the model. By estimating the flux of pollution over a plane near the aircraft, parallel to the aircraft direction, it is possible to estimate the total mass flow of emissions during an aircraft event leading to an estimate of the total emission of each gas species.

## 3.2. Weights of Noise and Emissions

This section discusses the weights $w_1$ and $w_2$. These two weights correspond to the impact of noise and emissions of aircraft events on near-airport communities. P.J. Wolfe et al. [6] analysed how people that live near airports experience an elevated impact of aircraft events, with the mean cost per person due to noise and emissions depending on aircraft operations. As one can conclude from Figure 3.1 [6], the ratio between damage due to air quality and noise differs depending on the amount of operations carried out at the airport annually (i.e. amount of flights landing and taking off, aircraft events). Therefore, the weights will be dependent on the airport/runway being analysed. The weights $w_1$ and $w_2$ will be calculated using Equation 3.3 and Equation 3.4, respectively;

$$w_1 = \frac{y_1}{y_1 + y_2}, \tag{3.3}$$

$$w_2 = \frac{y_2}{y_1 + y_2}, \tag{3.4}$$

In Equation 3.3 and Equation 3.4, $y_1$ is the mean expected damage per person in USD FY2006 due to noise and $y_2$ is the the mean expected damage per person in USD FY2006 caused by a decrease of air quality. It should be noted that this report uses EUR as standard currency. However, as a ratio

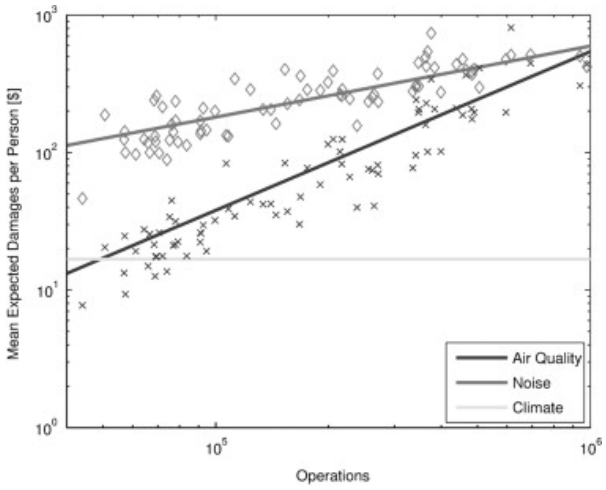


**Figure 3.1:** *Mean of expected damage per person living at airport boundaries in USD (FY2006) as function of amount of annual operations [6]*

is calculated to determine $w_1$ and $w_2$, the unit USD disappears in the weights. The same holds for the fact that it is expressed in FY2006. Therefore, the damages in USD FY2006 do not need to be corrected for inflation and currency rates. Lastly, the reader should be aware of the fact that the climate damage is not considered in the weights, despite being presented in Figure 3.1 [6]. That is because the climate damage stays constant and is not dependent on the amount of annual operations, nor on the distance a person lives from the airport. Furthermore, the damage experienced by a person living near an airport depends on the distance they live from that airport. The damage shown on the vertical axis is calculated for the airport boundary [6]. The weights for Schiphol Airport will be calculated to provide an example. In 2019, the year before the aviation industry got affected by the COVID-19 pandemic, Schiphol Airport had approximately 500.000 air traffic movements [1]. From Figure 3.1, one can see that for $5 \cdot 10^5$, $y_1$ is approximately 500 USD and $y_2$ is approximately 250 USD. Using this example with Equation 3.3 and Equation 3.4 leads to $w_1$ equal to 0.67 and $w_2$ as 0.33.

## 3.3. Weights of Emission Species

As mentioned above, different types of emission species have different impacts on human health and are emitted at different rates. To account for this, the weight $u_i$ was introduced in Equation 3.1. The weights for the five emission species used in the calculation of the total environmental footprint metric are displayed Table 3.1. The column called 'LTO Air Quality Cost Metric' accounts for the fact that different emission species have different impact on human health. It mentions the cost per tonne of emission species emitted, and it specific for landing and take-off operations and for Europe. The pollution has been quantified using VSL of Europe. [7]. If one wishes to use the system outside of Europe the weighting factors should be adjusted, as the values differ for different regions around the world. The costs have been written in USD and FY2015, but that does not pose a problem for the weighting as the the weights are determined as fraction of the total cost, so the units disappear.

The 'Share of emission' column in Table 3.1 consists of the ratio of different types of emission species weighted to the ratio in which they are emitted [2] [8]. This ratio is based on "a typical two-engine jet

[1] https://nieuws.schiphol.nl/jaarcijfers-2019/? [Cited 10 June 2022]

[2] https://www.easa.europa.eu/eaer/figures-tables/emissions-typical-two-engine-jet-aircraft-during-1-hour-flight-150-passengers [Cited 21 June 2022]

aircraft during 1-hour flight with 150 passengers"[3]. For LTO events this ratio could be different, but it serves as an initial estimate. Subsequently, the two weights have been multiplied, of which the result is provided in the column 'Shares multiplied'. Afterwards, these values have been normalise to obtain the final weight of the emission species, and seen in the right column of Table 3.1.

**Table 3.1:** *Calculation of weights for emission species used in total environmental footprint metric calculation*

| Emission Species | LTO Air Quality Cost Metric [$/tonne] [7] | Share of Total Cost | Share of emission [4] [8] | Shares multiplied | Weight of emission species ($u_i$) |
|---|---|---|---|---|---|
| CO | 1100 | 0.0037 | 0.846 | 0.003 | 0.064 |
| NO2 | 67000 | 0.2255 | 0.071 | 0.016 | 0.34 |
| PM2.5 | 120000 | 0.4038 | 0.056 | 0.023 | 0.489 |
| VOC | 56000 | 0.1885 | 0.003 | 0.001 | 0.021 |
| SO2 | 53061 | 0.1786 | 0.024 | 0.004 | 0.085 |
| Total | 297161 | 1.0001 | 1 | 0.047 | 1 |

Some remarks should be made:P.J. Wolfe et al. [6] uses the cost of $NO_x$ in \$/tonne $NO_x$ as $NO_2$. This value is used for weighting $NO_2$ emissions. NO is omitted from the calculation of $C$ and hence a weight is not required. Furthermore, the source notes the costs of black carbon (BC), not of $PM_{2.5}$. BC is the primary type of $PM_{2.5}$. Therefore, in the calculations for $C$, it is assumed that the weight of $PM_{2.5}$ is that of $BC$. Lastly, the source mentions sulfates in general and does not give the costs of $SO_2$ and $SO_4$ specifically. 98% of $SO_x$ is $SO_2$, and therefore the cost of sulfates mentioned in the source is divided by 0.98. This way the cost of $SO_2$ represents the health impacts of both $SO_2$ and $SO_4$.

## 3.4. Presenting the Total Environmental Footprint

In short, a total environmental footprint metric is calculated for a certain aircraft event. All these metrics will be uploaded to an FTP server, together with all the raw data as measured by the ground level sensors and drones. The footprint metric will be saved together with data about the type of aircraft and airport where the aircraft departed/is heading towards. From this FTP server the website will use data to present on the website.

The footprint calculated shall be displayed on a website that is available for everyone to see. So, if a person living near an airport wants to compare the impact of two (or more) aircraft events on the near-airport communities, they can check the values on the website. The basic metric presented on the website is calculated by Equation 3.1. However, other options will be available.

One could reason that an aircraft that can carry more passengers/cargo while producing the same amount of pollution is favorable over an aircraft carrying less passengers/cargo. The exact amount of cargo and passengers will be hard to obtain for each aircraft event as it requires data from airlines operating the aircraft, and therefore standard capacities for cargo and passengers will be used in the calculations depending on the specific aircraft type. In a similar manner, one could reason that an aircraft that flew a larger distance before arriving, ceteris paribus, is deemed favorable. However, as such choices are subjective they are left as an option to the user. Therefore, on the website it will be optional to add these factors in the total environmental footprint calculation. The equation

[3] https://www.easa.europa.eu/eaer/figures-tables/emissions-typical-two-engine-jet-aircraft-during-1-hour-flight-150-passengers [Cited 21 June 2022]

that would be used to calculate the total environmental footprint metric which these two options selected can be seen below in Equation 3.5.

$$E_2 = \frac{E \cdot \rho_p}{d \cdot \left(\frac{W_c}{W_p} + N_p\right)}, \tag{3.5}$$

$W_c$ is the cargo weight in kg, $W_p$ = 88 [kg] is the weight of an average passenger and is used as a normalisation factor, $N_p$ is the number of passengers, $d$ is the distance travelled by the aircraft in km, and $\rho_p$ is the population density in a certain area near the runway. Cargo weight is included in Equation 3.5 to be able to also generate a footprint metric for cargo aircraft. As the standard passenger weight is 88 kg [5] , the cargo weight is divided by 88 kg in the equation for the environmental footprint. By doing so, the cargo weight is represented compared to an equivalent number of passengers.

Another option is to see the total environmental footprint metric as function of the population density. One could reason that an aircraft flying over an area with a relatively high population density is worse than that aircraft flying over an area with lower population density while experiencing the same amount of pollution, all other parameters considered equal. However, making such a decision is left up to the user of the website. Therefore, adding this parameter in the calculation of the total environmental footprint will be optional too. The population density would be included in Equation 3.1 by multiplying the numerator by the population density, as a higher population density should lead to a higher environmental footprint value.

Furthermore, it will be possible to download the raw data from the website. This includes the ADS-B data and the data measured by the ground level sensors (GLS's), noise drones, and emissions drones. This option is meant for researchers who could use the raw data for more in-depth analyses than would be possible with merely the data presented on the website.

## 3.5. Future Recommendations

In the future development of ALEC, there are several components of the total environmental footprint metric that should be thoroughly analyzed for possible improvements.
First, the area of 20 km by 20 km should be reconsidered. Currently it is deemed the best area in which noise levels should be calculated for the environmental footprint, but further research could focus on analyzing whether this is indeed the best area or whether other regions would be better.
Furthermore, currently the values for $L$ and $C$ are normalized using the median values. The median values are based on all previous measurements made for a certain runway. However, further development should focus on whether an median should be taken for all previous aircraft events, or whether it is better to take the median for another time frame such as a week or single day. The weather can effect the noise and emissions produced, and therefore this time frame over which the median is taken should be analyzed in future development as the weather changes.

[5] https://www.easa.europa.eu/downloads/3860/en [Cited 10 June 2022]

# 4

# Emissions Drone Subsystem

To measure emissions and air quality near runways, a drone specialised in monitoring aircraft exhaust was designed. Compared to stationary air quality stations, the emission drone provides a more flexible approach with a short set up time and the ability to measure at more locations including differing altitudes. To measure different substances using a drone, a custom sensing subsystem has been designed, consisting of an array of sensors and a specialised sensor chamber.

The emission drone requirements are included in Section 4.1, an analysis of the air pollutants to analyse in Section 4.2 and the payload design in Section 4.3. The general design of the drone and its structure is shown in Section 4.4, the command and data handling in elaborated on in Section 4.5, the autonomous design in Section 4.6 and the regulations the drone should adhere to are described in Section 4.7. Additionally, the budget is included in Section 4.8, followed by the performance analysis in Section 4.9. Finally, the operations and logistics concept description can be found in Section 4.10.

## 4.1. Requirements and Verification

The requirements for the emission drone can be found below in Table 4.1 and those shared for both emission and noise drones are included in Table 4.2 under the flying vehicle requirements. They are presented as to provide the reader a summary of the goals set within the design of the hardware of the system. Additionally, a compliance matrix is included to indicate if the requirement met, as well as comments to indicate where they are addressed within the text. Finally, the tables includes a verification column which indicates the procedure required to validate the requirement. A ✓ indicates that the requirement has been met, ~ indicates partial compliance, and × shows that the requirement has not been met.

**Table 4.1:** *Emission drone requirements and compliance*

| Requirement ID | Requirement | Compliance | Comments | Verification |
|---|---|---|---|---|
| ALEC-SR-FV-ED-PL-01 | The emission sensing subsystem shall measure sulfur dioxide levels with an accuracy of 10% Full Scale (FS) | ✓ | Presented in Section 4.3 | Analysis - perform measurements at limit concentration |
| ALEC-SR-FV-ED-PL-02 | The emission sensing subsystem shall measure nitrous monoxide levels with an accuracy of 10% Full Scale (FS) | ✓ | Presented in Section 4.3 | Analysis - perform measurements at limit concentration |
| ALEC-SR-FV-ED-PL-03 | The emission sensing subsystem shall measure nitrous dioxide levels with an accuracy of 10% Full Scale (FS) | ✓ | Presented in Section 4.3 | Analysis - perform measurements at limit concentration |
| ALEC-SR-FV-ED-PL-04 | The emission sensing subsystem shall measure carbon monoxide levels with an accuracy of 10% Full Scale (FS) | ✓ | Presented in Section 4.3 | Analysis - perform measurements at limit concentration |
| ALEC-SR-FV-ED-PL-05 | The emission sensing subsystem shall measure total $PM_{2.5}$ levels with an accuracy of 10% Full Scale (FS) | × | Not covered by product specifications | Analysis - perform measurements at limit concentration |
| ALEC-SR-FV-ED-PL-06 | The emission sensing subsystem shall measure total Ozone levels with an accuracy of 10% Full Scale (FS) | ✓ | Presented in Section 4.3 | Analysis - perform measurements at limit concentration |

| | | | | |
|---|---|---|---|---|
| ALEC-SR-FV-ED-PL-07 | The emission sensing subsystem shall measure total VOC levels with an accuracy of 10% Full Scale (FS) | × | Not covered by product specifications | Analysis - perform measurements at limit concentration |
| ALEC-SR-FV-ED-PL-08 | The environmental science subsystem shall note the time of each measurement with accuracy of ± 1 second | × | Not covered by product specifications | Test - perform measurements at known time |
| ALEC-SR-FV-ED-TC-10 | The emission drone shall transmit the measured values to the ground station. | ✓ | Presented in Section 4.5 | Inspection - see if emission data is received by ground station |
| **ALEC-SR-FV-ED-PERF-01 (key)** | The emission drone shall have an operational time of at least 20 minutes with a fully charged battery. | ✓ | Presented in Subsection 4.9.1 | Demonstrate - operate emission drone until battery is dead |
| ALEC-SR-FV-ED-COS-01 | The emission drone shall cost no more than 4500 EUR. | ✓ | Presented in Subsection 4.8.1 | Inspection - sum hardware costs of components |

**Table 4.2:** *Flying vehicle requirements and compliance*

| **Requirement ID** | **Requirement** | **Compliance** | **Comments** | **Verification** |
|---|---|---|---|---|
| **ALEC-SR-FV-01 (key)** | The flying vehicle shall be able to take measurements autonomously. | ✓ | Presented in Chapter 9 | Demonstration - take measurements without human intervention |
| ALEC-SR-FV-02 | The flying vehicle be able to autonomously calculate its flight path. | ✓ | Presented in Subsection 4.5.1 | Demonstration - let system calculate its own, non-predetermined, flight path |
| ALEC-SR-FV-03 | The flying vehicle be able to autonomously follow its flight path. | ✓ | Presented in Section 4.6 | Demonstration - vehicle flies non-predetermined flight path |
| ALEC-SR-FV-04 | The flying vehicle shall have an operational set-up time of less than one hour. | ✓ | Presented in Section 4.10 and Section 5.7 | Demonstration - set up flying vehicle and record time |
| ALEC-SR-FV-05 | The flying vehicle shall have a minimum IP rating of IP33. | ✓ | Presented in Section 4.4 and Section 5.3 | Test - expose vehicle to IP33 conditions |
| ALEC-SR-FV-TC-04 | The flying vehicle shall communicate its position to the ground station every 1 second. | ✓ | Presented in Section 4.5 | Test - measure communication interval |
| ALEC-SR-FV-CAS-01 | The flying vehicle shall be able to land autonomously. | ✓ | Presented in Section 4.6 | Demonstration - test vehicle landing command. |
| ALEC-SR-FV-CAS-02 | The flying vehicle shall be able to autonomously take off. | ✓ | Presented in Section 4.6 | Demonstration - test vehicle take off command |
| ALEC-SR-FV-CAS-03 | The flying vehicle shall be controllable. | ✓ | Section 4.6 | Test - test controllability of vehicle |
| ALEC-SR-FV-EPS-02 | The flying vehicle's power source shall provide power to each subsystems at the required voltage. | ✓ | Presented in Section 4.6 | Analysis - check electric block diagram |
| ALEC-SR-FV-EPS-03 | The flying vehicle's power source shall be rechargable. | ✓ | Presented in Chapter 6 | Inspection - check product specifications |
| ALEC-SR-FV-EPS-04 | The flying vehicle's power source shall not leak fluids while operational | ✓ | Presented in Chapter 6 | Inspection - inspect power source while operational |

| | | | | |
|---|---|---|---|---|
| ALEC-SR-FV-CDHS-01 | The flying vehicle shall be able to receive commands from the ground station. | ✓ | Presented in Section 4.5 and Section 5.3 | Test - send commands from ground station to vehicle |
| ALEC-SR-FV-PERF-03 | The flying vehicle shall have a cruise speed of at least 5 m/s. | ✓ | Presented in Section 4.9 and Section 6.6 | Demonstration - fly vehicle at maximum velocity and measure that speed |
| **ALEC-SR-FV-SUST-01 (key)** | The flying vehicle shall not emit any harmful gasses during operation. | ✓ | Presented in Section 6.5 | Analysis - analyse all emissions vehicle produces during operation |
| ALEC-SR-FV-SM-01 | The structure shall not deflect more than 10% under operational loads. | ✓ | Presented in Section 4.4 | Test - subject vehicle to operational loads and measure deflection |
| ALEC-SR-FV-SM-01-01 | The material used for the structure shall have a Young's Modulus of at least 70 MPa. | ✓ | Presented in Section 4.4 | Test - test Young's Modulus of material used for the vehicle structure |
| ALEC-SR-FV-AE-01 | The flying vehicle shall be able to produce a L/MTOW ratio of 2.0 at ISA sea level conditions. | ✓ | Presented in Section 4.9 and Section 6.6 | Test - add weight vehicle and test hovering ability |
| ALEC-SR-FV-PEP-01 | The flying vehicle shall be able to associate a measurement with a wind direction with a precision of $\pm \pi/180$ rad. | ~ | Presented in Section 4.5 but precision not covered in design | Test - compare measurements with true value |
| ALEC-SR-FV-PEP-02 | The flying vehicle shall be able to associate a measurement with a wind speed with a precision of ± 0.1 m/s. | ~ | Presented in Section 4.5 but precision not covered in design | Test - compare measurements with true value |
| ALEC-SR-FV-PEP-06 | The flying vehicle shall be able to measure the atmospheric temperature with a precision of ± 1 K. | ✓ | Presented in Section 4.8 | Test - compare measurements with true value |
| ALEC-SR-FV-PEP-07 | The flying vehicle shall note the atmospheric humidity with a precision of ± 1 %. | ✓ | Presented in Section 4.8 | Test - compare measurements with true value |
| ALEC-SR-FV-OPER-06 | The mission shall be operable up to 1500 meters from the ground station. | ✓ | Presented in Section 6.9 and 7.6 | Analysis - review mission operations |
| ALEC-SR-FV-CAS-06 | The flying vehicle shall be able to avoid obstacles of size greater than 25 cm^2. | ✓ | Presented in Section 4.6 | Test - obstruct path of vehicle with obstacles and observe reaction |

## 4.2. Air Quality and Emission Analysis

All conventional fossil-fuel-powered aircraft create emissions during their operation. The emissions divide into two main sections, primary and secondary. Primary emissions are those that are directly emitted by the aircraft, and secondary emissions are a result of those primary emissions that form over time.

Aircraft emit mostly $CO_2$ and $H_2O$, making up more than 99% of the total emissions in nominal conditions [9]. Furthermore, $NO_x$ is created as a result of nitrogen in the air reacting with oxygen at high temperatures and pressures inside an aircraft engine. $SO_x$ is created as a result of sulphur

presence in the aircraft fuel. Particulate matter, referred to as PM, is also emitted, in the form of soot, resulting from incomplete combustion. CO is emitted during low thrust operations, also associated with incomplete combustion. VOC are emitted throughout this process as well.

The secondary emissions are harder to track, as the primary emissions can react in very different ways depending on the exact state of the environment that they are emitted into. As such, only the most important will be covered here. Starting with $NO_x$ as primary, two major systems are present. First, the $NO_x$ - $O_3$ cycle, where in the presence of UV light $O_3$ is created, otherwise it is consumed. Second, the formation of particulate matter through precipitation of salts, formed through a complex process where $NO_x$ leads to $HNO_3{}^-$ aerosols, which then reacts to create a salt, depending on what it reacts with. Within this cycle, the $HNO_3{}^-$ in and of itself can cause acidic rain, and in high concentrations directly impacts health through destroying living tissue [10]. $SO_x$ system is similar to the second $NO_x$ system, where it forms an acid, $H_2SO_4$, which can either directly negatively impact health or the environment, or will form particulate matter. Both the $NO_x$ and $SO_x$ cycle are affected by atmospheric conditions, hence their effect will be different at aircraft cruise level and near sea level.

**Emission Impact on Local Environment and Health**

As mentioned earlier, the two main aviation emissions by volume, $H_2O$ and $CO_2$, have a considerable climate effect. The latter is a powerful greenhouse gas that has been linked with global warming, and the former has an even stronger effect when released into upper atmosphere. However, neither carries any direct impact on human health, not in the anthropogenic emission levels. Within the scope of the local environment, $CO_2$ even promotes plant growth, having a marginally positive impact.

According to the 2016 EPA assessment [11], exposure to high concentrations of $NO_x$, specifically $NO_2$, has been linked to asthma exacerbation, respiratory infections, and early respiratory morbidity, among others. $NO_x$ is also directly linked to the creation of $O_3$, which is linked to both respiratory and metabolic health issues, reports EPA [12]. According to the same report, millions of Americans are currently living in areas where $O_3$ levels exceed air quality standards. Associated with the $NO_x$ creation of $O_3$ are VOCs, also emitted by aircraft engines. The CO emissions are likely to contribute to cardiovascular morbidity and have been linked to respiratory morbidity, however only in high concentrations [13]. It is nonetheless important to monitor the levels, since low-thrust operations, like some landing operations, or taxiing, produce significant levels of CO. The $SO_x$ emissions, on the other hand, have been proven to have a negative impact on human respiratory system in case of short term exposure. In terms of long term exposure at lower concentrations, research suggests a similar impact [14].

For both the $NO_x$ and $SO_x$, a wide range of secondary emissions is created. The acids formed by both emissions, $HNO_3{}^-$ and $H_2SO_4$, stay in the atmosphere in the form of acidic aerosol that can lead to acidic smog [10]. The smog then causes significant respiratory issues, and in higher altitudes can lead to acid rain. Furthermore, both acids can further react to create $PM_{2.5}$.

This $PM_{2.5}$, which is partly a result of $NO_x$ and $SO_x$ emissions, and partly a directly emitted pollutant, is one of the most problematic of the aforementioned substances. It is specified as particulate matter with diameter less than 2.5 µm. In terms of short-term exposure, it has been linked to issues with the respiratory system and the cardiovascular system. For long-term exposure, respiratory, cardiovascular, nervous, and metabolic, and it is linked to causing cancer [15]. Aviation also creates different particulate matter, both larger diameter $PM_{10}$, and ultra-fine-particles (UFP), also labeled $PM_{0.1}$. The impact of UFP in particular is a current subject of many studies, but the results on its health impacts are not yet exactly clear. It is however linked to many of the same problems associated with $PM_{2.5}$.

### Measuring Air Pollution

To measure air pollution, many techniques are available. First, a distinction is made between particulate matter, which is most often measured using optical methods, and gasses, that can be measured using chemical methods. For the application within the proposed system, only portable solutions are acceptable, which disqualifies most common and reliable methods such as gas chromatography - mass spectrometry (GCMS), or using heavy multi-gas analysers. Still, to map out every single possible method would be too extensive for this report, hence this section will focus on a few main types of sensors that can be used by the system.

For particulate matter, the general principle is to have a stable airflow in which the particles are then counted. For $PM_{2.5}$ and coarser material, this can be done using optical particle counters that use lasers to count the particles. For finer particulate matter, such as UFP, condensation particle counters (CPC) can be used, where the particulate matter is first enlarged in diameter by using the particles as nuclei for vapour droplet formation [1]. However, CPCs are quite large, heavy, and expensive, compared to their simpler, less sensitive counterparts.

For gasses, many options are available. First are electrochemical sensors. In these sensors, an electrode is used as a transducer, as the target gas is oxidised or reduced, producing measurable current [16]. Electrochemical sensors can be very light, as little as a few grams [2]. Another option are metal oxide (MOX) sensors (also sometimes referred to as metal oxide semiconductor = MOS). These sensors perform similarly to their electrochemical counterparts, and can be even further miniaturised. There are multiple options of measuring gasses with infrared image sensors and infrared point sensors which allow detection and location of gasses without being in direct contact, even at considerable distances of dozens to hundreds of meters [3]. However, these systems are only capable of detecting a limited amount of gasses, and are often heavy.

### Gas Sensor Parameters

Each gas sensor is suited to a slightly different detection environment, which is reflected in its parameters. Each sensor is limited to a certain range of concentrations, temperature, and humidity, but those are rather self-explanatory. In this section, the more complex parameters of interest are explained, and associated desirable values proposed.

Cross-sensitivity is one of the most crucial parameters of a gas sensor. It reflects how sensitive a sensor is to substances other than the target gas. In some cases, this cross-sensitivity can be higher than 100% of the target gas [4], or can be purposefully set at 100% as to create a sensor equally sensitive to multiple gases. For the purposes of researching the precise levels of gasses in the atmosphere, cross-sensitivity is not desirable.

Response time, often given as $t_{90}$ or $t_{50}$, is a measure of how quickly a sensor responds to a step change in concentration of the target gas. It is given in terms of $t_n$ seconds that the sensor takes to approach within n% of the change. For mobile systems and environments with rapidly changing concentration, a low response time is desirable, such that the quick changes are recorded by the sensor. Values less than 60 s are found acceptable by the EPA [17], however even lower values are preferred.

Linearity is a measure of how the sensor reacts to a change in concentration at that given concentration. For a fully linear response, the sensor response for a given change will be the same at any concentration level. Not so for a non-linear response, e.g. a sensor returns 20 $[\frac{\text{nA}}{\text{ppm}}]$ at 20 [ppm],

[1] http://www.cas.manchester.ac.uk/restools/instruments/aerosol/cpc/ [Cited 12 June 2022]
[2] https://www.alphasense.com/wp-content/uploads/2017/01/COAX.pdf [Cited 12 June 2022]
[3] http://www.rmi.cz/sigis-2 [Cited 12 June 2022]
[4] https://www.alphasense.com/wp-content/uploads/2021/05/NH3-B1.pdf [Cited 12 June 2022]

and 25 [$\frac{nA}{ppm}$] at 50 [ppm]. Such a sensor would not be ideal for applications where the concentration varies a lot over the measurement period. As such, a linear response is desirable.

**Target Gas Selection**

The ALEC system will use gas and particle sensors to measure local concentrations of gasses and particulate matter to establish the local air quality. For this purpose, it will observe the main pollutants attributable to aviation, which have a direct impact on human health or a direct impact on the environment on the local level. As such, $CO_2$ and $H_2O$ are not going to be measured, as their health impact on the local community is second to none. $NO_x$ will be measured, both in the form of NO and $NO_2$ to provide as much information as possible on the behaviour of $NO_x$ around aviation. $SO_x$ will be measured, though only $SO_2$, as $SO_4$ is much less present in the emission, and can be computed from the level of $SO_2$. The CO will be measured, as it can be attributed to specific operations, based on the engine thrust, and it can then help provide insight into the other emissions present with that specific engine setting. The $O_3$ will be measured, since it is crucial to the behaviour of the $NO_x$ - $O_3$ system and in and of itself is harmful. VOCs, also part of the system, will also be measured. Particulate matter will also be measured, given its undeniable negative impact on human health. Specifically, $PM_{2.5}$ will be measured. UFP was also considered, however the instrumentation necessary for its measurement is too heavy and expensive for the system.

## 4.3. Payload Design

In this section, the payload design is elaborated upon. In Subsection 4.3.1 the sensor selection is performed and reported. Subsection 4.3.2 details the integration of the sensors in the drone payload, so that optimal measuring conditions are created.

### 4.3.1. Sensor Selection

Following the identification of the substances of interest in Section 4.2, appropriate sensors have to be selected. This section will explain the selection and the mitigation of the limitations of the selected sensors.

**Sensor Trade-Off**

It was decided to measure the following substances: $PM_{2.5}$, VOC, CO, NO, $NO_2$, $SO_2$, $O_3$. As such, a sensor was selected for each target gas. The process of selection was divided into three parts. First, a large database of available sensors relevant to the target gases was compiled based on data from multiple companies (Alphasense, Honeywell/CityTech, Figaro, Winsen, and Flir). Second, the properties of each sensor were investigated and listed in the database. Third, based on the database, a trade-off was performed. Within the trade-off, first the unsuitable sensors were identified, using the criteria of operating temperature, humidity ranges, cost, and mass (single sensors with a price in the thousands of EUR or heavier than a kilogram were not considered). The final trade-off criteria in a decreasing order of importance were cross-sensitivity, reaction time ($t_{90}$), sensitivity, accuracy (linearity, zero and full scale error), and mass.

As a result of this selection process, the following sensors were chosen. Most sensors are electrochemical, with the exception of an MOX sensor for VOC, and an optical sensor for $PM_{2.5}$.

- **VOC**: Winsen MQ138
- **CO**: Alphasense CO-CX
- **NO**: Alphasense NO-B4
- **$NO_2$**: Alphasense NO2-AE
- **$O_3$**: Alphasense O3-AH
- **$SO_2$**: Alphasense SO2-A4
- **$PM_{2.5}$**: Alphasense OPC-R2

An important limitation of the electrochemical sensors to address is cross-sensitivity. Most sensors were chosen such that their cross-sensitivity to other gasses of interest and gasses that are normally present in the measuring environment is minimal. However, the $NO_2$ and $O_3$ sensors exhibit 100%

cross sensitivity to both gasses. According to research [18], using an $MnO_2$/PTFE powder filter on one of the sensors allows for the measurement of $NO_2$ without $O_3$ interference, and then by simple subtraction the correct value for $O_3$ can be found from the other sensor.

### 4.3.2. Sensor Integration

The sensors that were selected in the previous chapter only function optimally in very specific conditions. In this subsection, a payload layout is designed such that these conditions are met.

#### Sensor Support Circuitry

The electrochemical sensors themselves do not produce usable data. Instead, when in a circuit with a certain resistance and power source, they will create changes in the current in the circuit based on the exposure to a target gas. As such, a support circuit into which the sensor is placed is needed. For the alphasense electrochemical sensors, the ISB Individual Sensor Board supplied by the same manufacturer is used [5]. For the Winsen VOC sensor a custom circuit board will be made according to the information provided in the sensor specifications [6]. The optical sensor already provides a digital output, hence it does not require a support circuit.

#### Sensor Airflow Subsystem

For the sensors to measure optimally, a method of transport for the sampled air must be ensured, such that they are exposed to the most current concentration of the substances of interest and can react reliably. Otherwise, it is impossible to ensure that the air inside the sensor chamber hasn't stayed there since the beginning of the mission, and the data could not be reliably associated with current concentrations. According to the application notes provided by the sensor manufacturer [7], the flow around the sensors for best measurement must be parallel to their surface, while not laminar, to allow for diffusion.

It is also desirable to minimise pressure changes around the sensor, providing sufficient spacing between the inlet, the sensors, and the system creating the pressure difference to drive the airflow. A system was designed, in the form of a channel, to provide such environment. The sensors are located in a crown-like configuration around this channel. At the inlet on the top of the channel, guide vanes are used to angle the flow to graze the sensor surface. At the bottom, a fan drives the air through the channel. The air exiting the channel is distributed throughout the drone to cool the electronics and batteries, leaving the drone through one of the many openings in the structure. The placement of the payload is specific to the air disturbance pattern created by the propellers of a quadcopter. From simulation it has been shown that at the center of the body of a quadcopter, a quasi-stagnation is formed, where the disturbance is minimal. It is also lower with increasing vertical distance from the propeller level [19, 20].

The payload is placed such that it is centered on the drone, extending above the propellers. The distance between the sensors and the fan was designed to be equal to the diameter of the tube. While ideally the distance would be considerably larger, up to ten times the diameter, the vertical size of the payload was strongly limited by the constraints of the drone. Most specifically, the flight controller and landing camera have to be placed in the center of the drone, same as the payload, hence the tube cannot lead through the entire drone. A cross section of the subsystem is shown in Figure 4.1, and a rendering in Figure 4.2. Humidity and temperature sensors are mounted in the inlet to allow for measurement correction.

[5] https://www.alphasense.com/wp-content/uploads/2019/10/ISB.pdf [Cited 08 June 2022]
[6] https://www.winsen-sensor.com/d/files/mq138-(ver1_6)---manual.pdf [Cited 08 June 2022]
[7] https://www.alphasense.com/wp-content/uploads/2013/07/AAN_010.pdf [Cited 09 June 2022]

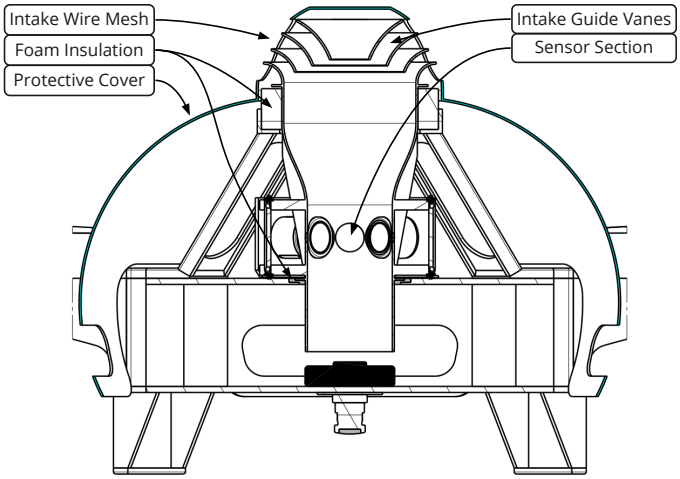


**Figure 4.1:** *Section view of ALEC emission drone*

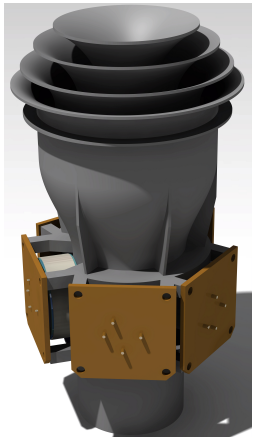

**Figure 4.2:** *Rendering of the channel with all sensors and sensor boards attached*

**Vehicle Integration**

The sensor assembly with the channel is fairly large for a drone. With an initial height of over 200 mm, it drove the design of the drone to an unacceptable extent. Through iteration, the height of 163 mm was achieved, which was deemed acceptable. The drone structure is conventional, with a top and bottom plate between which the drone arms are affixed. The top plate, however, has a large circular opening in which the sensor assembly is placed, set on a foam ring to insulate the system from vibration. The assembly extends more than 100 mm above the top plate, hence a supporting structure was added to fix it at the top, also equipped with a foam ring for insulation. To protect the system, a cover made out of HDPE is placed over it, and a wire mesh protects the intake from debris.

## 4.4. Structure & Materials

In Subsection 4.4.1, the main structure of the drone is explained. This is followed by an explanation on the material choice for the main structure in Subsection 4.4.2.

### 4.4.1. Design

The structure needs to comply with the requirements to protect the payload and withstand the load experienced during the mission. Furthermore, the structure needs to serve the payload by providing it with ideal positions to make accurate measurements. Therefore, the optimization for the position of the payload was the priority for the design to have the most ideal results. The most important payload for optimum results are the sensors. As the sensors need laminar flow to function ideally, a channel that would laminarise the flow was created as explained in Section 4.3. This tube is located in the center of the drone and laminarises the flow using a fan located at the end of the tube. This fan[8] will also be used to cool the flight controller down which is located exactly below it. The drone will be held together by the drone frame which will carry the load during the mission.

The drone frame will consist of detachable arms, the supporting structure, and the landing gear. For the detachable arms, of the drone, mainly two designs were considered. First, a hollow tube with a threaded end that would be easily detachable was considered. The second option considered was the channel beam type which would be much thinner towards the end where the motors and propellers are attached. Furthermore, it can be easily detached by sliding it in and out, and it is held in place using two screws. In the end, the later option was chosen as it would be more lightweight, and it would also be more easily manufactured. The drone also requires a strong land-

[8] https://www.amazon.com/GDSTIME-60mm-Bearings-Brushless-Cooling/dp/B07THX713H [cited 20 June 2022]

ing gear that would be able to withstand the impact caused during landing. For that four landing legs were chosen which were attached directly to the center part of the drone frame. These landing legs are lightweight and would provide some clearance with the ground. This design was chosen as there is no payload on the bottom of the drone.

In addition to a drone frame, a cover is needed to protect the payload during rainy weather conditions, for instance. This cover will be attached to the drone frame. Similar to the aerodynamic tube, it will not carry any loads. During operation, the fan attached at the bottom of the aerodynamic tube will be used to suck air in. When it starts raining, the fan will be turned off to make sure that no water enters the sensors.

### 4.4.2. Materials

For each part, a material had to be chosen that can be manufactured as required. First of all, a smooth lightweight material for the aerodynamic tube such that it does not create any turbulent flow was desired. An important requirement is that the material is lightweight, and it does not have to carry any load. Therefore, only polymers have been considered. Furthermore, a driving requirement is that the drone is sustainable. Therefore, only recyclable polymers that can be recycled at the end of life will be considered.

For the aerodynamic tube the following materials were considered: Nylon, Polyethylene (PE), Polypropylene, Polyurethane, PVC, and Polystyrene. These materials were considered as they can be manufactured in the required shape. However, it was concluded that all materials have similar properties and won't significantly affect the weight or the cost of the drone. However, the materials differ in sustainability, and thus, the most sustainable polymer, polyethylene, was chosen. It is the most recyclable polymer currently available. [9] The two types of polyethylene that can be used are HDPE (High-Density Polyethylene) and PET (Polyethylene Terephthalate). PET has a texture similar to glass and is transparent. On the other hand, HDPE is more crack resistance and has more strength. [10] Therefore, HDPE was chosen. The drone cover has very similar requirements as the aerodynamic tube as mentioned earlier. Thus, for the drone cover, HDPE will also be used.

Finally, for the drone frame, several materials have been considered. From the design options tree in the baseline report [21], it was concluded that a trade-off would be required between the aluminum alloys, carbon-fiber-reinforced polymers (CFRPs), chopped CFRPs, and polymers. The trade-off for the material of the drone frame is presented in Table 4.3, where the same scores and weighting system is used as in the Midterm report Section 2.4.

**Table 4.3:** *Trade-off table for the drone-frame material*

| **Materials** | **Sustainbility** | **Weight** | **Specific Strength** | **Cost** | **Manufacturing Complexity** | **Total score** |
|---|---|---|---|---|---|---|
| Aluminum Alloys | 4 (Green) | 2 (Orange) | 3 (Blue) | 3 (Blue) | 4 (Green) | **3.16** |
| CFRPs | 2 (Orange) | 4 (Green) | 4 (Green) | 2 (Orange) | 2 (Orange) | **2.84** |
| Chopped CFRPs | 3 (Blue) | 4 (Green) | 3 (Blue) | 3 (Blue) | 3 (Blue) | **3.26** |
| Polymers | 2 (Orange) | 3 (Blue) | 2 (Orange) | 4 (Green) | 3 (Blue) | **2.74** |
| Weighting Factor 1-5 | 5 | 5 | 3 | 3 | 3 | |

The scores in Table 4.3 are based on the material properties and are, therefore, very accurate. As can

[9] https://www-tc.pbs.org/strangedays/pdf/StrangeDaysSmartPlasticsGuide.pdf [cited 07 June 2022]
[10] https://silverspurcorp.com/hdpe-vs-pet-plastic-bottles/ [cited 07 June 2022]

be seen, the aluminum alloys and chopped CFRPs both provide reasonable solutions. However, as a more lightweight structure is required, it was decided to use the chopped carbon fibre reinforced polymers. It was aimed to use a completely recyclable material, and therefore, the CF15, which is a carbon reinforced reinforced nylon which can be completely recycled was chosen[11].

## 4.5. Command and Data Handling

The communications of an emissions drone with the ground station is important both to transmit measured data to the ground station and to get control inputs/flight plans. There are multiple directions of communicating: 1) from the ground station to the drone and vice versa, 2) from the drone to the server and vice versa 3) from air traffic control to the ground station and vice versa. The relations between the other elements of the control sub-system and other subsystems can be seen in Appendix C and it is noted that the control sub-system for the noise drone is similar. The Bayesian optimisation routines running on the ground station processors proposes a new location, and path planning routines are sending the information about the flight path to the on-board processor and controller. From here, data is sent to the Take off and landing sequence routines and to the flight controller software, via the path following functions, and to the emergency operations. Additional input is provided by the visual data sensors and used by the obstacle detection and landing and take-off sequence. LTO sequence, flight controller, emergency operations and obstacle detection send their commands to the propellers command routines.

### 4.5.1. Emission Flight Control Command and Data Handling

The flight plans and control inputs are sent by the ground station and received by the emissions drone using the Pixhawk 4 flight controller. The software use for the autopilot is "Ardupilot" due to its wide usage and compatibility with the used hardware. Ardupilot's mission planner is a software which computes the path of the drone such that it follows a pre-defined flight path. Telemetry radio can receive commands to change the flight path, which is used as the drones receive the next sampling location, as computed by the algorithm explained in Chapter 9. Moreover, Ardupilot is capable of performing sense&avoid maneuvers, both for airborne vehicles and object avoidance. The flight controller receives data from the telemetry radio and the Raspberry Pi - which receives data from the autonomous flight code, and sends commands to the electronic speed controller (ESC) which acts on the propellers in order to maneuver the drone. Moreover, Pixhawk flight controller relies on data provided by its sensors, namely its accelerometer, gyroscope, magnetometer and barometer. air traffic control (ATC) has the possibility to abort the mission at any moment due to safety reasons. ATC is able to send an 'Abort Mission' command to the drone. This is also valid for the noise drone.

### 4.5.2. Emission Sensor Data Handling

First thing to mention is that the second row of the sensor data handling diagram Figure 4.3 is identical to the data handling of the microphone data handling of the noise drone and ground level sensors (GLS). The description from the processor block onwards (last block of first row of Figure 4.3) is the same for all three systems so will only be described in this chapter. As described in Subsection 4.3.2, not all sensors produce an immediately usable signal. The signal is converted from analog to digital by sensor boards for these sensors. The board feeds that digital signal in a Arduino processor. The Arduino processor is also responsible for encryption of the data. After processing, the data is stored on local storage on a SD-card. This SD-card should be sized according to the quality of the cellular network in the area of interest. In the most extreme case of no cellular reception, the local storage will be used to collect all the data. Using only local storage means that an operator would need to manually switch the SD-cards when the capacity limits are reached. When a network is present, 3G or 4G will be used to send data to a remote File Transfer Protocol (FTP) server, and

[11] https://shop.fillamentum.com/products/nylon-cf15-carbon [cited 07 June 2022]

the local storage will be only used as a buffer. When the FTP server receives the data correctly, it will confirm this back to the emission drone and the correctly received file will be deleted on the local storage. In the case of a corrupted message or a transmission link failure, the files on the local storage will not be deleted. The files that had not been received correctly are stored on the local storage and the transmission is retried at a later point in time. The relation of the emissions data in the overall system can be seen in Appendix C. The raw pollution data is collected, filtered and then stored and transmitted to the ground station to be used for the ultimate outputs of the system. The humidity and temperature is obtained from the DHT22 sensor [12], and the wind direction and speed is obtained from the internal stabilization speed of the emission drones [22]. A schematic of the data handling is given in Figure 4.3.

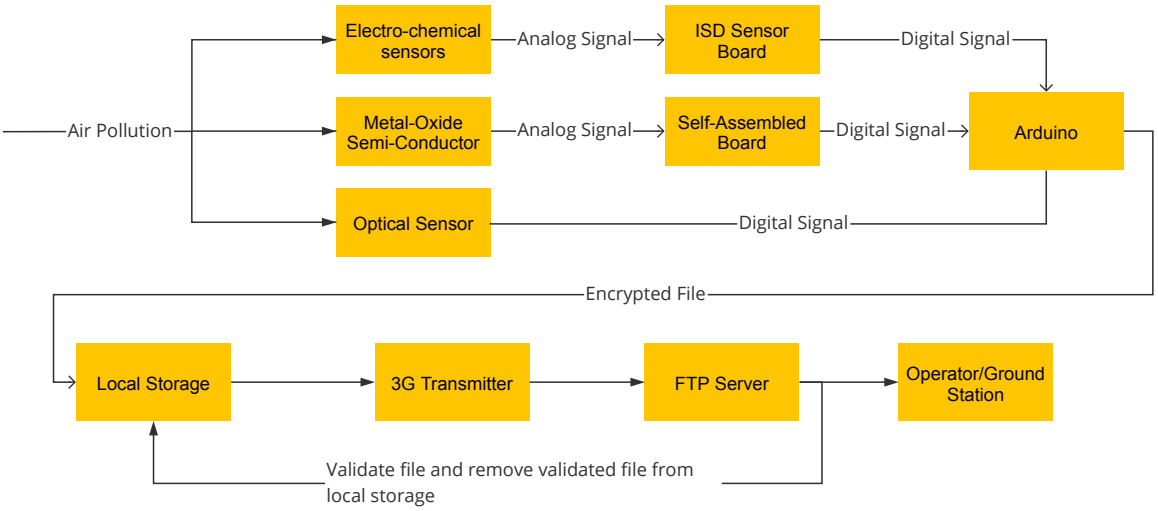


**Figure 4.3:** *Emission internal data infrastructure block diagram*

## 4.6. Autonomous Design

In order to comply with mission requirement **ALEC-UR-AUT-01**, the drones should have autonomous capabilities. The elements of interest for the autonomy of the system are the autonomous takeoff and landing, collision avoidance, path planning, and selection of sampling locations for the measurements, which are further described in the current section. Overall, the autonomy requirements are met by using Ardupilot, which is software that is able to perform sense&avoid, autonomous landing and path following maneuvers, in combination with the sampling algorithm described in Chapter 9. The choice for Ardupilot is because of its good reliability as it is a highly tested and proven concept.

### 4.6.1. Collision Avoidance

Autonomous flight in airports can be dangerous with temporary and moving obstacles close to the ground. To improve the safety of the system, sense and avoid technology should be included aboard. The focus for sense&avoid is on the front-facing part of the drone such that during the moving flight, the UAV is capable of analysing obstacles in front of itself and avoiding them. While the system is in hover mode, it is expected that it is unlikely for other objects, especially birds, to crash into it as the drone is relatively large and noisy. The three options for cameras are: single camera, double cameras, and depth cameras. Problem with single camera is that it is difficult to determine distance to object although it is possible. However, due to the greater safety required it would be better to

[12] https://www.adafruit.com/product/385 [Cited 20 June 2022]

include an optical subsystem capable of more quickly and accurately determining distance. Double cameras are feasible using stereo vision to determine distance from object. The drawback of the double camera is the computationally expensive image processing which would need to be computed on the Arduino/Raspberry Pi processor which has limited capabilities. Depth cameras have better performance as they are able to compute distances without using large amounts of computational power. The depth camera DOMINANCE: Drone Mine Obstacle Avoidance D435 intel [13] was chosen. As explained in Section 4.5, the software used for collision avoidance is Ardupilot.

### 4.6.2. Autonomous Take-Off and Landing

Using the aforementioned available hardware, the approach for autonomous landing and take-off takes two steps: symbol detection and landing. Firstly, the landing pads have a symbol with high color contrasts printed on them, e.g. [23] uses an *H*-shaped symbol. The Longruner LC20 wide angle Raspberry Pi camera [14] collects the image, and subsequently image pre-processing techniques are employed, namely gray scaling and the image's binarisation through a simple threshold method, as explained by [24], based on a Gaussian filter. The overall algorithm is run by Ardupilot.

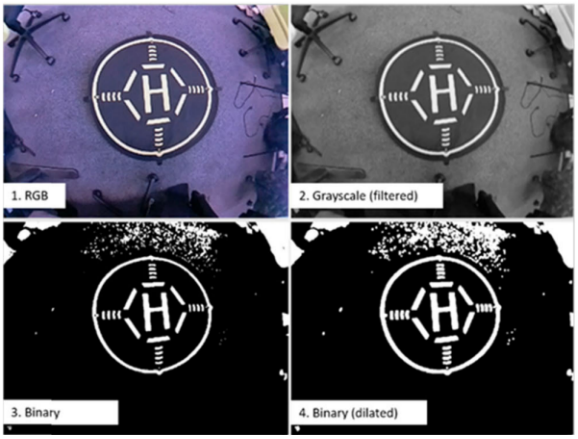


**Figure 4.4:** *Landing pad, as well as the image processing techniques [23]*

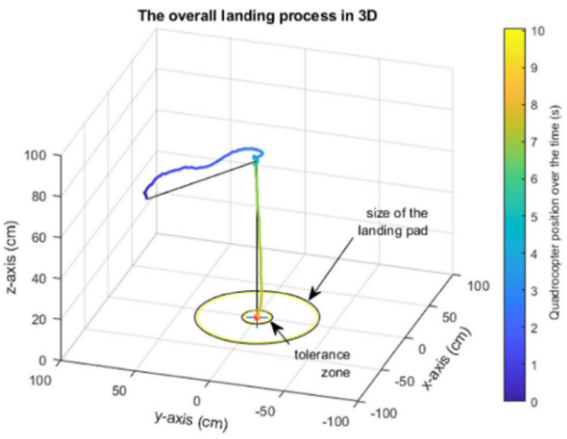


**Figure 4.5:** *Landing process visualisation [23]*

The second step concerns with the actual landing. After detecting the landing symbol as previously described, the drone flies towards it while keeping its height constant. In order to activate the second sub-step, it must be above the landing coordinates within a predefined tolerance, approximately 10 cm in radius for several seconds, needed in order to avoid overshooting or transient effects. The target height is set at −3 cm under the ground, in order to tackle the possible ground camera. The second step of the landing process can be visualised in Figure 4.5.

**Table 4.4:** *Optical subsystem of drones*

| Name Component | Mass (g) | Cost (Eu) | Volume [mm] |
|---|---|---|---|
| Intel RealSense Depth Camera D435[13] | 72 | 273.55 | 25x25x90 |
| Longruner LC20 [14] | 18 | 19.32 | 114x64x20 |

### 4.6.3. Path Finding

Autonomous flight implies that the drones have to fly from the ground station to the sampling points and back without human intervention. This feat is achieved using the Ardupilot's mission planner,

[13] https://www.dateks.lv/en/cenas/videokameras/305976-intel-intel-realsense-depth-camera-d435 [1 June 2022]
[14] https://www.amazon.de/-/en/Raspberry-Fisheye-Longruner-Adjustable-LC20/dp/B074W6TPHF [1 June 2022]

which is able to set a flight path to the drones. The flight path is computed by the location sampling algorithm in the ground station, which is described in Chapter 9, and subsequently the flight commands are transmitted to the drones.

### 4.6.4. Autonomous Wind Stabilization

An important reason why Ardupilot was chosen as the software for the drones is its ability to provide stability in heavy wind conditions. Due to the Beaufort 4 wind requirement, the drone should remain stable and maintain the ability to take measurements. According to documentation on Ardupilot, the software can estimate the wind velocity experienceed quite accurately[15]. Because Ardupilot is a heavily trusted software it is assumed that the wind condition requirement is met if the drone can provide the necessary velocity to counter it.

## 4.7. Drone Regulations

All the drones and their accompanying missions should adhere to the regulations of regulatory bodies such as, the EASA, the airport, and the air traffic control. Firstly, a look will be taken at the requirements of EASA to have the drones and the operations authorized. There are 3 categories under which civil drones can fall [16].

- The **open** category, is meant for low-risk recreational use and anyone is allowed to fly an open category drone.
- The **specific** category, for riskier drone operations, where the safety is assured by an operator. An example of drones falling under the specific category, are the drones operational at the port of Rotterdam [17] which were taken as an example of the feasibility of the deployment of the ALEC system.
- The **certified** category, for high risk operations. This category is for very special UAV operations and examples provided are an autonomous A320 transporting cargo from Paris to New York or 'dangerous' drone operations such as autonomous package deliveries in residential areas.

The aim of the design is to have the drone be authorized under the **specific** category as the requirements for the certified category are much more difficult to adhere to. Most of the requirements for the specific category, on the other hand, can be adhered to rather easily. Such as UAS.SPEC.020 (1)(iii) [18] that states that the drone shall not be larger than 1 meter due to the 'beyond visual line of sight' requirement. However, there is also a part of the approval regarding the operations performed with the drone. The information provided is quite limited and it essentially states "Before starting an Unmanned Aerial System (UAS) operation in the 'specific' category the UAS operator shall obtain an operational authorisation from the national competent authority of the Member State of registration"[18]. This could prove to be a bottleneck in getting approved for the specific category rather than the certified category, because the drones would be flying around 50 meters from the airport. For EASA regulations nothing has been found on flying at an airport, but there are cases of Luchtverkeersleiding Nederland (LVNL or Air Traffic Control Netherlands) flying drones over Rotterdam airport for runway inspection [19]. However, this test case was executed with a lot of preparation and training of the pilot in order to have a safe flight. Therefore, one of the first things to do when the design phase is nearly done is applying for authorisation to determine the required certification.

Continuing on the example of the drone flying at Rotterdam airport, the LVNL was highly involved

[15] https://ardupilot.org/copter/docs/airspeed-estimation.html[Cited 20 June 2022]
[16] https://www.easa.europa.eu/domains/civil-drones[Cited 13 June 2022]
[17] https://www.portofrotterdam.com/nl/haven-van-de-toekomst/innovatie/drones[Cited 13 June 2022]
[18] https://eur-lex.europa.eu/legal-content/EN/TXT/PDF/?uri=CELEX:32020R0639&from=EN [Cited 13 June 2022]
[19] www.dutchdronedelta.nl[Cited 13 June 2022]

in the process. When executing the mission of the drones, the regulatory bodies for air traffic control (ATC), such as the LVNL, will be updated frequently and will have access to the location of the drone at any time. If desired by the air traffic control, control over the drone should also be provided to kill the operations of the drone if deemed necessary by ATC.

The final entity that needs to be discussed is the airport. Due to the location of operations, the mission will need to be explained and approved by the governing body of the airport. Without this approval the mission can not take place even if all other regulatory bodies agree. For this reason, an in-depth safety and risk analysis plan should be presented, in addition to the mission profile. Furthermore, there are frequencies used for supporting the aviation on the airport [20] [21], these should not be used to prevent interfering with the airport operations.

## 4.8. Budgets

As the payload and materials are chosen, it is possible to create detailed mass, financial, and power budget. Therefore, in this section, first the mass and financial budgets are presented in Subsection 4.8.1. Afterwards, the power budget is presented in Subsection 4.8.2.

### 4.8.1. Mass & Financial Budgets

To create detailed mass and financial budgets, all the components have been listed. Afterwards, the mass and cost of each component was researched and presented in Table 4.5.

**Table 4.5:** *Mass & financial budgets for the emission drone*

| Component | Financial | Mass | Component | Financial | Mass |
|---|---|---|---|---|---|
| Sensors | €770.00 | 144.00 g | Obstacle Avoidance | €292.87 | 90.00 g |
| Cover & channel | €0.15 | 150.45 g | Raspberry Pi 3B | €33.01 | 42.00 g |
| Main Structure | €67.24 | 750.00 g | channel Fan | €3.30 | 68.00 g |
| Motors & Esc | €315.56 | 440.00 g | SiK Telemetry Radio V3 | €52.30 | 50.00 g |
| Propellers | €28.26 | 180.30 g | Wiring + Redundancy | €50.00 | 50.00 g |
| Flight Controllers & GPS | €177.27 | 81.00 g | 3x SD Card 64 GB | €24.77 | 6.00 g |
| Arduino | €17.36 | 25.00 g | Huawei E3372H-320 | €41.32 | 50.00 g |
| 2x Battery | €137.65 | 908.00 g | DHT22 | €4.92 | 6.00 g |
| | | | **Total per drone** | **€2,015.97** | **3040.75 g** |

### 4.8.2. Power Budget

In this section the power budget is elaborated on. The power budget was calculated for two different states of an emission drone. The first is while taking measurements and the second is when the drone is not measuring. For both states the power was calculated for hovering. This was done to be able to make a fair comparison and to be able to see the effect of the differences. The power budgets can be found in Table 4.6. The values are obtained from data provided by the component manufacturers, or measurements done by independent researchers. Either the power was provided directly, or the voltage and current were provided, which are then multiplied with each other to obtain the power. When the drone is not measuring, all the sensors will draw no power, and the Huawei cellular internet dongle will be turned off. The processor related to measurements will also run idle. How the voltage and current of the motor were obtained is elaborated on in Chapter 6. It is

[20] https://www.faa.gov/about/office_org/headquarters_offices/ato/service_units/techops/safety_ops_support/spec_management/engineering_office/rfb.cfm[Cited 14 June 2022]

[21] https://833radio.com/about[Cited 14 June 2022]

seen that the measuring has a very small impact on the power usage, as most power is used by the motors.

**Table 4.6:** *Power budget for hovering for three different cases*

| | | Power at hovering | | | |
|---|---|---|---|---|---|
| | | During measuring | | While not measuring | |
| | | [Watt] | % of total power | [Watt] | % of total power |
| **Payload** [22] [23] [24] *sc = support circuit | CO-CX | 0.00975 | 0.00331 | 0 | 0 |
| | NO-B4 | 0.00975 | 0.00331 | 0 | 0 |
| | SO2-A4 | 0.00975 | 0.00331 | 0 | 0 |
| | O3-AH | 0.00975 | 0.00331 | 0 | 0 |
| | OPC-R2 | 0.55 | 0.19 | 0 | 0 |
| | NO2-AE | 0.00975 | 0.00331 | 0 | 0 |
| | MQ138 | 0.00975 | 0.00331 | 0 | 0 |
| | channel fan | 1.68 | 0.571 | 1.68 | 0.580 |
| **Motors** | | 279.17 | 94.89 | 279.17 | 96.31 |
| **Raspberry Pi** [25] | | 2.4 | 0.82 | 2.4 | 0.83 |
| **Arduino** [26] | | 1.1 | 0.37 | 0.4 | 0.14 |
| **Huawei E3372** [27] | | 2.5 | 0.85 | 0 | 0 |
| **Pixhawk 3B** | | 2.1 | 0.71 | 1.58 | 0.54 |
| **Obstacle Avoidance** [28] [29] [30] | Intel camera | 3.403 | 1.157 | 3.403 | 1.174 |
| | Raspberry Pi camera | 1.25 | 0.425 | 1.25 | 0.431 |
| **Total** | | **294.2** | 100 | **289.9** | 100 |

The wind tunnel fan is included in the payload, since it regulates the flow over the sensor, but it is also used for cooling purposes. For this reason it is not turned of when no measurements are being taken.

The Pixhawk 3B flight controller in this table includes a GPS module, a transceiver and other modules. The GPS module does not need to be used when the operator is using camera footage to fly the drone.

To calculate whether the battery capacity of 10000 $mAh$ is sufficient the power required for hovering during measuring is used. 294.2 Watts for a flight time of 25 minutes means 8283 $mAh$ is required. This means 83 percent of the battery capacity is used. Quan Quan [25, p. 80] advises to use a value between fifteen and twenty percent for the minimum battery capacity, which is the unused capacity during operations. In this case the value for the minimum battery capacity is seventeen percent, which means the battery capacity is viable. The electric block diagram is included in Figure 4.6.

[22] https://www.alphasense.com/wp-content/uploads/2019/10/ISB.pdf [Cited 10 June 2022]
[23] https://www.alphasense.com/products/optical-particle-counter/ [Cited 10 June 2022]
[24] https://www.allekabels.nl/koeler/214/1085668/koeler-60-x-60-mm.html?[Cited 10 June 2022]
[25] https://www.pidramble.com/wiki/benchmarks/power-consumption [15 June 2022]
[26] https://www.researchgate.net/publication/327132935_A_practical_microwatt-meter_for_electrical_energy_measurement_in_programmable_devices[Cited 10 June 2022]
[27] https://www.handleidi.ng/huawei/e3372/handleiding?p=10 [Cited 15 June 2022]
[28] https://www.intel.com/content/dam/support/us/en/documents/emerging-technologies/intel-realsense-technology/Intel-RealSense-D400-Series-Datasheet.pdf[Cited 10 June 2022]
[29] https://www.amazon.de/-/en/Raspberry-Fisheye-Longruner-Adjustable-LC20/dp/B074W6TPHF[Cited 10 June 2022]
[30] https://www.raspberrypi.com/documentation/accessories/camera.html[Cited 10 June 2022]

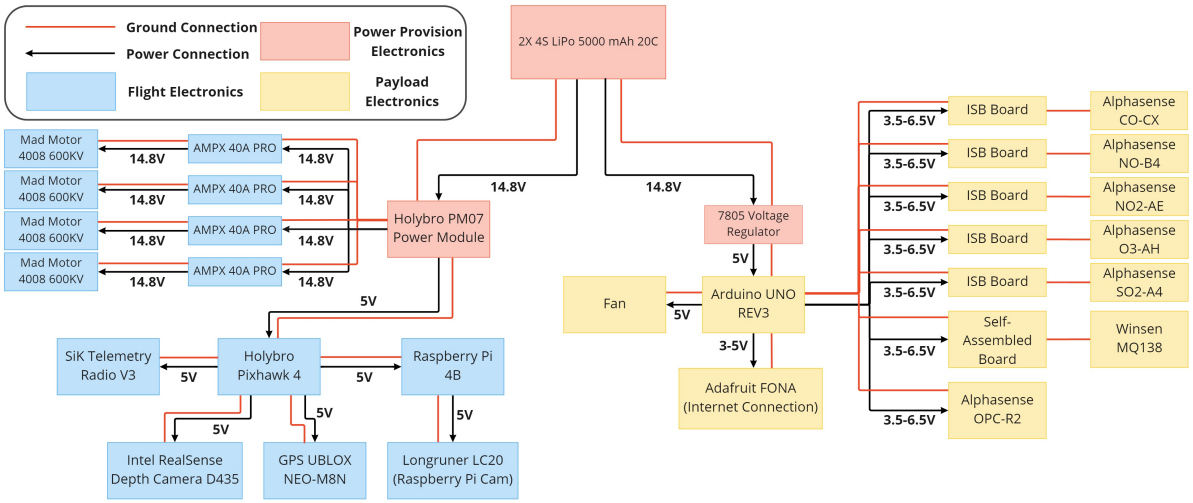


**Figure 4.6:** *Electrical block diagram of the emissions drone*

## 4.9. Performance Analysis

This section is concerned with the performance analysis of the emissions drones. It will start by discussing the maximum hovering time in Subsection 4.9.1. Thereafter, it will provide the maximum velocity and maximum take-off altitude in Subsection 4.9.2 and Subsection 4.9.3, respectively.

### 4.9.1. Maximum hovering time

The maximum hovering time was set to be 25 min. The battery was sized accordingly. A longer hovering time would require a battery with a larger capacity. Requirement **ALEC-FVSR-ED-PERF-01** states that the emission drone shall have an operational time of at least 20 minutes. Horizontal flight requires less power than hovering. However, taking off requires more power than hovering. Also, a small percentage of the electrical energy stored in the battery is used by other components than the propulsion system, such as the sensors and flight controller. Hence, the emissions drone has been designed such that it has 5 min of redundancy. This 25 min of hovering time is achieved by using a battery with a capacity of 10 000 mAh. The calculations for this can be found in Section 6.5.

### 4.9.2. Maximum velocity

The maximum velocity is an important parameter as it determines the distance the drones are capable of flying within a certain time. The forward flight speed $V$ can be calculated using Equation 4.1 [25].

$$V = \sqrt{\frac{2W\tan(\theta)}{\rho S\left(C_{D_1}\cdot\left(1-\sin^3(\theta)\right)+C_{D_2}\cdot\left(1-\cos^3(\theta)\right)\right)}} \tag{4.1}$$

In Equation 4.1, $\theta$ is the pitch angle, $W$ is the weight of the drone, $\rho$ is the air density, and $S$ is the cross-sectional area. Furthermore, $C_{D_1}$ and $C_{D_2}$ are the drag coefficient when the pitch angle $\theta$ is 0° and 90°, respectively.

The drag coefficient could be obtained by performing a computational fluid dynamics (CFD) analysis on the drone design. However, this is deemed outside the scope of the project. An estimation for the drag coefficient $C_{D_1}$ (hence at 0° pitch angle) for a quad-copter using CFD analysis is given in a study by Felismana [26] and was estimated to be 0.0464. The Felismana article also provides drag coefficient values for 15° and 30° pitch angles [26]. However, a drag coefficient estimate for 90° pitch angle is not given. After creating a trend line with the 0, 15 and 30∘ data points, the following

second-order polynomial is given as approximation for the relation between these data points;

$$C_D = 3 \cdot 10^{-5}\theta^2 + 0.0005\theta + 0.0464$$

Extrapolation can be used to estimate the drag coefficient for $C_{D_2}$. This method results in an approximation for the drag coefficient at 90° pitch of 0.3344. It should be noted that the accuracy of this estimation is low as it uses a second-order polynomial and extrapolation to approximate the drag coefficient. Nevertheless, it serves as a good starting point for the performance analysis. In future design and development of the system a CFD analysis should be performed on this design to calculate more accurate drag coefficients.

The maximum velocity is obtained when the drone has the highest possible pitch angle as then the most force is generated in horizontal direction, creating the highest horizontal speed. The highest possible pitch angle can be calculated using Equation 4.2

$$L_{max} \cdot \cos(\theta_{max}) = W \tag{4.2}$$

Equation 4.2 states that the lift generated by the four propellers multiplied by the pitch angle should equal the weight of the drone. It should be noted that the lift is defined as the force generated by the propellers and it is always oriented perpendicular to the propellers. I.e. when the drone pitches, the value of lift generated stays the same. $L_{max}$ denotes the maximum lift that the propellers can generate and it is a function of the rotational velocity of the propellers. Maximum lift is achieved at maximum rotational speed of the propellers, which is 6000 RPM. Rewriting Equation 4.2 gives an expression for the maximum pitch angle, which can be seen below in Equation 4.3.

$$\theta_{max} = \cos^{-1}\left(\frac{W}{L_{max}}\right) \tag{4.3}$$

With a maximum angular velocity of 6000 RPM the maximum lift generated per propeller is 22.62 N. As the quad-copter has four propellers, the maximum lift it can generate is 90.48 N. Furthermore, the weight is 3.0 kg multiplied by the gravitational acceleration 9.81 m/s$^2$. Filling in these numbers in Equation 4.3 gives a maximum pitch angle $\theta_{max}$ of 71°.

The exact surface area $S$ is unknown for this emissions drone design. Thus, it will need to be approximated. This will be done based on the top view technical drawing Figure D.1. The top view area was chosen as the surface area because the maximum pitch angle is 71°, which is closer to 90° than to 0°. As at 90° pitch the surface area in direction of flight is the top view area, using the top view at 71° is a good approximation. When looking at the top view in Figure D.1, one can conclude that it consists of two main shapes, namely a central circular area and four rectangular arms. These areas will be calculated separately and subsequently added to get an approximation for the total surface area.

The surface area of the circular center part can be calculated by $S_{circ} = \pi r^2$, where $r$ is the radius. The radius for this circular central section of this design is 135 mm. Hence, $S_{circ}$ is 0.0573 m$^2$. The length of one arm is 290 mm and the width is approximately 50 mm. Hence, the area of the four arms is 0.058 m$^2$. Adding the area of the four arms and the circular center section together leads to a total surface area of 0.1153 m$^2$. The blade area covered by the propellers nor the surface area of the propellers itself was considered in the calculation of top view surface area as the propellers generate the lift required to counteract the drag created by the other parts of the drone.

Equation 4.1 also requires the air density $\rho$, which is assumed to be 1.225 kg/m$^3$ (the ISA sea level value) [27]. Filling in all these values leads to a maximum velocity of 61 m/s, or 218 km/h. However, this speed is the absolute maximum velocity when the throttle is at 100%. This speed would require a lot of electrical energy from the battery, greatly reducing the operational time of the drone.

For that reason, the maximum velocity has also been calculated at 60% throttle. At this throttle setting the propellers generate a lift of 42.4 N in total (10.6 N per propeller). This leads to a maximum pitch angle of 46°. The maximum velocity at 60% throttle is 41 m/s, or 149 km/h. This throttle setting and hence speed can be maintained for longer time spans that the absolute maximum velocity of 61 m/s mentioned above and it is therefore a more relevant parameter.

### 4.9.3. Maximum take-off altitude

The maximum take-off altitude is dependent on mainly the weight of the drone (3.0 kg), the maximum angular velocity of the propellers/motor (6000 RPM), and the air density. If the drone is deployed at higher altitudes, the air density will reduce. This limits the lift that the propellers can generate. There is a maximum altitude where the air becomes too thin for the drone to safely lift off. The maximum take-off altitude is the maximum altitude at which the drone can safely lift off. Safely lifting off means that the lift over weight ratio should be at least 2.0, as described by requirement **ALEC-FVSR-AE-01**. The lift generated is calculated by Equation 6.2.

A Python script was created to calculate the air density at a certain altitude conform the international standard atmosphere (ISA) values and subsequently calculate the lift generated at that altitude. Furthermore, a plot was created which visually shows the maximum take-off altitude.

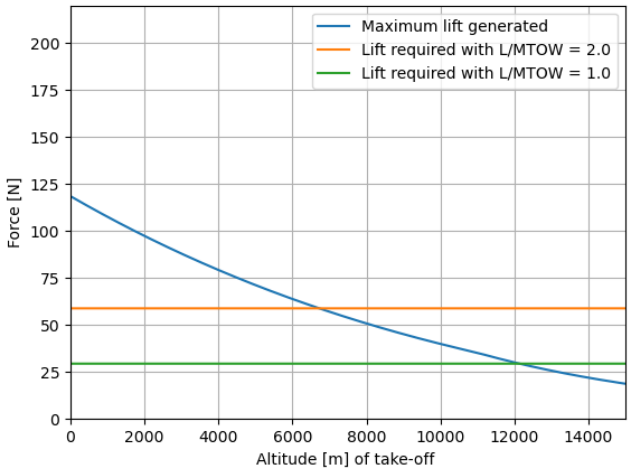


**Figure 4.7:** *Maximum take-off altitude*

The maximum take-off altitude at which the drone can safely take off with lift over weight ratio of 2.0 is approximately 6.7 km. In Figure 4.8 this is the point where the blue graph crosses the orange line. Furthermore, the emissions drones could theoretically take off up to an altitude of approximately 12.1 km (where the blue graph crosses the green line), but above 6.7 km it would not be able to produce a lift over weight ratio of 2.0, which means that its operations would be less safe.

## 4.10. Operations and Logistics

The emission drones play an important role in the larger system, as the only air quality-measuring component. The operations of the drones are described in this section. As mentioned in Section 2.3. the drones are operated on a day-to-day mission basis. This section will thus describe what this mission within a working day looks like.

### Setup and Take-Off

The drones are removed from their secure stowage, and assembled. The four arms are attached to the center-body using two bolts for each. The protective cover is then placed over the body and attached to the structure with plastic clips on all four sides. The drones are visually inspected throughout the process for any indications of damage; if required, minor maintenance can be performed at this stage. The drones are then placed on the landing pads, and charged batteries are connected. After powering up, each drone is checked to see if all systems are operating nominally. The fan of the emission payload should begin spinning upon power up. One by one, the drones begin to take off based on instructions received from the ground station. It is estimated that the set up of each drone will take approximately 15 minutes, taking the two operators a total of 15 minutes for the four drones.

### After Take-Off

The drones climb to a certain altitude and travel towards the runway of interest. It hovers nearby until it is given a command with the first measurement location determined by the ground station algorithm. At all stages including this one, a path is computed to reflect all no-fly zones, e.g. the drone will not fly over a runway. The no-fly zones for the drones are instated in order to minimize the chance of disturbing the regular airport operations. Besides being barred from flying over the runway at any time, the drones are not allowed to hover over taxi-ways. The number of taxi-way crossings are also limited. By not allowing the drones to fly or hover over the runways and taxi-ways respectively, the chance of a failure of a subsystem such as the propulsion or power delivery leading to interrupted airport operations is drastically lowered. In order to allow for access to both sides of a runway during operations, the GS is placed at a corner of the runway, thus allowing for the drones to access both side with minimal crossing of taxi-ways. A visualization of the zones can be seen for a specific runway at LAX. It can be noted that quite some area besides the runway is not available for measurements. In order to improve this situation, in coordination with ATC, some taxi-ways could be closed as not all taxi-ways are used concurrently for a single runway.

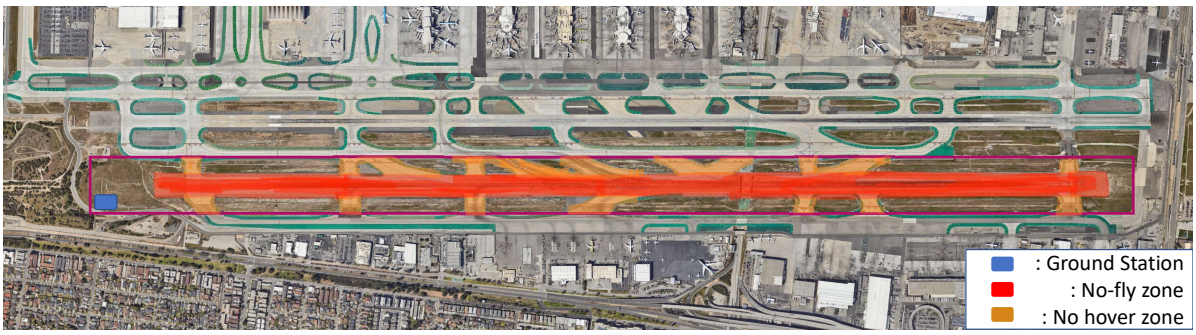


**Figure 4.8:** *No-fly zones for drones around a runway. Purple box indicates area of operation*

### Performing Measurements

Once at the given location, the drone will begin logging data with the set sample rate. The data is transmitted to the ground station via an FTP server for processing, and saved locally for backup. The drones perform measurements for as long as the runway is not in use, that is until the next aircraft event. The system is aware of the locations of aircraft through the included ADS-B receiver in the GS. If the drone does not receive information on the next way-point by this time, it will either hold, or land, depending on the exact conditions.

**Battery Recharging**
When a drone is running low on power, it will be directed by the ground station to return. Upon landing on the landing- and take-off (LTO) platforms, the batteries will be manually removed, and exchanged for new ones. The discharged batteries are then charged at the ground station for the next rotation. Since only three of the four drones are used concurrently for measuring, the fourth is afforded ample time to go through the process of landing, getting its batteries replaced and taking-off and returning to the measurement location. This means that there are always three drones constantly available for measuring.

**Connection Issues**
In case of connection issues, the drone will automatically land to minimise all risks. The data collection will be halted, and the data stored locally.

**Before Landing**
Given the mission ends, the drones will return to their respective LTO platforms, taking into account airport operations. The drones will approach the ground station and land one after another to minimise any risks of collision.

**After Landing**
All systems are checked for any unexpected behaviour. The drones are then powered off, and the batteries are removed. The drones are disassembled, and checked for any signs of damage or dirt. If none are found, the drones are stowed away in custom crates.

# 5

# Noise Drone Subsystem

For measuring noise levels, as well as providing a frequency spectrum of data obtained from near-aircraft operations, a flying system was designed. Near-airport research is often conducted using rigidly placed ground stations like NOMOS[1]. Although providing good data, ground stations have a long set-up time, and a limited spatial flexibility. A more flexible alternative is to use a quadcopter which would perform measurements while flying. To measure noise while flying has inherent difficulties: providing un-corrupted data while experiencing its self-induced noise pollution is very difficult. A middle-ground option was to use a drone which would transport a microphone to one location, land, and perform noise measurements while stationary on the ground. This concept was chosen, as it allows for flexible yet accurate measurements to be taken.

This chapter will explain the design process, starting with the requirements listed in Section 5.1. Ground effect and mitigation strategies are explained in Section 5.2, after which the design of the payload is elaborated on in Section 5.3. Then the structure of the drones is shown in Section 5.4, after which Section 5.5 shows the mass and financial budgets. Furthermore, Section 5.6 explains the data handling of the subsystem. The operations and logistics are included in Section 5.7. A conclusion and future recommendations are shown in Section 5.8 and Section 5.9.

## 5.1. Requirements and Verification

The design of the noise drone starts from the requirements that the noise drone needs to fulfill. The requirements and compliance are presented in Table 5.1. A ✓ indicates that the requirement has been met, ~ indicates partial compliance, and × shows that the requirement has not been met.

**Table 5.1:** *Noise drone requirements and compliance*

| **Requirement ID** | **Requirement** | **Compliance** | **Comments** | Verification |
|---|---|---|---|---|
| **ALEC-SR-FV-ND-COM-01 (key)** | The noise drone shall be able to transmit uncompressed audio data near real-time | ✓ | Presented in Section 5.7 | Demonstrate - transmit uncompressed audio data near real-time |
| ALEC-SR-FV-ND-DH-01 | The noise drone shall be able to store one day's worth of uncompressed audio measurements. | ✓ | Presented in Section 5.6, Section 5.7 | Demonstrate - record sound measurements until data storage capacity is reached |
| ALEC-SR-FV-ND-PN-01 | The noise sensing subsystem shall record sound between 40 and 140 dB SPL. | ✓ | Presented in Subsection 5.3.2 | Test - perform sound measurements from 40 dB to 140 dB SPL |
| ALEC-SR-FV-ND-PN-02 | The noise sensing subsystem shall record sound between 20 and 20000 Hz. | ✓ | Presented in Subsection 5.3.2 | Test - perform sound measurements from 20 Hz to 20000 Hz |
| ALEC-SR-FV-ND-PN-03 | The noise sensing subsystem shall record the frequency with an accuracy of ±10% Hz. | ~ | Presented in Subsection 5.3.2 | Analysis - perform sound measurements with known frequency |
| ALEC-SR-FV-ND-PN-04 | The noise sensing subsystem shall record sound intensity with an accuracy of ±2 dB | ~ | Presented in Subsection 5.3.2 | Analysis - perform sound measurements with known sound intensity |

[1] https://noiselab.casper.aero/ams/#page=actual[Cited 10 June 2022]

| | | | | |
|---|---|---|---|---|
| ALEC-SR-FV-ND-OPER-01 | The noise drone shall be able to land near the runway without sustaining damage | ✓ | Presented in Section 5.7 | Demonstrate - performn landing near the runway |
| ALEC-SR-FV-ND-OPER-02 | The noise drone shall stay stationary at wind speeds under 7.9 m/s when landed near a runway. | ~ | Presented in Section 5.4 | Test - test maximum velocity noise drone can withstand in wind tunnel |
| ALEC-SR-FV-ND-PERF-01 | The noise drone shall have an operational time of at least 8 hours with a fully charged battery. | ✓ | Presented in Subsection 5.5.2 | Demonstrate - operate drone until battery is dead |
| ALEC-SR-FV-ND-COS-01 | The noise drone shall cost no more than 1500 EUR. | ✓ | Presented in Section 5.5 | Inspection - sum hardware costs of components |

## 5.2. Ground Effect

In order to create a drone design capable of measuring noise accurately, the ground effect had to be dealt with. Certain frequencies get attenuated by destructive interference patterns, while other frequencies get amplified by constructive interference [28]. As the amount of interference each frequency experiences is dependent on the angle, the distance from the noise source to the microphone, the reflectivity of the ground surface and the height of the microphone from the ground, it is nearly impossible to theoretically predict how exactly the ground effect influences the results. Thus, finding solutions to mitigate the ground effect as much as possible was desired.

The ground effect causes interference patterns for an observer that heavily influence the recorded/-experienced audio. This interference happens because of two sound paths: the direct path and the ground reflected path. When the two paths arrive simultaneously at an observer (person, microphone, etc) at different angles, this causes sound interference. This causes doubling of the sound (+6dB) at the peaks of interference and (theoretical) complete deafening of the sound. The effect of the ground effect can be seen in the difference between Figures 5.1a and 5.1b. In Figure 5.1b the curved interference patterns are distorting the measured samples very heavily, while in Figure 5.1a no such patterns are visible, giving much cleaner data.

The ground-effect by itself does not necessarily cause a problem. When a microphone is placed flush to an infinite perfectly reflecting plate, its measured response will be a flat 6 dB. An infinite plate on the ground is not possible, but the plate should be as big as possible for the best possible result. Several solutions were considered to mitigate impact of the ground effect on the microphone,

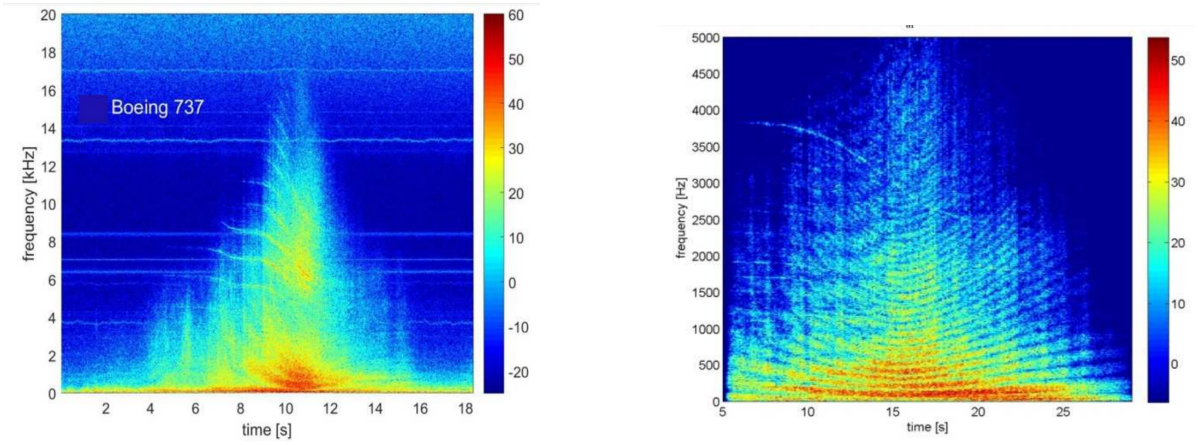


**(a)** ***without*** *interference pattern*

**(b)** ***with*** *interference pattern*

**Figure 5.1:** *Spectrograms with and without ground effect interference patterns from [28]*

an overview of which is provided below. The solution that was chosen to have the best possible noise measurement was a plate on top of the drone.

Firstly, it was envisioned that careful placement of two microphones at different heights would result in interference at different frequencies. Then a comparison can be made between the two respective spectrograms, filters applied for the given incidence angle and microphone height and their data combined to get a more accurate measurements.

However, numerically modelling Equation 5.1 [28], showed that the combined data of the two microphones at different heights would be too chaotic to be usable for this purpose: comparing the two spectrograms in a way that would result in more useful data was considered to be of such complexity in practice that it would not be feasible to implement. This was also deemed infeasible due to the effect of the changing incidence angle.

$$\Delta \mathrm{SPL}(r,\theta) = 10\log\left[1+\left(\frac{r_1}{r_2}\right)^2 |Q_p|^2 + 2\left(\frac{r_1}{r_2}\right)|Q_p|\cos\left(\frac{4\pi f}{c}h_m \sin\psi + \beta\right)\right] \tag{5.1}$$

The formula describes the difference between measured sound pressure levels and real sound pressure levels due to the ground effect. A few assumptions were made for the plotting of Equation 5.1. First of all the 'direct path' $r_1$ and the 'bottom reflected path' $r_2$ were considered to be equal $r_1 = r_2$ because the aircraft is relatively far away. The incidence angle $\psi$ was taken at 90°. This incidence angle and a hard boundary assumption led to the assumption of the 'normal surface impedance' coefficient $Q_p$ to be equal to 1 and the phase shift angle $\beta$ to be 0. The speed of sound $c$ was taken as the speed of sound at sea-level standard conditions (340 $m/s$). Figure Figure 5.2 shows the theoretical interference effects as experienced by two microphones placed at 4 and 7 cm of a perfectly reflective flat surface using formula Equation 5.1.

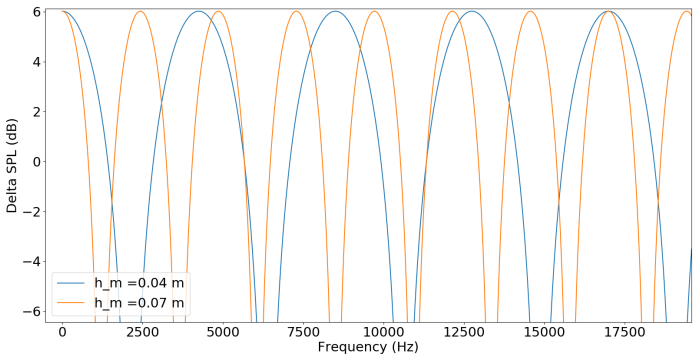


**Figure 5.2:** *Ground effect of microphones placed at 4 and 7 cm from a hard flat surface at an incidence angle of 90°*

Secondly, it was considered to place a plate below the quadcopter, in-between the landing legs. This option would be perfect for mitigating the ground effect as the plate would be as similar as possible to an infinite plate as it is located on the ground. Although this option was explored, the main drawback is due to the interference of the drone itself. The noise measurements are first of all distorted by the drone that is located above the microphone which will create extra distortions as well as air pushing down the plate; resulting in a lower propeller efficiency. It was deemed that the audio data and performance would decline too much with this configuration.

The last -chosen- option was to add a plate on top of the quadcopter, in which a microphone would be mounted flush to the surface. Such a surface would provide a more predictable interference pattern. The problem with this option is that the plate is not placed on the ground and not big

enough to assume its performance is similar as it would be on the ground. This option will have a reasonable audio measuring performance if edge effects are mitigated as much as possible, and the plate does not interfere with aerodynamics. The plate should also be made as big as possible to resemble an infinite plate on the ground as much as possible. The plate is designed with an absorptive surface by using sound absorbing foams. This option was chosen as it reduces unwanted reflection-related related measurement disturbance.

## 5.3. Design Configuration

As has been explained in Chapter 2, a quadcopter was chosen for performing near-airport noise measurements. Such a configuration would provide a noise measurement node that is very versatile in deployment. It should be noted however that these measurements will not be performed while flying. This is because of the many problems encountered with ego-noise of any flying vehicle. While solutions such as dirigible balloons, aerostats, or stationary flying measurement stations could theoretically work, a quadcopter which is able to provide measurements at any desired location at a short travel time was considered ideal.

In addition, in order to obtain a high level of certainty on the obtained data, the interference problems caused by the ground effect had to be addressed. Its most viable solution was deemed to be to add a small plate on top of the drone, which would serve as a basis from which sound waves would be absorbed and reflected in a more predictable manner; allowing for more accurate results.

### 5.3.1. Interference-effect Reducing Plate

Research has been performed into the shape of such plates to improve the accuracy of the sound measurements. Research by Albert et al. [29] show that the original round plate can be improved. Namely, by means of a "daisy shaped plate" a reduction in the magnitude of edge effects is achieved. Especially the elevated microphone experiment by Albert et al. is relevant to this case. In the daisy plate experiment (pp. 9 [29]) when a sound source has a zero incidence angle and the microphone is elevated above the plate, a heavily increased performance by the daisy plate relative to a round plate is seen on the frequency response above 1500 Hz. This led to the choice of using a daisy plate pattern instead of a round plate.

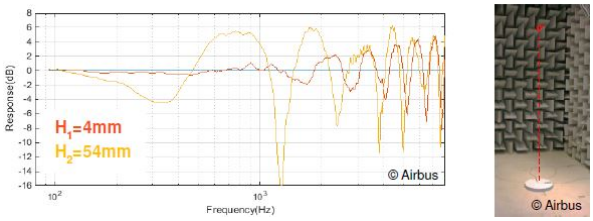


**Figure 5.3:** *Standard model round plate tested in anechoic chamber [29]*

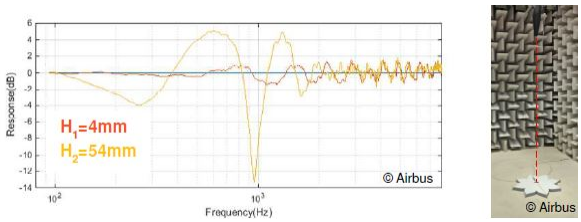


**Figure 5.4:** *Airbus designed daisy plate tested in anechoic chamber [29]*

Thus, taking all of the aforementioned considerations into account, it was deemed that for the pur-

pose of the noise measurement drone, a small "daisy" shaped plate with embedded microphone would result in the least possible distortion as caused by multipath interference and edge diffraction.
Although the project team is aware of the novelty of the new plate design, as well as the novelty of using a quadcopter for measuring aircraft noise -potentially resulting in issues that have not yet been discovered or thought off- this solution is deemed to be as good as possible within the constraints of the ALEC mission. Research and testing will have to be performed to find how closely the daisy plate resembles a flat plate. Calibration tests have to be performed anyway on the microphones.

### 5.3.2. Microphone Selection

There are several factors which were taken into account for selecting the final microphone that would be mounted on top of the noise drone.

First of all, the mission profile for the noise drone is non-standard, as it aims to perform noise measurements closer to the source than is done conventionally. More specifically, a higher maximum SPL was required (140 dB was selected as upper limit). Furthermore, a high signal to noise ratio (SNR) (and thus a low ego-noise) was deemed at first to not be of high priority. However, a good SNR would result in the microphone being able to also capture the higher frequencies, which get attenuated more quickly than the lower frequencies of aircraft in landing/take-off configuration several hundreds of meters away from the noise drone; potentially resulting in useful data. Thus, a good SNR was listed as a "nice to have" requirement.

Ultimately it was decided to use an omnidirectional microphone. This choice was made on the basis of omnidirectional microphones providing sufficient performance, while being less complex in operation because of the pointing necessary when using directional microphones. Another big drawback of using directional microphones is that directional microphones do not perform well in measuring low-frequency sound, which is dominant in aircraft noise. Nevertheless, further investigation of this option is listed as a potential future improvement.

The frequency responses of the microphone candidates were investigated as well. It was deemed by the client as desirable to be able to capture high-pitched noise data, in order to better understand engine characteristics. Thus, a conscious choice was made to allow frequencies of up to 20 kHz to be measured; as opposed to the 10 kHz which the ground level sensors will be able to measure. Furthermore, an as "flat" as possible frequency response was deemed as beneficial.

Lastly, the weight of the microphone system was taken into consideration, as a heavy payload would severely limit the flight time of the quadcopter. Thus, next to just the microphone itself, the additional components necessary for certain microphones had to be taken into consideration. Microphones requiring high-weight components like a dedicating signal conditioning unit, or a separate high-voltage pre-amplifier were deemed as infeasible.

The final chosen microphone is the MKE Essential Omni microphone by Sennheiser. It is a lightweight, high resolution microphone that is able to handle very high SPL levels. Its intended use is for live-theater productions, which also causes its design to be waterproof as it should be able to handle sweat of performers. Another additional benefit of this microphone is that it has a 3.5mm jack which makes it easily connectable. Although relatively expensive (EUR 187.21), it was deemed that this microphone will likely meet all the specified requirements. The requirements **ALEC-SR-FV-ND-PN-03** and **ALEC-SR-FV-ND-PN-04** can not be proven to be met at this point in time and the compliancy of these requirements need to be tested in a soundproofed studio in future development. A summation of the most important Sennheiser microphone specifications are given in Table 5.2[2]. The

[2]https://nl-nl.sennheiser.com/mke-essential-omni-distortion-free-small-omnidirectional-condenser-microphone-for-live-stage-includes-ke-4-capsule

microphone calibration procedure is described in Subsection 8.5.2.

**Table 5.2:** *Chosen microphone specifications*

| Characteristic | Value |
|---|---|
| Directionality | Omnidirectional |
| Frequency range | 20 Hz - 20 kHz |
| Signal to noise ratio | 66 dB |
| Maximum SPL | 140 dB |
| Weight | 16 g |

### 5.3.3. Final Configuration

The noise drone design is a culmination of the results achieved by the work on the ground level sensors, as well as the emission drone. While a completely unique solution could have been devised, the noise measurement system of the ground level sensors was deemed to be ideal, and only the type of microphone was changed. Out of reasons of ease of replacability, reusability, it was considered beneficial to use the same flight enabling components for the noise drone as for the emission drone. Thus, ultimately, the noise drone uses the same electronic architecture as the GLS, the same flight system as the emission drone, and is unique by means of addition of the ground-effect plate, and the different choice of microphone. The final list of components is provided below.

**Components identical to emission drone**

- Main structure
- Motors & Esc
- Propellers
- Flight controllers & GPS
- Arduino
- 2x 5000 mAh Battery
- Obstacle avoidance
- 2x SD card 64 GB
- GSM/GPS Module for Raspberry Pi
- Wiring+Redundancy
- Obstacle Avoidance
- DHT22
- SiK Telemetry Radio V3

**Components identical to GLS**

- Raspberry Pi 4B
- Ugreen Audio card
- Huawei E3531 3G dongle
- Ugreen USB audio card
- SD Card 64GB

**Components unique to noise drone**

- Sennheiser MKE Essential Omni-Black
- Ground-effect daisy plate

A render of the final configuration has been provided in Figure 5.5. The electronics are housed in a waterproof encasing, placed in the center of the drone. A daisy plate has been added on top of the drone which seals the internal electronics from rain/dirt from the top, at the center of which a microphone has been embedded flush to the surface.

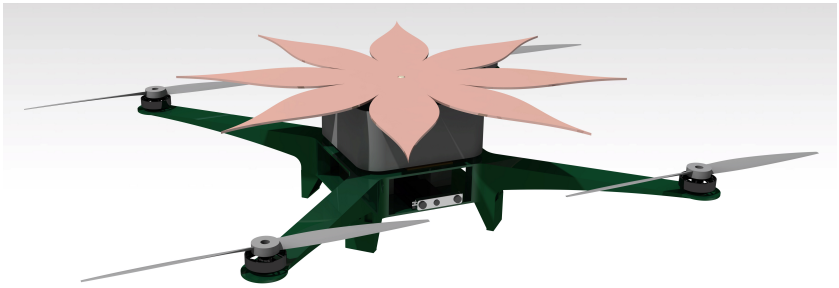

**Figure 5.5:** *Daisy plate on noise drone, artist impression*

## 5.4. Structure & Material

The payload weight of the noise drone is slightly lower than that of the emission drone, but it was chosen to still use the same batteries, propellers, and motors. A requirement for the noise drone is that it should be able to function for 8 hours. Therefore, efficient propellers and heavy batteries are required. Also, the structure of the drone frame should be lightweight. The hole in the middle will be removed. However, the noise drone frame will be made out of the same material, Nylon CF15. However, the noise drone will not require a cover and a wind-tunnel, but as has been discussed in the previous section, a daisy plate will be added to the system. The batteries are mounted in the centre at the bottom of the drone to have a low centre of gravity for stability while stationary. The standing stability under wind still needs to be tested but it is assumed that the drone will likely meet requirement **ALEC-SR-FV-ND-OPER-01**.

The daisy plate is added to reduce the unwanted ground effect of the measured acoustic data. Several methods of manufacturing for this plate were envisioned, in the end a carbon fibre sandwich plate with a foam core was used [3]. This material has sufficient stiffness at a low weight, while being partially recyclable and partially downcyclable, which is further explained in Section 14.3. On top of this sandwich plate an absorptive foam is attached, since the top of the plate should be absorbing, and not reflecting sound.

## 5.5. Budgets

This section presents the mass and financial budget for the noise drone in Subsection 5.5.1 and the power budget for the noise drone in Subsection 5.5.2.

### 5.5.1. Mass & Financial Budget

All the components required for the drone explained in the previous sections are summarised in Table 5.3 with the mass and cost of each component.

**Table 5.3:** *Mass & financial budgets for the noise drone*

| Component | Cost | Mass | Component | Cost | Mass |
|---|---|---|---|---|---|
| Main Structure | €46.10 | 514.27 g | 2x Raspberry Pi 3B | €66.02 | 84.00 g |
| Motors & Esc | €315.56 | 440.00 g | 3x SD Card 64 GB | €24.77 | 6.00 g |
| Plate | €97.02 | 60.00 g | UGREEN Audio Card | €10.33 | 50.00 g |
| Propellers | €28.26 | 180.30 g | Huawei E8372h-320 | €41.32 | 40.00 g |
| 2x Battery | €134.29 | 854.00 g | Wiring + Redundancy | €50.00 | 130.00 g |
| SiK Telemetry Radio V3 | €52.30 | 50.00 g | Obstacle Avoidance | €292.87 | 90.00 g |
| 1x Sennheiser MKE Essential | €148.76 | 53.00 g | Flight Controllers & GPS | €177.27 | 81.00 g |
| DHT22 Temperature Sensor | 4.92 | 6.00 g | **Total per drone** | **€1,489.79** | **2568.57 g** |

[3] https://www.r-g.de/en/art/650800AX [15 June 2022]

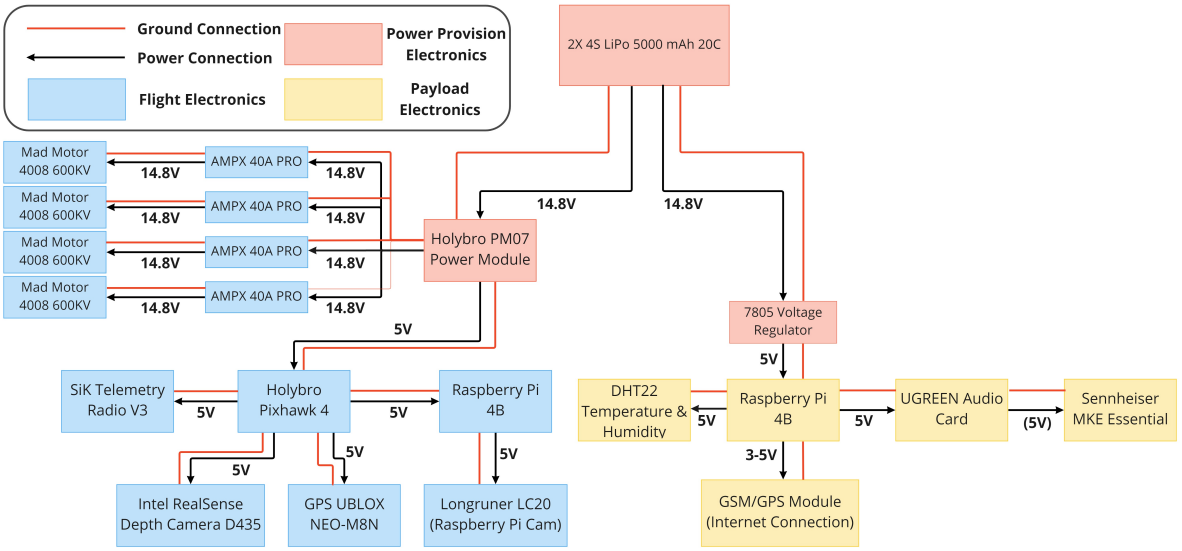


**Figure 5.6:** *Electrical block diagram noise drone*

### 5.5.2. Power Budget

The power consumption of the noise drone changes dramatically between its mission phases. The distinction is made between the flying phase and the stationary phase. In the flying phase, the drone flies to a location of interest where it lands and starts measuring. This measuring part is the stationary phase. During the flying phase, the internal electronic systems have a negligible power consumption in comparison to the propulsion system. The internal electronics are not negligible anymore during the stationary phase, due to the large amount of time the system will stay at a certain location and measure there. The power usage of the motors is only during flight from the ground station to the location of interest and back, the power required in the flight phase is 290 W, see Section 6.6. As the drone flies a max of 2km with 7 m/s and a 1.5 safety factor is used, 69Wh for moving back and forth to the ground station.

During the stationary measuring phase, the main power consumers are the Raspberry Pi 3B that is running and used for the noise data handling, the Raspberry Pi 3B that is used for flight control and will be idle, and lastly the Huawei transmission link dongle. It is assumed that the microphone and components (other than the Raspberry Pi) related to flight controllers all use negligible power while stationary. The active Raspberry Pi draws 2.4W [4], the idle Raspberry Pi draws 1.4W [5] and the Huawei tranmission dongle draws 2.5W [6]. This totals to a power consumption of 6.3W while measuring. For an 8 hour measuring day, this accounts to 50.4Wh used. The total Wh of the chosen 10000 mAh 14.8V batteries is 148 Wh. It is unsafe to discharge the battery below 15% so a 20% discharge depth is chosen to have a margin there. This means that the available battery power is 120Wh. 119.4 Wh are used for the minimal requirements of 2km range and an 8 hour operating day which is within budget especially given the 1.5 safety factor applied for the flying phase. The voltage and ground connections of the electrical components are displayed in Figure 5.6.

## 5.6. Data Handling

This section discusses the pre-processing of data in the noise drone in Subsection 5.6.1. Thereafter, the way in which the data is transmitted from the microphone to the ground station is presented in Subsection 5.6.2. The overall handling of the data can be seen in Appendix C, where the raw

[4] https://www.pidramble.com/wiki/benchmarks/power-consumption [Cited 15-06-2022]
[5] https://www.pidramble.com/wiki/benchmarks/power-consumption [Cited 15-06-2022]
[6] https://www.handleidi.ng/huawei/e3372/handleiding?p=10 [Cited 15-06-2022]

noise data input is filtered, optionally it is compressed and afterwards stored and transmitted to the ground station.

### 5.6.1. Data Pre-processing

The noise signal obtained by the chosen microphone will either be output as digital signal or analog signal. The signal needed to be conditioned by means of an analog to digital converter (ADC) in the latter case. This functionality will be provided by the Ugreen audio cards used in the system. Once a quantized digital signal has been obtained, a fast Fourier transform (FFT) will be performed. The FFT is a mathematical operation which converts a given time response to the frequency domain. One advantage of the FFT is its special property of being a matrix operation that scales only to the power $\mathcal{O}(n \log n)$ [30] in terms of computational complexity.

Once the spectral information has been obtained, it can be decided to transmit the complete information, or perform compression first. The data size can be reduced by limiting the information to $\frac{1}{3}$ octave bands, using lossless compression as FLAC [31], or lossy compression such as MP3.

### 5.6.2. Data Transmission

As mentioned in Chapter 4, the data handling after the processor is the same for the emission drone, noise drone, and ground level sensor, so that description will not be reiterated.

The Sennheiser microphone needs a USB-connected audio card that transmits the output from the microphone to the processor which is a Raspberry Pi in this case. The processor then proceeds to compress the measured audio data. Uncompressed audio data will be sampled at 16 bits with a frequency of 44.1kHz which constitutes to a 711 kbit/s bitrate. The uncompressed data will be stored in a WAV file. Any desired type of file compression is easily implementable within the Python code provided on GitHub of the SAFE Project [7]. The SAFE project will be elaborated on in Chapter 8. MP3 can be used for compression from a maximum of 320 kbit/s to a minimum of 32 kbit/s. The choice is up to the user to compress the data to e.g. Variable Bit Rate (VBR) MP3 to save bandwidth and necessary storage space. The processor is also responsible for encryption of the data for obvious privacy and safety reasons. The difference from the emission drone to the noise drone and GLS considering internal data handling is mainly that the bitrate of audio data is a lot bigger than the single metrics of emission. The 64 GB local storage amounts to 200 hours of uncompressed audio data, while it is estimated that the bitrate of the emission drone is about 1/100th of the noise capturing devices (20000 hours of uncompressed emission data for 64GB card). A schematic of the data handling is given in Figure 5.7. When a network is present, 3G or 4G will be used to send data to a remote File Transfer Protocol (FTP) server, and the local storage will be only used as a buffer. When the FTP server receives the data correctly, it will confirm this back to the GLS and the correctly received file will be deleted on the local storage. In the case of a corrupted message or a transmission link failure, the files on the local storage will not be deleted. The files that had not been received correctly are stored on the local storage and the transmission is retried at a later point in time. A schematic of the data handling is given in Figure 5.7.

The data handling of the Ground Level Sensor is identical to the Noise drone except for the difference in microphone selection. This section will not be repeated in the GLS section due to their equivalence.

## 5.7. Operations and Logistics

[7] https://github.com/sarabsethi/rpi-eco-monitoring [Cited 10 June 2022]

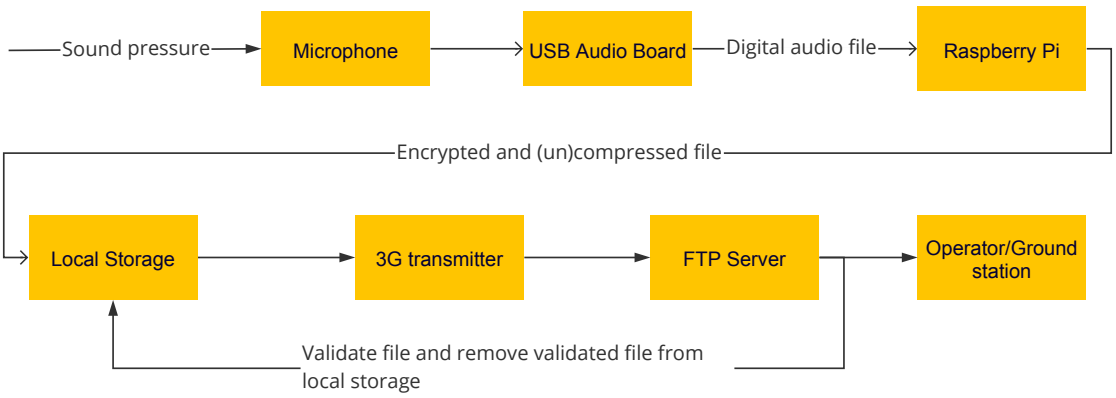


**Figure 5.7:** *GLS/Noise Drone data handling block diagram*

### Take-Off

The drones are removed from their secure storage, and assembled. The four arms are attached to the center-body using two bolts for each. The interference-reducing plate is then placed on top of the body and attached to the structure on four aluminium spacers. The drones are visually inspected throughout the process for any indications of damage; if required, minor maintenance can be performed at this stage. The drones are then placed on the landing pads, and charged batteries are connected. After powering up, each drone is checked to see if all systems are operating nominally. This procedure is expected to take 15 minutes per drone, leading to a total working time of 15 minutes for two operators. One by one, the drones begin to take off based on instructions received from the ground station.

### After Take-Off

The drones climb to a certain altitude and travel towards the runway of interest. It lands precisely at a location determined by the ground station algorithm, which could be close to and further from the runway, depending on the predetermined measurement location. At all stages including this one, a path is computed to reflect all no-fly zones which are also in effect for the emissions drones.

### Performing Measurements

Once landed at the specified location, the drone will turn off its motors and begin recording data. The data is stored locally but also transmitted to the ground station via an FTP server in near real-time. The drones remain on the ground in the chosen location for the duration of the day. In case of connection issues, the drone has all data stored locally.

### Before Landing

At the end of the mission, the drones will take off again and fly towards the ground station. The drones will approach the ground station and land one after another to minimise any risks of collision.

### After Landing

All systems are checked for any unexpected behaviour. The drones are then powered off, and the batteries are removed. The drones are disassembled, and checked for any signs of damage. Components will need to be cleaned once every week or more frequently if deemed necessary by the operator. If no flaws are found, the drones are stowed away in custom crates.

## 5.8. Conclusion

A quadcopter has been designed which can provide noise measurements at a versatile set of locations due to its capability to fly. The propulsion system was optimized for range to allow for a wide spatial coverage, and the measurement payload was designed to provide for noise data to be obtained which is useful in determining specific aircraft characteristics, as well as being as "clean" and un-corrupted as possible. The final configuration uses the same propellers, batteries, and motors as the emission drone in order to improve reliability and replaceability. A custom structure was then designed which would allow the measurement system to fulfill its specific requirements. The final design is one that can provide noise measurements up to 2 km away from the ground station.

## 5.9. Future Improvements

Several improvements to the noise drone design could be made, given a continuation of the ALEC project. An overview of possible optimisations is given below.

Firstly, further research can be put into the selection of the microphone used. A condenser type microphone of the Sennheiser brand was chosen for the current iteration of this project. However, significant developments in the field of digital MEMS microphones have made them usable and used for a variety of noise research projects. An array of MEMS could possibly provide better results than a limited number of "conventional" microphones, and could thus provide large advantages. In addition, the usage of "pressure zone microphones" has also become more widespread. Whilst not commonly seen in research, these microphones could also provide benefits specific to the project.
Secondly, one variant of a number of patented "Daisy" plate design was chosen. However whether other variants, or as of now unexplored options, would provide even better results should be investigated.
Thirdly, a more extensive knowledge of temperature and humidity gradients of the medium through which aircraft noise is propagated will result in a better understanding and classification of aircraft noise. Thus, a future system would make better use of open-source data, and/or allow for meteorological measurements to be taken at a better spatial resolution than is currently feasible.
Lastly, selecting a foam which exhibits better absorption properties as compared to the type which is now used would provide additional benefits in reduced interference effects. Research on this topic seems to be steered toward aerosols, such as those made using graphene. As well as bio-produced, and bio-degradable sound-absorbing foams.

# 6

# Drone Propulsion Subsystem

In this chapter the propulsion system design will be presented for both the noise drones and the emission drones. The propulsion subsystem heavily influences the power and mass budgets presented in Chapter 4 and Chapter 5. Therefore, a separate chapter is presented for this subsystem to clarify some driving choices. The process in which the propulsion system has been designed is as follows: First, the approach taken to design the propulsion system for the emission drone is elaborated on in Section 6.1. Secondly, in Section 6.2 the driving design parameters will be explained. Furthermore, in Section 6.3 the propeller sizing will follow. With the information about the propeller, in Section 6.4, a motor and an accompanying electronic speed controller (ESC) will be selected, which fulfil the requirements and in Section 6.5 the battery will be designed. Moreover, in Section 6.6 the propulsion subsystem design of the noise drone is explained. Finally, in Section 6.7 the validation and verification of the code is presented with a sensitivity analysis on the chosen propulsion subsystem for the emission drone.

## 6.1. Design Philosophy

The design of the propulsion subsystem is conducted for the emission drone as this was determined to be the heavier drone due to the nature of the scientific payload, see Chapter 4. The propulsion subsystem for the noise drone was sized after the emission drone, as the mass was still rather unclear due to the research that needed to be conducted. However, as will be explained further into the report, the mass was actually rather similar which mitigated the need for a resizing of the propulsion subsystem.

The actual design of the propulsion subsystem was done with help of the book "Introduction to Multicopter Design and Control" by Quan Quan [25], referred to in the rest of the report as Quan Quan (2017). The book was used as the main source of reference as other available options were all from hobbyist websites, or papers where a propulsion subsystem is described, but the design process is not explained. It must be noted that Quan Quan (2017) was not always accurate with respect to experimental data provided by manufacturers, which will be shown in Section 6.7.

The method proposed by Quan Quan (2017) of propulsion subsystem sizing is an approach of modelling the different components, see Figure 6.1. Modelling approach means that performance is computed for multiple individual components. Based on the computed performance the optimal components are chosen.

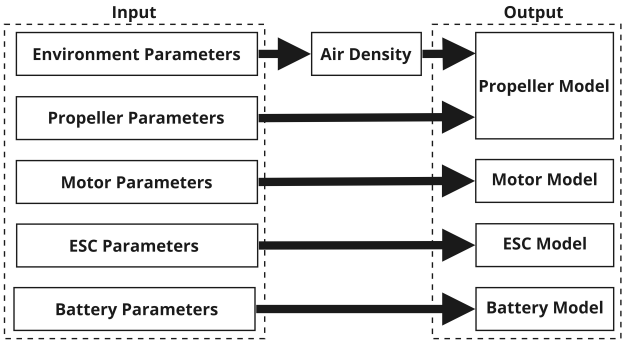


**Figure 6.1:** *Modelling of the propulsion subsystem*

## 6.2. General Parameters

To design the propulsion subsystem, it was necessary to establish general parameters, which drive the design process. The required parameters were: the number of arms ($n_{arms}$), the thrust to weight ratio ($T/W$), and the preliminary mass ($m_{pre}$).

### 6.2.1. Number of Arms

A N-copter has an N amount of arms, each of them attached to the main body carrying the propulsion unit. The unknown N is set to four, making the current design a quadcopter. This is because the emission drone will need to hover to take measurements, and if more arms are included, more propulsion units will be necessary, increasing the weight of the structure. Using smaller motors is not a good idea for the current design, as the smaller motors generally require more power, resulting in a larger battery mass, elaborated on in Section 6.5 [1] [2] [3] . A larger weight will require a larger thrust to be generated, leading to the same battery charge being drained quicker. Furthermore, multiple drones are desired for the current mission profile making cost also of importance, more parts means more cost [1] [2]. Finally, the agility of a quadcopter is generally speaking also better than a drone with more arms.

Nevertheless, there are also drawbacks of taking a quadcopter rather than e.g. a hexacopter (6 arms). The amount of payload that can be carried and the maximum speed will decrease significantly, because more motors provide more thrust in total in the end [2]. In addition, the stability and manoeuvrability will be slightly worse, and a hexacopter can land in the case of an engine failure[1] [3].

The latter point would be a reason to opt for the hexacopter, but as the quadcopter will be functioning far away from the runway, the crash will not impact the airport operations. The cost necessary for damage on the quadcopter can in most cases be maintained relatively easily as most of the structure exists of separate components. Therefore, in case of any damage the damaged parts only need to be replaced and the other components can still be utilized.

### 6.2.2. Thrust to Weight Ratio

The thrust to weight ratio (T/W) is one of the most important parameters to establish before the propulsion unit can be sized. The T/W needs to be set for two conditions for the current mission, hovering and the maximum desired value. For hovering, the T/W needs to be 1 as the drone should hold its position and not ascent or descent, assuming it has a pitch ($\theta$) of 0 degrees. The maximum T/W is set to be 2.5, this stems from **ALEC-FVSR-AE-01** which says that the maximum T/W ratio shall at least be 2. To make sure this value is attained in practice after the theoretical sizing has been conducted, it has been increased to 2.5. The emission drone is primarily assessed on its hovering performance at a T/W of 1, the requirement for 2.5 T/W is more to select a motor with an adequate performance rather than carrying out operations with.

### 6.2.3. Preliminary Mass

The final step before the propulsion unit could be designed was to determine a preliminary mass budget for the emission quadcopter. The initial mass budget is displayed in Table 6.1 and is determined to be 3.028 rounded down to 3 kg, as several parameters are overestimated in the preliminary mass estimation, while other components might be missing. The breakdown of this initial mass estimation can be found in Table 6.1.

[1] https://lucidcam.com/hexacopter-vs-quadcopter/#:~:text=as%20a%20helicopter.-,What%20Are%20The%20Difference%20Of%20Hexacopter%20vs%20Quadcopter,easier%20to%20repair%20and%20build. [Cited 10 June 2022]

[2] https://droneista.com/hexacopter/ [Cited 10 June 2022]

[3] https://www.droneybee.com/tricopter-vs-quadcopter-vs-hexacopter/ [Cited 10 June 2022]

**Table 6.1:** *Initial mass estimation*

| **Payload Masses** [4] [5] **[g]** | | | | | |
|---|---|---|---|---|---|
| **CO-CX** | **NO-B4** | **SO2-A4** | **IRC-AT** | **OPC-R2** | **NO2-AE** |
| 8 | 13 | 6 | 15 | 30 | 6 |
| **O3-AH** | **MQ138** | **Airpump** | Windtunnel | Sensor Adapters | |
| 6 | 4 | 10 | 80 | 100 | |
| **Component Masses** [6] [7] [8] **[g]** | | | | | |
| **Structure** | **Motors** | **Propellers** | **Flight Controller** | **ESC's** | **Arduino** |
| 800 | 500 | 60 | 49 | 70 | 25 |
| **Raspberry Pi** | **Battery** | **Wiring** | **Obstacle Avoidance** | | |
| 46 | 900 | 50 | 200 | | |

With this preliminary mass and the thrust to weight ratios, the thrust values for hovering ($T_{hov}$) and the maximum attainable value ($T_{max}$) can be calculated. The quadcopter will hover when the thrust is equal to the weight and the maximum value is 2.5 times the value for the hovering thrust. This results in the values displayed below, using a value for $g$ of $10\,\mathrm{m\,s^{-1}}$ rather than 9.81 to account for inaccuracies later on. The thrust required will be provided in kg and in N, as manufacturers usually give the thrust produced per motor in kg. The motor thrust required per arm (pa) is also provided.

$$T_{hov} = 3\,\mathrm{kg} = 30\,\mathrm{N} \qquad T_{hov_{pa}} = 0.75\,\mathrm{kg} = 7.5\,\mathrm{N}$$
$$T_{max} = 7.5\,\mathrm{kg} = 75\,\mathrm{N} \qquad T_{max_{pa}} = 1.88\,\mathrm{kg} = 18.8\,\mathrm{N}$$

## 6.3. Propellers

The propeller is responsible for generating the thrust for the drone and thus needs careful sizing. In Subsection 6.3.1, an elaboration is provided on the selection of the propellers to be analysed. This is followed by the modelling process for the propeller of the emission drone in Subsection 6.3.2.

### 6.3.1. Propeller Selection

Before the modelling process started, a literature study was conducted. The main goal of this literature study was to determine what were the ranges of viable propeller diameters ($D_p$) and propeller pitches ($H_p$). These two parameters are of importance when calculating the thrust produced and the torque required by the propellers. From the literature study, it was observed that 2 main aerodynamic effects of the propellers needed to be taken into account, these are the vortex ring state and the airflow stalling of the propellers.

The vortex ring state (VRS) or settling with power, is an aerodynamic phenomenon where the propellers are enveloped in a vortex ring, a vortex in the shape of a torus. The vortex ring forms when a moving fluid is injected into a stationary fluid, resulting in friction between the two different masses. The friction causes the moving fluid on the outer core of the said torus to rotate back inwards, decelerating it initially, but the moving fluid is accelerated due to the continuous injection of moving fluid [9].

The VRS impacts the controllability and the aerodynamic performance of a N-copter, as the vortex ring moves with the N-copter and the lift produced by the propellers is reduced. Therefore, it is important to take precautions in the design so that the risk of the VRS occurring is minimised. The probability of a VRS occuring increases significantly when a high descent rate is coupled with a slow forward speed [9], but also if the pitch of the propeller is too high, bigger than $0.66 \cdot D_p$ [10]. The latter provides a limitation on the plausible propellers.

[9] https://pilotinstitute.com/vortex-ring-state/ [Cited 10 June 2022]
[10] https://www.ecalc.ch/calcinclude/help/xcoptercalchelp.htm#vrs [Cited 10 June 2022]

The other aerodynamic effect that has to be considered is the stalling of the flow at the propeller blade [10]. A propeller is essentially an airfoil, and an airfoil will stall if the angle of attack becomes too large. The higher the propeller pitch, the more prone the propeller is to stalling at low speed [11], but a pitch that is too low will result in a low thrust at high speed. For this reason, the selected propeller needs to have a balance between too high of a pitch and too low of a pitch.

Next to technical research, a market research was also performed to see what propellers N-copters with a similar mass and flight time use. The only quadcopter that was seen as relatively similar, was the DJI Matrice 100 [12] with a mass of 2.4 kg and being able to carry 1 kg. This Quadcopter used a 13x45 propeller and because DJI is a market leader in commercial drones this was used as a reference value to determine the $D_p$ and $H_p$ range that should be analysed. Eventually, it was decided to inspect propeller sizes ranging from, 10-15 inch in $D_p$ and 3-6 inch in $H_p$. This range includes smaller and bigger propellers than the DJI reference value, providing a diverse range for inspection. The choice for the pitch values is also based on propeller motor combinations available on websites, such as T-motor [13] and Mad Motor [14].

Furthermore, some 3-blade propellers were also included to investigate the possible benefits. However, it is expected that 3-blade propellers will be less efficient than 2-blade propellers [15]. The propellers in the database are from different manufacturers and also made from different materials. The material is of importance for the maximum rotations per minute the propeller can handle, as the propeller should not be subject to rpm above the limits as the propeller might break and get ejected at high velocities, possibly damaging the quadcopter. To summarise, in the database propellers are present with their diameter ($D_p$), pitch ($H_p$), amount of blades ($B_p$), aspect ratio ($A$) and the maximum rpm ($N_max$).

### 6.3.2. Propeller Modelling

With the help of the general parameters and the propeller data base, the propeller modelling can start. Equation 6.2-Equation 6.6 present all the modelling equations. These are the equations for Thrust ($T$), Torque ($M$), Thrust coefficient ($C_T$), Torque coefficient ($C_M$), and Drag coefficient ($C_d$). A list of parameters is presented in Table 6.6. The constants displayed in Table 6.6 are provided by Quan Quan (2017) and derived from matching their theoretical model with that of experimental data.

One peculiarity that should be mentioned is the aspect ratio ($A$), Quan Quan (2017) suggests to use an aspect ratio of 5 which was the product of modelling/inspecting multiple propellers. For the thrust calculations this value proved to be quite accurate and the data matched well with experimental data from motor manufacturers such as T-motor and Mad motor, see Section 6.7. However, when the torque values are inspected for an aspect ratio of 5, they are significantly higher than they should be according to experimental data.

Unfortunately, manufacturers do not provide any information about the aspect ratio of the propellers. The equation to calculate the aspect ratio is shown in Equation 6.1. The mean chord ($C_p$) was measured at 2/3 of the propeller radius. With the help of Equation 6.1 the aspect ratio was measured from images provided by the manufacturer. This method results in high inaccuracies as the accuracy with which the measurements were mm, and the measured $C_p$ was in all cases in the same order of magnitude, e.g. 8 mm. Therefore, a mismeasurement of 1 mm results in a high inaccuracy.

[11] https://aerotoolbox.com/propeller/#Engine_and_Propeller_Combination [Cited 10 June 2022]
[12] https://www.dji.com/nl/matrice100 [Cited 10 June 2022]
[13] https://store.tmotor.com/ [Cited 10 June 2022]
[14] https://www.mad-motor.com/ [Cited 10 June 2022]
[15] https://dronesgator.com/how-many-blades-for-a-drone-propeller/#:~:text=3%2Dblade%20propellers%20are%20better,we%20consider%20efficiency%20and%20portability. [Cited 10 June 2022]

**Table 6.2:** *Value and description of the constants used in the propeller modelling equations*

| Parameter | Description | Value | Parameter | Description | Value |
|---|---|---|---|---|---|
| $\eta$ [-] | Correction factor for downwash | 0.85 | $C_{fd}$ [-] | Zero-lift drag coefficient | 0.015 |
| $\lambda$ [-] | Correction factor for lift | 0.75 | $\alpha_0$ [rad] | Zero-lift angle of attack | 0 |
| $\zeta$ [-] | Correction factor for weight | 0.5 | $K_0$ [rad$^{-1}$] | Theoretical value thin wing sections | 6.11 |
| $e$ [-] | Oswald efficiency factor | 0.83 | | | |

$$A = \frac{D_p}{2C_p} \tag{6.1}$$

$$T = C_{\mathrm{T}}\rho\left(\frac{N}{60}\right)^2 D_{\mathrm{p}}^4 \tag{6.2}$$

$$M = C_{\mathrm{M}}\rho\left(\frac{N}{60}\right)^2 D_{\mathrm{p}}^5 \tag{6.3}$$

$$C_{\mathrm{T}} = 0.25\pi^3\lambda\zeta^2 B_{\mathrm{p}} K_0 \frac{\varepsilon \arctan\frac{H_{\mathrm{p}}}{\pi D_{\mathrm{p}}} - \alpha_0}{\pi A + K_0} \tag{6.4}$$

$$C_{\mathrm{M}} = \frac{1}{8A}\pi^2 C_{\mathrm{d}}\zeta^2\lambda B_{\mathrm{p}}^2 \tag{6.5}$$

$$C_{\mathrm{d}} = C_{\mathrm{fd}} + \frac{\pi A K_0^2}{e}\frac{\left(\varepsilon \arctan\frac{H_{\mathrm{p}}}{\pi D_{\mathrm{p}}} - \alpha_0\right)^2}{(\pi A + K_0)^2} \tag{6.6}$$

After all the parameters were determined, the sizing followed with equations Equation 6.2-Equation 6.6. Initially, all the propellers are tested for the required thrust per arm for hovering and the maximum thrust within the prescribed maximum rotations per minute ($N_{max}$) of the manufacturer. Most of the propellers passed this stage, especially if the pitch was higher. For these propellers, the torque at the speed ($N$) for hovering and the maximum thrust was calculated. At this stage it was decided to not go for 3-blade propellers, as the required torque for the smallest 3-blade was the highest out of all options, even the largest 2-blade propeller. In Section 6.4, an explanation will be given on the influence of required torque. For the remaining propellers, the propeller efficiency was plotted, this was done with the help of Equation 6.7, where $N$ is in rad s$^{-1}$ instead of rpm. In Figure 6.2, the most efficient propeller for each diameter size is plotted. The most efficient propeller was determined to be the APC 15x6E.

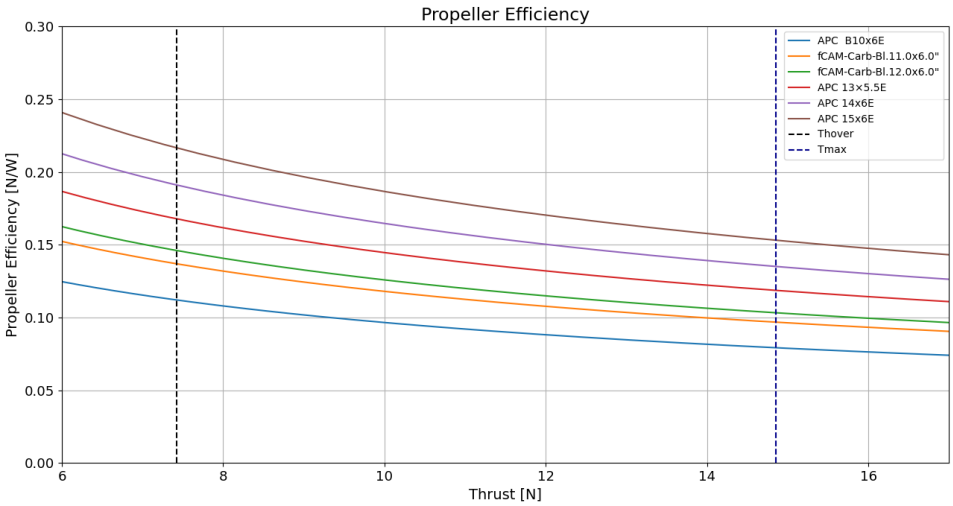


**Figure 6.2:** *Propeller efficiency vs thrust for the best propellers of each diameter size*

This method of selecting a propeller is rather unfair, as the larger the propeller is the lower the required rotational speed to generate the same amount of thrust, hence increasing the efficiency. Also, It should be noted again, that the aspect ratio has a significant impact on the final result. The aspect ratio of the 14x6E and 15x6E was checked by three individuals and all obtained an aspect ratio within a range of $\pm$ 0.3 of the assigned value. A change of this magnitude would not replace the 15x6E as the winner, but it would bring the 14x6E closer as a contender in the case where the aspect ratio would

be increased. Therefore, a look was taken at all the values in an excel sheet with conditional formatting applied to the $N$ and $M$ at hovering and maximum conditions, see Table 6.3. It was analysed that indeed there were other options that would have been just as viable, such as the APC 14x6E, but the extra added weight, ~ 30 grams in total, by the 15 inch propeller was outweighed by the fact that it performs better, even when decreasing the aspect ratio by a value of 0.3. The size of the propellers was not deemed to be to an issue, as they would be detached during transport and the overall size would stay roughly around 1 m. Furthermore, on first look it seems like the 13x5.5E would be a good compromise, but after consulting websites of motor manufacturers it became clear that the motor would mostly be running around 60% throttle to produce the required amount of thrust, making it an inefficient choice. The same holds for the other smaller propeller sizes. This is mostly due to the required rpm.

$$\eta_{prop} = \frac{T}{M \cdot N} \tag{6.7}$$

**Table 6.3:** *Value and description of the constants used in the propeller modelling equations*

| Name | Diameter [m] | Pitch [m] | Maximum Allowed RPM | Blade number [n] | Aspect Ratio |
|---|---|---|---|---|---|
| APC B10x6E | 0.254 | 0.1524 | 15000 | 2 | 6.5 |
| fCAM-Carb-Bl.11.0x6.0" | 0.2794 | 0.1524 | 13000 | 2 | 7.1 |
| fCAM-Carb-Bl.12.0x6.0" | 0.3048 | 0.1524 | 13000 | 2 | 7.1 |
| APC 13×5.5E | 0.3302 | 0.1397 | 11538.46 | 2 | 7.8 |
| APC 14x6E | 0.3556 | 0.1524 | 10714.29 | 2 | 8.1 |
| APC 15x6E | 0.381 | 0.1524 | 10000 | 2 | 8.7 |
| **Name** | **Hover RPM** | **Max Thrust RPM** | **Nominal Torque** | **Maximum Torque** | |
| APC B10x6E | 6400 | 10100 | 0.103 | 0.256 | |
| fCAM-Carb-Bl.11.0x6.0" | 5500 | 8700 | 0.0949 | 0.237 | |
| fCAM-Carb-Bl.12.0x6.0" | 4900 | 7700 | 0.105 | 0.258 | |
| APC 13×5.5E | 4500 | 7100 | 0.0970 | 0.241 | |
| APC 14x6E | 3900 | 6100 | 0.0990 | 0.249 | |
| APC 15x6E | 3500 | 5500 | 0.0992 | 0.245 | |

## 6.4. Motors and Electronic Speed Controllers

The motor is the driver for the propulsion subsystem, a propeller generates thrust but the motor provides the required RPM. The commands for the motor are given by the flight controller to the ESC. The design of the motor is explained by going into the motor selection in Subsection 6.4.1 and followed by the modelling of the motor and the selection of an ESC in Subsection 6.4.2.

### 6.4.1. Motor Selection

For the motor selection a literature study was conducted to determine what aspects to look at when selecting a motor. The main takeaways from the literature study are the type of motor and the understanding of the parameters that need to be established before calculations can be executed.

There are 3 main types of commonly used motors on UAV's. These are permanent magnet synchronous motors (PMSM), superconducting motors (SCM), and permanent magnet brushless DC motors (BLDC). From these options the BLDC is the only feasible option, because:

- The PMSM usually need to be paired with gearboxes which increases the weight significantly, and there is a problem with demagnetisation of the permanent magnets. The latter point makes the PMSM unable to output high power for an extended period of time, hence also affecting its reliability. Nevertheless, there also positive sides to the PMSM such as an increased operating temperature and power density. It also has a high efficiency and low technical risk. If the current design was for a heavier UAV, this option would be a strong contender.

- The SCM shows a lot of promise as it combines the low current loss characteristics of superconducting materials with high power density, but it is still in its theoretical phase.

On the other hand, the BLDC motor has a lower power density, but is widely used in UAV application and has the best reliability, a low noise, a compact size and it is easy to maintain.

The selected motor should be able to produce the required amount of thrust for hovering ($T_{hov}$) at approximately 50% throttle to not over-engineer the design. If the $T_{hov}$ would be achieved at much lower throttle values, it indicates that the motor is too heavy and too powerful for the current design. Important parameters to consider when selecting a motor are: the produced thrust ($T_m$), the motor current ($I_m$), the motor voltage ($U_m$), and the motor torque ($M_m$). This will become more clear later on when the motor selection for the database is explained. The final thing that was researched was the electronic speed controller (ESC). The ESC is responsible for communicating the required speed to the motors. The manufacturer always recommends an ESC for the motor that they deemed most optimal. Therefore, it has been chosen to select the ESC provided by the manufacturer. In addition, an ESC for the current design will weigh around 30 grams per ESC and it is not deemed necessary to construct a database in order to obtain a slightly lighter ESC, $\pm$ 5 grams, if the manufacturer already provides a compatible one.

With the information that a BLDC motor is the best option, websites were consulted for the available options. Initially, BLDC motors for more industrial application, such as Maxon Motor [16] and Faulhaber [17] were consulted due to the provided data about the motors, but one electronic speed controller (ESC) would weigh four times the weight of one motor required. Therefore, this option was discarded. Maxon motors also had a UAV line, but the ESC for the motor which would suite our need was not available and the weight of the available one was around 2/3 of the motor.

Attention then shifted to commercial UAV motor manufacturers. The websites that were used in the end are T-motor [18] and MAD motor [19] due to the available data about the motors, and the variety of motors for the required hovering and maximum thrust.

When selecting a motor, the experimental data provided by the manufacturer for a propeller size of 15x5 was analysed. The motors combined should be able to provide the $T_{hov}$ at around 50% throttle and before 100% throttle is reached the $T_{max}$ should be reached. Due to problems with verifying the motor modelling approach proposed by Quan Quan (2017), verification of the produced results was not possible elaborated on in Section 6.7, it was opted to not use this, but rather assess the motors on their motor efficiency. The current and voltage were acquired from the experimental data provided on the websites. The voltage stayed relatively constant, the change in voltage was usually 1 to 2 magnitudes lower than the voltage. However, the current values obtained were for a 15x5 propeller, but the propeller chosen is a 15x6. In Figure 6.3, it becomes clear that torque and current have a linear relation, thus more torque would require more current. Therefore, the current was taken where the torque required for the chosen propeller was met. In the final iteration, this resulted in a database with 8 motors, 3 from Mad motor and 5 from T-motor.

### 6.4.2. Motor Modelling

The aim of the design process for the motors is to get the best ratio of motor efficiency to weight at hovering. The motor efficiency for a thrust to weight ratio of 2.5 is also considered, but is considered less important as the quadcopter will mostly be operating at hovering conditions. The equation for

[16] https://www.maxongroup.nl/maxon/view/content/index [Cited 2 June 2022]
[17] https://www.faulhaber.com/nl/ [Cited 2 June 2022]
[18] https://www.mad-motor.com/series-motors.html [Cited 08-06-2022]
[19] https://store.tmotor.com/category.php?id=2 [Cited 08-06-2022]

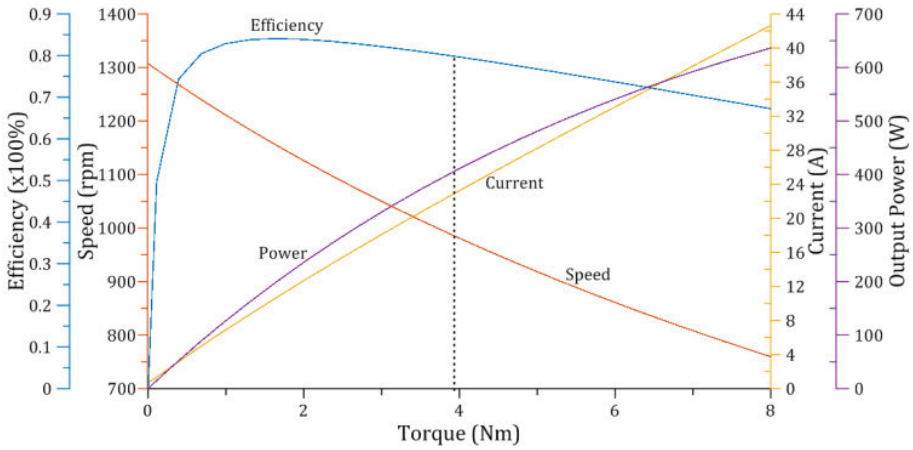


**Figure 6.3:** *Characteristic curves of a BLDC motor [32]*

the motor efficiency $\eta_m$ is given in Equation 6.8 [20]. In Equation 6.8:

- M is the motor torque in N m, which is equal to the propeller torque calculated with Equation 6.3.
- N is the motor speed in rad s$^{-1}$, which is equal to the propeller speed. The propeller speed is calculated using Equation 6.2 by filling in the thrust needed for hovering and for a thrust over weight ratio of 2.5.
- $U_m$ and $I_m$ are the motor voltage and current as explained in Subsection 6.4.1.

$$\eta_m = \frac{M \cdot N}{U_m \cdot I_m} \tag{6.8}$$

The torque and speed used for these calculations depend on the chosen propeller, which is explained in Section 6.3. To provide a certain thrust the propellers need a certain speed which requires a certain torque from the motors. The efficiency for the motors varies with the thrust they provide depending on the motor characteristics. The best option is the motor with highest efficiency over weight ratio at hovering thrust, provided that the efficiency does not drop too far under the other options for a thrust to weight ration of 2.5. The motor options are plotted for weight versus efficiency at hovering thrust and at a thrust over weight ratio of 2.5 in Figure 6.4. [21] [22]. The plot is for the final design iteration.

As can be seen in Figure 6.4 the best motor option for this quadcopter is the 'MAD Motor 4008 600KV' [23]. The motor combines a low weight with a slightly lower efficiency. It is recommended to use a 4S LiPo connection for this motot, which is another reason why this motor is a good choice in terms of weight, elaborated on in Section 6.5

The next decision to be made was which electronic speed controller (ESC) to use. The motor manufacturer has provided a recommended electronic speed controller for this motor, the 'AMPX 40A Pro (2-6S)' [24]. It was decided to use the ESC provided by the motor manufacturer. This was done because the ESC needs to be compatible with the motor and the manufacturer has the most complete information on compatibility, which is most of the time not available to the public. The most important properties of the motor and ESC are given in Table 6.4.

[20] https://www.tytorobotics.com/blogs/articles/brushless-motor-power-and-efficiency-analysis [Cited 03-06-2022]
[21] https://www.mad-motor.com/series-motors.html [Cited 08-06-2022]
[22] https://store.tmotor.com/category.php?id=2 [Cited 08-06-2022]
[23] https://www.mad-motor.com/products/madcomponents4008eee.html [Cited 08-06-2022]
[24] https://www.mad-motor.com/products/mad-ampx-esc-40a-2s-6s.html [Cited 08-06-2022]

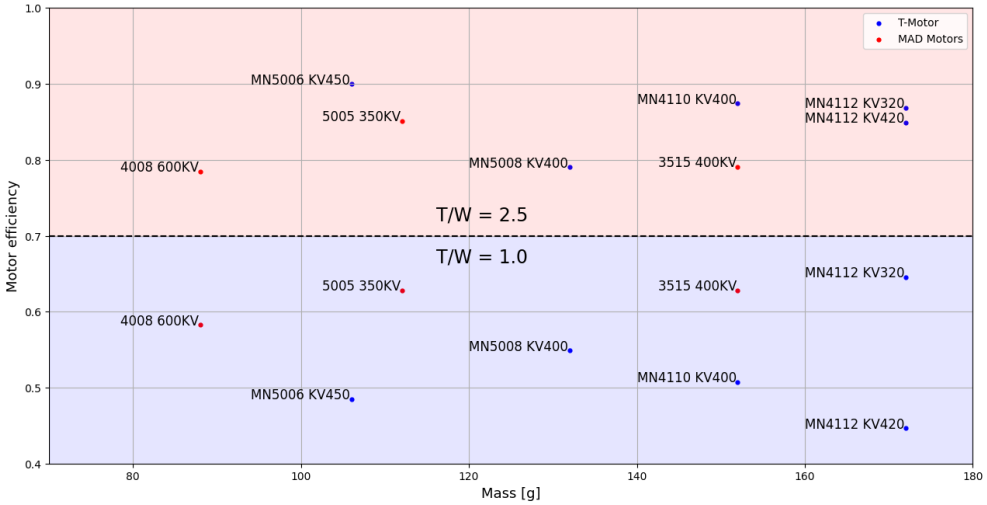


**Figure 6.4:** *Motor efficiencies for hovering and for T/W = 2.5*

**Table 6.4:** *Motor and ESC parameters*

| Motor | | | | ESC | Total |
|---|---|---|---|---|---|
| Mass | 88 g | Current at Hovering | 3.91 A | 22 g | 440 g |
| Cost | €52.89 | Current at T/W=2.5 | 12.49 A | €26.00 | €315.56 |
| Motor KV | 600 rpm/V | Voltage at Hovering | 15.95 V | | |
| Nominal Voltage | 14.8 V | Voltage at T/W=2.5 | 14.39 V | | |

## 6.5. Battery

The battery is the powerhouse of the propulsion subsystem, it provides power for the propulsion subsystem but also for the flight and scientific payload aboard the drone. In Subsection 6.5.1, a short literature study on battery types is presented. Furthermore, in Subsection 6.5.2 the battery for the emission drone is sized.

### 6.5.1. Battery Selection

There are 2 types of batteries that can be used for a quadcopter, Lithium-Ion (Li-ion) and Lithium(-Ion) Polymer (LiPo). The advantages (+) and disadvantages (-) of a lithium-ion battery are [25] [26] [27] [28]:

- (+) Lower Cost
- (+) Higher volumetric energy density
- (+) Not harder to charge over time, the so-called memory effect
- (-) Needs a battery protection circuit for safe operations
- (-) Few high discharge rate Li-ion batteries available
- (-) Highly sensitive to high temperatures, increased chance of combustion
- (-) Can not be discharged as much as LiPo batteries, less available capacity
- (-) Suffers from aging, even when discharged upto 40%

[25] https://blog.ravpower.com/2017/06/lithium-ion-vs-lithium-polymer-batteries/ [Cited 12 June 2022]
[26] https://batteryuniversity.com/article/is-lithium-ion-the-ideal-battery#:~:text=Despite%20its%20overall%20advantages%2C%20lithium,dropping%20too%20low%20on%20discharge.[Cited 12 June 2022]
[27] https://www.theengineer.co.uk/content/opinion/solving-the-problem-of-lithium-ion-battery-ageing [Cited 12 June 2022]
[28] https://www.epectec.com/batteries/cell-comparison.html [Cited 12 June 2022]

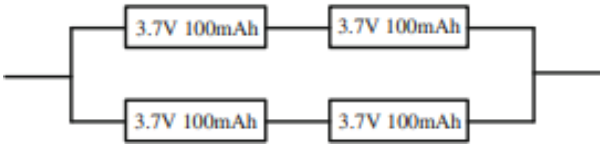


**Figure 6.5:** *Batteries connected in [25]*


**Figure 6.6:** *Batteries connected in series [25]*

The advantages (+) and disadvantages (-) of a lithium-polymer battery are [25] [28]:

- (+) Flexible, can be formed into many shapes
- (+) Reduced chance of leaking electrolyte
- (+) Can be discharged up to 15% capacity [25]
- (+) Higher Gravimetric energy density
- (+) Many available options for high discharge rate batteries
- (-) Higher cost
- (-) Increased weight
- (-) Supports Less recharge cycles
- (-) Should be charged in a safebag in case of combustion due to overcharging

The advantages and disadvantages did not display a clear winner, both options seemed equally viable. That is why an attempt was made to see if lithium-ion is actually used commercially and one drone was found, namely the DJI Matrice 30. All the other DJI Drones have a LiPo battery as the power source [29]. It is assumed that this originates from the maturity of the LiPo batteries in the UAV industry, which is also the reason for choosing a LiPo battery for the current design.

Another research point was the way the battery cells are connected with respect to each other. LiPo batteries for UAV application have a N-amount of cells connected in series and a M-amount of batteries in parallel, see Figure 6.5 and Figure 6.6, in order to obtain the capacity required [25]. In the example, 2S2P means two cells in series and two in parallel connection, each of the cells has a nominal voltage of 3.7 V and a capacity of 100 mh, resulting in a 7.4 V and 200 mh battery.

Finally, understanding the discharge rate is of high importance when selecting the battery. The equation for the discharge rate is displayed in Equation 6.9 [25] and the definition is " The steady current in amperes (A) that can be taken from a battery of defined capacity (Ah) over a defined period (h) [33]". For the design of the battery this means that the battery should be able to provide the maximum needed current, which is needed at 100% throttle. The selected motor has a $I_m$ of 21.21 A at 100% throttle for a 15x5 propeller. This value has been increased to 25 A for the current propulsion configuration. Consequently, the battery should be able to provide a current of 100 A, because each motor needs 25 A at maximum throttle. The required discharge rate can then be calculated once the required capacity is known.

$$\text{Discharge Rate (unit: } C\text{)} = \frac{\text{Current of Discharge (unit: mA)}}{\text{Capacity (unit: mAh)}}. \tag{6.9}$$

### 6.5.2. Battery Modelling

The battery is the heaviest component of the power and propulsion system. Therefore, the battery is optimised for minimal weight. However, due to the configuration of the quadcopter, it is also restricted in size. The battery should have a minimal weight while still achieving a chosen hovering time. A hovering time of 25 minutes is used, which is based on **ALEC-FVSR-ED-PERF-01** which states that a 20 minutes hovering time shall be achieved. A margin is included on top of this value to make sure it will be reached in practice. The equation for the hovering time in minutes is given in Equation 6.10 [25, p. 80]. $C_b$ is the battery capacity in $mAh$ and $C_{min}$ is the minimum capacity that is not used during operations. This minimum capacity should never be used as the LiPo battery can

[29] https://www.dji.com/nl/products/enterprise?site=insights&from=nav#drones [Cited 13 June 2022]

be damaged, reducing its lifespan. As advised by Quan Quan [25, p. 80], the minimum capacity is set at 15% of the $C_b$. To determine the battery capacity for the flight performance this value was not used yet, as the required power from the power budget of the emission quadcopter still needed to be added. Finally, $I_b$ is the battery current.

$$T_b = \frac{C_b - C_{min}}{I_b} \cdot \frac{60}{1000} \tag{6.10}$$

The battery current is calculated using Equation 6.11 [25, p. 79,80]. $n_r$ is the number of propellers, which is four in this case. $U_m$ and $I_m$ are the motor voltage and current respectively, which are given in Table 6.4. $U_b$ is the battery voltage. The battery voltage for this system is 14.8 $V$, since the motor is a 4S $(4 \cdot 3.7V)$ motor and the battery voltage should be compatible. $I_{other}$ is the current needed for other systems such as cameras. However, a power budget has been established for the emission quadcopter and this value is set to 0, so the equation will output the required battery current for the motors.

$$I_b = n_r \cdot \frac{U_m}{U_b} \cdot I_m + I_{other} \tag{6.11}$$

Equation 6.10 was rewritten to calculate the required battery capacity for a hovering time of 25 minutes. Again consulting experimental data, the required current and voltage for hovering are 14.5 V and 3.91 A for the 15x5 propeller, but looking at the required torque for the APC 15x6E and the linear relation between Figure 6.3, it is suggested that only a current draw of around 3 A would be needed. This value is not used as it does not seem realistic, instead the current at the achieved thrust for the 15x5 propeller is used with an additional margin of 0.5. This resulted in a $I_m$ of 4.8 A and the $U_m$ did not fluctuate too much, $\pm$ 0.05, and is taken at 14.5 V. In Figure 6.7, the battery capacity required for a 2S connection and higher is displayed. The 4S battery would require a battery capacity of 7859 rounded to 7900 mAh. Again, this is excluding the other subsystems and the extra margin required.

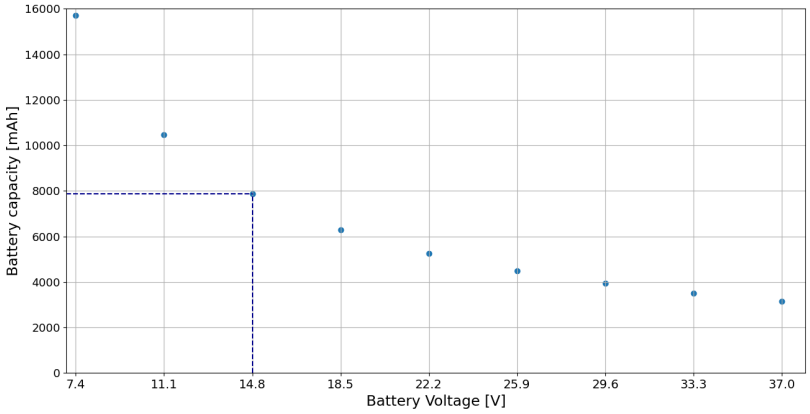


**Figure 6.7:** *Required battery capacity for the motor at a 3. 7V interval*

From the power budget it became apparent that the other subsystems would need 16.55 W to operate for a period of 25 minutes. This is translated into 470 mAh. Adding this value to the power required by the motor, the total battery capacity without margin is 8370 mAh, dividing this value by 0.85 to account for the 15% unused capacity of the LiPo battery results in a battery capacity of 9847 ~ 9850 mAh. Therefore, the quadcopter will have a battery capacity of 10000 mAh.

Coming back to the discharge rate explained in Subsection 6.5.1, the required discharge rating is 10C. This factor should be kept in mind when selecting the battery. The selected battery is "TopFuel LiPo 20C ECO-X 5000mAh 4S MTAG"[30] with a mass of 454 grams, the total mass of the batteries is then 908 grams.

At this stage the whole design iteration is finished and the other subsystems were also designed, therefore a new mass was determined. The breakdown of the mass can be found in Section 4.8. This mass was actually the final mass and a new iteration was not deemed necessary as the new mass was 3059 grams. The calculations included ample redundancies and extra margins to provide certainty that a 59 gram mass increase would still suffice, e.g. a $g$ of $10\,\mathrm{m\,s^{-2}}$ was used instead of the conventional $9.81\,\mathrm{m\,s^{-2}}$.

## 6.6. Mobile Noise Measuring System

Initially, the idea was to scale down the structure of the emission drone to get a structure for the noise drone. However, after the preliminary weight analysis for the noise drone, displayed in Table 6.5 it became apparent that the drones would have a mass relatively close to each other.

**Table 6.5:** *Preliminary mass distribution noise quadcopter without propulsion subsystem and structures*

| **Payload [g]** | | | | | | **Total [g]** |
|---|---|---|---|---|---|---|
| **Sennheiser MKE Essential** | **Raspberry Pi +SD Card** | **3000 mAh 4S LiPo** | **UGREEN Audio Card** | **Huawei E8732h-320** | **Daisy Plate** | 922 |
| 53 | 48 | 300 | 50 | 40 | 60 | |
| **Component Masses [g]** | | | | | | |
| **Flight Controller + SD Card** | **Raspberry Pi + SD Card** | **Obstacle Avoidance** | **GPS** | **Wiring + Redundancy** | **Telemetry Radio** | |
| 51 | 48 | 90 | 32 | 100 | 50 | |

The battery capacity required for continuous measurements is derived from the maximum power needed by a noise drone when standing on the ground and measuring. The maximum power needed is 6.3 W and an operating day is 8 hours, meaning that 50.4 Wh is required. Assuming that the same battery would be used as the one for the emission drone 51.2/14.8 = 3.41 Ah, rounded to 3500 mAh to include uncertainties, would be needed for a full day of operations.

After this had been established, the weight of the current propulsion subsystem and structure was added without the battery and this resulted in a mass of 1542.3 grams. For a preliminary estimation 30% of the quadcopter can be taken as an estimate of the structural mass [34]. Before this can be estimated the battery mass/capacity needed for the flight time should be determined. The noise drone will take the measurements stationary and will only use battery when flying to the location of interest. The required battery capacity was initially estimated to be around 7000 mAh, based on the knowledge acquired during the sizing of the battery for the emission drone. The mass of a 4S 7000 mAh battery is around 550 grams [31]. This results in a mass of 2074 gr, dividing this by 0.7 resulted in a mass of 2963 gr.

This was basically the mass of the emission drone. However, after a discussion the structure where the electronics are mounted for the emission drone can be used and that mass is 515 gr. So, the mass of the noise drone was estimated at 2600 gr with the current propulsion subsystem. Using the experimental data provided on Mad motor for the 4008 600 KV motor, the hovering performance is achieved around 50%. It is difficult to determine the required thrust to achieve a certain constant velocity as the drag can only be determined through CFD simulations. Therefore, an assumption

[30] https://www.hacker-motor-shop.com/Batteries-and-accessories/Battery-search/TopFuel-LiPo-20C-ECO-X-5000mAh-4S-MTAG.htm?shop=hacker_e&SessionId=&a=article&ProdNr=95000431&p=11452[Cited 13 June 2022]

[31] https://nl.banggood.com/ZOP-Power-14_8V-7000mAh-35C-4S-Lipo-Battery-T-Deans-XT60-Plug-for-RC-Car-p-1759201.html?cur_warehouse=CN&rmmds=buy[Cited 13 June 2022]

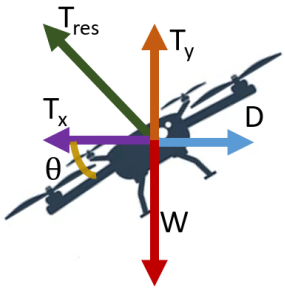


**Figure 6.8:** *Forces acting on a drone during steady flight*

will be made that the drone will be flying at 55-60% throttle in forward flight to reach the maximum distance of 2 km from the ground station. A higher throttle than for hovering is required because the weight of the drone has to be counter acted, while a component of the angled thrust vector needs to provide an horizontal component as well, see Figure 6.8.

A thrust of 8 N per arm, the approximate value produced at 55-60% throttle, results in a resultant Thrust of 24 N. It is assumed that all the motors will produce the same amount of thrust, however in reality this is not true as the drone needs to be pitched in order to obtain a tilted thrust vector. This means that the motors will be running at different throttle values. This means that some motors will use more power than others but assuming that they all produce the same thrust is a decent estimate for the average power used. Of course, the desired pitch angle has a heavy influence on the throttle settings as a larger pitch angle requires the motors to produce more thrust. For this calculation a relatively small pitch angle is assumed of 5 degrees based on results from Theys et al. [35]. For steady horizontal flight the horizontal thrust component is equal to the drag, the drag equation is displayed in Equation 6.12.

$$D = C_D \frac{1}{2} \rho V^2 S \tag{6.12}$$

The final parameters that need to be determined before the speed can be calculated are the drag coefficient and the surface area. The surface area is obtained from CATIA and is equal to 0.64 $m^2$. The drag coefficient is estimated with the derived equation provided in Section 4.9, for a pitch angle of 5°, the $C_D$ is 0.06065. Resulting in a speed of 9.379 $m\,s^{-1}$. Due to the inaccuracy of the equations and assumptions this value has been reduced to 7 m/s. This would mean that the distance is travelled in 2000/7=285.714 s ≈ 5 min in optimal conditions, this has been increased with a safety factor of 1.5 to 7.5 min. In total this means a flight time of at least 15 min is required, using the calculations explained in Section 6.5 with the voltage and ampere (5 A, 14.5) at 55%-60% throttle, again extra ampere is added to the provided value due to a different propeller, a battery capacity of 4898 ~ 5000 mAh is required for flight only, see Figure 6.9. The ampere value is based on the required torque which is approximately 0.1 N m and the experimental data. Combining the battery required for both systems a capacity of 8500 is needed for a full day of operations, including the 15% unusable capacity, results in a 10000 mAh battery. This is again the same as that of the emission drone. So, the initial assumption that the emission drone would not take as much mass was not correct due to the negligence of the 8-hour operating day without recharging.

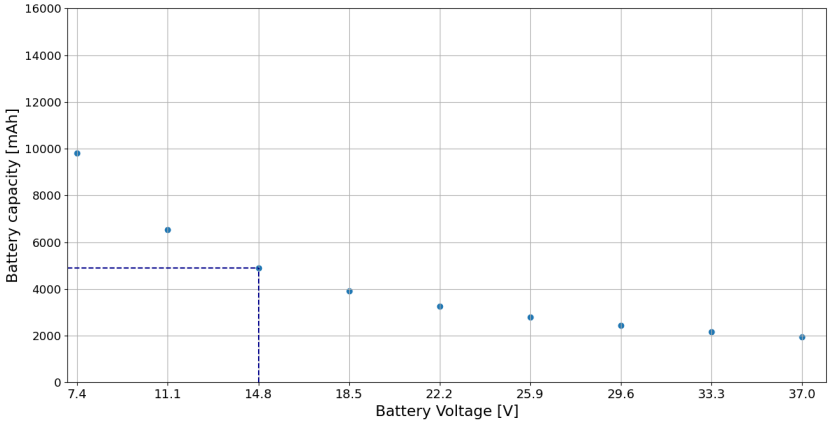


**Figure 6.9:** *Required battery capacity for the noise drone at 15 minutes flight time*

## 6.7. Verification & Validation

All the calculations and plotting in this chapter were done using python models. These models had to be verified and validated to proof the validity of the results. This was done using unit tests, and by checking the results with experimental data. The V&V is done separately for the propellers, the motors, and the batteries.

### 6.7.1. Propeller Modeling

The verification and validation will be provided for the Fluxer Pro 15x5.0 Matt[32] and the experimental data with the propeller mounted on the Mad Motor 4008 600KV [33], because this motor and propeller example have been used heavily for the design of the propulsion subsystem. The verification of the model was executed by running the code for the parameters displayed in Table 6.6. The difference between the default and the tuned values is only the aspect ratio. in Figure 6.10, a graph is provided displaying the predicted and produced thrust and torque values at different speeds. In addition, the root mean square error is provided for the default and tuned lines compared to the actual data, see Table 6.7. The equation for the RMSE can be seen in Equation 6.13, where $y_i$ is the observed value, $\hat{y}_i$ is the predicted value, $i$ is the index of summation, and $n$ is the upper limit of summation.

**Table 6.6:** *Value and description of the constants used in the propeller modelling equations*

| Constants | | | | | |
|---|---|---|---|---|---|
| **Parameter** | **Description** | **Value** | **Parameter** | **Description** | **Value** |
| $\eta$ [-] | Correction factor for downwash | 0.85 | Cfd [-] | Zero-lift drag coefficient | 0.015 |
| $\lambda$ [-] | Correction factor for lift | 0.75 | $\alpha_0$ [rad] | Zero-lift angle of attack | 0 |
| $\zeta$ [-] | Correction factor for weight | 0.5 | K0 [rad$^{-1}$] | Theoretical value thin wing sections | 6.11 |
| e [-] | Oswald efficiency factor | 0.83 | | | |
| **Variables** | | | | | |
| $A_{Th_{def}}$ [-] | Aspect Ratio Thrust Default | 5 | $A_{Th_{meas}}$ [-] | Aspect Ratio Thrust Measured | 7.5 |
| $A_{Tq_{def}}$ [-] | Aspect Ratio Torque Default | 5 | $A_{Tq_{meas}}$ [-] | Aspect Ratio Torque Measured | 7.5 |

$$\text{RMSE} = \sqrt{\frac{1}{n}\sum_{i=1}^{n}\left(y_i - \hat{y}_i\right)^2} \tag{6.13}$$

[32] https://www.mad-motor.com/products/fluxer-matt-pro-15x5in.html [Cited 16 June 2022]
[33] https://www.mad-motor.com/products/madcomponents4008eee.html [Cited 16 June 2022]

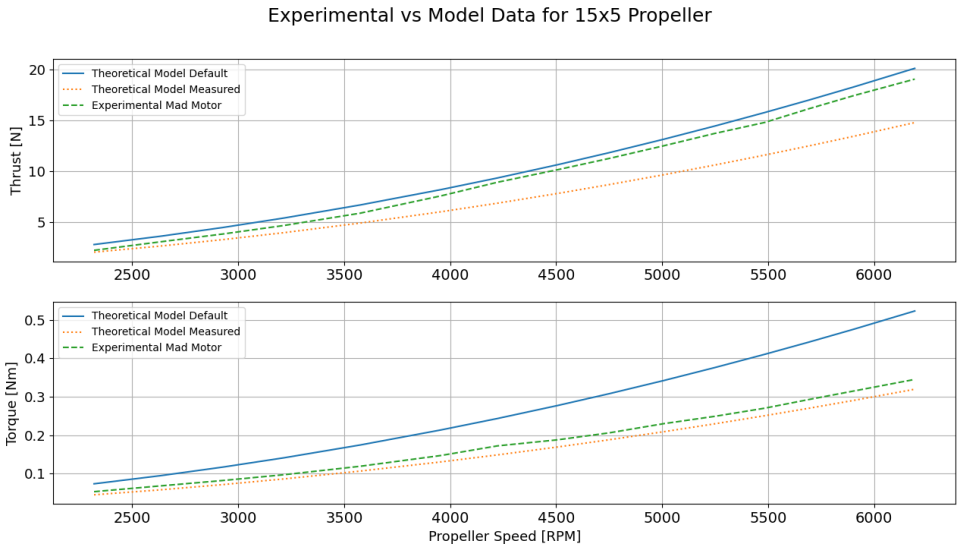


**Figure 6.10:** *Thrust and torque produced and predicted by the model for the measured and default aspect ratio*

**Table 6.7:** *The root mean squared error using a 15x5 propeller with the default and tuned models*

| | **RMSE in N** | | **RMSE in Nm** |
|---|---|---|---|
| Default Thrust Model | 0.72 | Default Torque Model | 0.104 |
| Measured Thrust Model | 2.53 | Measured Torque Model | 0.0183 |

A line in Figure 6.10 from the theoretical model has a higher accuracy if it is closer to the dashed experimental line. From this something peculiar can be noted, the thrust model has a higher accuracy for the default aspect ratio rather than the measured value and for the torque model the opposite is true. It is assumed that this is because the constants are not tuned properly for the analyzed propeller, but this can also not be done as the information is not provided by the manufacturer. The difference is not negligible as can be observed in Table 6.7, as there is an order of difference between the RMSE. Upon finding this issue, other propeller sizes were also immediately checked and it turned out that this is also the case for different propeller sizes, than the currently displayed 15x5 propeller. Therefore, it was chosen to work with an Aspect Ratio ($A$) of 5 for the thrust model and measure it for the torque model from the image provided by the manufacturer. By doing this, the accuracy of the model increased significantly and a more accurate propulsion subsystem could be designed.

### 6.7.2. Motor Modeling

The desired values to obtain from the motor modeling were the efficiencies of the motors at hovering. This was done using Equation 6.8. The torque and speed equations were verified in Subsection 6.7.1. The motor voltage and current were originally obtained using the equations given by Quan Quan [25] shown in Equation 6.14 and Equation 6.15. In these equation $K_T$ is the torque constant in $Nm/A$, $I_{m0}$ is the no-load current in $A$, $R_m$ is the internal motor resistance in , and $N_0$ is the no-load speed in $rad/s$.

$$U_m = (\frac{M}{K_T} + I_{m0}) \cdot R_m + K_T \cdot N_0 \quad (6.14) \qquad I_m = \frac{M}{K_T} + I_{m0} \quad (6.15)$$

To verify this model the model was used to solve an example problem in the Quan Quan book. The results matched the results of the book. To validate the model the values for the voltage and current were compared to experimental data provided by the motor manufacturers. The voltage and

current values for the MAD Motors '4008 600KV' using the model were 15.2 Volts and 7.52 Ampere respectively. These values were obtained using a torque of 0.99 $Nm$. The motor parameters are provided by the motor manufacturer [34]. The experimental voltage and current values for a comparable torque are 14.6 Volts and 2.89 Ampere [34]. An overview of the current and voltage values is given in Table 6.8.

**Table 6.8:** *Current and voltage comparison between model and experimental data*

| | **Model result** | **Experimental data** |
|---|---|---|
| Voltage [V] | 15.2 | 14.6 |
| Current [A] | 7.52 | 2.89 |

The values can have a slight offset, since it is not the exact same propeller, torque, and thrust. They should however be close. The value for the voltage is close enough, but the model value for the current is more than twice the experimental value. The model therefore failed the validation. Another approach was then taken to obtain the current and voltage values, namely interpolating from the experimental data to get the values for the torque and thrust required.

### 6.7.3. Battery Modeling

The battery model, that is the battery current and capacity calculations, were verified using manual calculations and calculations using other software, such as excel. Unit tests were performed on the battery current function and the battery capacity function. The tests were completed successfully.

### 6.7.4. Sensitivity Analysis

For the propulsion subsystem, a sensitivity analysis was performed to see up to what mass,the 10000 mAh battery was able to fulfil **ALEC-FVSR-ED-PERF-01** which states that at least a hovering time of 20 min shall be achieved for the emission drone. In Figure 6.11, it can be seen that the drone will still adhere to the requirement until a mass of 3.75 kg. Therefore it can be confidently said that the requirement is adhered to. Furthermore, lower masses are also included to display the increase in endurance. For this reason, the first thing that should be done in further development would be to decrease the mass of the structure as to increase the endurance.

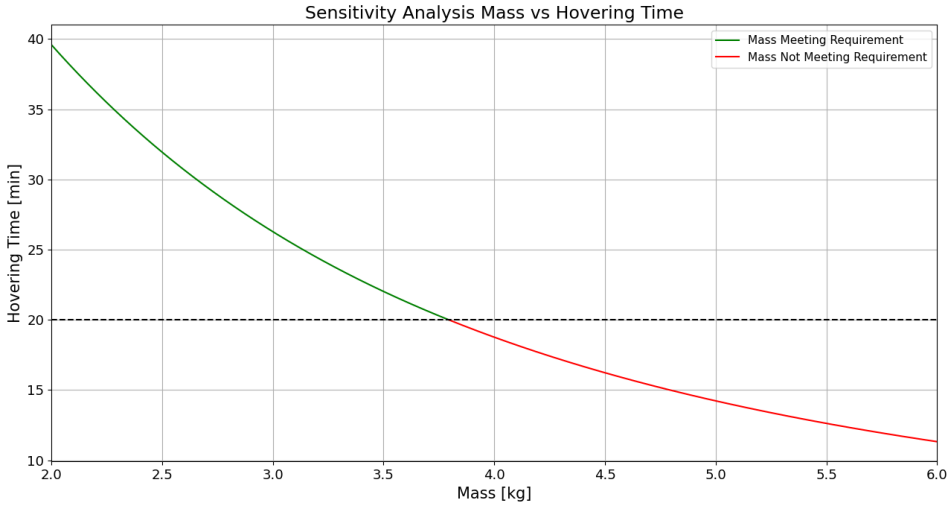


**Figure 6.11:** *The hovering time of the emission drone for different total masses*

[34] https://www.mad-motor.com/products/madcomponents4008eee.html [16-06-2022]

# 7

# Ground Station Subsystem

The ground station is another subsystem which plays a crucial supporting role for the two drone types. Furthermore, it controls the complete system and is responsible for most of the data handling. This chapter will document the design process of this particular subsystem. First, the requirements for the ground station (GS) and verification thereof will be elaborated on in Section 7.1. Then, Section 7.2 presents all the components which make up the subsystem. The operation of the GS is described in Section 7.3.

## 7.1. Requirements and Verification

Defining the requirements of the ground station aids in identifying the boundary of what the subsystem must be capable of. The requirements stem from the overall system requirements and the mission profile for the drones. The requirements and compliance of the design to the requirements are presented in Table 7.1. A ✓ indicates that the requirement has been met, ~ indicates partial compliance, and × shows that the requirement has not been met.

**Table 7.1:** *Ground station requirements and compliance*

| **Requirement ID** | **Requirement** | **Compliance** | **Comments** | Verification |
|---|---|---|---|---|
| ALEC-SR-GS-01 | The ground station shall provide the electrical charge required for 8 hours of operation for all drones in the system. | ✓ | Presented in Section 7.2 | Test - endurance shall be tested |
| **ALEC-SR-GS-02 (key)** | The ground station shall communicate with the flying vehicles at least every 1 second. | ✓ | Presented in Section 7.2 | Test - communication interval measured |
| ALEC-SR-GS-03 | The ground station shall allow the operator to order the vehicle to abort the mission at any time. | ✓ | Presented in Section 7.2 | Demonstration - operator demonstrates that it can abort mission |
| ALEC-SR-GS-04 | The ground station shall transmit the vehicle's real time flight path to airport authorities. | ✓ | Presented in Section 7.2 | Test - airport authorities test transmission |
| ALEC-SR-GS-05 | The ground station shall allow airport authorities to order the vehicle to abort the mission at any time. | ✓ | Presented in Section 7.2 | Demonstration - airport authorities demonstrate that they can abort mission |
| ALEC-SR-GS-06 | The ground station shall not be larger than 10 by 6 meters in area. | ✓ | Presented in Section 7.2 | Inspection - measure ground station |
| ALEC-SR-GS-07 | The environmental science processing subsystem shall display the processed data. | ✓ | Presented in Section 7.2 | Inspection - visually check display |
| ALEC-SR-GS-08 | The ground station shall track the position of all flying vehicles. | ✓ | Presented in Section 7.2 | Test - track all positions |
| ALEC-SR-GS-09 | The ground system shall be able to determine the locations of interest for a flight event. | ✓ | Presented in Section 7.2, elaborated in Chapter 9 | Test - test implementation of Bayesian optimisation model |
| ALEC-SR-GS-10 | The ground station shall be able to be set up in less than an hour. | ✓ | Presented in Section 7.3 | Demonstration - set up ground station |

| | | | | |
|---|---|---|---|---|
| ALEC-SR-GS-11 | The flying vehicles shall be able to land and takeoff from the ground station | ✓ | Presented in Section 7.3 | Demonstration - take-off and land flying vehicle from ground station |

## 7.2. Choosing Components

Similar to the GLS kit, the approach taken to designing the ground station is to select off-the-shelf components. As can be seen from the requirements, there are four main capabilities that the ground station must provide; charging drone batteries, communication, computing power, and an LTO (landing & take-off) platform.

### Drone Charging

As stipulated in **ALEC-SR-GS-01:**, the GS must provide sufficient electrical charge for an entire operational day. The initial approach was to utilize a large battery to provide the amount of power needed to charge the drone batteries throughout the day. However, the amount of energy required and the nominal charging speed prove it to be infeasible to charge the drone batteries at a similar rate at which they are discharged by the multiple drones. This would mean a large number of spare batteries would be required. Due to the infeasibility of this approach, the GS will have to be connected to the regular power grid through a power outlet.

For the charging of the drone batteries, a charging module with the capability to provide a large current is chosen. This is done in order to reduce the charging time of a single drone battery as much as possible. The HOTA D6 Pro[1] is theoretically capable of charging a single drone battery of 5000 mAh at 15 A within 24 minutes. For a more realistic estimate of the time required to charge from 0% to 100% it is assumed to take 30 minutes. With a flying time of approximately 25 minutes for the emission drone, it is deemed that two sets of spare batteries are required for each emission drone to allow for continuous operation of the drones. The GS must thus be capable of charging the two sets simultaneously, this means two HOTA D6 Pro are required per emission drone. To be able to connect all the charging stations simultaneously, a power strip is included. Another component included in the GS which is required for charging is a charging safe-bag. This is included for the safety of the operator. In the case that the batteries catch on fire, the bag ensures the fire does not spread and the operator is not injured. One bag is included per battery.

The noise drones have a large enough battery to operate for the entire day without charging. The batteries must be charged in between missions. Because the battery used by the noise drone is of the same type and uses the same connector, the same charging stations can be used for the noise drone batteries as well. The characteristics of the HOTA D6 Pro are listed in Table 7.2 and an image of the dock can be found in Figure 7.1.

**Table 7.2:** *Specifications charging station*

| **Characteristic** | **Value** | **Characteristic** | **Value** |
|---|---|---|---|
| Dimensions | 108 × 105 × 76 mm | Charging Current | 15 A |
| Charging Power | 2 × 325 W | Input Voltage | AC100~240V / DC 6.5~30V |

### Communication

Four communication functions are necessary for the mission. These are for commanding of the drone, receiving the measurement data, communicating with ATC, and receiving ADS-B transmission respectively. The communication system needs to both receive and deliver data to the drone.

[1] https://www.banggood.com/nl/HOTA-D6-Pro-AC-200W-DC-650W-15A+2-Dual-Channel-Lipo-Charger-With-Wireless-Charging-for-NiZ html?rmmds=detail-topright-recommendation&cur_warehouse=CN&ID=477596175626&trace_id= fb1d1654774880672 [cited 20 June 2022]


**Figure 7.1:** *Charging Station.*


**Figure 7.2:** *Landing pad*

For the commanding of the drones, a SiK Telemetry Radio V3 is included which comes with the antennas for both ends of the communication link. On the GS end, the antenna is connected through USB. Due to the use of multiple drones simultaneously, a 10 port USB hub is included.
In the case of the noise drone, transmitting measurement data is handled over the internet. The emission drone makes use of the previously mentioned SiK Telemetry Radio V3 as the measurement data has a very small bit-rate.
The communication link with ATC is necessary to allow for the airport authorities to abort the mission at any time. In this case, the drone either returns to the GS or performs an emergency landing. This communication link is realized through the internet and an online portal which the airport authorities have access to.
A Nooelec ADS-B receiver is used in order to be independent of third party open source ADS-B data providers. The data is crucial for the execution of the mission. The receiver will be placed within the GS component of the system and will thus be ensured of being in range to be able to detect the relevant aircraft.

### Computing Power

The computing power is required for running the algorithm which selects the locations for the drones to perform measurements at needs to be run by the GS component. For the system, a laptop is selected due to its mobility and low power usage. A Lenovo Thinkpad is selected since it has a capable Intel i5 CPU. The laptop will also be responsible for communicating with the airport authorities through the internet in order to report the location and destinations of the drones.

### LTO Platform

Another task of the GS is to accommodate the landing and take-off of the drones. For this to take place autonomously, the drone cameras must be aided with visual guides. For this, a foldable pad is used. An image of the landing pad can be seen in Figure 7.2. One landing pad will be included per drone in the system.

After the components have been selected a cost budget can be established. The budget is presented in Table 7.3 below.

**Table 7.3:** *GS component cost*

| Component | Price | Component | Price |
|---|---|---|---|
| Spare Batteries | 4 × €136.65 | USB 10 Port Hub | €23.96 |
| HOTA D6 Pro | 4 × €105.84 | 10 Outlet Power Strip | €12.36 |
| Leslaur Lipo Protection Bag | 8 × €5.39 | Nooelec ADS-B Antenna | €59.46 |
| LTO Platform | 6 × €20.65 | Camping Table | €16.52 |
| Lenovo Thinkpad | €668.80 | Camping Chair | €14.04 |
| **Total** | | **€1,936.14** | |

## 7.3. Operations and Logistics

The ground station consists of six LTO platforms to accommodate each drone and four charging stations which are used to charge the emission drone batteries. These can be easily stored in the two transportation vans along with the drones. One of the vans must be parked close to the the landing pads to act as the home for the charging stations. The second van will be parked at the garage that will be used when the vans are not operating. At the beginning of the mission, the LTO pads must be distributed across the available area with at least 1 meter of space in between individual LTO pads. A visualization of the top-down of the GS area can be seen in Figure 7.3. The four charging stations are connected to the power strip and placed in the trunk of the van. It is assumed all batteries are charged before arriving to the mission site. The table can be put outside and the laptop placed on it. The USB 10 port hub, ADS-B Antenna and SiK Telemetry Radio V3 are connected to the laptop. This constitutes the mission ready state of the GS. The setup of the GS takes approximately 15 minutes. Once operations finish at the end of the day, the system can be packed up and stored in the van in a similar amount of time.

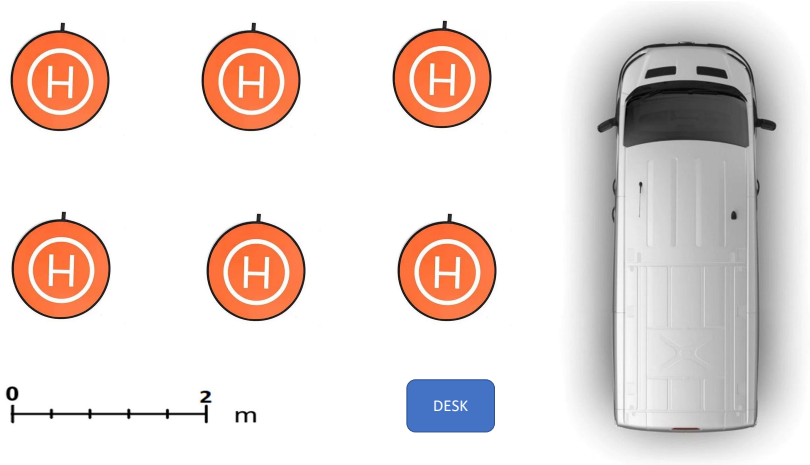


**Figure 7.3:** *The layout of the deployed GS*

# 8

# Ground Level Sensors Subsystem

One of the subsystems in ALEC is the ground level sensor (GLS). The aim of the GLS is to provide a flexible and robust audio sensing system that is capable of being deployed in a multitude of locations, particularly outside airport ground. This chapter will document the steps taken in the design process of the GLS subsystem. The chapter starts with Section 8.1, which expands on the requirements set for the GLS subsystem. Section 8.2 then offers insight on the developments of wireless acoustic sensor networks (WASNs). After this, Section 8.3 documents the trade-off performed for choosing the GLS configuration. Section 8.4 then presents the winning configuration. What follows is a description of the operations of the subsystem in Section 8.5. Finally, Section 8.6 covers some possibilities for future developments.

## 8.1. Requirements and Verification

An important step in the design phase of the GLS subsystem is determining a set of requirements. Selecting the components of the GLS is facilitated by considering a list of objectives the design needs to be able to fulfill. Many requirements also stem from the general system requirements of ALEC as a whole. This section includes the requirements and the process to verify and ensure the system is compliant, which can be found in Table 8.1. A ✓ indicates that the requirement has been met, ~ indicates partial compliance, and × shows that the requirement has not been met.

**Table 8.1:** *Ground level sensors requirements, compliance, and verification*

| Requirement ID | Requirement | Compliance | Comments | Verification |
|---|---|---|---|---|
| ALEC-SR-GLS-COM-01 | The GLS shall be capable of sending the collected data to the ground station within 1 minute. | ~ | Presented in Section 8.4, but frequency of communication not covered | Test - time communication procedure |
| ALEC-SR-GLS-COS-01 | The total cost of the GLS shall be no more than 10000 euros. | ✓ | Presented in Subsection 8.4.1, specifically in Table 8.4 | Analysis - add cost of individual components |
| ALEC-SR-GLS-DH-01 | The data collected by the GLS shall be encrypted. | ✓ | Presented in Subsection 5.6.2 | Analysis - analyse encryption of data |
| ALEC-SR-GLS-MES-01 | The GLS shall collect measurements continuously during the entire mission duration. | ✓ | Presented in Section 8.2 | Demonstration - demonstrate ability of system to continuously take measurements |
| ALEC-SR-GLS-MES-02 | The GLS shall be able to record sound at levels of 40 dB and above | ✓ | Presented in Table 8.3 | Test - compare measurements to real values |
| ALEC-SR-GLS-MES-03 | The GLS shall record sound between 20 and 20000 Hz. | ✓ | Presented in Table 8.3 | Test - compare measurements to values measured by calibrated microphone |

| | | | | |
|---|---|---|---|---|
| ALEC-SR-GLS-MES-04 | The GLS shall record sound intensity with an accuracy of ±2 dB. | ~ | Presented in Section 8.5 with unknown accuracy | Test - compare measurements to values measured by calibrated microphone |
| ALEC-SR-GLS-MES-05 | The GLS shall be able to attribute noise recorded to aviation events. | ✓ | Presented in Section 8.5 | Demonstration - demonstrate in test environment |
| ALEC-SR-GLS-STR-01 | The GLS shall have a protection rating of IP65. | ✓ | Presented in Section 8.4 | Test - test using CENELEC guidelines |
| **ALEC-SR-GLS-OPS-01 (key)** | The GLS shall be able to function without human interference for 30 days. | ✓ | Presented in Section 8.5 | Demonstration - demonstrate in test environment |
| ALEC-SR-GLS-OPS-02 | An individual GLS can be installed within 1 hour. | ✓ | Presented in Section 8.4 | Demonstration - run through installation procedure |
| ALEC-SR-GLS-OPS-03 | An individual GLS can be uninstalled within 1 hour. | ✓ | Presented in Section 8.4 | Demonstration - run through uninstallation procedure |

## 8.2. Overview of WASN Developments

Due to the large amount of ready-made options available on the market, it was deemed that designing the subsystem from scratch would not be the most efficient use of resources. Instead the hardware selection of the GLS would be carried out through a trade-off of readily available options, with the software and operational aspects of the component being designed instead. In order to make an informed decision on which system best suits the ALEC system, an overview of wireless acoustic sensor network (WASN) developments is required.

In the past fixed ground stations have been used as noise monitoring systems. However, these systems are costly and highly inflexible: the NOMOS (NOise MOnitoring System), situated around North-Holland, Netherlands, takes around 9 months to a year to set-up for a single unit according to their website[1]. The advance of Internet of Things (IOT) technology allows for the design and development of affordable wireless acoustic sensor networks (WASNs). These sensor networks are becoming cheaper and better, and have seen tremendous improvement in the past fifteen years. An overview will now be given on the development of these acoustic sensor networks, and how this will influence the GLS subsystem design. Developments show an increase in the quality and decrease in the price of microphones, enabling newer systems (such as SAFE [36], SONYC [37], GUARDIAN RFXc [2]) to send out full spectrograms at a fraction of the cost.

### Further Developments

Several projects are available focused on providing noise level data with a high spatial resolution, providing as many data points within a city as possible. Because processing data (costing in the order of picojoules/bit) is more energy efficient than transmitting data (costing several to tens of microjoules per bit) [38], these set-ups nearly always measure the full audio spectrum, and subsequently perform analysis which converts the signal of the microphone into single dB values. Often, A-weighted filtering is performed, which is a metric based on psycho-acoustic research performed

[1] https://noiselab.casper.aero/ams/#page=n_locaties_meetposten[cited 12-06-2022]
[2] https://rfcx.org/guardian Cited 21-06-2022

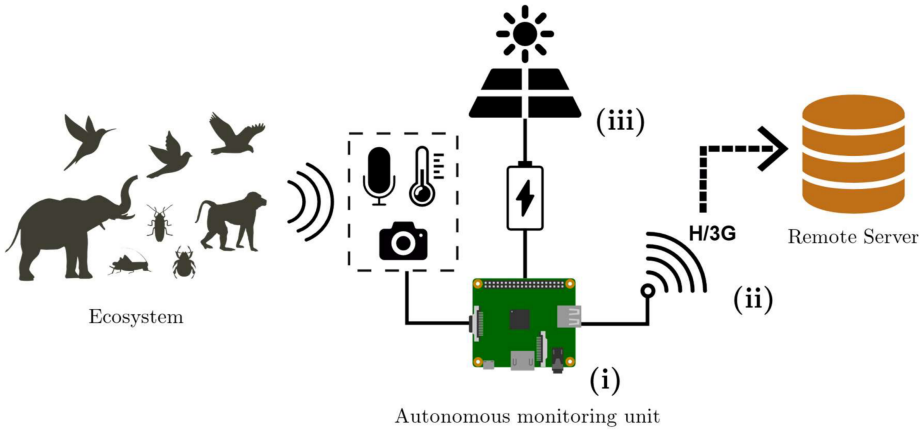


**Figure 8.1:** *Project SAFE's description of an eco-acoustic measuring system*

on humans [28]. In many projects, either time-averaged data, or maximum noise level data in certain time interval, and/or a combination of A-B-C-weighted metrics is transmitted. Examples of such projects are RUMEUR [39], MONZA [40], and DYNAMAP [41].

However, for the purpose of ALEC, to accurately capture aircraft noise and link aircraft events to noise levels within cities, a full spectrogram is greatly desired, as opposed to exclusively the equivalent noise level ($L_{eq}$) values. That being said, these projects still offer a lot of value as they show what steps researchers are currently taking in order to create monitoring networks for improving audio quality in cities.

### Spectrogram Solutions

Multiple projects exist that aim to better understand urban noise levels. However, these projects are limited in the type of audio output data. Therefore, research was conducted into whether it would be feasible to design a ground level sensor capable of transmitting full spectrograms. This was indeed possible, and is mainly covered by the field of eco-acoustics. Eco-acoustics is a branch of noise monitoring aimed at understanding sounds produced by nature, as well as monitoring external threats, such as illegal logging activities [38].

Currently, two eco-coustic projects have succeeded in creating a long-term battery-less (and thus independent) system, capable of transmitting full spectrograms of audio data [38]. Although bio-acoustics are of course not directly relevant for measuring urban noise levels caused by aircraft, some remarkable breakthroughs in science have come into fruition by applying results of one sector to another. Following this reasoning; applying the knowledge gained by the projects run into the highly variable climate of rain-forests will be of great use for designing urban monitoring systems. Below, two examples are provided of the systems providing full spectrograms which are currently in use.

The RFCx guardian is made by a nonprofit organisation which aims to detect sounds of illegal logging activities in Ecuador, Indonesia, and the Philippines. It repurposes an old Huawei smartphone, which is encased in a weatherproof box and equipped with an omnidirectional microphone, which then transmits real-time acoustic data. It uses a solar panel as built-in energy harvesting tool. The smartphone does not perform any feature extraction nor sound event detection on the edge: instead, it transmits compressed audio to a central server via cellular network typically 2G or 3G. As transmitting data costs in the order of picojoules/bit, whereass transmitting to the cellular network costs several to tens of microjoules/bit [38], the power requirements for these spectrogram providing solutions is much higher than comparable, $L_{eq}$ projects.

The next project, which will be featured as one of the selected options, is one by project SAFE. SAFE is a multidisciplinary collaboration between several faculties of the Imperial College, England. A team of several PHD's, and one professor have built a cheap, pragmatic solution, who shared their assembly procedure as well as data-processing code on Github [3]. SAFE [36], proposes to combine a large solar panel, a large deep-cycle battery, and 3G connectivity. The main difference between RFCx Guardian and SAFE is that the former operates on smartphone hardware whereas the latter operates on a Raspberry Pi computer. It should also be noted that SAFE uses a 64GB microSD card as a high-capacity buffer (200 hours of audio) in case of connectivity losses. With these differences in mind, the RFCx Guardian and SAFE both aim to fulfill a similar purpose, and does so with relatively small differences in concept.

**Figure 8.2:** *RFCx model in use*

To realise truly-autonomous monitoring, their method relies upon an existing mobile network in the study area, and access to direct sunlight for the solar power system. Despite these limitations, the system is designed with redundancy and is able to operate seamlessly over temporary inclement weather and disruptions to the mobile network. Its utility has been demonstrated in real-world ecological surveys by deploying a network of monitoring units in the challenging environment of the tropical forests of Borneo.

Full spectrograms are sent continuously when availability of the local cellular network allows so. An SD card is used to provide a buffer for instances when there is no access to the network. As the Guardian RFCx aims to provide full spectrograms at a low price, it was very similar to the requirements of the ALEC project. This is way it has been taken this extensively into consideration.

### Concluding Section

There has been a tremendous amount of development in the field of wireless acoustic sensor networks. Decades ago, there was little information available on the concentration of noise in many parts of cities. Professional, often government endorsed, enterprises were set-up in order to gain a better understanding. However, these operations often require expensive equipment, as well as permits for construction of permanent sound stations.

Then, advancements in the field of microprocessors, microphones, and transmission protocols made it possible to create affordable and effective wireless acoustic sensor networks (WASN). Further improvements allowed researchers to create systems capable of transmitting full spectrograms. This is still a relatively new, but promising field. The overview of aforementioned projects has been

[3] https://sarabsethi.github.io/autonomous_ecosystem_monitoring/ Cited on 21-06-2022

used in order to gain an understanding of current solutions researchers use to tackle a variety of noise monitoring problems.

## 8.3. Trade-off GLS Options

As previously mentioned, the subsystem was not designed from scratch. Instead, the approach was taken to investigate existing configurations which provide the capabilities which are stipulated by the requirements. Many different noise monitoring systems were found and a selection of the four most suitable options was made. A trade-off of these options was conducted and will be presented in this section. Subsection 8.3.1 presents the options which were considered. Then, Subsection 8.3.2 describes the criteria used for the trade-off. Lastly, Subsection 8.3.3 elaborates on the scores given to each option.

### 8.3.1. Description of the Design Options

Four concepts were chosen which are all less than or about 5 years old, as these were deemed to be better in terms of performance than other, older, configurations. All of them make use of current improvements in microphone quality, micro-processor capabilities, and transmission protocols. Images of the four options can be seen in Figure 8.3. The following four concepts were selected.

Option 1: the aim of Project SAFE is to create an open, low-cost, networked device which performs robust, real-time and autonomous monitoring of ecosystems. The authors provide a guide on how to build the system and also provide open-source software in a GitHub repository [42]. This project aims to capture high-quality audio files from rain-forests, but the system can be customized to other monitoring activities like videotaping. The concept is proven to work in both London, as well as the tropical climate of Borneo. The system included solutions for outages of the cellular network, days that are low in solar intensity, as well as monsoon effects.

Option 2: this project's solution uses solar power in order to act as an independent measurement node. In comparison to option 1, the researchers were aiming to answer questions on the classification of noise and advanced digital signal processing, and less so on designing a system of sensor nodes. Thus, the documentation concerning specific components is limited, as well as the documentation on the total mission profile [43].

Option 3: this option relies on a power socket and Wi-Fi in order to provide data. Its advantage is the relatively low cost, and the design of a custom casing which helps in alleviating weather effects. Its main limitations are the dependency on a domestic power supply and Wi-Fi, although researchers claim that the power supply problem will be solved for future iterations [44].

Option 4: the cheapest option. This system consists of several sensor nodes. These nodes subsequently transmit data to a central sink unit using the Zigbee protocol. This data is subsequently uploaded by the sink node to a central network. However, the allowable bandwidth of the Zigbee bandwidth is limited, allowing only single metric values to be sent (such as DB(a) or $L_{eq}$ values). Furthermore, the range of the sensors to the node is limited as well. Additionally, there is no effort made to weather-proof the nodes. Lastly, this system is dependent on a domestic power socket and Wi-Fi connectivity [45].

### 8.3.2. Selected Trade-off Criteria

The criteria chosen to include in the trade-off were hardware cost, value of recorded data, ease of installation, deployability, and level of independence. Weights between 1-4 were apportioned to each criteria based on how much the criteria affects the concept's suitability to the mission.

*Hardware cost* is relevant because it will determine the number of sensor packages which will fit in the budget of 10000 euros. This in turn determines the number of unique data points which the GLS

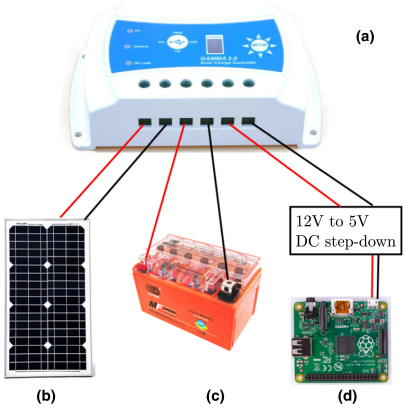


**(a)** *Option 1 [46].*

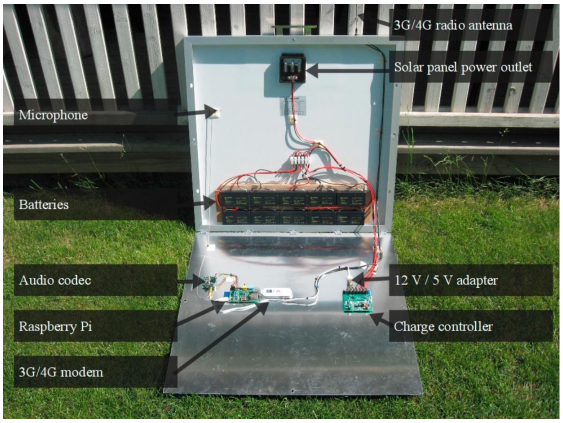


**(b)** *Option 2 [43].*

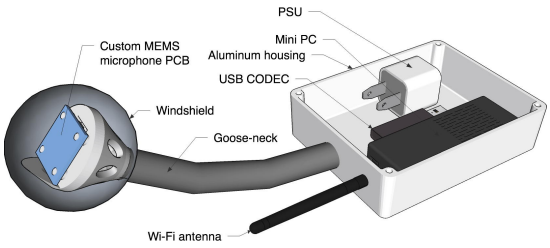


**(c)** *Option 3 [44].*

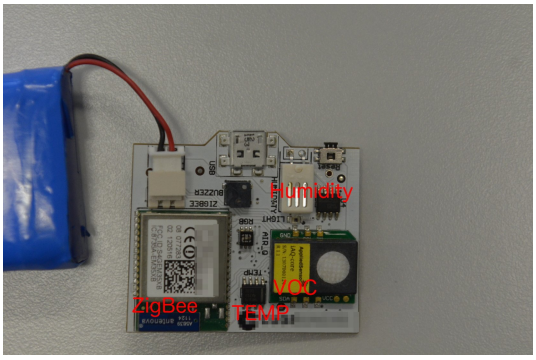


**(d)** *Option 4 [45].*

**Figure 8.3:** *Configurations considered for the trade-off*

subsystem will be able to provide. A larger number of data points leads to either having a larger area of coverage for the system or having a higher density of measurement points. These are obviously desirable qualities and thus options which have a lower unit cost will score higher. The cost criteria is given a weight of 3 as it influences the results from the experiment directly.

*Value of individual data* was given the highest weight of 4 because the aim of the project is to collect data. The actual value of the data is thus of high importance. The requirement for the mission is to provide noise levels, but this can be done to differing levels of detail. The system can be more useful for aircraft-noise researchers if more information is recorded. WASN's are currently divided into two distinct groups based on the data provided. The first includes systems that sample noise data which is then processed into $L_{eq}$ values or similar single value metrics. The second includes systems which transmit the full spectrogram of measured noise. The systems will be judged on based on whether they provide the possibility to provide a spectrogram or $L_{eq}$, and the quality of the audio in terms of bits per sample, and sampling frequency.

*Ease of installation* is the third criterion. Ease of installation is used to score the concepts on amount of effort for the installer of the system to setup the GLS system. This is an important factor since tens of GLS kits will have to be installed before the mission can begin. If the effort and thus time to install a single kit is substantial, the operational costs will rise. Factors which influence the ease of installation include the size of the kit and the options for mounting the system in place. This criterion is given a weight of 2 since it does not influence the measurement phase of the mission and thus does not affect the data collected.

*Deployability* is defined as the breadth of locations or countries the subsystem can be deployed in. This is mainly influenced by the method of communication and power delivery. Availability of communication services like Wi-Fi or 4G depend heavily on the place where the system is deployed. Similarly for power, autonomous power delivery by e.g. a solar panel is more desirable than a fixed power outlet like a domestic power socket. It is desirable for the system to have the possibility to be deployable in places where there is no external power source available or where connectivity to communication services like Wi-Fi is limited. Another consideration is the weather-robustness of the system. If a system is able to operate in harsh conditions, this is deemed desirable as well. Because the versatility of possible operating locations of the system is deemed very important, this criterion is weighted with a 4.

*Level of independence* is the last criterion that will be considered. The level of independence is defined as the possibility for the system (given its described configuration) to operate for a long time without any operator having to intervene. A system will score high if that system is reliable, robust and has a relatively low downtime. This criterion is different from deployability as this criterion looks at performance given the described operation. If the system will only work perfectly inside of a house with a reliable power and Wi-Fi supply, then the system will score high in this criterion while scoring low for deployability. Because of the perceived relative insignificance to deployability, this criterion is weighted with a 1.

Discarded Trade-Off Criteria

Two criteria, namely *looks* and *assembly complexity* were not considered in the trade-off. The assembly complexity was left out as it was deemed that all the options had fairly similar complexity. Besides this, the assembly of the system is a process which takes place once, when the operator receives the package for the first time and thus does not affect the use of the system after that. The looks of the system had to be considered for social sustainability and in order to keep one of the stakeholders; the residents in mind. People generally do not like their field of view obstructed by ugly objects. Nonetheless, the looks of the system were not considered in the trade-off as it highly dependent on the location of deployment which is not a design factor. If the GLS gets rolled out,

effort should be put towards minimizing visual nuisance caused for the environment and its local population.

### 8.3.3. Scoring

This subsection will focus on providing and explaining the scores for each option per criterion. The reasoning is provided first, after which the scores and final result are presented in Table 8.2.

Hardware Costs

Option 1 is the most expensive one at 260 EUR because of the more expensive microphone, SD card and more robust packaging. A cost breakdown per component can be found in [46]. Option 2 costs approximately 150 EUR as stated in [43]. The authors do no provide a cost breakdown per component but they just mention that the solar panel is 'the most expensive component'. The stated hardware cost of option 3 is 75 EUR [44]. Most hardware costs of option 3 are because of the relatively expensive mini pc that is used which constitutes more than 60% of the total cost. The authors also provide a cost breakdown. Option 4 is the least expensive option at approximately 20 EUR excluding the sink node. The stated hardware cost of a sensing unit is around 40 EUR but that includes a volatile organic compound (VOC) sensor of 20 EUR which is not of interest in the GLS mission. Additional to this sensing unit, a central 'sink node' is necessary to acquire data from the sensing units. This sink node consists of a Raspberry Pi and a Zigbee Communication Module (ETRX357). The cost of this sink node is assumed to be between 60 and 100 EUR. It is unclear how many nodes can be connected to a single node [45].

Value of Acquired Data

The four systems were judged based on the amount of noise data the system was able to transmit. Option 1 and 3 score the highest in this category, as they are able to send full uncompressed audio data which can be used to construct high quality spectrograms. Thus, a score of 5 is given. Option 2 is ,in its current configuration, only able to send compressed but quite complete data so it gets a relatively high score of 4. Option 4 scores lowest, as its small microprocessor is just able to calculate single values for $L_{eq}$. As $L_{eq}$ does not provide information on the respective levels of each frequency, its data does not allow for the determination of specific characteristics, such as what variables play a role on the attenuation of certain frequencies.

One remark on the quality of measured data will be made. MEMS microphones have been developed up to a point where they are superior in terms of provided quality, as well as meteorology related consistency. Because ECM show large variances in measured pressure levels when temperature, humidity, and wind velocity are varied as compared to MEMS. Thus, the configuration which allows for MEMS to be used are rated higher than those only capable of supporting ECM. However, all options seem to be capable of supporting both microphone options, and thus are rated equally in this regard.

Ease of Installation

Option 1 relies on a 30W solar panel which typically has a size around 30cm by 30cm. This introduces complexity and extra steps in the setup process. The solar panel needs to be installed in a fixed position which optimizes the angle of incidence. Option 2 is physically similar in size to the first option as it also relies on a solar panel. However, this configuration includes a larger solar panel at 60W. Such a solar panel has a size of around 60cm by 60cm. Option 3 differs from the first two in the fact that it operates without the use of solar panels. This makes the packaging of the configuration much smaller, approximately of 10cm by 20cm. It does need to be plugged in for its power supply, this means that a cable must be routed to the nearest outlet. Finally, option 4 requires a node hub and a connection to this hub. This node must be installed inside a building. Thus, access

**Table 8.2:** *Trade-off Ground Level Sensors*

| Concepts | Cost | Data Value | Installation | Deployability | Independence | Total Score |
|---|---|---|---|---|---|---|
| Option 1 | 2 (Orange) | 5 | 4 | 5 | 3 | **4.1** |
| Option 2 | 3 (Yellow) | 4 | 3 | 4 | 2 | **3.5** |
| Option 3 | 4 (Blue) | 5 | 2 | 2 | 5 | **3.5** |
| Option 4 | 5 (Green) | 1 (Red) | 1 | 1 | 4 | **2.1** |
| Weights | 3 | 4 | 2 | 4 | 1 | |

to the inside of all buildings where modules will be installed is required. This is not necessary for the other options and is very detrimental to the installation process.

Deployability
The deployability of option 1 is deemed to be very good, as they have shown in their research that even after six months they were able to reliably deploy their sensing units in a rainforest environment where temperatures ranged from 2.0 to 31.5°C with high humidity and precipitation. The system has not been tested in a very cold environment, but it can be assumed that the system performs well in almost any type of environment if it can survive in a rainforest. For environmental deployability, option 2 is much less specific on its performance results in extreme environmental conditions but the system is made for outside use and mounted inside a solar panel. This is still relatively positive, but inferior to option 1 because there are no results on robustness specified. Option 3 has an aluminium casing which is used for shielding against the elements but has also not been tested in harsh conditions. Option 4 is designed for domestic usage, so its environmental robustness is weak.

Both option 1 and 2 use a solar panel and batteries for power, and use cellular data (3G/4G) for data transmission. The fact that a solar panel is used is beneficial to the deployability of the systems as the systems are not confined to locations with existing power grids. The difference between option 1 and 2 is again the thoroughness and transparency on its respective performance. Option 2 only mentions that the battery was used "to keep the system running during the dark hours" while option 1 is specific on its up- and downtime. Cellular data is used for the data transmission in both option 1 and 2 which limits the operable locations to places where there is such a (stable) network present. Option 3 and 4 both need a regular power socket and Wi-Fi connectivity to be able to operate which massively limits the operable range and flexibility.

Level of Independence
The level of independence has been evaluated for the 4 configurations while noting that the conditions of the four configurations is completely different. Option 1 and 2 are both located in the outside environment and are dependent on solar panels which makes them relatively unreliable. Option 1 showed positive results though, with the system still working according to plan after 6 months of autonomous operations in a rain forest. Option 2 is unspecific regarding its operation conditions and downtime, thus scoring lower than option 1. Option 3 is deployed in a protected domestic environment with a power socket, which means there are very few threats to both its power supply and electronics. Both option 3 and 4 are not influenced by weather conditions thus it is expected that they will work continuously without major outages.

From the table it can be seen that option 1 achieves the highest score. This option is selected as the final configuration which will be used for the GLS kits. One of the main reasons for this choice was the availability of documentation and because option 1 is a widely used proven system.

**Table 8.3:** *Chosen microphone specifications*

| Characteristic | Value |
|---|---|
| Directionality | Omnidirectional |
| Frequency range | 20 Hz - 20 kHz |
| Signal to noise ratio | 67 dB |
| Maximum SPL | 110 dB |
| Sensitivity | -35 dB |
| Dynamic range | 83 dB |

## 8.4. Configuration

The chosen concept, project SAFE, consists of the following components. Firstly, noise is measured by use of an electret microphone; the "Rode SmartLav+" [47]. Its specific details are as follows can be found in Table 8.3.

A 12V, 10Ah deep cycle battery was used for storing energy. Thus, this battery is able to supply 120 Wh to the device. Assuming, crudely, a power usage of 3 W; 40 hours of audio data can be transmitted without external power supplied by the solar panel. As a final note; because the required input of the raspberry PI is 5V, whereas the power output of the battery is 12V, a 12V to 5V DC step down converter is needed.

The other components in the system are as follows:

- **2x15W Solar panel:** The exact type is not specified, but it is assumed that any type will do. A (slightly) larger/smaller model could be requested depending on the data availability wishes of the customer. In a low solar-irradiance areas far from the equator, a bigger solar panel can be selected to still provide sufficient power. Two solar panels are used to give the possibility to mount a microphone flush in between the 2 solar panels.
- **Solar charge controller:** Needed to regulate energy transfer from the solar panel to the battery.
- **Weatherproof box:** The project team uses a special box for keeping the electronics unaffected by the weather providing a rating of IP55. The brand that was used was DRi-Box. [4].
- **SanDisk 64GB SD card:**. As was specified by the SAFE team, a large SD card is needed for operating in regions were cellular reliability is low, such as in Borneo. For deploying the system in a more stable region, a smaller storage card is sufficient.
- **12V 10Ah DC step down converter:** this is required for the conversion of voltage.
- **Huawei E3531 3G dongle:** An antenna is needed for transmitting data.
- **Ugreen USB sound card:** While converting the analog signals to digital output can be performed on the raspberry PI, this sound card is needed in order to convert the 3.5mm output of the SmartLav+ microphone USB, as the Raspberry does not provide support for 3.5mm audio cables.
- **64GB data sim card:** A subscription to the local cellular network is bought for each sensor unit.
- **Anker powered USB hub:** the system requires two USB ports (one for the 3g dongle, and one for the audio card) while the raspberry PI A+ provides only one. Thus, an additional hub is required.
- **NEO-7M Gps Module:** GPS module that is compatible with Raspberry-Pi.

[4] http://dri-box.com/

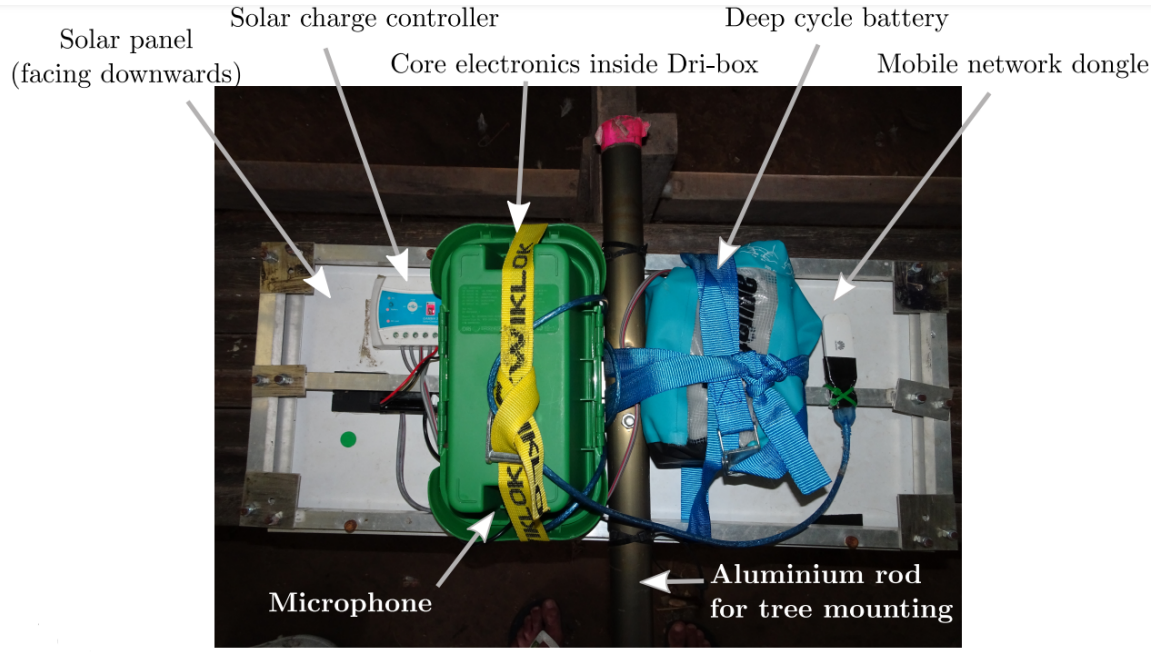


**Figure 8.4:** *Backside GLS configuration (solar panel facing downwards) [46]*

### 8.4.1. Component Configuration

As can be seen in figure Figure 8.4, all components have been placed below the solar panel. For the ALEC system, the configuration would be nearly identical. One difference would be in the method for attachment; the SAFE project added an aluminium rod for mounting the sensor unit to trees, whereas the ALEC sensor unit will operate in cities. The second difference would be the microphone location: while for the SAFE project the microphone was oriented below the solar panel (in order to capture sounds from nature), the ALEC GLS microphone should be on top of the solar panel, in order to capture aircraft noise from the sky.

A second addition to the system is a Raspberry-Pi compatible GPS location module. This was deemed necessary to be able to easily track the exact location of the system for theft prevention. An additional alteration to the original SAFE system needed to be made due to the ground effect. The ground effect is heavily influenced by the height of the microphone with respect to the ground and the incidence angle of the incoming sound [28]. Because the incoming sound of an aircraft in fly-over has a constantly changing incidence angle it was deemed to hard to create a filter that would compensate for the ground effect. Instead of trying to compensate for the ground effect in post-processing, it was chosen to mount the microphone flush in between the two solar panels and fill the gap of the solar panels with resin. This would create a hard uniform plate with a flush mounted microphone, and it is known that a flush mounted microphone causes a relative uniform 6dB increase in measured sound over the whole frequency range [28]. This mounting of the microphone means that in post-processing, just 6dB across the whole frequency range needs to be subtracted in post-processing to get to the correct audio levels. It is assumed that the surface of the two solar panels combined is large enough to make the assumption of the uniform 6dB increase due to the ground effect. Furthermore, an electret microphone was chosen. Electret microphones are shown to exhibit a high variability on results due to temperature and humidity differences [48]. It is not sure whether the *Rode Smartlav+* microphone does not show this behaviour but this should be researched in practice in future developments. Lastly, the same measurement data infrastructure as in the noise drone are used as described in Subsection 5.6.2.

**Table 8.4:** *Cost budget of GLS sensor kit*

| Component | Cost | Component | Cost |
|---|---|---|---|
| Raspberry Pi 3B | €40 | Solar charge controller | €12.86 |
| SD Card 64 GB | €8.26 | 30W solar panel | €52.74 |
| Huawei E3531 3G dongle | €24.57 | Ugreen USB audio card | €8.18 |
| Dri-box weatherproof box | €11.81 | Rode SmartLav + Electret Microphone | €51.48 |
| 12V 10Ah AGM deep-cycle battery | €28.06 | GPS | €12.39 |
| 12V to 5V DC step down converter | €7.36 | Solar Panel connector | €9.08 |
| | **Total per kit** | **€227.64** | |

A table with the cost of all components is included in Table 8.4.

## 8.5. Operations and Logistics

This section will describe the operation of the actual GLS subsystem and what this will look like. Starting with describing how these measurement points will be distributed in Subsection 8.5.1. Then, Subsection 8.5.2 discusses the calibration required for the GLS kits. The installation of the sensor network in a desired area of interest is documented in Subsection 8.5.3. Finally, Subsection 8.5.4 describes how the measurements of the GLS subsystem are performed.

### 8.5.1. Locations

The GLS is only a subsystem of the entire design. This subsystem has a specific mission which consists of various phases. The budget allocated to the GLS subsystem and the purchase price of individual units means 40 GLS kits are included in one system. This means 40 unique measurement points can be simultaneously used. The placement of these points throughout the area of interest must be considered carefully. Ultimately, the desired spatial density of measurement points is a choice to be made by the customer. Some considerations are presented in this section which should be taken into account when placing the GLS kits.

The first thing to keep in mind is that one of the methods to distinguish between aviation noise and background noise is the use of multiple sensors in a common area. The idea is that two or more of the 40 sensors have a similar distance to the aircraft throughout a large portion of the flyover. This means the sensors at a similar distance are supposed to record similar noise levels and spectrograms. In the case of local alternative noise sources, these noise levels should only be recorded at one of the sensors and thus can be filtered out. Due to this method of filtering, two individual sensors should not be placed in such close proximity that they will both record the same disturbance.

A second consideration is privacy. Seeing that the mission involves placing microphones in communities, the privacy of inhabitant should be taken into account. For this reason, a preference for placing the sensors in public spaces should be maintained.

Based on these considerations, an example of how the GLS kits could be deployed for operating a mission from Schiphol runway 18R for arrivals and 36L for departures can be seen in Figure 8.5. Each star represents a cluster of closely placed GLS kits. As mentioned, placing two GLS kits near each other is done to aid in filtering out disturbance noise sources other than aviation pollution. The placement is more concentrated near inhabited areas near the approach and departure paths in attempt to provide information most relevant to communities.

### 8.5.2. Calibration

It is necessary to carefully calibrate the microphone of every GLS before the operation starts. The calibration should be performed in an isolated lab environment. The chosen calibration option is to mount an already calibrated high-quality reference microphone directly next to the microphone

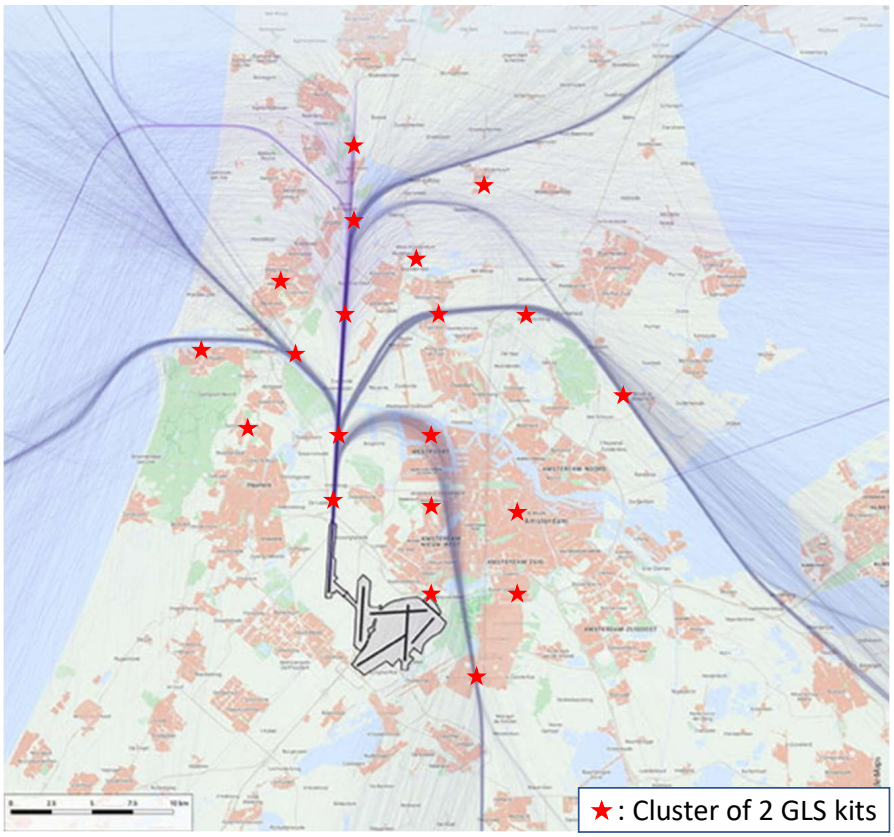


**Figure 8.5:** *Example placement of GLS kits for observing Schiphol runway 18R arrivals and 36L departures* [5]

that is used in the GLS. It is assumed that the reference microphone has a flat frequency response over the full spectrum. Sound is then played with the swept sine technique which is a known sound sequence in the full frequency spectrum. The response of the reference microphone is then compared to the microphone of the GLS. When the difference is known, an inverse of the difference between the GLS microphone and the reference will be constructed into a filter, used to compensate the frequency response deficiencies of the GLS microphone. Another additional procedure is to use a piston phone or other type of device that outputs a sound wave at an exactly known SPL level. This gives the opportunity to calibrate the exact sensitivity of the microphone. In Figure 8.6 the frequency response as provided by the microphone manufacturer is given [47]. It shows an almost perfectly flat frequency response between 30Hz and 3.5kHz. This graph will be validated with the procedure of the frequency response with the swept sine technique. This process shall take one working day for all the kits.

### 8.5.3. Installation

After the desired location for a sensor is determined and the GLS are calibrated, they can be deployed. The methods applied for the calibration are presented in Subsection 8.5.2. A specific mounting point must be found. The chosen GLS kit design has high flexibility in the possible installation locations, however, the solar panel is exposed to sun as much as possible. As can be seen in Figure 8.4, there is an aluminum rod which can be used as the attachment point for the installation in the case where the system needs to be attached to a vertical pole or a tree. Alternatively, when there is a flat surface available and there is a guarantee that the system will not be interfered with, the kit can also just be placed without a fixed attachment point. As is stipulated by the requirements, an individual kit can be installed within one hour. With two operators independently installing the kits, three to five working days are dedicated to installing the 40 GLS kits.

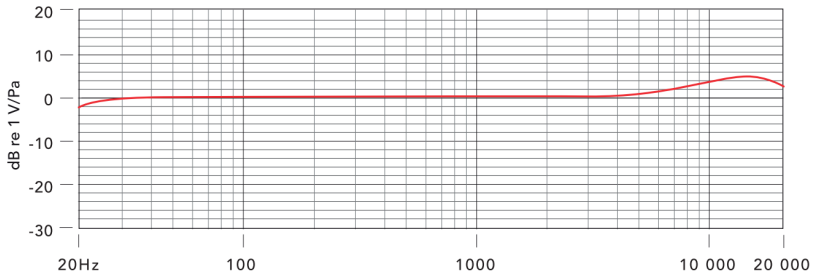


**Figure 8.6:** *Factory given frequency response of Smartlav+ microphone as used in the GLS [47]*

### 8.5.4. Measurements

Once the kits have been installed the measurements are performed. Although the kits have the capability to constantly record and transmit the data, doing this would significantly shorten the battery life. In order to extend it, GLS will not transmit measurement data constantly. Instead, the operator is able to set a fixed threshold dB level, under which the GLS kit will not transmit the data. This level will vary heavily depending on the location in which the kit is placed. In a city street, the background noise level will be much higher than at a farm house. For this reason, the operator has to set these levels accordingly. As stipulated by the requirements, the noise data accumulated must be attributable to specific aviation events. For this, filtering of alternative noise sources must be performed. The GLS incorporates three methods to achieve this goal. Firstly, multiple sensors are dispatched in the same area to filter out loud outlier noise sources, as described in detail in Subsection 8.5.3. Secondly, the time signal is recorded and transmitted to the ground station so that the spectrograms can be analysed to identify the specific aircraft, since each produces a unique spectrum. The third is the use of ADS-B. By obtaining the altitude and location of an aircraft during the fly-over, another layer of confirmation can be gained. Once the measurement is performed, the data is sent to the server through mobile internet connection.

### 8.5.5. Final Phase

Once the mission is completed, the GLS kits are retrieved by the operator. The requirement of being able to operate without human intervention for at least a month stipulates the achievable performance of the GLS kits. The duration of the mission for the GLS kits is also a variable which can be determined by the customer. After the mission duration has elapsed, the kits can be retrieved. A similar requirement for the time to uninstall a kit of one hour is stipulated. This means the same two working days is dedicated to the termination phase of the GLS mission. As the kits are exposed to the outside environment for an extended period of time, the GLS need to be thoroughly but carefully cleaned after pick-up to ensure its correct future operations.

## 8.6. Future Improvements

Investigations show that for several research projects, use is made of a very low-cost processing unit, going for as low as 2 euros [49]. Compared to a raspberry PI, this is a significant reduction in price. Secondly, investigations would be performed into "multi-hopping" techniques, which allow for more efficient data transmission by making use of the benefit of certain low-power local transmission options. Thirdly, the effects of temperature, humidity, wind velocity, and time on the effectiveness of the sensors would be studied. As shown in [48], ECM type of microphones show great variability depending on these parameters. While less affected, MEMS microphones also show excursion effects. Fourthly, to study the effects of weather effects on frequency attenuation, a temperature and humidity sensor could be added to the sensor nodes. Lastly, more research would be conducted into the details of transmission.

# 9

# Model Generation & Sampling

The ultimate goal for designing ALEC is to autonomously perform measurements concerning emissions and noise pollution due to aviation, both near the runways and in near-airports communities, and producing environmental metrics, according to the mission requirement **ALEC-MR-08**. Regarding the near runway operations of the system, the noise and emissions drones have to autonomously collect measurements, as it follows from **ALEC-UR-AUT-01**. The present chapter offers an overview on the problem the team had to tackle, the mathematical tools employed, as well as the results of the experiments performed. Concretely, the chapter presents an overview of the autonomous data sampling and model generations problems in Section 9.1, and briefly introduces the theoretical aspects employed in tackling these problems in Section 9.2. Some results motivating the approaches used are discussed in Section 9.3. The data handling is discussed in Section 9.4 while the model verification procedures are presented in Section 9.5.

## 9.1. Problem Description

For every aircraft event measurement conditions change such that the location to maximises information about the event changes: for example, a change in wind direction influencing the direction of the aircraft exhaust or additional information obtained from a previous sample. The problem faced by developing an effective sampling and model generation model can be formulated as: given the ability to sample different points in a restricted spatial domain and a history of previous samples, what is the optimal approach in deciding the next measurement position. In order to satisfy mission requirement **ALEC-MR-08**, the information provided by the measurements has to be processed in order to derive an environmental metric for both the noise and emissions pollution.

### 9.1.1. Data Sampling

The goal of data sampling is to decide the best locations to be sampled next, given the history of already performed samples, such that the confidence on the predictions generated by the data increase as much as possible, in order to generate an accurate model of the pollution and noise as fast as possible, while the energy used to perform the measurements is as low as possible. As the energy available for the drones is limited, a sampling strategy has to be carefully decided upon.

For deciding the locations of data sampling, three main approaches were considered: grid search, random sampling and intelligent decision making. All three methods have their own advantages and weak points especially given that over time, with a sufficiently large database all three methods converge to the same predictions. However, the main difference between the sample strategies is their rate of convergence: as the ALEC product is envisioned as a service provided to airports to generate emissions and pollution models, a significant goal of the system is to generate these models as quickly as possible which leads to the importance of selecting meaningful sampling locations to understand the underlying phenomena.

Grid search refers to discretising the search domain into a meshgrid and sampling sequentially all the mesh points, using heuristics based on simple physical models. The main advantage of this approach is its simplicity, however, it requires a large number of measurements in order to be able to predict an accurate model. Moreover, it is expected that a high level of redundancy will be present in the data at the end of the measurements if this technique is employed which makes the method unfeasible for the ALEC system.

Random sampling refers to randomly choosing points to sample in the searching domain, which was considered unfeasible due to the high complexity of the problem. Finally, an intelligent decision making approach refers to using statistical learning methods in order to determine the location of the next sampling point; due to the changing environment of aircraft events, such as wind, humidity, and incoming aircraft type there are conditions which make it advantageous to intelligently select sample location as to optimise the information obtained. Consequently, this latter method has been selected for both emission and noise drones of ALEC.

Figure 9.1 offers an overview on the Design Option Tree (DOT) of the possible techniques. A red cell indicates an option considered unsuitable, a white cell indicates an option theoretically possible, while a green cell indicates a method considered appropriate for the problem at hand. Regarding the nodes on the second layer of depth in the DOT, the justification for the categories they are included into are:

- **Regression algorithms** are suitable for the problem at hand as they are able to produce predictions even for new data, as well as some algorithms are able to infer probability distributions. Moreover, regression algorithms are useful to fit complex functions using the collected data as training data.
- **Classification algorithms** are considered unfeasible for the model sampling as the number of classes for the dimension positions needed is unreasonably high to be able to generate meaningful predictions, due to the large spatial dimensions involved in the problem.
- **Clustering algorithms** is considered an unsuitable approach due to the large number of categories needed to produce meaningful predictions. Moreover, this class of algorithms usually suffers from the "curse of dimensionality", and the problem at hand involves a relatively large number of variables.
- **Dimensionality reduction algorithms** might be useful to be employed after the database is constructed in order to remove redundant dimensions, however the new dimensions might not have physical meaning and would render the interpretability of the data gathered much more difficult and therefore it was not considered suitable to perform it at this step.

It is to be noted that all the aforementioned techniques might be useful in later stages, when the pollution and noise database is already constructed in order to be used by scientists working on developing more sophisticated models. However, the previous discussion concerned itself solely with the use of the algorithms for sample location proposal and initial model generation.

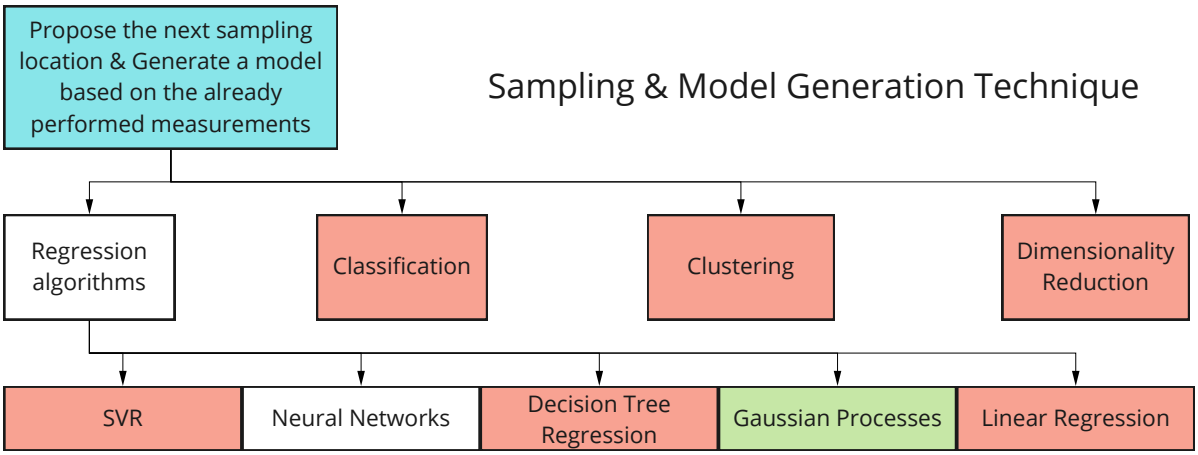


**Figure 9.1:** *Design Option Tree for Sampling & Model generation*

Regarding the possible regression algorithms, the following options are identified and listed below,

along with a short discussion regarding their suitability for the problem at hand:

- **State Vector Regression** are considered unfeasible due to their poor performance when dealing with noisy data, which will inherently be produced by the measurements performed. Moreover, they are a parametric method and require precise knowledge about the shape of the functions to be fitted.
- **Neural Networks (NN)** are a very flexible method which are useful in numerous contexts, however for the current mission it is considered it might not be the most suitable, as they require a large amount of data and their training takes a significant amount of time. As it is desired to provide real time information about the models, this aspect is considered a drawback for the NN methods.
- **Decision Tree Regression** are considered unsuitable mainly due to their tendency to overfit data, their inherent weakness when dealing with continous data and especially due to their instability, i.e. producing wildly different outputs when provided with slightly different inputs, due to the inherent noise in the collected samples.
- **Gaussian Processes Regression** Gaussian Processes is a stochastic process where every linear combination of its variables is normally distributed. They are well suited for a variety of problems due to their non-parametric nature and ability to deal with noisy data while quantifying uncertainty. Additionally, they have high computationally simplicity [50].
- **Linear Regression** is considered unfeasible as it only associates values to predictions and it does not offer any information whatsoever regarding its confidence in the predictions it generates, which hinders the software to achieve its goal of sampling such that the confidence of the predictions of the model improves.

Reviewing the available options for the model generation, Gaussian Process Regression has been selected due to their ability to quickly generate a model which is needed for the near-real time generation of the total environmental metric. Additionally, Bayesian Optimisation, a sampling strategy often combined with Gaussian Processes, has been selected as a suitable approach for the problem. As the sample location has to be chosen in between aircraft events, an algorithm with low computational cost needs to be implement, a requirement which Bayesian Optimisation fulfills. More details on the theoretical background of the method are presented in Subsection 9.2.1. As a note, using Stochastic Gradient Descent (SGD) as an optimiser is considered unfeasible in the current context, due to the high complexity of both the noise and emissions environmental functions. Thus, obtaining accurate data regarding the first derivatives of these functions, which are required as an input for SGD methods, is considered unobtainable, especially when possible noise when sampling is taken into account.

### 9.1.2. Model Generation

Justification for the need of theoretical models in the context of the ALEC is twofold: firstly, as it will be explained further in Section 9.2, Bayesian Optimisation needs an a priori model as an initial guess of the black box objective function, which should be as close as possible to the real function in order to ensure fast convergence. Secondly, due to the lack of three dimensional real data collected for near-runways experiments, the verification for the techniques employed were using fabricated data based on a theoretical model in order to test the correctness and the speed of convergence of the software, as well as the accuracy of the system. It is reasoned that, even though much simpler than the real environmental function, if the software fails to emit reasonable predictions on the fabricated data, its performance when deployed is going to be unsatisfactory. Moreover, it is expected that the real predictions will have a lower accuracy than the test's accuracy, but the test accuracy is useful to serve as an upper bound of the performance of the system.

For the emissions model, desired properties of the model are: it should be a reasonable approxi-

mation of the shape of an aircraft jet exhaust's plume's concentration of pollutants, it should take into account the effect of a moving source, and it should take into account the effect of wind on the plume - which of special interest as otherwise the system might sample points with no plume whatsoever. The noise model should produce the $dB$ levels of noise and take into account the ground effect.

## 9.2. Theoretical Aspects

After deciding upon using certain mathematical tools to model the problem at hand, a thorough understanding of the theoretical concept is required in order to ensure sound decision are made during the modelling process. The current section presents a brief overview of Gaussian Processes, Bayesian Optimisation as well as some details regarding their implementation, such as the acquisition function used. Furthermore, the models used as a base for the a priori kernels for noise and emissions, as well as during verification, are discussed.

### 9.2.1. Bayesian Optimisation

Bayesian Optimisation is a machine learning technique used to maximise knowledge about a black-box model while using a minimum number of samples [51]. It is best used when the function is costly to analyse and possibly noisy, such as the phenomena monitored by the ALEC system. This is due to the time, energy, and opportunity cost of sampling the aircraft event at a certain location rather than another, and the noise associated with the measurements by the sensors for both the noise and emissions drone. If performing the measurements were cheap to evaluate in terms of energy used, it would be possible to use a grid search or random sample, but the cost of each measurement motivates the choice of evaluating the optimal sample locations for each aircraft event. Bayesian Optimisation is an iterative process with two main components, an estimate of the function, better known as the surrogate function, and an acquisition function used to select the optimal location to sample [52]. The acquisition function is usually dependent on the surrogate function. The Bayesian Optimisation process illustrated in Figure 9.2, where an initial estimate of the model and an acquisition function are generated using previous observations, and subsequently the next sample is taken at the maxima of the acquisition function. This sample is then added to the posterior which is used to update the surrogate and acquisition function, after which the the sampling process can be repeated as often as desired. For ALEC, a significant benefit of Bayesian Optimisation is that the algorithm is constantly developing a best estimate of aircraft pollution while determining the subsequent sample location.

Within Bayesian Optimisation, Gaussian Process are commonly used to calculate the surrogate function. A Gaussian Process (GP) Regression is a non-parametric method which infers a distribution based on sampled data and quantifies the uncertainty of the predictions. A GP relies on a multivariate Gaussian distribution which describes the surrogate function [54], the fit of the objective function $\mathbf{f}$, i.e. the emissions or noise function. A GP therefore can be fully described by a mean vector $\mu$ and a covariance matrix $K$, also known as a kernel, which can be seen as a similarity metric between points in the domain space. Prior knowledge of the measured system can be incorporated by selecting a kernel which approximates the expected distribution of results. Proper kernel selection ensures faster rates of convergence for the model, as well as minimises unwanted numerical phenomena, such as un-physical oscillations of the surrogate function, caused by the GP which tries to fit the sample points.

Gaussian processes have a very powerful property, namely they are able to update their a priori distribution based on new training data. More formally, given a training dataset with values $f$ at inputs $X$, a GP prior can be updated to a GP posterior $p(\mathbf{f}_* \mid \mathbf{X}_*, \mathbf{X}, \mathbf{f})$, which can be used for predictions

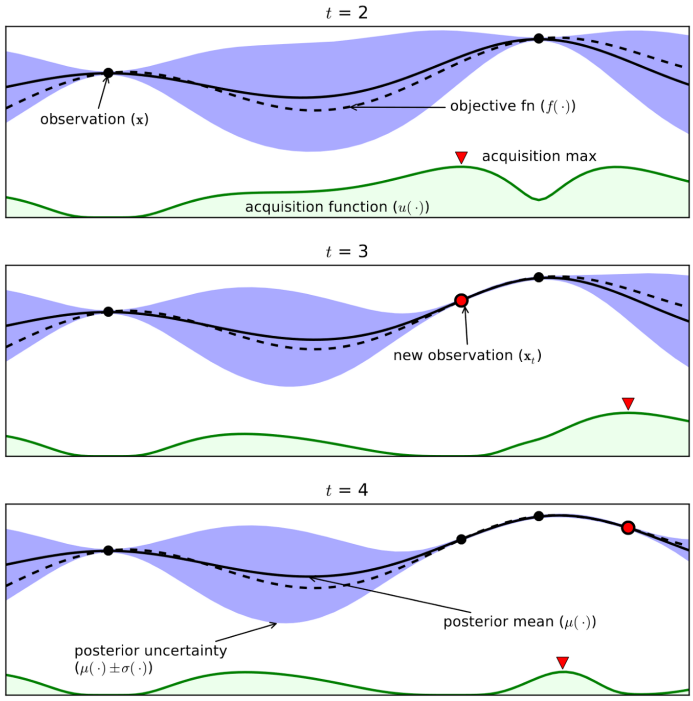


**Figure 9.2:** *Gaussian Processes and Bayesian Optimisation algorithms, in the case of noise-free sampling of a generic function [53]*

$\mathbf{f}_*$ corresponding to new inputs $\mathbf{X}_*$. From the definition of a GP, the joint distribution of observed values and predictions is a Gaussian of the form:

$$\begin{pmatrix} \mathbf{f} \\ \mathbf{f}_* \end{pmatrix} \sim \mathcal{N}\left(\mathbf{0}, \begin{pmatrix} \mathbf{K} & \mathbf{K}_* \\ \mathbf{K}_*^T & \mathbf{K}_{**} \end{pmatrix}\right) \tag{9.1}$$

With $\mathbf{K}_* = \kappa(\mathbf{X}, \mathbf{X}_*)$ and $\mathbf{K}_{**} = \kappa(\mathbf{X}_*, \mathbf{X}_*)$. Moreover, using standard rules for conditioning Gaussians, the predictive distribution is given by:

$$\begin{aligned} p(\mathbf{f}_* \mid \mathbf{X}_*, \mathbf{X}, \mathbf{f}) &= \mathcal{N}\left(\mathbf{f}_* \mid \boldsymbol{\mu}_*, \boldsymbol{\Sigma}_*\right) \\ \boldsymbol{\mu}_* &= \mathbf{K}_*^T \mathbf{K}^{-1} \mathbf{f} \\ \boldsymbol{\Sigma}_* &= \mathbf{K}_{**} - \mathbf{K}_*^T \mathbf{K}^{-1} \mathbf{K}_* \end{aligned} \tag{9.2}$$

The specific kernels selected for the emissions and noise model will be based on a prior understanding of the distribution of the natural phenomena and will be explained in the sections describing on the respective models in Subsection 9.2.5 and Subsection 9.2.6. When selecting a kernel, there are certain parameters known hyper parameters that are used to control the learning process of the algorithm. Using optimal hyper-parameters, the kernel is structure is adapted in an optimal representation of the sampled data. The optimal set of hyper parameters $\boldsymbol{\theta}^*$ is found by maximising the log marginal likelihood (LML) goal function [55]:

$$\boldsymbol{\theta}^* = \max_\theta \mathrm{LML}(y, X, \theta) \tag{9.3}$$

With:

$$LML(y, X, \theta) = -\frac{1}{2} y^T K_X^{-1} y - \frac{1}{2} \log \| K_X \| - \frac{n}{2} \log 2\pi \tag{9.4}$$

### 9.2.2. Acquisition Function

A key component of Bayesian Optimisation is the acquisition function which is used to determine the next location to sample. This is especially important for the drones in the ALEC system, as each sample can be considered costly in terms of time, power, and opportunity cost, of carrying out each measurement. By balancing the exploitation of knowledge obtained by already evaluated locations and the exploration of areas with high uncertainty, the acquisition function is key to balance the exploitation-exploration trade-off and maximise the knowledge obtained from each sample. Additional consideration in this trade-off needs to be conducted for environmental monitoring as it is desirable to be more accurate in areas with higher concentration of pollutants rather than those in lower concentration [55]. Before selecting the location to sample, the model has to generate an acquisition function considering the predicted value, uncertainty, and cost of sampling at each location and subsequently select the position which maximise the value of the acquisition function. Depending on the type of drone, the acquisition function needs to be evaluated for the concentration of multiple types of gasses or for the magnitude of an individual noise metric ($dB$) which motivates an acquisition of form:

$$\alpha(x) = c(\boldsymbol{x}, \boldsymbol{x}^{-}) + \sum_{i=1}^{N} \alpha_i(x), \tag{9.5}$$

where the overall acquisition function $\alpha$ is composed of the cost of evaluating the new proposed location $\boldsymbol{x}$ considering the last sampled location $\boldsymbol{x}^{-}$ with cost function $c$, and the sum of a separate acquisition function $\alpha_i$ for each variable being tracked in the samples. The advantage of this method is that the cost $c$ and benefit $\alpha_i$ are decoupled from each other and can therefore can be assessed separately: this can assist in the eventual parallelisation of the program and is useful when analysing scientific research on acquisition functions for Bayesian Optimisation, which is mostly based on the benefit $\alpha_i$ [56].

Commonly used acquisition functions [57] include:

- Probability of Improvement:

$$\begin{aligned} \alpha_{PI}(\mathbf{x}) &= P\left(f(\mathbf{x}) \leq f\left(\mathbf{x}^{+}\right) + \xi\right) \\ &= \Phi\left(\frac{\mu(\mathbf{x}) - g\left(\mathbf{x}^{+}\right) - \xi}{\sigma(\mathbf{x})}\right), \end{aligned} \tag{9.6}$$

  The Probability of Improvement (PI) is one of the earliest proposed acquisition functions and estimates the probability that a sample at a new location $\mathbf{x}$ is greater than the largest observed value $f(\mathbf{x}^{+})$. Function $\mu$ is the estimate of the surrogate function, function $g(\mathbf{x}^{+})$ is the highest value of the posterior, $\sigma(\mathbf{x})$ is the variance, variable $\xi$ is an exploration-exploitation tuning parameter, and $\Phi$ is the normal cumulative distribution function. However, PI has been shown to not choose solutions from a Pareto Optimal trade-off between exploration and exploitation, which may account for the poor empirical performance of the acquisition function [56]. For this reason, the function has not been selected for the Bayesian Optimisation model of the ALEC.

- Expected Improvement:

$$\alpha_{EI}(\mathbf{x}) = \sigma(\mathbf{x})[Z\Phi(Z) + \phi(Z)] \tag{9.7}$$

  where

$$Z = \frac{\mu(\mathbf{x}) - g\left(\mathbf{x}^{+}\right) - \xi}{\sigma(\mathbf{x})}, \tag{9.8}$$

where variable $\phi$ is the normal probability distribution function. Expected Improvement (EI) is a commonly used acquisition function due to its guarantee to converge to a global optimum under certain conditions [56]. Additionally, the location selected belongs to the Pareto set maximally trading-off exploration and exploitation. However, the function is slow at finding the global optimum as only points close to the current best point have high expected improvement and therefore requires a relatively exhaustive search around a local optima before changing measurement location [58]. Some authors have propose a Weighted Expected Improvement which can help balance the exploitation-exploration trade-off although the function prioritises Pareto dominated solutions. Overall, this has resulted in the EI function not being viable for the model.

- Upper Confidence Bound

$$\alpha_{UCB}(\mathbf{x}) = \mu(\mathbf{x}) + \xi\sigma(\mathbf{x}), \tag{9.9}$$

An intuitive acquisition function is the Upper Confidence Bound (UCB) which overestimates the mean by adding uncertainty multiplied by an exploration-exploitative variable $\xi$. UCB selects samples from a Pareto non-dominated location although it may converge to a local optima too quickly, which leads to the recommendation of occasionally selecting a purely explorative sample. A considerable advantage of the UCB acquisition function is that it is an effective exploratory metric while the previously mentioned functions are better suited for obtaining the global maximum of the function. For emissions and noise modelling, the global maxima is already known to be located at the aircraft, whereas for the models developed by ALEC the overall distribution of the pollutants are of interest. Overall, the Upper Confidence Bound has been identified as an effective acquisition function for the model and has already been used in Bayesian Optimisation frameworks for environmental modelling [55].

Cost function $c$ is determined as to optimise the energy usage of the drone: reducing the energy consumption leads to a longer time during which the UAV is capable of carrying out its mission and a proportionally larger up time of the system during which measurements are able to be carried out. The cost function for the drone is then done by considering the energy consumption through equation:

$$c(\boldsymbol{x}, \boldsymbol{x}^{-}) = t_{move}P_{move} + t_{hover}P_{hover} = \frac{d(\boldsymbol{x}, \boldsymbol{x}^{-})}{v_{drone}}P_{move} + \left(t_a - \frac{d(\boldsymbol{x}, \boldsymbol{x}^{-})}{v_{drone}}\right)P_{hover}. \tag{9.10}$$

In total, the equation considers the total power consumed in-between aircraft events with time $t_a$. As the time spent moving $t_{move}$ during this period increases, the time spent hovering $t_{hover}$ decreases, leading to the cost function being divided between the power consumed while moving from one location $P_{move}$ to the other and the power used while hovering $P_{hover}$. This is done by considering the velocity at which the drone moves $v_{drone}$ and the distance of the minimum path between the last sampled location $\boldsymbol{x}^{-}$ and location $\boldsymbol{x}$ based on the domain further explained in Subsection 9.2.3. Combining the proposed cost-benefit acquisition function from Equation 9.5 with Equation 9.9 and cost function Equation 9.10 results in the selected acquisition function:

$$\alpha(x) = \gamma\frac{c(\boldsymbol{x}, \boldsymbol{x}^{-})}{\|c(\boldsymbol{x}, \boldsymbol{x}^{-})\|} + \sum_{i=1}^{N}\frac{u_i\left(\mu_i(\mathbf{x}) + \xi\sigma_i(\mathbf{x})\right)}{\|\mu_i(\mathbf{x}) + \xi\sigma_i(\mathbf{x})\|}. \tag{9.11}$$

Both the cost and benefit components of the acquisition function have been normalised to facilitate comparison between the two, with the cost multiplied by a cost variable $\gamma$ which can be used to select the ratio of importance between the two components when computing the acquisition function. However, the energy cost of each measurement is only of importance for the emissions drone while for the noise drone $\gamma = 0$; this is because the noise drone has only enough power to land at

the location of interest and is not designed to change measurement position before returning to the ground station. Therefore, the location is only selected based on the benefit offered by sampling at the position and energy cost is not considered. The exploration-exploitative variable $\xi$ and cost variable $\gamma$ are parameters which are difficult to optimise and are based on specific properties of the drone, such as power consumption and velocity, and airport characteristics, such as runway length and measurable area. Consequently, these parameters are recommended to be tuned throughout the operations of the system.

Weighting factor $u_i$ is selected according to the weightings determined in the total environmental metric described in Chapter 3; as a goal of the measurements made by the ALEC system is to calculate this total environmental metric for each aircraft event, it is useful to prioritise the location of measurements which can help optimise the accuracy of metric. However, NO and $O_3$ were not considered within the metric, and consequently the acquisition function will not be evaluated using those gasses despite them being measured and estimated throughout the operations of the emission drone. Additionally, the noise drone is measuring only one value, resulting in the weighting factor being equal to 1.

### 9.2.3. Domain Constraints

As it follows from the user requirement **ALEC-UR-SAR-02** and mission requirement **ALEC-MR-03**, ALEC's activity should not interfere with the airport operations, which poses restrictions on the domain where the noise and emission drones are allowed to operate. Moreover, additional constraints are imposed before the model is run, as, the farther from their source are, the emissions tend to diffuse in the atmosphere and their concentrations might not be detectable by the sensors. Given the exploratory nature of the acquisition function used, as described in Subsection 9.2.2, the Bayesian optimisation would tend to explore the entirety of the domain, and therefore some limits on the domain's extension have to be set in order to ensure reasonable mapping times and avoid measuring null values of pollution - as the sensors have limited accuracy. The limits of the domain the drones are sampling is defined in Section 4.10.

The effect of the geocaging on the modelling algorithm is two-fold: firstly, it is not possible to sample outside the permitted domain, even though the GP would try to infere values in the prohibited areas and, secondly, as the drones were not allowed to pass through the restricted areas the distance computation metric between two points in the domain, as used by the acquisition function, is modified. The modified metric relies on the Euclidean distance metric and the distance $d$ between two points $A$ and $B$ in the Cartesian space belonging to the set of allowed points $\mathscr{S}$ is defined as follows:

- 1. If a straight line which passes exclusively through points is set $\mathscr{S}$ can be drawn between $A$ and $B$, then $d$ is the Euclidian distance between $A$ and $B$.
- 2. If condition 1. is false, then the distance is computed as the shortest distance which passes exclusively through $S$, which in the case of rectangular restricted domain, the shortest path corresponds to a line from $A$ to the closest reachable (in a straight line) corner of the restricted domain, and from there it will try recursively to reach point $B$ using the described method.

The pseudocode of the algorithm described previously is shown in Algorithm 1.

### 9.2.4. Parallelisation

In the design of the ALEC system, multiple drones are employed to minimise the time required to obtain an accurate model of the emissions and noise generated by aircraft events. For a single drone, maximising the acquisition function is a straightforward process but for multiple drones a simultaneous sampling strategy needs to be selected to optimise the overall return of the acquisition

**Algorithm 1** Modified Minimum Distance DISTANCE(A,B,C,D)

**Require:** Coordinates for points $A$ and $B$, the domain $\mathscr{D}$ and the list of constraints $\mathscr{C}$
  **if** ISSTRAIGHTLINE(A,B) == TRUE **then**
    **return** EUCLIDIANDISTANCE(A,B)
  **else**
    $FRC \leftarrow$ FARTHESTREACHABLECORNER(A)
    **return** EUCLIDIANDISTANCE(A,FRC) + DISTANCE(FRC,B,C,D)
  **end if**

function. When selecting a sample location for a drone, it is expected that the acquisition rate for the other drones change at the same time resulting in an overall acquisition function dependent on the sample location of each individual drone. A combined true optimal solution can be highly computationally expensive to obtain, but the system needs to be able to compute these locations fast enough to provide the drones with enough time to relocate before the next aircraft event occurs. Wang et al. propose [59] an infinitesimal perturbation analysis to construct a stochastic gradient estimator to optimise the multi-points expected improvement of the sample but as the posterior distribution of the Gaussian process is to be recalculated at each step, the process is expected to be too computationally expensive and not practical .

To overcome this limitation, a greedy alternative of the Synchronous Thompson Sampling (synTS) method was developed by the team. While the conventional method waits for all workers to finish and then simultaneously re-deploys all workers at their respective maxima, this simultaneous approach was not optimal for the mission design due to the limitations explained above [60]. Instead, an algorithm was designed such that it assigns a location to the drone with the highest individual acquisition rate, and then adds the expected value for the location of this sample to a dummy posterior, initially equal with the actual posterior. This process is repeated using the dummy posterior until all idle workers are assigned a location to sample. When this process is complete, the drones will then move to their assigned location and conduct the real sample, which will be then added to the real history of samples. While this process is not optimal, it provides the computational cost to conduct this calculates in real-time. Furthermore, due to the nature of the experiments performed, namely the measurements are collected through the entirety of an aircraft event, the idle times are not going to be significant as the workers will finish their work approximately at the same time. Thus, it is expected that the overall idle times will not be significant compared to the total operational times. The pseudo-code of the algorithm is presented in Algorithm 2, along with several explanatory comments:

**Algorithm 2** Greedy Synchronous Parallel Thompson Sampling SYNTS($\mathscr{GP}$)

**Require:** Prior GP $GP(0,\kappa)$
  $D_1 \leftarrow \varnothing$, $GP_1 \leftarrow GP(0,\kappa)$
  **for** i = 1,2,... **do**
    $D_{i,1} \leftarrow D_i$ ▷ Generate dummy domain
    $GP_{i,1} \leftarrow GP_i$ ▷ Generate dummy GP
    $A_i \leftarrow \varnothing$
    Wait until all n workers are idle
    **for** j = 1,2,...n **do**
      $B_1 \leftarrow \varnothing$
      **for** each idle worker with index k **do**
        Sample $g \sim GP_{i,j}$ ▷ Generate acquisition function from dummy domain
      **end for**
      $x_k \leftarrow \text{argmax}_{x\in\chi} g(x)$ ▷ Determine best location for each worker
      $B_{j+1} \leftarrow B_j \cup (x_k)$ ▷ Save best location for each worker
      $w \leftarrow \text{argmax}_{x_k\in B_j} x_k$ ▷ Select winning worker index
      $x_j \leftarrow \max_{x_k\in B_j} x_k$ ▷ Select winning location
      $A_i \leftarrow A_i \cup x_j$ ▷ Save winning location
      $D_{i,j+1} \leftarrow D_{i,j} \cup \{x_j, E(x_j)\}$ ▷ Add expected value to dummy domain
      $GP_{i,j+1} \leftarrow GP_{i,j}(\mu_{D_{i,j+1}}, \kappa_{D_{i,j+1}})$ ▷ Update dummy domain
      Move worker $w$ to $x_j$ and set as busy
    **end for**
    $y_n \leftarrow$ Query $f$ for all $x_n \in A_i$ ▷ Query real function
    $D_{i+1} \leftarrow D_i \cup \{(x_1, x_2, ..., x_n), (y_1, y_2, ..., y_n)\}$ ▷ Update real domain
    $GP_{i+1} \leftarrow GP_i(\mu_{D_{i+1}}, \kappa_{D_{i+1}})$ ▷ Update real posterior
  **end for**

### 9.2.5. Emissions Model

Modelling emissions through Gaussian process regression requires a prior understanding of the aircraft plume to obtain a quicker convergence for the model. Although, aircraft plumes have a highly complex behaviour dependent on multiple variables, such as wind, temperature, and chemical interaction, a relatively simple prior model needs to be analysed to derive a kernel for the Gaussian process. The Gaussian Plume Model is considered a suitable prior model due to its simplicity - and therefore its fairly low computational cost - and previous application in the modelling of aircraft emissions [61]. The classical Gaussian plume model for a specific concentration is as follows:

$$C_{con}(x,y,z) = \frac{Q_{con}}{2\pi u \sigma_y \sigma_z} \exp\left(-\frac{y^2}{2\sigma_y^2}\right)\left[\exp\left(-\frac{(z-H)^2}{2\sigma_z^2}\right) + \exp\left(-\frac{(z+H)^2}{2\sigma_z^2}\right)\right], \tag{9.12}$$

where $Q$ is the intensity of the concentration source located at the origin of the Cartesian plane, $u$ is the sum of the vertical wind and emission velocity, $\sigma_y$, $\sigma_z$ is the horizontal and vertical standard deviations, $H$ is the height of the source, and $x, y, z$ are the sample location. Equation 9.12 takes into account the effect of the ground on the ground: namely, the second term represents an imaginary source situated symmetrically to the ground with respect to the real source. Although the Gaussian Plume model suffers from a number of drawbacks such as it not considering the chemical phenomena of the plume, the rise due to difference in temperature between the exhaust and the environment, and the effect of the wind, it is computationally efficient and takes into account fundamental physical mechanism such as the conservation of mass and, thus was rendered suitable to serve as an a priori for the Bayesian Optimisation. Due to the Gaussian distribution of the plume,

it was observed to be similar to the radial basis function (RBF) kernel, the kernel most commonly used for GPs:

$$\kappa\left(\mathbf{x}_i,\mathbf{x}_j\right)=\sigma_f^2\exp\left(-\frac{1}{2l^2}\left(\mathbf{x}_i-\mathbf{x}_j\right)^T\left(\mathbf{x}_i-\mathbf{x}_j\right)\right) \tag{9.13}$$

The advantage of using a Gaussian kernel function is that due to the properties of GPs, the posterior distribution is also guaranteed Gaussian [62]. Even if the true distribution of the emissions of the plume are not Gaussian the estimate offered by the kernel are expected to help the model converge faster than without a kernel. However, the standard model is insufficient due to the simplicity of the model, which led to a more sophisticated version being employed, as it also accounts for external wind velocity and a moving source [63].

$$\begin{aligned}C_{con,t}(x,x_0,y,y_0,z,z_0,t)=&\frac{Q}{(2\pi)^{3/2}\sigma_x\sigma_y\sigma_z}\mathrm{e}^{-\left((x-x_0)u-(y-y_0)v-(u^2+v^2)(t-t_0)\right)^2/2\sigma_x^2(u^2+v^2)}\\&\cdot\mathrm{e}^{-\left((x-x_0)v+(y-y_0)u\right)^2/2\sigma_y^2(u^2+v^2)}\left(\mathrm{e}^{-(z-(z_0+h))^2/2\sigma_z^2}+\mathrm{e}^{-(z-(z_0+h)+2H)^2/2\sigma_z^2}\right)\end{aligned} \tag{9.14}$$

Where $t$ is time, $t_0$ is the emission time, $Q$ the intensity of the source, $u$, $v$ the wind velocity components, $\sigma_x$, $\sigma_y$, $\sigma_z$ the horizontal and vertical standard deviations, $H$ the mixing layer height, $x_0$, $y_0$, $z_0$ the source coordinates, $h$ the effective stack height. Furthermore, the emissions are calculated based on an instantaneous emission of source, which means that an estimate for the total concentration measured by a receiver at $x,y,z$ at time $t$ with time step $\Delta t$ by a moving source with time dependent location $x_{0,t},y_{0,t},z_{0,t}$ is:

$$C_{con}(x,y,z,t)=\sum_{i=1}^{N}C_{con,t}(x,x_{0,N\Delta t},y,y_{0,N\Delta t},z,z_{0,N\Delta t},t-N\Delta t) \tag{9.15}$$

Parameters $\sigma_y$ and $\sigma_z$ are crucial for Gaussian models, but no analytical expressions are available. Semi-empirical estimates, as described in [64] are used instead:

$$\sigma_x=Ax(1+Bx)^C,\sigma_y=Dx(1+Ex)^F,\sigma_z=Gx(1+Hx)^I \tag{9.16}$$

Where $x$ represents the horizontal distance from the source, and $A$, $B$, $C$, $D$, $E$, $F$, $G$, $H$, $J$ and $I$ are coefficients depending on the atmospheric conditions. According to [64], for moderate values of wind, i.e. higher than $6m/s$, in urban conditions and moderate or slight solar radiation, the value of coefficient in Equation 9.17 are: $A=E0.16$, $B=F=0.0004$, $C=G=-0.5$, $D=H=0.14$ ,$J=0.0003$, $I=-0.5$. Therefore the equation can be rewritten as:

$$\sigma_x=0.16x(1+0.0004x)^{-0.5},\sigma_y=0.16x(1+0.0004x)^{-0.5},\sigma_z=0.14x(1+0.0003x)^{-0.5} \tag{9.17}$$

Gas concentration measured by the emission drone will be dependent on a variety of directly measurable factors such as position of measurement $x,y,z$, the wind-speed $w_{speed}$, wind direction $w_{dir}$, aircraft velocity $A_v$, aircraft position $A_{3D}$, $A_{thrust}$ (which will be further explained in Subsection 9.2.6, aircraft type $A_{type}$, aircraft event $A_{event}$, aircraft origin/destination $A_{od}$, estimated aircraft thrust, airliner $A_{company}$, environmental temperature $T$, and environmental humidity $\phi$. Some of these parameters, such as aircraft type, event, and airliner represent a non-continuous characteristic of the underlying phenomena and will be difficult to represent using a Gaussian process. Consequently, a separate Gaussian process needs to be assigned to each of these combinations. Furthermore, for brevity of notation the continuous parameters will be noted under variable

$\boldsymbol{A}_e = \{w_{speed}, w_{dir}, A_v, A_{3D}, A_{thrust}, T, \phi\}$. It is important to track these values as they can help obtain a better understanding of the variables which influence the measurements and reduce the uncertainty in the estimates. However, as more and more variables are tracked, the size of the design space increases exponentially, which is known as the curse of dimensionality in machine learning. Based on the power of the computational system used with GLS and amount of data collected, it is recommended to start with a limited dimensionality of $\boldsymbol{A}_e$ and later scaling the amount of variables considered within the Gaussian Process, or by employing sparse matrix methods [65]. Additionally, the measurements obtained by the sensors are concentrations of each pollutant over time during the aircraft event, leading to the state space matrix of each measurement $X(t)$ and output of system $Y(y)$ as:

$$X(t) = \begin{bmatrix} x & y & z & t & Ae \end{bmatrix}^T \quad (9.18) \qquad Y(t) = \begin{bmatrix} C_{VOC}(t) & C_{CO}(t) & \dots & C_{PM2.5}(t) \end{bmatrix}^T \quad (9.19)$$

The order in which actions will be carried out by the emission drone for the sampling strategy of the emission model are included in Figure 9.3. Before the acquisition function can be determined, prior knowledge of the upcoming aircraft event needs to be obtained: this includes certain information related to the aircraft event which are known before the events such as aircraft type, aircraft origin/destination, wind direction, and so on. This is then used by the acquisition function to determine the best location to sample from the already available information. In block 3, the drone will select the location corresponding to the global maxima of the acquisition function and move there to prepare to take the sample.

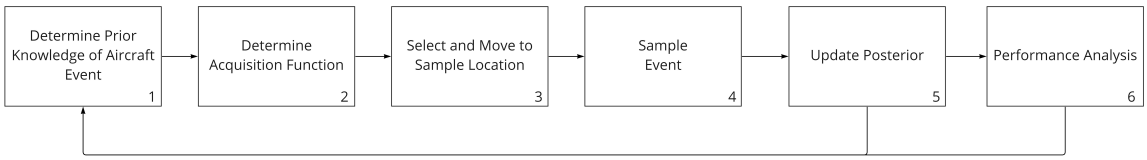


**Figure 9.3:** *Emissions Model Sample Strategy*

After the aircraft event has been observed, the results of the sensor measurements can be saved and further elements of the aircraft event can be tracked. These include important factors such as the aircraft speed, aircraft thrust, and aircraft position which are key to estimating the total pollution emitted by the event but are only possible to track after the observations. Finally, the values of the state space and output of the system can be used to update the Gaussian process posterior. This process is then repeated for as long as required, after which the performance analysis of the whole process can be conducted. This is where the measurements and uncertainty of the model can be analysed by the operator, and the exploration-exploitative variable and cost variable of the acquisition function can be accordingly tuned.

### 9.2.6. Noise Model

For modelling noise emissions the following equation is employed. It models an aircraft event fly over the observed sound pressure level as a function of horizontal distance $r$, direct path $r_1$, and frequency $f$:

$$SPL(r,f) = PWL - 10.8 - 20log(r_1) + \alpha(f)r_1 + \Delta SPL_G(r,f) \quad (9.20)$$

with $\alpha(f)$ the attenuation for each frequency and $\Delta SPL_G(r,f)$ as the ground effect. The formula considers the environmental impact of a homogeneous atmosphere where there are no temperature or wind gradients. It is also assumed that the source moves slow enough that the Doppler effect can be neglected [28]. Nonetheless, even having built the priori model with these assumptions,

it is expected that over time the model is capable of developing an understanding of the relation between these variables. As effective sound pressure decreases quadratically with distance from the source, the kernel used as the basis for the noise GP is the quadratic rational kernel:

$$k_{\mathrm{RQ}}\left(x, x'\right) = \sigma^2 \left(1 + \frac{\left(x - x'\right)^2}{2\alpha\ell^2}\right)^{-\alpha}. \tag{9.21}$$

The optimal values of $\alpha$, $\sigma$ and $l$ are found by maximising Equation 9.4 [66]. RBF kernel was not employed as it rendered worse predictions than the Quadratic Kernel for smaller number of data points. For larger amounts of data points both kernels predicted very similar functions as the GP updates its predictions based on the new training data, and in time, abandons its initial beliefs. Thus using Rational Quadratic Kernel ensures a faster convergence. An example of the GP with Bayesian Optimisation fitting the noise model can be seen in Figure 9.4. A simulation for the noise produced by an aircraft passing at a minimum distance of $d = 100m$ from the noise drones is passing by is fitted and the results plotted.

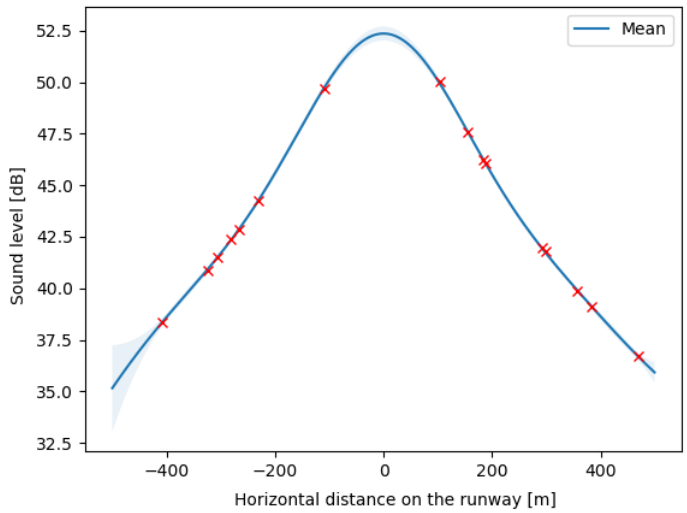


**Figure 9.4:** *Noise model function fitted using GP based on Rational Quadratic Kernel, for a larger number of samples, i.e. 16 training data points*

As the noise drone will be measuring the spectrum of noise in SPL, the state space matrix $X(t)$ of each measurement will be the same as for the emissions drone, but the output of the system will be the measured SPL in dB per frequency over time:

$$Y(t) = \left[SPL(f, t)\right] \tag{9.22}$$

The results of the noise models can also be used to estimate the thrust during the aircraft event, which can help significantly improve the atmospheric pollution estimate of the emission drone [67]. Considering the Doppler effect, which is caused by the relative motion of the source with respect to the observer, the observed frequency $f'$ can be used to calculate the emitted frequency $f$:

$$f' = \frac{f}{1 - \|M\| \cos(\theta)}, \tag{9.23}$$

where $M$ is the Mach number velocity and $\theta$ is the angle between the relative position of of the source with respect to its velocity and the observer. The fundamental frequency of the sound $f_1$ can then be used to calculate the fan rotational speed of the blades $n$, i.e. $f_1 = \frac{Bn}{60}$ with $B$ as the number of blades.

Finally, the fan percentage speed $N1\% = 100n/n_{max}$ is calculated considering the maximum fan rotational speed $n_{max}$ which is then used to calculate the estimated net thrust per engine in pounds force $F_n$ with:

$$F_n = \delta\left(E_0 + F_0 V_C + G_A h + G_B h^2 + HT + K_3\left(\frac{N1\%}{\sqrt{\theta_T}}\right) + K_4\left(\frac{N1\%}{\sqrt{\theta_T}}\right)^2\right), \tag{9.24}$$

where $\delta$ is the ratio of the ambient air pressure at the aircraft altitude to the standard air pressure at sea level, $V_C$ is the airspeed in knots, $h$ is the aircraft altitude in feet, $T$ is the atmospheric temperature at the aircraft in $C^\circ$. $\theta_T$ is the ratio of of the absolute total temperature at the engine inlet to the standard air temperature at mean sea level The constants $K_3$ and $K_4$ are derived from engine data for the $N1\%$, and the variables $E_0$, $F_0$, $G_A$, $G_B$, and $H$ are engine constants for temperatures below the engine flat rating temperature at the thrust rating in use [67]. By keeping these constants and variables in a database per aircraft type, it is then possible to actively estimate aircraft thrust levels.

### 9.2.7. Performance metric

In order to be able to quantify the quality of a certain model in tackling a certain problem, as well as to be able to track the progress- or lack thereof, a performance metric is needed. For regression problems usually performance metrics reflect how closely the surrogate function fits the target function, over the whole domain. Root Mean Squared Error (RMSE) is a very popular metric for regression problems, measuring the error in estimation independently of the predicted value, therefore it does not take into account if a certain absolute error took place in a point with high or low absolute value. Other metrics, such as Weighted Root Mean Squared Error (WRMSE), are applying a weight proportional with the normalised mean of the predicted value. Thus, more importance is placed on the error in areas with higher values of the studied phenomenon. However, due to the mission's goal to create an accurate pollution map through the entire domain, RMSE [55] is considered more suitable:

$$\text{RMSE} = \sqrt{\frac{1}{n}\sum_{i=1}^{n}\left(y_i - \hat{y}_i\right)^2} \tag{9.25}$$

WRMSE is is based on RMSE, but multiplies the error by a vector proportional with the . Thus, more importance is placed on the error in areas with higher values of the studied phenomenon, a natural assumption when dealing with harmful pollutants. A more refined version, which takes into account the confidence of the predicted value, is the Mean Log Loss (MLL), which evaluates the negative log probability of the true data point under the prediction [57].

## 9.3. Results & Discussion

Once the mathematical tools are selected, the noise and emissions models are implemented, as well as the model prediction algorithm. The current section present the preliminary results obtained using the Gaussian Processes with Bayesian Optimisation techniques as a base for model predictions, as well as a discussion regarding estimates of the total duration of a mission.

### 9.3.1. Model

The ability of the Bayesian Optimisation to produce accurate predictions can be seen in Figure 9.5, where the fitted functions for the concentrations of a pollutant modelled using a 3D Gaussian Plume is plotted. Overall, the Bayesian Optimisation fits well the target function, even though some slight

over fitting can be noticed in the form of the non-physical minimum, as well as the fact that the singularity at the source is not captured by the surrogate function.

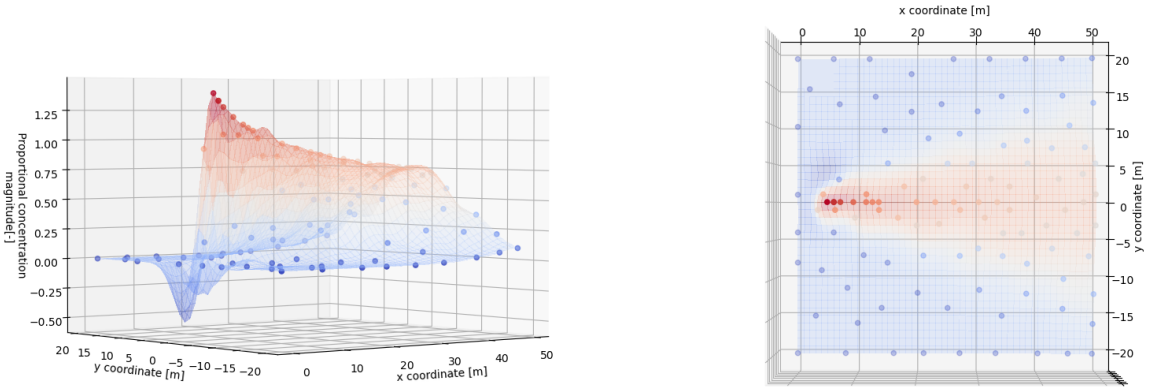


**Figure 9.5:** *Noise-free Bayesian optimisation after parameter optimization: l=2.37, $\sigma_f$ =0.38 modelling the 3D concentration of a pollutant based on the Gaussian Plume model*

As a first experiment, a simple Gaussian Plume Model was modelled and used as the objective function, and then two algorithms are employed to fit the objective function: firstly, the Gaussian regression receives as training data from 40 randomly chosen sampling points, representing 2% of the total number of points in the domain. The fitted function can be seen in Figure 9.6, the part immediately near the source of the plume is outside of the permitted domain, and therefore the predictions are not accurate in that particular area. Secondly, Bayesian Optimisation uses the same amount of training data, but for 35 data points it chooses alone the best points to sample next are. The resulting fitting function, along with the target function, are presented in Figure 9.6. As expected, Bayesian Optimisation manages to offer a significantly better global fitting, due to its exploratory properties. Moreover, during the sampling artificial measurement noise has been introduced in order to simulate real-life conditions.

Finally, the ability of a Gaussian regression using points sampled in a grid search to fit an objective function is analysed. Again, in order to ensure fair comparisons, the Gaussian process receives the similar number of training data as in the other two experiments. As the training data is well distributed among the domain, the grid search fits better than the random sampling Gaussian regression. However, due to the fact that Bayesian Optimisation is able to sample areas about which it is unsure, it performs much better than the regular grid search: on average, its RMSE score is 50% lower for the Bayesian Optimisation, compared to the grid search. It is thus concluded that the extra complexity and calculations introduced by the Bayesian Optimisation pay off in terms of the quality of the model produced. In terms of distance travelled, the random search, as expected, performed the worst: on average, it travelled a distance 50% larger than the distance travelled when using Bayesian Optimisation, and rendered a worse model. However, the Bayesian Optimisation suggests a distance about 50% longer compared to grid search. However, the quality of Bayesian Optimisation is better, and it is expected than, when the models are deployed, the real life results are going to be much more skewed in favour of the Bayesian Optimisation: for example, wind conditions affect greatly the location of the plume, and grid search does not take them into account, therefore performing redundant measurements, whereas Bayesian Optimisation can be tuned to explore locations where pollutants are present, through the exploitative properties of the acquisition function.

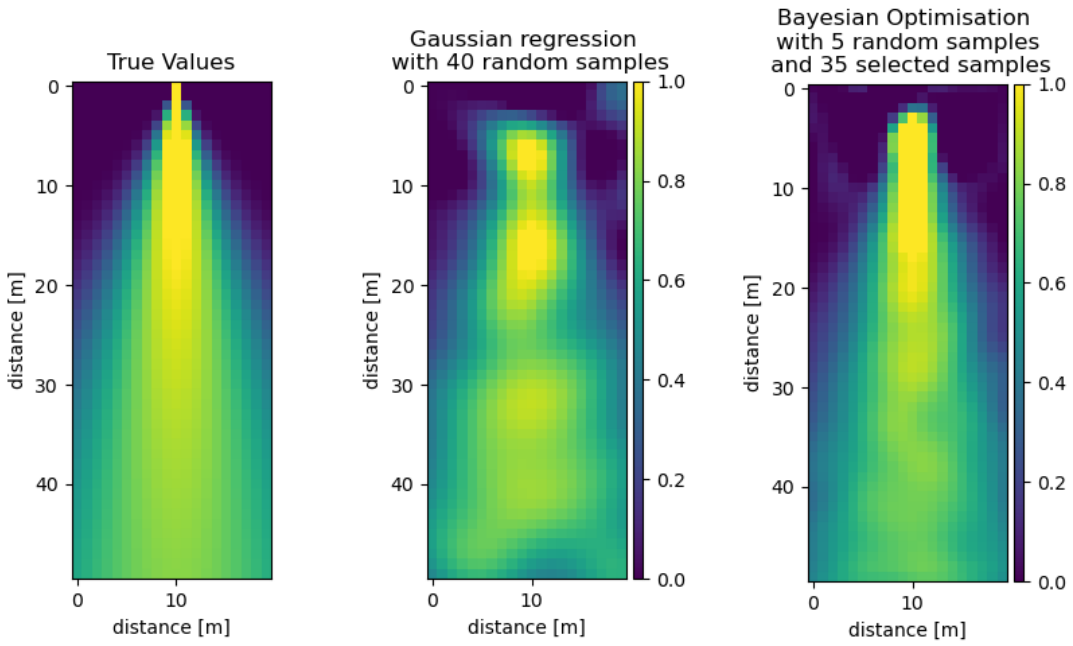


**Figure 9.6:** *Normalised concentration of a pollutant reconstructed using Gaussian regression with 40 random samples and with Bayesian Optimisation*

The increasing performance of the modelling algorithm with increasing number of samples is presented in Figure 9.7 and Figure 9.8. The sampled locations are highlighted in red, and the algorithm tries to reconstruct the objective function of the normalized concentrations of a two-dimensional plume, whose graph is presented on the left side of the figures. As the number of samples is increased the fit is increasingly better, however, after about 20 samples the increase in the quality of the predictions with each new sample decreases significantly, as discussed in Subsection 9.3.2.

The more refined Gaussian Plume Model, as defined in [63], takes into account the effects of a moving source and the presence of external wind. It assumes instantaneous emission, and the state of a particular puff at three different time frame can be seen in Figure 9.9. Both the effect of the wind, as the puff is moving sideways, and of the diffusion can be noticed in the figures.

### 9.3.2. Acquisition Rate

Based on the theoretical aspects discussed in Section 9.2, some first order estimates regarding the acquisition rate can be made. They are useful in order to approximate the amount of time needed to generate a model, based on the desired accuracy of the model, as well as to offer an overview on the required number of drones. Knowing the number of samples required to achieve a certain level of accuracy prior to taking the measurement is often an imprecise process, but as a rule of thumb for Gaussian Processes $n = 10d$ is commonly used, where $n$ is the number of samples and $d$ is the dimensionality of the input space [68]. Analysis of the guideline has shown that predictions on average are within 10% of the true value. As the limiting factor for the duration of the mission is the emissions model as there are only three active drones, but 40 ground level sensors working with the two noise drone, the acquistion rate is calculated only for the emissions.This estimate will later be verified using the Gaussian Plume of Equation 9.12 and noise model of Equation 9.20 in Section 9.5.

For a preliminary estimate of the duration of the mission, a case study of Schiphol's de Polderbaan is used, as follows from the example presented in Chapter 8. Considering the state matrix Equation 9.18, it can be seen that an initial estimate for the input space of the Gaussian Process for each

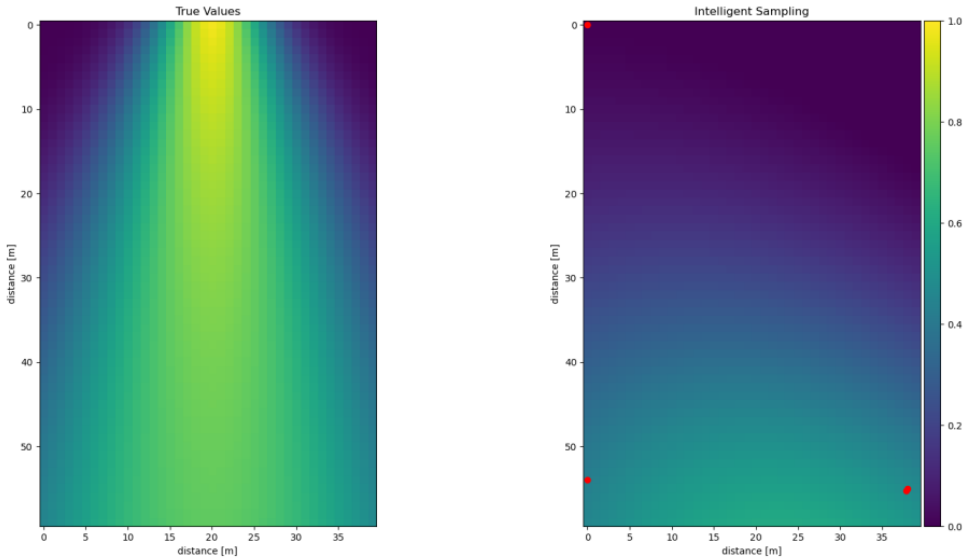


**Figure 9.7:** *True function based on the normalised concentrations of a pollutant modelled using a 2D Gaussian Plume and the function fitted by the intelligent sampling for $n = 3$ samples*

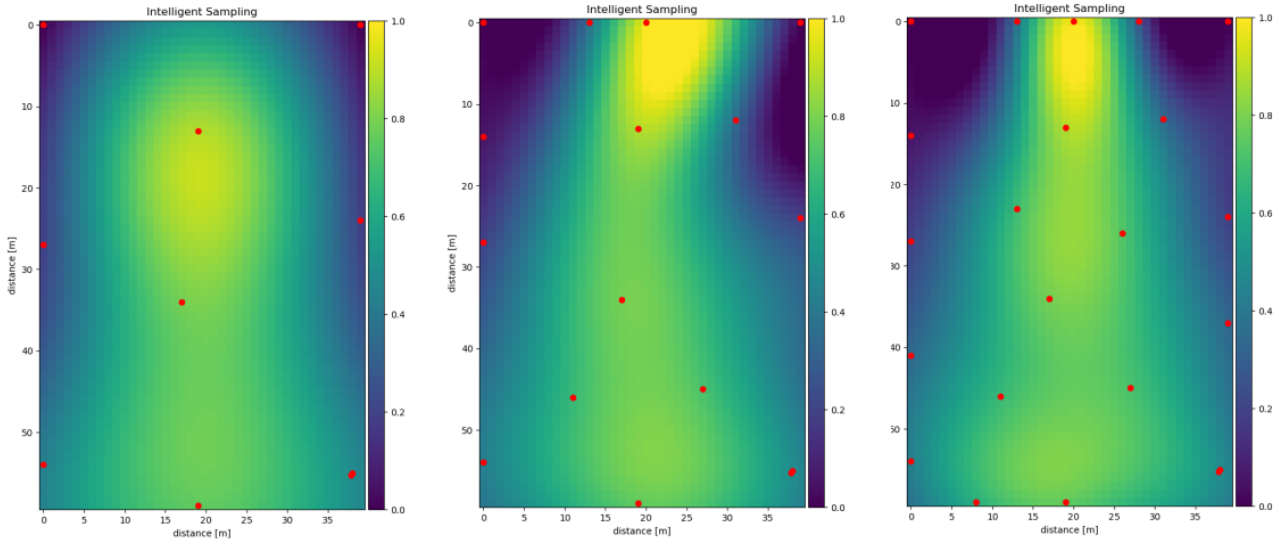


**Figure 9.8:** *Fitted functions for a objective function based on the normalised concentrations of a pollutant modelled using a 2D Gaussian Plume sample for $n = 9$, $n = 15$ and $n = 21$ samples*

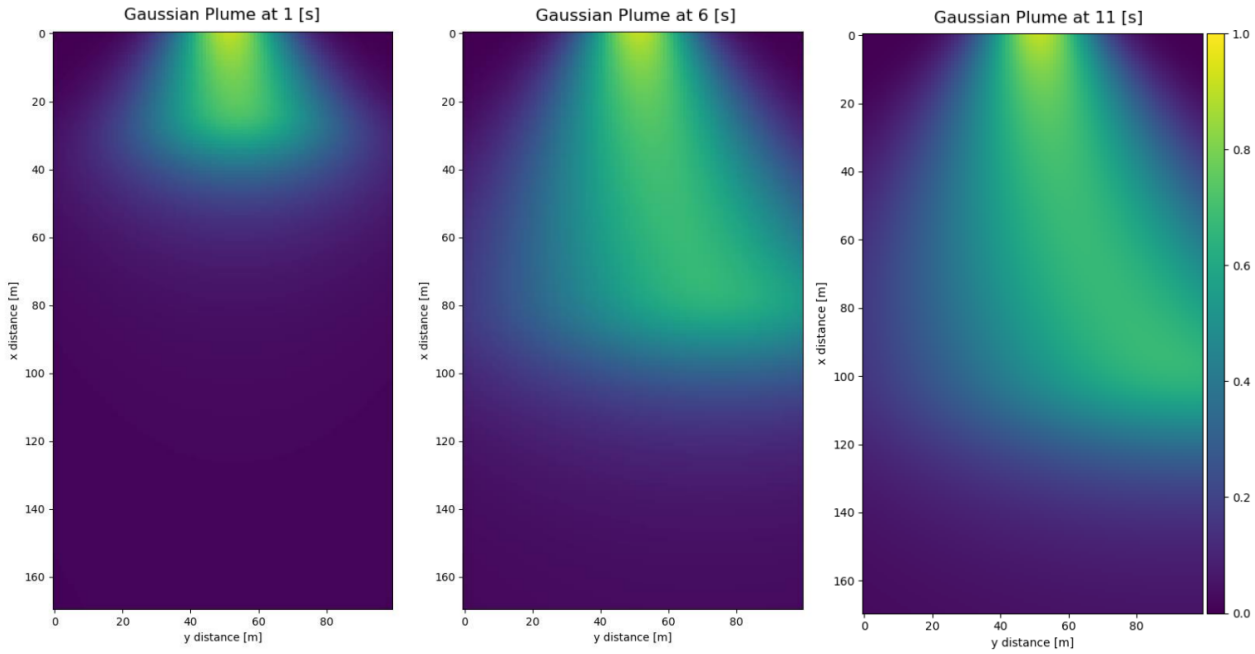


**Figure 9.9:** *Visualisation of the normalised concentrations of a pollutant emmited at $t = 0s$ modelled using a modified Gaussian Plume model as defined by [63], at three time frames*

aircraft type, aircraft event, and airliner is 11, therefore 110 samples of each combination are required to satisfy the $n = 10d$ guideline. An analysis can be conducted to observe how long it would take to reach this principle for each aircraft type/event/airliner combination passing by the Polderbaan.

First, the total amount of aircraft type/event/airliner which fly by Schiphol in a year was considered [1]. Due to the impact of Covid-19 on the total number of aircraft movements within the airport, this was done using values from 2018. Next, the percentage of aircraft taking off and landing from the de Polderbaan was considered, which was 24% and 39% respectively [2]. As almost all aircraft which land at Schiphol have to take-off, this percentage was combined to an average percentage of 31.5% and the "aircraft event" characteristic for the Gaussian Process was removed. This meant that the estimates were only done considering the aircraft type - airliner combination passing Schiphol. The ten most frequent combinations are included in Table 9.1 [3].

The total number of required samples $n_{req}$ was then estimated using:

$$n_{req} = \frac{10 \cdot d \cdot F_s}{f_p \cdot n_{drones}}, \tag{9.26}$$

**Table 9.1:** *Ten most frequent aircraft type - airliner combination in 2018*

| Frequency in 2018 | Aircraft Type | Airliner |
|---|---|---|
| 34677 | Embraer 190 (IGW) | KLM |

[1] https://schiphol.dutchplanespotters.nl/ [19-06-2022]
[2] https://news.schiphol.com/why-do-i-always-fly-from-de-polderbaan/ [19-06-2022]
[3] https://schiphol.dutchplanespotters.nl/ [19-06-2022]

| | | |
|---|---|---|
| 26120 | BOEING 737-800 WINGLETS | KLM |
| 19807 | EMBRAER175(170-200 STD) | KLM |
| 18832 | BOEING 737-700 Winglets | KLM |
| 13343 | BOEING 737-800 WINGLETS | Transavia |
| 9892 | AIRBUS A320-200 | EasyJet |
| 9064 | AIRBUS A319-111 | EasyJet |
| 4647 | B737-900/Winglets | KLM |
| 4181 | AIRBUS A320-200 | Vueling |
| 4125 | DASH 8 DHC SERIES 400 | Flybe |

where $F_s$ is a safety factor used to consider that not all aircraft events can be measured due to operational limits because of weather or light. As a preliminary estimate, this value was set as 2. $f_p$ is the percentage of aircraft which pass by de Polderbaan, and $n_{drones}$ is the number of active drones. As ALEC is designed to always have one drone in the charging phase, the real number of drones in the system is one more than considered in the acquisition rate. Furthermore, rather than considering the total number of aircraft type-airliner combinations which reach the criteria set out by Equation 9.26, the estimated percentage of aircraft events modelled was calculated considering the frequency of the combination divided by the total number of aircraft which pass by Schiphol. For example, being able to accurately model the Embraer 190 (IGW)-KLM combination implies that at least 13.4% of all aircraft operations at Schiphol can be accurately modelled. The results are shown in Figure 9.10.

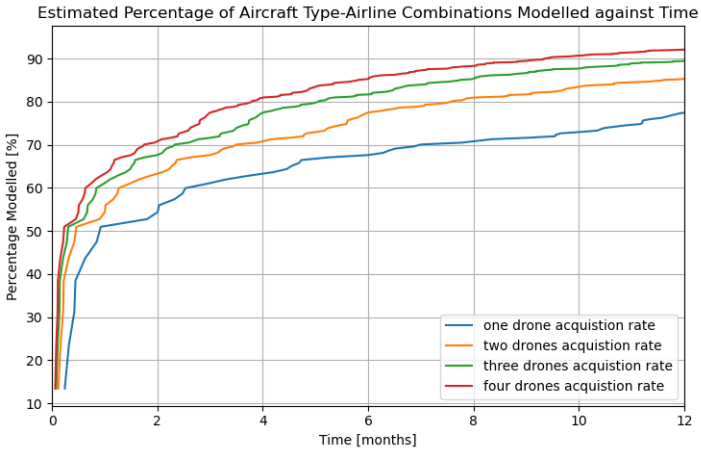


**Figure 9.10:** *Acquisition rate per number of drones for Polderbaan, Schiphol, based on 2018 flight data*

Results show that with two active drones, 80% of total events can be modelled in 7.6 months and 90% in 18.7 months, with three active drones 80% in 5 months and 90% in 12.47 months, and with four active drones 80% in 3.8 months and 90% in 9.35 months. It can be seen that increasing the number of drones in the system improves the acquisition rate, although with a diminishing rate of returns. This preliminary analysis was conducted assigning a separate Gaussian Process to each aircraft type-airline combination as to obtain a conservative estimate of the duration of the ALEC mission. Despite this, it can be seen that in reality there should be a correlation between all aircraft of the same type independent of airliner. However, due to the fact that the drones are continuously collecting measurements during the entire of an aircraft event these preliminary estimates are overestimating the time required to map a runway. Future research is recommended in obtaining a way

to couple the Gaussian Process of same aircraft type as to potentially reduce the duration of the mission and obtain more accurate estimates of noise and emission.

## 9.4. Data Handling

The drones operate by taking some initial samples, needed to be able to start the Bayesian Optimisation process. The location of the initial samples is selected in the middle of the permitted domain in order to ensure it provide useful information. Moreover, the drones, after being deployed to a certain location, are sampling continuously the entire aircraft event, send their data to the ground station, receive the new locations to sample and move there.

The final purpose for collecting the measurements is to create a raw database to be used as a reference in the future work of environmental scientists, as well as to generate a preliminary near real time environmental metric, based on aircraft events. The pipeline for the measurements' data, from the moment of collection to the moment of storage in a database, is as follows: firstly, the data will be pre-processed on board: cleaned, filtered and packed in order to be prepared for transmission. The data will then be transmitted from the drones to the ground station, where concurrently, the data will also be stored on board on the SD cards. After arriving at the ground station, the data is unpacked, and then used to update the model by the Bayesian Optimisation routines, and information regarding the next sampling locations is sent to the drones. In order to create a clean, raw database for further use for scientists, the data is stored in a several databases, based on its labels, referring to the aircraft type and aircraft event it measured. Moreover, a normalisation is applied to the data to account for the varying fuel mass aboard, depending on the destination. As more data is collected, the databases can be split in more databases based on extra labels, such as company operating the polluting aircraft. However, "the curse of dimensionality" has to be kept in mind, as the number of required data increases exponentially with an increasing number of labels.

The overall role of the Bayesian optimisation in the system's software can be seen in the Software diagram in Appendix C. The data provided as input to the Bayesian Optimisation routines by the ground station processor, after being received and pre-processed. The output of the modelling algorithm is used to generate the final outputs, namely the total environmental metric function, the environmental database and the environmental model output. Moreover, the Bayesian Optimisation proposes the next location and send this information to the control&autonomy software running on the noise and emission drones.

## 9.5. Verification

In order to ensure the correctness of the modelling algorithm verification has to be performed. Validation is not yet possible due to a lack of real data. This section concerns itself with the verification procedures performed on the modelling algorithm and its subroutines.

### 9.5.1. Code Verification

The code is verified by performing unit tests in order to ensure the atomic parts of the code work as intended, as well as subsystem tests which are useful to test the overall correctness of the subroutines. Moreover, the models for noise and emissions are used to perform system tests by introducing artificial noise in the theoretical model and checking the performance of the model when trying to fit the environmental functions. Furthermore, the parallelisation algorithm and custom distance routine are tested against dummy examples in order to verify they behave as expected.

### 9.5.2. Sample Size Verification

In Subsection 9.3.2, the guideline $n = 10d$ was used to estimate the number of samples required to accurately model aircraft events. Loeppky et al, 2009 [68] have noted in experiments that with

$n = 10d$, predictions using Gaussian Processes are on average accurate to within 10% of the true value. Beyond the scientific literature which supports this rule of thumb, it was important to independently verify this metric by measuring the change in error as the number of sample size increases. This was first done using a Gaussian plume and then with noise model of Equation 9.20.

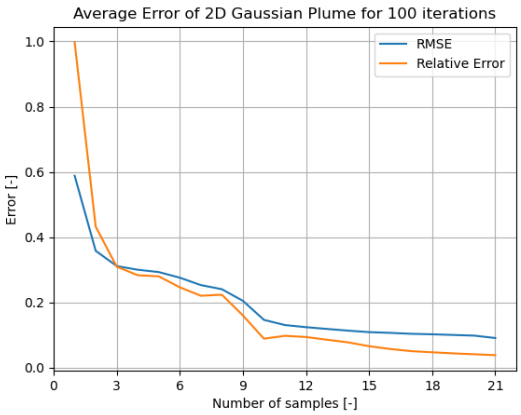


**Figure 9.11:** *2D Gaussian Plume experiment's error per number of samples*

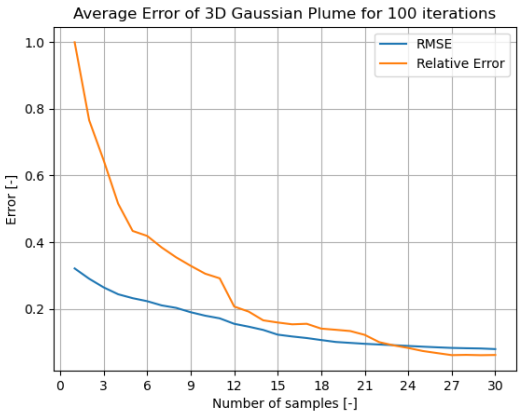


**Figure 9.12:** *3D Gaussian Plume experiment's error per number of samples*

Figure 9.11 and Figure 9.12 shows the effect of the size of sample size for the Gaussian Plume for both a 2D plume and a 3D plume respectively, using 100 iterations. The relative error was calculated by adding the total concentration estimated by the model with respect to the true value, this was because in the true model there were several locations where the concentrations were 0, leading to a singularity in the relative error metric per individual location. In both cases, the number of samples were considered in batches of 3 due to it being the number of drones which will actively sample emissions in the ALEC system. Occasionally, the log marginal likelihood function of Equation 9.4 would not converge, which would lead to the iteration being run again. Results show that for the 2D Gaussian Plume, reaching the $n = 10d$ sample threshold with 21 samples results in a relative error of 3.8% and a root mean square error of 0.091, while for the 3D Gaussian Plume at the 30 sample value the relative error is 6.0% and root mean square error of 0.078. Overall, preliminary results for the Gaussian Plume show that for the emissions model the sample size rule of thumb is valid, with the GP performing better than the initial estimate of 10% accuracy.

## 9.6. Future Improvements

Gaussian Processes are known to scale up poorly [65], and sparse techniques have to be applied to decrease the asymptotic complexity of the algorithm. Due to the rather low number of samples needed to model an aircraft-airline combination, in the order of hundreds, the feasibility of the mission is not affected by this issue.

The $n = 10d$ rule has to be further investigated as well as the models used as kernels. As discussed in Section 9.3, the estimations for the mission duration to map one runway are overly pessimistic and the fact that one aircraft event is continuously sampled by the drones reduces the time needed. The results of the parallelisation as well as an in depth analysis of its performance would ensure the model distributes work to its drones optimally, and therefore further work in this direction has to be done. Additionally, more refined performance metrics, incorporating the uncertainties of the GPs, such as MLL, could be incorporated in the model. Moreover, the current software is still in prototype phase and a significant work is needed to deploy the software.

# 10

# Manufacturing, Assembly, Integration Plan

In this chapter, it is described how the timeline for manufacturing, assembly, and integration of the various subsystems is envisioned. A time estimate is given on the duration of individual elements, and a total estimate is given for each segment. For the ground level sensors, it is estimated that the manufacturing will take 12 hours, the assembly 6.5, and the integration 12, for a total of 30.5 hours. For the drones, it is estimated that the manufacturing of the drones will take about 25 hours (with small differences between the emission and noise drone), the assembly 12 hours, and the integration 12 hours; the combined time being 49 hours.

But, it should be noted that these are conservative estimates. It is expected that a more accurate estimation can be made once the product has been further developed. In addition, it is assumed that due to experience gained each subsequent part will be produced in less time than before.

As all parts will either be purchased off-the-shelf, or 3-D printed, a quick note is made on its manufacturing process. As has been explained in Chapter 4, the material of choice for manufacturing the main load-bearing components of the structure will be Nylon 15CF; this is a filament consisting of chopped carbon fiber which strengthens the polymer it is added to. The main method of manufacturing such material is using 3D printing. 3D printing at low production numbers offers significant benefits over traditional manufacturing methods. Furthermore, the chosen carbon fiber reinforced polymer is usable on consumer-grade printers, such as the Prusa i3. It should be taken into account that the heated bed of the used printer can perform up to 80 Celsius, and allow for a working temperature of at least 235 Celsius [1]. The MAI plan for the separate subsystems are discussed in Section 10.1, Section 10.2, and Section 10.3 for the GLS, the ground station, and the drones.

## 10.1. Ground Level Sensors

In this section, the Manufacturing, Assembly, and Integration (MAI) plan for the ground-level sensors will be presented. Two components need to be manufactured -the recyclable dry-box, and the frame of the solar panel- whilst the remainder of the parts will be purchased. Assembly is straightforward, but has to be done precisely in order to ensure the components are connected correctly. The estimated hours as provided in Figure 10.1 are for the first production, which is assumed to take the largest amount of time.

## 10.2. Ground station

The GS only consists of components that are purchased in an already assembled state. The only modification of the ground station vans that needs to be manufactured are custom racks for the safe transport of the processing unit, batteries and (most importantly) drones/GLS. It is assumed that this has a negligible influence on the financial budget. The USB dongle, SiK telemetry radios, and ADS-B can be plugged into the laptop to integrate the subsystem.

## 10.3. Noise and Emission Drones

A large part of the components of the noise drone are identical to those of the emission drone. The only difference is in the components and configuration of the payload; a wind tunnel with electrochemical sensors for the emission drone, and a microphone with a ground plate for the noise drone.

[1] https://fillamentum.com/collections/nylon-filament/nylon-cf15-carbon-filament/

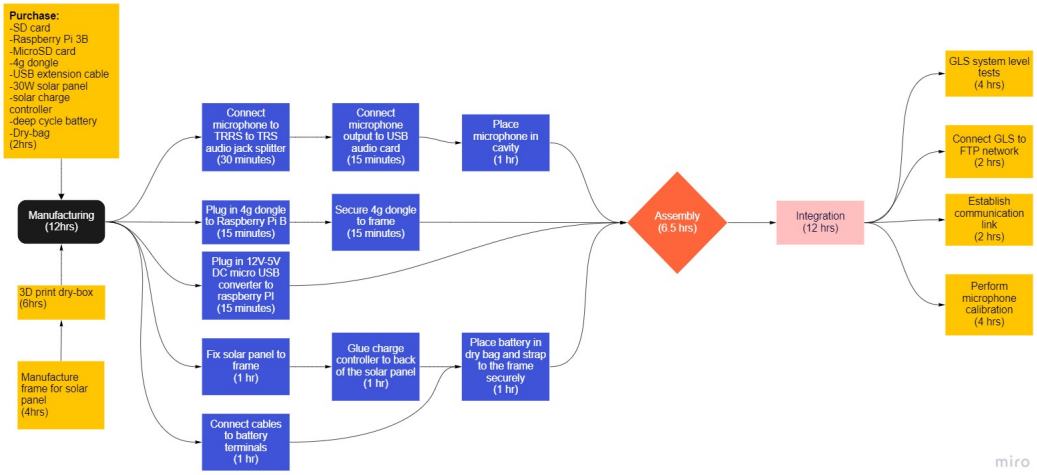


**Figure 10.1:** *Manufacturing, Assembly and Integration flow diagram GLS*

Additionally, the structure will be slightly changed, to accommodate the change in the payload. The combined MAI has been provided in Figure 10.2. The time taken is given as the total duration for creating the parts; the amount of "hands-on time" the operator needs to spend on these parts is much lower, as the printers can run autonomously.

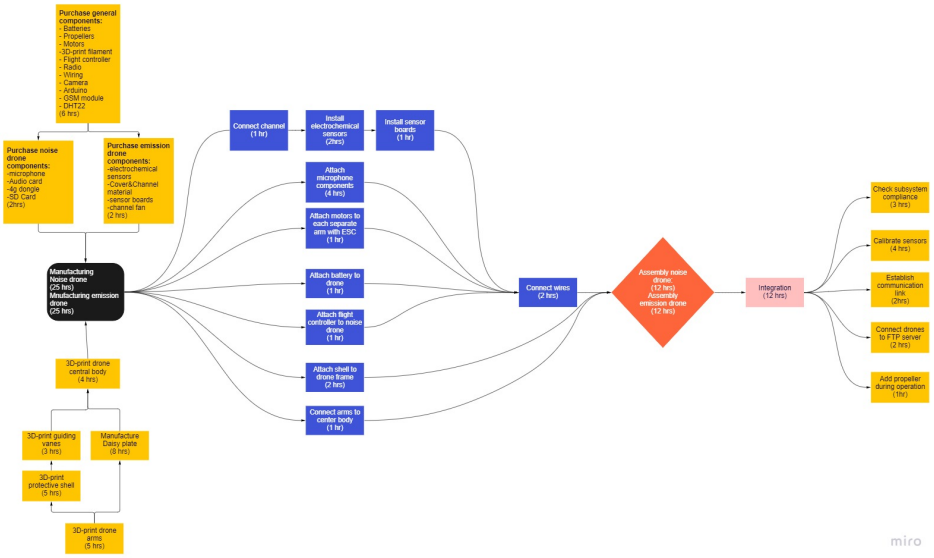


**Figure 10.2:** *Manufacturing, Assembly and Integration flow diagram for noise and emission drone*

# 11

# Verification & Validation

This chapter presents the verification and validation of the design. Verification is essential to make sure the requirements are met. Validation is done to ensure that the system actually performs as desired. Section 11.1 discusses the verification and compliance of the design with the requirements. Validation of ALEC is discussed in Section 11.2.

## 11.1. Verification

The verification of ALEC is subdivided into the verification of the requirements per subsystem, where the relevant requirements together with design compliance and a description of how it would be verified for a subsystem is presented. The verification of the requirements for the emission drone is shown in Section 4.1 together with the verification of the requirements on the flying vehicle for both drone types. Section 5.1 shows the verification for the noise drone. The verification of the requirements for the ground station and ground level sensor are given in Section 7.1 and Section 8.1 respectively. Although most requirements were met, there are some that are not met by the current design. These requirements should be re-evaluated and, if necessary, incorporated in future development. There are also some requirements for which it is uncertain whether they have been met at this stage. They will be verified when testing the system.

## 11.2. Validation

This section presents the validation of the emission drone, noise drone, ground level sensor, and ground station in Subsection 11.2.1, Subsection 11.2.2, Subsection 11.2.3, and Subsection 11.2.4, respectively. Thereafter, validation of the system as a whole will be described in Subsection 11.2.5.

### 11.2.1. Emission Drone Validation

This subsection describes the validation of the emission drone. First, separate components are tested, and afterwards, the subsystem is tested as a whole.

#### Components Validation

The first component of the emission drone that will be tested is the payload. Afterwards, the power and propulsion system is checked, and lastly the communications are validated. The payload will be tested to check whether the sensors output the desired data. First, the sensors with their sensor support circuits are tested separately to check whether they work and whether the output is in the expected format. Then, the payload is tested as a whole by testing the sensors with the wind tunnel and the wind tunnel fan. These tests will be done in a controlled environment where the concentrations of the pollutants is known.

The power and propulsion subsystem will be tested for hovering endurance and maneuverability. The hovering endurance will be tested by having the drone hover until 85 percent of the battery capacity is depleted. This way the real hovering time can be recorded. The maneuverability will be tested by having the drone fly in one direction and then making a turn. Both of these tests will be done on an empty field.

The communications will be tested for the transmission of measured data and the communication with the flight controller. After the payload has been tested, the same payload test will be done again, but instead of directly recording the data, the communication system will be attached to the

payload, and the data will be send to a laptop two kilometers away. The communication with the flight controller will be tested by giving the drone a flight path to the other side of an empty field, and the telling it to come back.

**Subsystem Validation**
The complete emission drone subsystem will be tested by having it perform a simulated mission. It will be given measurements points in a safe area, but not an empty area in order to test the obstacle avoidance, and it will perform the mission as if it was an actual mission. The measurements taken might not show much air pollution, since the test will not be done on an airport, but as long as the data is received by the ground station and the drone completes the mission the test will be successful. This mission also includes the autonomous take-off and landing using the landing pads of the ground station.

### 11.2.2. Noise Drone Validation
This subsection starts by presenting the validation of the separate components of the noise drone. Thereafter, the validation of the complete noise drone is discussed.

**Components Validation**
The validation of the communications, power, and propulsion of the noise drone is the same as for the emissions drone. Hence, if the reader wishes to read about validation of those components the author recommends to consult Subsection 11.2.1.

The payload of the noise drone consists of the Sennheiser MKE Essential Omni-Black microphone, ground-effect daisy plate, and DHT22.

The Sennheiser MKE Essential Omni-Black microphone should be tested in a laboratory where it is exposed certain noise. Thereafter, the another, calibrated microphone should be exposed to the exact same noise. The measured noise of the Sennheiser MKE Essential Omni-Black microphone and calibrated microphone should be compared to analyze the accuracy of the measurements made by the Sennheiser MKE Essential Omni-Black microphone.

The ground-effect daisy plate should be validated by comparing the noise measured by a microphone with daisy plate to a microphone with a circular plate and a microphone without any plate. It is important that the noise created is the same in all three instances and that it is performed in the same conditions. When comparing the measurements, it can be concluded whether the daisy-plate reduces the ground-effect. In this manner validation of the ground-effect daisy plate is performed.

The DHT22 temperature and humidity sensor should be validated by using it in a controlled environment with known temperature and humidity. By comparing the temperature and humidity measured by the DHT22 with the conditions it was exposed to the DHT22 sensor can be validated.

**Subsystem Validation**
After all the individual components have been validated, the noise drone as a whole should be validated. This should be done by letting it perform a simulated mission in a controlled environment. This means that it will have to fly to a certain location, measure noise there, and later fly back to the LTO pad. This way it can be analysed whether the emission drone works as desired and adheres to all the standards the client has.

### 11.2.3. Ground Level Sensor Validation
This subsection first discusses the validation of the individual ground level sensors. Thereafter, it presents the validation of the ground level sensor as a complete subsystem.

**Components Validation**
The ground level components that need to be validated are the solar panel, solar charge controller,

weatherproof box, and the Rode SmartLav+.

The Rode SmartLav+ microphone will be validated by comparing noise meausured by that microphone with the measurements of a calibrated microphone.

The solar panel will be validated by exposing the panel to controlled light conditions. That way, the electrical energy generated by the solar panel can be compared with the expected generation. This comparison allow validation of the solar panel.

The charge controller will be validated by checking whether the charge controller accurately controls the amount of electrical energy sent from the solar panel to the battery. This can be done by giving a certain amount of electricity as input, and comparing the output to the settings of the charge controller. If these match, the charge controller works correct and it is validated.

The weatherproof box can be validated by exposing the box, with a dummy payload inside, to weather conditions it should be able to withstand. If the dummy payload inside is sufficiently protected and the weatherproof box withstands the tests than the weatherproof box is validated.

**Subsystem Validation**
The ground level sensor can be validated by using the sensor in a simulated mission. If the ground level sensor works as expected and meets the standards set by the clients then the ground level sensor is validated.

### 11.2.4. Ground Station Validation
This subsection describes the validation of the ground station by first explaining the validation of separate components and then testing the complete ground station.

**Components Validation**
The components of the ground station that need to be tested are the charging station, the communications, and the data processing. The charging stations will be tested by simply charging a drone from 15 percent battery capacity to 100 percent, and measuring how long this takes and how much power is drawn.

The test for communication includes having both a noise drone and an emission drone measure at two kilometers away and sending the data to the ground station. Whether ADS-B data and other required data from external sources is received will also be checked. The drones will then be told to come back to the ground station. The data being send from the drones to the ground station is then processed and put into the algorithm described in Chapter 9. It is then checked whether this data is in the correct format to get actual results from that algorithm.

**Subsystem Validation**
The validation of the complete ground station will be conducted after the noise and emission drone are validated. It will be validated by using the ground station to have a noise and an emission drone perform part if a mission. Specifically, the drones will be given a measurement point by the ground station, the drones will measure there and send data to the ground station. Afterwards the drones will go back to the ground station and be charged. Before the mission itself starts, the ground station will be set up in order to get an estimate on the set up time.

### 11.2.5. Validation of System
After all subsystems have been validated, the system as a whole will be tested. The interaction within and the performance of the complete ALEC system will be evaluated by performing three different missions. These missions will include all aspects of the system in the exact way they would be used in a commercial mission. The missions will only differ from real commercial missions in their length, the test missions will be much shorter. The duration of the test missions will not be set

beforehand. Instead, the test missions will continue until there is confidence in all aspects of the system under different circumstances. The first circumstance is a sudden change in weather. It is required to know how the system will behave if it starts raining, or when the wind suddenly changes direction or velocity. The response of the system to such (change of) conditions should be analysed.

Another circumstance is when a certain subsystem fails. The rest of the system should then still continue to operate if possible. This circumstance will be simulated by taking out different subsystems at a time. The ground station can not be taken out, since there is only one of them, but all the other subsystems will be taken out one by one. This is done to ensure safety and reliability of the system.

The first type of test that will be performed is testing the whole system, with its four subsystems, at a location where the risk of creating harm or damage is as low as possible. Suitable locations would be for example an airport no longer in use, a football field, or just a patch of grass of sufficient size without trees or other objects near. The most important part to test is the communication/cooperation between the various different subsystems. When these tests are successful, the system will be tested at an airport with very low traffic. By doing so, it can be tested whether the drones adhere to the spatial limitations set, and whether the emergency procedures work correctly. If all these tests go as planned, the system should be tested at a busy aircraft with many aircraft events. This is the final type of testing in which should be checked whether the system adheres to all the clients desires and standards. If all tests are completed successfully, the system has been validated, the design team can be sure that the system works as desired and subsequently it can be deployed commercially.

# 12

# Financial Analysis

ALEC has an economic aspect as well as a scientific aspect attached to it. Performing financial analysis is important in order to ensure the economic viability of the product, which represents the topic of the current chapter. First, the stakeholders of our projects are identified in Section 12.1. Section 12.2 analyses the financial impacts of aviation pollution. Then an overview on aviation noise and emission measurements market is given in Section 12.3, followed by a Strengths, Weaknesses, Opportunities, and Threats (SWOT) analysis. Thereafter, the cost breakdown structure will analysed in Section 12.4, and finally, the operational profit will be analyzed in Section 12.5. It should be noted that all prices are mentioned in EUR and price listings in foreign currencies are converted using the rates announced at the moment of writing the report, e.g. for the USD-EUR a rate of 0.93 euros per dollar is used [1].

## 12.1. Stakeholders

In order to perform a good financial analysis, it is important to analyze the stakeholders of the mission. Stakeholders are considered any party influencing or being affected by the mission. The stakeholders identified for this autonomous environmental sensing mission are;

- **Researchers** - researchers creating noise and emissions models of airports and investigating aviation noise and emissions in general, will benefit from this system as the open source data gathered allows researchers to analyze and model noise and emissions pollution. As a result of this gathered data, currently existing noise and emissions models can be improved.
- **Near-airport communities** - they are disproportionately affected by the noise and emissions produced by aircraft flying over at a low altitude during take-off and landing. ALEC's database can serve as a trusty source for implementation of effective mitigating measures to reduce the nuisance caused by aviation, which benefits the near-airport communities. They benefit not only in overall well being, but they also have a lower chance on illnesses which increases productivity and the price of their house will rise if the noise and emissions from aircraft is reduced.
- **Local and national governments** - the noise and emissions caused by the aircraft create health risks for near-airport communities. By using this system, more effective mitigating measures can be taken to reduce noise and emissions pollution which reduces health care costs for the government. Furthermore, municipalities located near airports can benefit as, when the pollution is lower, their community becomes more attractive for both new residents to move to and tourism, which increases the income for that municipality.
  In addition, governmental bodies will have to grant permission to fly the drones near the aircraft as that is currently prohibited by law in the European Union.
- **Policy makers** - policy makers mainly benefit from the data gathered by ALEC. When ALEC is used, a detailed map of noise and emissions is created both near the airport and farther from the airport in near-airport communities. This allows researchers to create more accurate noise and emissions models, which subsequently allows policy makers to implement more effective, mitigating measures to reduce pollution from noise and emissions.
- **Airports** - airports benefit from accurate noise and emissions data as it allows them to reduce noise nuisance experienced by near-airport communities as they can optimise approach and

[1] https://www.wisselkoers.nl/dollar-euro [Cited 30-05-2022]

take-off flight paths. As a result, airports receive less complaints from residents, which could allow the airport to increase the number of aircraft landing and taking-off while still adhering to noise regulations. This could increase their revenue and hence they can benefit financially. Furthermore, airports influence the project as the system will have to be used in close co-operation with the airport under investigation. Without their permission the drones will not be allowed to fly near the aircraft to measure noise and emissions as it is prohibited by law. Hence, extensive cooperation with the airport is required.

- **The producer/designer of this system** - the producer/designer of this system mainly benefits financially when the product would be put on the market. If the producer/designer ensures that there is a high demand for its product, they can financially benefit from the product.

## 12.2. Financial Impacts of Aviation Pollution

The impact of the pollution due to the aviation industry not only impacts nature. It has also a significant financial impacts. In this section, the costs of death due to aviation and the depreciation of house prices due to aviation will be analyzed.

**Costs of deaths due to aviation**

As mentioned above, it is estimated that annually 16,000 people die prematurely due to aircraft emissions worldwide [2]. Assuming that the global population is 7.76 billion and the Dutch population is 17.44 million[2], the amount of premature deaths in the Netherlands due to aviation emissions is approximately 36. Cost-benefit analyses require a monetary value for a life. A method used for this is the value of statistical life (VSL). The OECD advises to use a value of 1.53 million EUR for environmental measures which is the value used by the European Commission [69] (approximately 1 million EUR for 2000 prices, correcting for inflation gives 1.53 million EUR)[3]. This number has been corrected for the age of people prematurely dying from air pollution. This means that, if all the Dutch deaths due to aviation air pollution would be prevented, the annual benefit is approximately 55 million EUR.

**Depreciation of house prices near Airports**

Besides the health effects due to noise and emissions disproportionately affecting near-airport communities, people living near airports are also disadvantaged by the fact that their houses have lower values due to the noise nuisance. According to research by the Centraal PlanBureau (CPB, a Dutch government body making economic forecasts and analyses), the Noise Depreciation Index (NDI), which a measurement for the depreciation of house prices to due noise nuisance caused by aircraft, around Schiphol Airport is 0.8 %. This means that, for every increase of 1 dB(A) of aircraft noise nuisance, the average house price decreases by 0.8 %. The total annual benefit of reducing the aircraft noise by 1 dB(A) per aircraft event is 49 million EUR for Schiphol Airport area. This is obtained by using the total value of houses exposed to at least 45 dB(A), based on data from the RIVM, NVM, and Dutch Association for Estate Agents (Nederlandse Vereniging van Makelaars). It should be noted that this analysis corrected for background noise levels. [70]

It should be noted that performing a cost-benefit analysis using the value of statistical life is controversial. The VSL is often dependent on the income/GDP per capita [71] and can also be corrected for age [69]. Hence, using VSL in cost-benefit assessments assumes that the life of a person living in a country with lower GDP per capita is worth less than in a country with higher GDP per capita. For example, the life of a person in Switzerland (GDP per capita of 71,745 USD) is worth more than the life of a person in Italy (GDP per capita of 41,902 USD)[4]. Therefore, financially valuing human lives

[2] https://data.worldbank.org/indicator/SP.POP.TOTL?end=2020&start=1960 [Cited 02-06-2022]

[3] https://www.inflationtool.com/euro/2000-to-present-value?amount=1000000&year2=2022&frequency=yearly [Cited 06-02-2022]

[4] https://data.worldbank.org/indicator/NY.GDP.PCAP.PP.CD?most_recent_value_desc=true&year_high_desc=true [Cited

is controversial. Other methods, such as quality-adjusted life-years (QALY), exist, but are harder to implement as they depend not only on the length of life but also on the quality of life [72]. Such methods are deemed to be outside the scope of the project. Hence, the VSL method used above serves as rough estimate when assessing the benefit of reducing aviation noise and emissions.

## 12.3. Market Valuation and Competitors

In 2022, the total emissions monitoring systems market was valued at approximately 2.79 billion EUR, and it is expected to reach 4.2 billion EUR by 2027, with a compound annual growth rate (CAGR) of 8.8 %[5]. The noise measuring market was valued at approximately 637 milion EUR in 2021 and is expected to grow to 912 million EUR by 2030, representing a CAGR of 5.6 %[6]. The current market of emissions monitoring systems consists mainly of three types of systems, namely fixed, mobile, and satellite monitoring systems. However, the current systems all lack functionalities that are of importance for the mission of ALEC as will be presented below.

**Satellite Emissions Monitoring Systems**

To start with satellite monitoring systems, they have very high expenses per system and a low resolution. For example, TNO designed the TANGO satellite for the ESA Copernicus CO2M mission. The satellite would measure carbon dioxide emissions from industrial facilities once every three to four days, and it would have a spatial resolution of 300 m by 300 m[7]. For that mission, ESA in the end signed a contract worth 445 million EUR with OHB System AB to create only two satellites measuring carbon dioxide emissions[8]. The price of satellites is too high for high-volume production, and satellites are not capable of accurately measuring noise. For these reasons, satellite based monitoring systems are deemed infeasible for the goal this project has.

**Fixed Emissions Monitoring Systems**

In the United States of America, the government scientific standard for air-quality monitoring are categorized in federal reference methods (FRM) or federal equivalent methods (FEM). Monitoring systems belonging to either one of these categories have to meet strict requirements, as the data collected is used by regulatory bodies. However, these systems have two main downsides. The first is that they are large, stationary systems. That means that it is not possible to create a dense map of data[9]. The United States Environmental Protection Agency also discusses the use of low-cost sensors with a price between approximately 190 EUR and 4600 EUR. However, these sensors are less reliable and the gas sensors tend to lose responsiveness over time, typically one year, and therefore require regular replacement. This increases the cost of the system and reduces the accuracy of the measured data[10]. Furthermore, as these low-cost sensors are stationary, they do not create a dense map of data points.

**Mobile Emissions Monitoring Systems**

The benefit of mobile monitoring systems is they are not fixed to one location and therefore can make measurements at various locations in a given time frame. The benefit of this flexibility is that a dense map of data can be created over time. Mobile monitoring systems currently available

06-02-2022]

[5] https://www.marketsandmarkets.com/Market-Reports/emission-monitoring-systems-market-72002872.html [Cited 30-05-2022]

[6] https://www.verifiedmarketresearch.com/product/noise-monitoring-market [Cited 31-05-2022]

[7] https://www.tno.nl/en/focus-areas/industry/roadmaps/space-scientific-instrumentation/earth-observation/tango-satellite [Cited 30-05-2022]

[8] https://www.ohb.de/en/news/2020/ohb-and-esa-sign-contract-for-copernicus-atmospheric-co2-monitoring-mission [Cited 30-05-2022]

[9] https://www.clarity.io/blog/air-quality-monitoring-2-0-how-different-types-of-air-monitoring-technologies-are-contributing-to-a-more [Cited 31-05-2022]

[10] https://www.epa.gov/sites/default/files/2018-01/documents/collocation_instruction_guide.pdf [Cited 31-05-2022]

are for example the Teledyne Muve C360[11] and the Scentroid DR100 Flying Lab[12]. Both systems are drones capable of measuring gases, which enables them to analyze the concentration of gases three-dimensionally. These systems can send their measured data real-time to a ground station which allows for live analysis of the measurements. Therefore, these systems are deemed the closest competitors of ALEC. A downside is that their level of autonomy is relatively low as they require a person actively flying the system and the systems operate individually, limiting the amount of data gathered in a certain time frame. Hence, there is a market gap which can be filled by ALEC.

**Noise Monitoring Systems**

The market of noise monitoring systems consists of a great variety of products. There exist small, mobile, hand-held systems and large, stationary systems ranging from tens of Euro's up to thousands of Euro's[13]. Schiphol Airport has been measuring noise produced by aircraft since 1993 using a network of microphones called NOMOS (short for Noise Monitoring System). It currently consists of 41 systems continuously measuring noise. Each system consists of a 6 m to 10 m pole with at the end a calibrated microphone. This microphone is accompanied by a station analyzing the data and ensuring a connection to a central computer[14]. The downside of such a system is that it is very expensive, requires large systems (poles of 6 m - 10 m) and is not mobile. ALEC also has the possibility to immediately provide spectrograms. Due to its flexibility and high quality of audio data including spectrograms, ALEC is deemed to be able to fill a market gap. The real value lies in the combination of the data of the multiple systems. It is hard to quantify the exact worth of the combination of all the data, but it is assumed that the combination of data is worth more than the sum of its individual components. All in all, there is a market gap regarding systems creating a dense, accurate map of both noise and emissions data as this has not been done before, and doing so with high autonomy. This gap should be filled by ALEC.

### 12.3.1. SWOT Analysis

A SWOT analysis has been performed to provide extra understanding of the position of ALEC in the market. The figure with SWOT analysis can be found below in Figure 12.1, and it is further elaborated on below.

**Strengths**

- **S1** - ALEC will provide both noise and emission measurements which distinguishes it from other available systems which only measure noise or emissions, not both.
- **S2** - The high level of autonomy of the noise and emissions drones means that, once all systems are set up, the system requires little human intervention to work properly.
- **S3** - The short set-up time of the drones allows for a quick start of measurements at the beginning of the day.
- **S4** - The high mobility and flexibility of the drones means that it can safely be operated close to aircraft.
- **S5** - Collecting data both close to aircraft on airports and in near-airport communities enables clients to create a detailed map of noise pollution caused by aircraft close to and further from airports.
- **S6** - Using a Bayesian optimisation model enables measuring at the optimal location, where the data collected will be of highest value.

**Weaknesses**

[11] https://www.flir.eu/products/muve-c360/ [Cited 31-05-2022]
[12] https://scentroid.com/products/analyzers/dr1000-flying-lab/ [Cited 31-05-2022]
[13] https://www.pce-instruments.com/eu/measuring-instruments/test-meters/noise-meter-sound-meter-kat_40410.htm [Cited 31-05-2022]
[14] https://noiselab.casper.aero/ams/#page=n_over_nomos [Cited 31-05-2022]

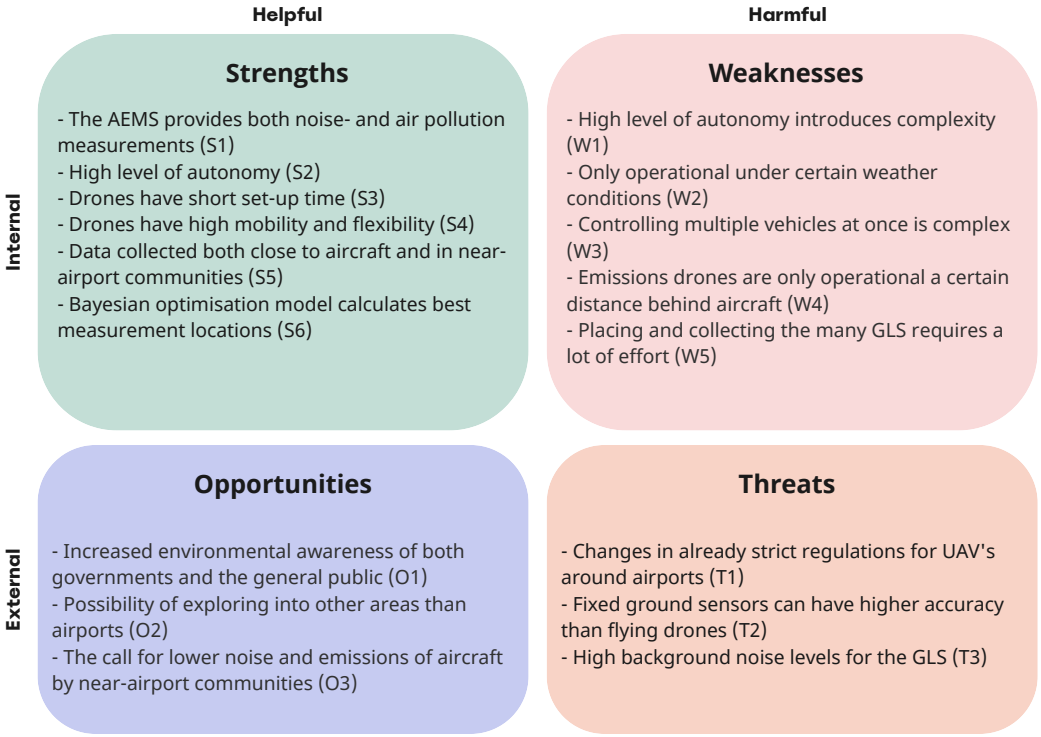


**Figure 12.1:** *SWOT analysis of ALEC*

- **W1** - The high level of autonomy introduces complexity as it requires complex systems to let the drones operate safely.
- **W2** - The drones are only operational up to Beaufort 4 wind conditions. This limits the versatility of the drones.
- **W3** - The system will consist of multiple emissions drones and noise drones operating simultaneously, which increases complexity as the system will need to control multiple drones autonomously and safely.
- **W4** - The emissions drones can only safely fly behind aircraft once the velocity and temperature of the plume created by aircraft engines are sufficiently low. This limits the operations of the emissions drone.
- **W5** - The ground level sensors (GLS) have to be manually placed before the measurements begin and collected once they have ended. This requires a lot of effort which is a downside of the GLS.

**Opportunities**

- **O1** - Global warming is a real threat endangering the whole planet and thus also the human population. Rising temperatures have increased the awareness of both governments and the general public that measures have to be taken in order to stop climate change. ALEC provides data on emissions created by aircraft and hence can help policy makers take adequate mitigative measures to reduce those emissions.
- **O2** - The system might be useful not only for measurements near airports but also for, for example, factories emitting high levels of emissions. For example, Tata Steel in IJmuiden creates many emissions disproportionately affecting communities in close proximity to that factory. Obtaining data of how exactly those emissions spread allows effective mitigative measures to be taken.
- **O3** - The need for lowering the noise and emissions produced by aircraft by near-airport com-

munities is stringent. For example, in 2019, London Heathrow airport received 75,838 noise complaints[15]. With the data gathered by ALEC mitigative measures can be taken to reduce the noise and emissions and hence reduce the nuisance caused by aircraft near airports.

**Threats**

- **T1** - The current regulations for drones near airports are, in the EU, strict. Legislation can always change, however. This poses a threat to the use of the noise and emissions drones of ALEC near airports.
- **T2** - The emissions drones will take measurements will flying. The location of the drone in three-dimensional space can very slightly whilst taking measurements. Ground measuring systems have higher accuracy as they can stand still. This could pose a threat to ALEC as some potential clients might prefer the high accuracy of fixed ground sensors.
- **T3** - The ground level sensors measure noise in near-airport communities when aircraft fly over when approaching or taking-off from an airport. High background noise levels can disturb the measurements and can make it hard to filter the noise generated by an aircraft from other noise sources. This poses a threat to ALEC, and specifically to the noise data obtained by the GLS.

## 12.4. Cost Breakdown Structure

The total cost for ALEC is split into one-time costs for the development, one time product cost for a single ALEC system and operational costs of ALEC as can be seen in Figure 12.2. The development costs are the initial expenses that need to be made before the system is ready to be sold on the market e.g. prototype development and certification. The one-time product costs of ALEC are the costs related to a single ALEC system e.g. manufacturing cost. Afterwards, the operational cost are the costs that will be made while using the system. First, the development costs are going to be explained in Subsection 12.4.1, secondly the one-time product costs are explained in Subsection 12.4.2 and lastly the operational costs are going to be explained in Subsection 12.4.3.

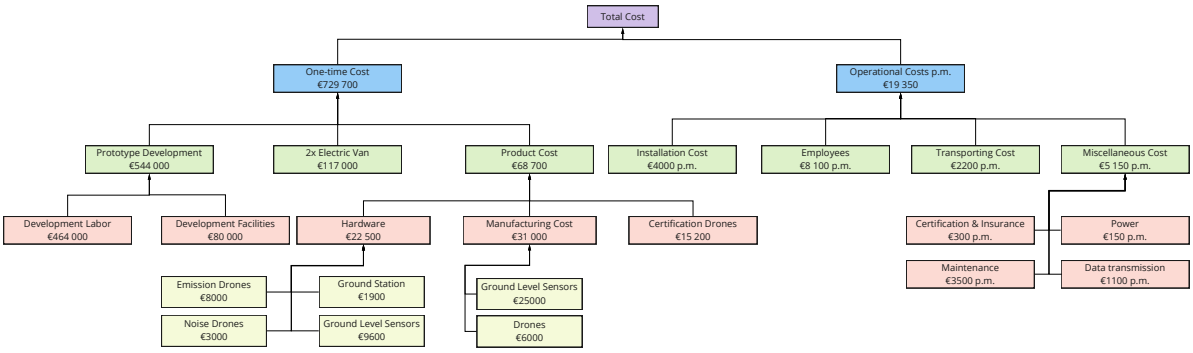


**Figure 12.2:** *Cost breakdown structure*

### 12.4.1. Development costs

The (prototype) development costs are hard to quantify but it is assumed that this is a very cost-intensive phase as it both includes testing and iteration of the design. The prototype phase is also used for certification by the authorities. Effort is put into certification from the start of the prototype design phase. Verification and validation of all systems and the compliance to requirements will all be tested and the design is iterated. Development and testing of the prototype includes unit testing

[15] https://www.heathrow.com/content/dam/heathrow/web/common/documents/company/local-community/noise/reports-and-statistics/reports/noise-complaint-reports/annual-reports/Heathrow_Noise_Complaints_Report_2019.pdf [Cited 01-06-2022]

of all separate components, testing of subsystems (e.g. the noise drone) and the testing of the entire system on the top-level to see if the components work together as they should. The time and costs related to testing and iteration is heavily dependent on the results of the test which makes the time and costs hard to predict. At the time of writing, the testing phase has not been worked out more than is shown in Figure 15.1 and described in Chapter 15. Given that crude estimation and given the fact that a team of 8 people would work on ALEC full time up until August 2023, this would consist of approximately 290 working days or 18560 working hours. Assuming that the employees are paid a gross salary of €25/hour this would cost an additional €464,000 for the labour needed for development. On top of the labour needed for development, facilities and equipment will also be needed. This would include things like an office, a soundproofed studio to test the microphones, a lab to test the emission sensors and facilities for structural testing of the drone frames. A first estimate for these costs is €80,000. This leads to a total development cost of €544,000.

### 12.4.2. One-time Product Costs

When a satisfactory prototype has been developed and certified, one-time costs per unit consists of hardware costs, manufacturing costs, vehicle specific certification and set-up costs. The **hardware costs** for a single ALEC system has been set to €25,000 by the clients. However, it has been decided to keep a 10 % margin to have a sufficient margin during further development after the DSE to account for unexpected increase in certain hardware components. The total hardware cost per ALEC system is presented in Table 12.1. This includes both off-the-shelf components and custom components like the emissions drone cover.

**Table 12.1:** *The total hardware costs*

| Subsystem | No. | Unit Cost | Total Cost | Percentage |
|---|---|---|---|---|
| Emission Drone | 4 | €2,000 | €8,000 | 35.8 % |
| Noise Drone | 2 | €1,500 | €3,000 | 13.2 % |
| GLS | 40 | €240 | €9,600 | 42.5 % |
| No. of GS | 1 | €1,900 | €1,900 | 8.5 % |
| Total | | | €22,500 | 100% |

As can be seen in Chapter 10, the manufacturing time for each GLS is 30.5 hours and the manufacturing time for each drone is 47 hours. The average technician salary per hour is €21.00 per hour[16]. Therefore, the total manufacturing labour cost for the GLS is $40 \cdot 30.5 \cdot 21 \approx 25000$ euros. The total manufacturing cost for the drones is $6 \cdot 47 \cdot 21 \approx 6000$ euros. This makes the total manufacturing costs to be around €31000.

After manufacturing and assembly, the drone needs certification. The one-time costs consist of approval by the ILT which will cost €2,000.00, license for prove of registration which will cost €77.00, and the RPA-L pilot license given by the ILT which will cost €125.00. Therefore, a total of €2,202.00 for the certifications for each drone, and a total of €13,212.00 for six drones. The total cost for the certification of the drones equals €15,212.00[17].

Transportation vehicles are necessary to transport all the equipment to the area of interest. The one-time cost that needs to be added to the budget is the cost of an electric van. Although relatively expensive, an electric van is deemed necessary instead of a van on fossil fuels. The electric van that has been selected is the Mercedes eVito Tourer which will cost €58,685.00[18]. It has cargo storage for dimensions of 2.290 m x 2.078 m x 1.261 m. Two vans will be used because of the number of

[16] https://www.salaryexplorer.com/salary-survey.php?loc=152&loctype=1&job=849&jobtype=3 [Cited 14-06-2022]
[17] https://droneshop.nl/roc-vergunning [Cited 14-06-2022]
[18] https://voc.mercedes-benz.com/voc/nl_nl/stage/44770313NEL0001-0#paint [Cited 14-06-2022]

drones and GLS that need to be transported. Using only one van would cause a daily delay because all drones cannot be transported in a single van. The cost of the two vans will be €117,400. The vans should be bought every time a new ALEC system is bought.

### 12.4.3. Operational Costs

For the **employee cost**, two drone operators are required for operation of the drones. Drone operators have a salary of approximately €4,052.00 a month [19]. This constitutes to €8,100 per month.

The **installation costs** are the costs required to set-up the system to operate. To operate the system, it needs to be installed at the operational area. Installing and dismantling are assumed to be similar operations that take a similar amount of time. As mentioned earlier, an average cost for a technician is €21.00 per hour. For the installation of each drone, it has been estimated that approximately 15 minutes are required. For each GLS, approximately one hour is required. For the GS, approximately 30 minutes is required. The GLS needs to be setup once a month, while the drones and GS have to be setup and dismantled everyday. 190 installing hours are necessary every month when using these estimations. The monthly operating set-up and dismantling costs accumulate to an approximate €4000.

The **transportation cost** can be calculated using the 27.8 kWh/100 km power that the van uses[20]. Electricity costs around €0.67 per kWh[21]. This means that a single electric van costs €18.63/100km. It is assumed that a 150 km range is enough to transport the drones from and to the operational area given the fact that a warehouse is reasonably close. This drone transportation needs to be done everyday for an entire operational month (30 days) with two vans. This would conclude to an approximately €1800,- (30days x 150km x €18.63/100km x 2 vans) transportation electricity bill per month. The GLS on the other hand need to be transported once at the beginning of the month and picked up once at the end. Because there are 40 GLS that all operate in different locations, a lot of distance needs to be covered during installing/removing which is estimated at a safe 1000km as a 20x20km square needs to be covered with GLS subsystems. Given the assumption that the GLS are installed and removed by a single van once per month, the GLS transportation costs are approximately €400. The total transporting costs sum up to approximately €2200.

The **miscellaneous** include the cost for the power, data transmission, certification, insurance and maintenance for each system. The power usage includes the power for charging the drone batteries, and the laptop of the ground station. The laptop will require 160 Wh a day[22], which is almost neglible compared to the drones as it has been estimated that the drones will require 7.5 kWh using Subsection 4.8.2 and Subsection 5.5.2. Therefore, again using the €0.67 per kWh, the monthly (30 day) power cost for the system is €150.

Furthermore, the cost of mobile data subscription (3G/4G) is €25.00 per month for unlimited data transmission for each device[23], and it is required for each GLS and drone. Therefore, the total monthly data cost for 46 units (40 GLS + 6 drones) is €1150.00. The operational cost also consists of insurance and certification costs. The S-Bvl certificate for each drone needs to be renewed yearly which costs €125.00. Also the insurance for each drone costs €495.00. Therefore, this would result

[19] https://www.erieri.com/salary/job/drone-operator/netherlands [Cited 14-06-2022]
[20] https://voc.mercedes-benz.com/voc/nl_nl/stage/44770313NEL0001-0#paint [Cited 14-06-2022]
[21] https://www.consumentenbond.nl/energie-vergelijken/kwh-prijs [Cited 14-06-2022]
[22] https://www.lenovo.com/nl/nl/laptops/thinkpad/edge-series/E14-G2/p/20TA00F8MH?cid=nl:sem%7Cse%7Cgoogle%7CG-NL-SEM-COMMERCIAL-PUBLIC-CCF-LF-Shopping-PLA-Brand-CommercialLaptops%7CBrand-CommercialLaptops&gclid=CjwKCAjw14uVBhBEEiwAaufYx_x44zv_GP9u4eMT0a694RSuTRF3M0QxWN2jCmi2Ism8DfTd-Xgz7xBwE [Cited 14-06-2022]
[23] https://www.tele2.nl/mobiel/sim-only?shop=product&ch=es&cc=con&sc=acq&dr=24&pr=T2C01,T2A12&lp=1 [Cited 14-06-2022]

in a monthly cost of €310.- for 6 drones[24]. The maintenance cost is approximated to be 35% of the total hardware cost every three months[25]. This would mean that the maintenance cost is approximately €2500 monthly. The maintenance cost covers the cost of when a battery or a part needs to be replaced. Additionally, the operational cost also consists of insurance and certification costs. The Special Certificate of Airworthiness (S-Bvl) for each drone needs to be renewed yearly which costs €125.00 per drone. Also the insurance for each drone costs €495.00. Therefore, this would result in a monthly cost of €310.- for 6 drones[26].

## 12.5. Return on Investment

As is shown in Section 12.3, the monitoring market is a big and expanding market. The total emissions monitoring systems market was valued at approximately €2.79 billion and is expected to grow to €4.2 billion by 2027. Furthermore, the noise measuring market is valued at €640 million and is expected to reach €910 million by 2030. From Section 12.4, it has been found that the total one-time cost is €729,700.00 and that the monthly operational cost is €19,350.00. It has been decided that a break-even point of 3 years at the worst case scenario, which is for only one unit operating at a time, would be the only case in which it would be worth operating. As a result, the service will be provided at a monthly cost of €39,995.00, but given the novelty of the ALEC system, it is considered a reasonable price.

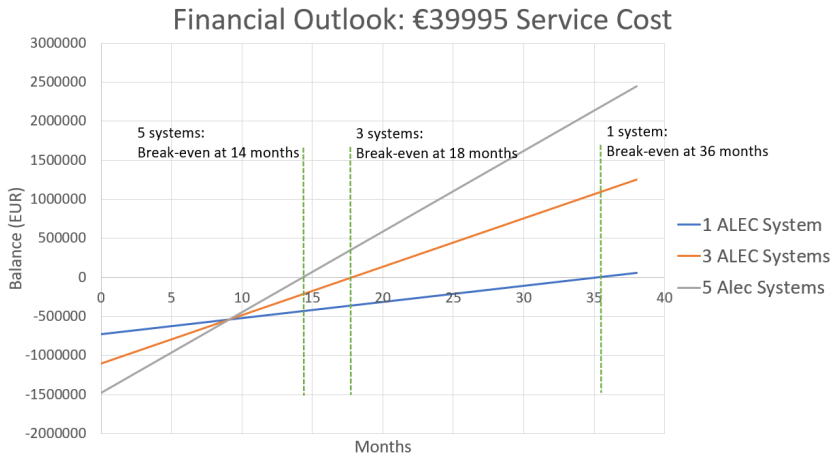


**Figure 12.3:** *Financial outlook with break-even points indicated*

The return on investment in 36 months for 1, 3 or 5, respectively, systems service subscriptions sold is shown in Table 12.2.

| **Subscriptions** | 1 | 3 | 5 |
|---|---|---|---|
| **RoI(%)** | 1.9 | 102.5 | 152.4 |

**Table 12.2:** *Return on investment in 36 months for 1, 3 or 5 service subscriptions*

It is expected to have more then one subscription at a time, but even for the worst case in which only one subscription at a time is provided, the break-even point is in less than 3 years as shown in Table 12.2.

[24] https://www.droneverzekering.nl/drone-verzekering-afsluiten-stap-1/ [Cited 14-06-2022]
[25] https://www.droneblog.com/cost-to-repair/ [Cited 14-06-2022]
[26] https://www.droneverzekering.nl/drone-verzekering-afsluiten-stap-1/ [Cited 14-06-2022]

# 13

# Risk Analysis

Throughout the report, four subsystems has been designed. The design choices made for the subsystems and system as a whole can introduce risks to the success of the mission. Section 13.1 provides an explanation on the method and terms used for this risk analyses. Section 13.2 identifies the risks relevant to ALEC. Finally, Section 13.3 documents the most critical risks and goes into more detail on the mitigation measures for these.

## 13.1. Method

The first step in the process is identifying the risks. After this, each risk is analysed by estimating the probability and determining the consequence. The probability indicates the chance that a risk will affect the mission during the lifetime of the product. The consequence dictates how detrimental the effect of a risk is on the success of the mission. The explanation for the terms used to rank the probability and consequence are given in Table 13.1. The next step involves mitigating the risks by implementing prevention and contingency procedures. The prevention methods aim to lower the probability of the risk occurring. The contingency on the other hand, is aimed at lowering the consequence. With the mitigation measures implemented, the risks are reanalysed and the updated probability and consequence are documented. Finally, the risks are visualized with a risk map.

**Table 13.1:** *Ranks for probability and consequence*

| **Probability** | **Explanation** |
|---|---|
| Very likely | The risk is almost guaranteed to happen on every flight or is almost guaranteed to happen after the vehicle achieves a certain age. |
| Likely | There is a significant possibility that the risk occurs at least once throughout an operational day. |
| Possible | The risk can occur after multiple operational days. |
| Not likely | The risk is unlikely to happen, even during a longer time span. |
| **Consequence** | **Explanation** |
| Catastrophic | The consequence is catastrophic to the operation of the mission and the planned operations of the day cannot continue. |
| Critical | The consequence is critical to the operation as the mission will not necessarily fail, but time might be lost since processes need to be redone. |
| Marginal | The consequences are very marginal and do not have permanent effects on the system or operations. Only minor delays might be incurred. |
| Negligible | The risk has almost no effect on the operation. |

## 13.2. Identifying Risks

As mentioned in the introduction of the chapter, the first step in the risk analysis process is identifying the risks. A comprehensive overview of the risks is provided in Table 13.2.

**Table 13.2:** *Identified and mitigated risks for ALEC system*

| | | | |
|---|---|---|---|
| **ID:** | **R-DRONES-01** | | |
| Risk: | Emission drone cannot reach exact measurement location designated by algorithm | | |
| Driver: | Obstacles are detected by autonomous flight system. This prevents the drone from taking the optimal path to the location. The likelihood of the drones encountering objects in the air is low, since the operations are at an airport, but can still be caused by animals, fellow emission drones or malfunctions in the obstacle avoidance system. | Probability: | Possible |
| Effect: | Measurement data gathered is not in the correct location and does not contribute optimally to the model of the emission plume. This lowers the rate of improvement of the model and means in a future flight event, the missed location must be sampled again. | Consequence: | Critical |
| Prevention: | - | Mitigated Probability: | Possible |
| Contingency: | Remaining emission drones adjust target locations to still obtain highest value of information with measurements | Mitigated Consequence: | Marginal |
| **ID:** | **R-DRONES-02** | | |
| Risk: | Emission drone runs out of battery prematurely | | |
| Driver: | Drone attempts to perform one more measurement before returning to GS but power consumption is higher than expected. This can be due to increase in wind velocity or gusts. | Probability: | Likely |
| Effect: | The drone must return to the GS halfway through a measurement which invalidates the result. In some cases, the drone will not be able to return to the GS and must perform an emergency landing. | Consequence: | Critical |
| Prevention: | Drones must retain a certain battery reserve and start returning to GS when battery level reaches 20%. The rotating scheme of having a drone always at the GS charging while the other three are flying means the 15% margin can be afforded. | Mitigated Probability: | Not likely |
| Contingency: | Drones perform emergency landing and must be manually picked up by operator. This is not very effective contingency and thus the consequence remains the same. | Mitigated Consequence: | Critical |
| **ID:** | **R-DRONES-03** | | |
| Risk: | Noise drone runs out of battery power prematurely | | |
| Driver: | External factors like raised ambient temperature or interrupted cellular connection lead to the battery draining quicker than expected. | Probability: | Possible |
| Effect: | The drone cannot continue measurements until the end of the mission and cannot perform the return flight to the GS. | Consequence: | Critical |
| Prevention: | - | Mitigated Probability: | Possible |
| Contingency: | Drones must return to GS when battery reaches 15%. This means the drone is ensured of being able to perform its return flight. This means at the end of the day, the number of near runway noise measurement points is reduced from two to one. If this occurs at a particularly early stage in the day, the batteries can be swapped and the drone sent out to the measurement point again. But there will be a gap in the measurements. | Mitigated Consequence: | Marginal |
| **ID:** | **R-DRONES-04** | | |
| Risk: | Access to ADS-B information is not available | | |
| Driver: | External APIs which provide the ADS-B information experience technical issues or internet connection which carries this information fails. | Probability: | Possible |
| Effect: | The emission drones are not capable of determining the location of the aircraft and thus cannot perform the required measurements. The drones must return to the GS and the mission cannot continue. | Consequence: | Critical |

| | | | |
|---|---|---|---|
| Prevention: | Include an onboard ADS-B receiver in the GS so there is no reliance on third parties | Mitigated Probability: | Not likely |
| Contingency: | - | Mitigated Consequence: | Critical |
| **ID:** | **R-DRONES-05** | | |
| Risk: | Drones collide with each other during take-off, flight or landing | | |
| Driver: | The drones will be flying simultaneously whilst being in close proximity to each other, especially during the first take-off of the day and the last landing. Especially since they operate autonomously and depend on cameras for detecting obstacles, there is a chance of collisions. | Probability: | Possible |
| Effect: | The collision can cause damage to the propellers, structure and payload. This would lead to parts having to be replaced and the mission not being able to continue for that day. | Consequence: | Catastrophic |
| Prevention: | The drones will communicate their locations constantly to the GS using the telemetry link. The GS is aware of the locations of all drones and can calculate the direction they are heading in. If the paths intersect, the GS will command one of the drones to slow down or momentarily stop moving. | Mitigated Probability: | Not likely |
| Contingency: | - | Mitigated Consequence: | Catastrophic |
| **ID:** | **R-DRONES-06** | | |
| Risk: | Drone disturbs regular airport operations | | |
| Driver: | The drones fly on the airport grounds and could experience failures in critical subsystems such as power and propulsion. | Probability: | Likely |
| Effect: | The drones could obstruct the use of taxiways or runways or cause damage to other aircraft. | Consequence: | Catastrophic |
| Prevention: | The drones are restricted in their flight paths through no-fly and no-hover zones. Which means if failures occur, they are less likely to interrupt airport operations. | Mitigated Probability: | Possible |
| Contingency: | There are always two operators on site who are able to quickly retrieve damaged drones in accordance with the airport authorities | Mitigated Consequence: | Critical |
| **ID:** | **R-GS-01** | | |
| Risk: | Drone battery catches fire during charging | | |
| Driver: | Lipo batteries have an inherent risk of overheating and catching fire during charging. | Probability: | Possible |
| Effect: | The battery gets damaged and must be disposed of. For that day, there will be a chance that there is some down time for the emission drones as one fewer battery is in circulation. Besides this, there is a chance that the operator get injured and the fire spreads and other items are damaged. | Consequence: | Critical |
| Prevention: | The batteries should not be charged under direct sunlight. Space is available in the transportation van to place the charging stations and batteries. | Mitigated Probability: | Not likely |
| Contingency: | Charging safe bags are included for each battery in the GS. These prevent the fire from spreading in the case a fire is started. This protects the operator and prevents the fire from spreading. | Mitigated Consequence: | Marginal |
| **ID:** | **R-GS-02** | | |
| Risk: | No access to power grid in desired location of deploying GS | | |
| Driver: | Some airports may not provide the required infrastructure which allows for power outlets to be placed near a runway. | Probability: | Possible |
| Effect: | The GS cannot provide power to charge the drone batteries, only one flight cycle is possible for the emission drones. This would mean about 30 minutes of measuring is possible. | Consequence: | Catastrophic |
| Prevention: | - | Mitigated Probability: | Possible |

| | | | |
|---|---|---|---|
| Contingency: | The GS will have to be deployed in a location where there is a power outlet available. Realistically, this will still be within the grounds of the airport. This situation will lead to larger distances between the GS and the measurement location. Consequently, the travel time for a single drone is higher and the measuring time is lower. Thus, the number of events which can be captured or the number of measurement points for these events is lower. | Mitigated Consequence: | Critical |
| **ID:** | **R-GLS-01** | | |
| Risk: | GLS kit runs out of battery | | |
| Driver: | Power use during a particular day is higher than expected or the solar power generated is lower due to a damaged solar power or detrimental weather effects. | Probability: | Possible |
| Effect: | The GLS kit shuts down until the solar panel is able to provide enough power to recharge the battery to a sufficient level. This means that for a certain duration of time one fewer GLS measurement point is available. | Consequence: | Marginal |
| Prevention: | - | Mitigated Probability: | Possible |
| Contingency: | - | Mitigated Consequence: | Marginal |
| **ID:** | **R-GLS-02** | | |
| Risk: | Cellular connection is disturbed | | |
| Driver: | The cellular network provider has issues with providing service. Besides this, certain weather conditions can cause lower signal to noise ratio for the cellular link. | Probability: | Possible |
| Effect: | The GLS kit is not able to send the measurement data to the FTP server. | Consequence: | Critical |
| Prevention: | - | Mitigated Probability: | Possible |
| Contingency: | In the case that real time data cannot be sent to the FTP server, information is stored on the local SD card. The data can then be sent to the server once the cellular connection is re-established. | Mitigated Consequence: | Marginal |
| **ID:** | **R-GLS-03** | | |
| Risk: | Sensitive conversations or interactions could be recorded by the microphones on the GLS kits | | |
| Driver: | Microphones are placed throughout communities. | Probability: | Possible |
| Effect: | Residents will not be pleased with the placement of the GLS kits in their environment. | Consequence: | Marginal |
| Prevention: | There is a lower threshold for the minimum dB level required for the system to transmit and store the audio data. Besides this, the kits are preferably placed in public spaces. | Mitigated Probability: | Not likely |
| Contingency: | The data is encrypted before it is transmitted over the internet, this means the likelyhood of an information breach is low. | Mitigated Consequence: | Negligible |
| **ID:** | **R-GLS-04** | | |
| Risk: | GLS kit unable to produce good measurements | | |
| Driver: | Microphones in GLS kits are damaged or covered unexpectedly. | Probability: | Not likely |
| Effect: | One fewer measurement point is available in the grid of GLS measurement points. | Consequence: | Marginal |
| Prevention: | - | Mitigated Probability: | Not likely |
| Contingency: | Due to the fact that two GLS kits are always placed near each other for the filtering, in the case one fails there will be another measurement point in the vicinity. The ability to filter unwanted noise sources will be diminished however. | Mitigated Consequence: | Marginal |

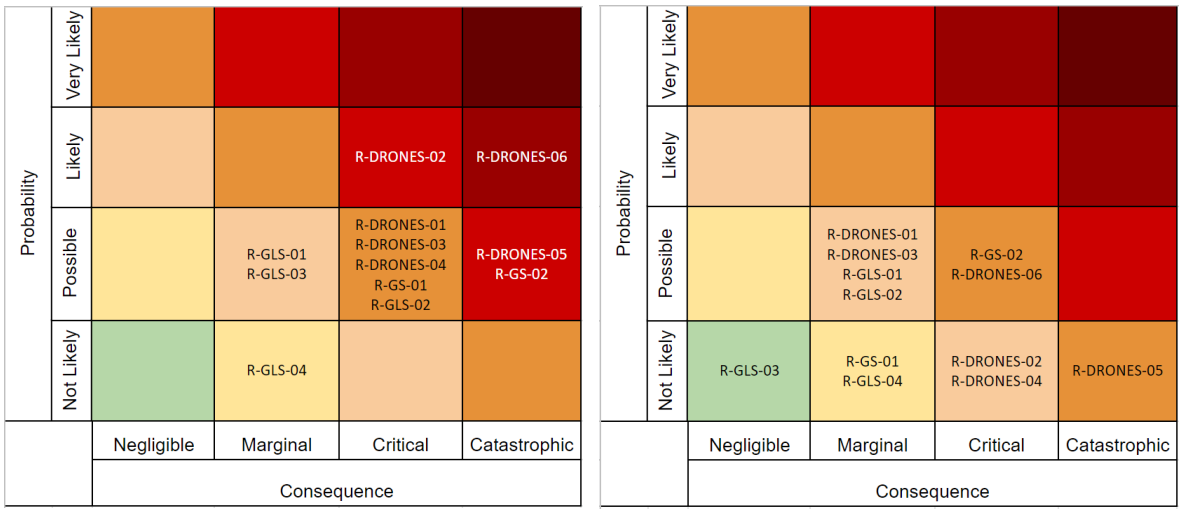


**(a)** *Before mitigation* **(b)** *After mitigation*

**Figure 13.1:** *Technical risk severity plots for ALEC system*

## 13.3. Critical Risks

Now that the risks have been identified, they can be visualized using the risk map. This is done for both before mitigation and after. This can be seen in Figure 13.1. From the risk map after mitigation, it can be seen that there are three risks which are the most critical. These are R-GS-02, R-DRONES-06, and R-DRONES-05. These will be afforded some more attention and discussed below.

In the case of there not being a power outlet available to charge the drones, only a single flight of the emission drones can be performed before the batteries are depleted. If the contingency plan of placing the GS further from the runway leads to the drones not being able to reach the target location and hover for a sufficient time to perform a proper measurement, a different solution needs to be evaluated. Before a mission for a specific runway is deployed, it must be investigated whether the required power outlet is available. In situations where this is not the case but a mission is still desired, an additional battery pack solution must be employed. This would involve a BLUETTI PowerOak EB55 for each emission drone. This portable power station has sufficient energy to power one emission drone for the entire day. Single power stations are required for each drone since one power station is not able to provide the required current to charge multiple drone batteries at once at the required speed. The power station costs €649.00 for a single item. Powering all four drones would add significant cost to the entire system and is thus not considered for the main package. This would be an optional package in case it is necessary for a specific mission.

The drones interfering with the airport operations is something that will need to be carefully monitored by the operators and perhaps adjustments in the no-fly zones will have to be made if it becomes clear the operation of the drone introduces too many risks for the airport.

The drones clashing into each other is something that is more difficult to prevent or deal with in addition to the contingency. If drones are damaged to such an extent that they cannot function anymore, replacement parts must be purchased.

All risks, but especially the critical risks will have to be monitored during the operation of the mission and the probabilities and consequences can be adjusted.

# 14

# Sustainability of Design

In this report a system has been designed to measure emissions and noise close to airports. The larger objective is to help communities near airports through the promotion of the sustainability of aviation. To obtain this objective the system itself should be developed in a sustainable manner. This chapter will elaborate on how this was done. A sustainable development strategy was set up before designing. Section 14.1 will summarise this strategy and then explain how this strategy was implemented. The results of the strategy, the sustainability of the system, will be analysed in Section 14.2. And end-of-life plan is shown in Section 14.3.

## 14.1. Sustainable Development Strategy

A sustainable development strategy was used in the design process to ensure the inclusion of sustainability in this design [21]. In this strategy the three aspects of sustainability are included; social, environmental, and economic sustainability [73].

### 14.1.1. General Strategy

This strategy includes five guidelines for the team members to adhere to, and seven objectives for the design. The five guidelines are based on 'Professional Engineers and Geoscientists of British Columbia' [74] and were established in the project plan [75]:

- "1. The group members shall obtain and maintain knowledge of current sustainability information and developments."
- "2. The group members shall make use of the knowledge and expertise of other group members and external experts."
- "3. The group members shall plan how to incorporate sustainability in decision making and document all decisions."
- "4. The group members shall review the consequences of project choices on its sustainability and investigate how they can be improved."
- "5. The group members shall apply the sustainability principles while carrying out the design, for the duration of the entire project."

The seven objectives are based on the United Nations Environment Programme in 2009 [76] and were established in the baseline report [21].

- "1. **Choosing low-impact materials:** The impact of the materials depends on multiple things. First, the social impact of producing the materials. This can be negative, for example if workers are not treated fairly. It could also have a positive impact, for example creating local income [76]. A positive social impact of course contributes to a material being low-impact. Second, the recyclability of the material, but also whether it is already a recycled material, is part of the impact. Another important consideration is whether the material are renewable, since this has a large influence on economic sustainability. [76]"
- "2. **Minimising amount of materials used:** Even when choosing low-impact materials there is always some impact. Therefore, it is important to minimise the amount of materials used. [76]"
- "3. **Sustainable production and manufacturing:** This includes the emissions caused during the production of the materials and of the complete parts. This consists of the emission of greenhouse gasses due to the power used, but also the emission of other harmful pollutants.

Some materials can be produced with methods that have a different impact on sustainability. The logistics of the assembly of parts and of a complete product also cause emissions, which should be taken into account. [76]"

- "4. **Optimising operations and logistics:** The product will have to be transported before, during, and after a mission. People working on any missions conducted will also have to be transported. This causes emissions. [76] The effect of of the logistics on sustainability is influenced by the amount of people needed to operate the product and by the size of the product."
- "5. **Minimising impact during operation:** The product will use power during operations. The power used should be minimised. The method used to generate the power is also of influence. Furthermore, the noise and other disturbances caused during operation influence social sustainability. [76]"
- "6. **Optimising the lifetime of the product:** The reliability and difficulty of maintenance and repair influence the sustainability. Parts should only be chosen if their expected lifetime is equal to or longer than the intended lifetime of the complete system. If parts have to be changed or repaired, more materials will be used and a larger workforce is required. The lifetime of the complete system before it has to be discarded also influences the sustainability. The degree of difficulty for changing or repairing parts will also lead to an increased workforce, as there is a demand for specialists. [76]"
- "7. **Optimising the end of life plan:** All parts that can be reused or recycled, should be reused or recycled. The other parts should be disposed of safely and as sustainable as possible. [76]"

### 14.1.2. Strategy Application Trade-off

As shown in Section 2.4 trade-offs were done for the main concepts of the flying vehicles of the system. The strategy was used to properly include sustainability in the trade-off with four criteria. Objective 1 was included in the criterion 'type of materials used', and objective 2 in 'amount of material'. Objective 5 was included in the criteria 'power usage' and 'noise produced'. [5] The type and amount of material are related to both environmental and economic sustainability, since the environmental impact and the renewability of materials was considered. The power usage relates to environmental sustainability and the noise produced is social sustainability.

### 14.1.3. Strategy Application Mission Configuration

The mission the system can carry out is designed with especially social sustainability in mind. The choice was made to not fly drones over the near airport communities. This way, the communities will not hear any noise produced by the system and no nuisance is caused to the people this system is designed to help.

To measure sound in the communities ground level sensors are used instead of drones to still measure noise without disturbing residents. The GLS's are placed on public buildings to not cause privacy issues, which would impact the social sustainability of the system as well.

### 14.1.4. Strategy Application Detailed Design

In the detailed design different departments have made choices on components and designs. These choices were made with the seven objectives for sustainability in mind. The departments included this themselves, after which the sustainability department checked whether the objectives were properly implemented. When choosing off-the-shelf components, recyclable components were chosen when possible. Some main points of attention in the detailed design will be discussed below.

The power and propulsion system of the drones has a large influence on the sustainability of the system, because it is the subsystem using the most power. Thus, the power and propulsion system was designed to be as efficient as possible. This is explained in Chapter 6. Another main point of

attention for sustainability was the main material of the structure. A trade-off was done for this material where sustainability was one of the two highest weighted criteria. The material chosen was chopped carbon fibre reinforced nylon. This is a recycled and recyclable material. The other sustainability aspects of this material will be discussed in Subsection 14.2.2. Furthermore, the ground level sensors are not plugged in to the grid, but instead use solar panels, thereby reducing the impact on environmental sustainability. The social sustainability impact of the GLS's were also considered in terms of the way the systems look.

## 14.2. Sustainability Analysis

This section concerns itself with an analysis of the sustainability of the project, especially from the point of view of the recyclability of the components in Subsection 14.2.1 and the sustainability of the main materials in Subsection 14.2.2. An overview of the carbon dioxide footprint of operations is presented in Subsection 14.2.3.

### 14.2.1. Recyclability

The recyclability of all components of the system was investigated. The recyclability of the components is shown in Table 14.1. along with the source that describes the recyclability. For some electrical components specific information on materials and recyclability is not available. Printed circuit boards and wiring can be recycled [1] [2]. Thus, the components that consist mostly of printed circuit boards and wiring, such as the ESC and the flight controller, are assumed to be recyclable. The different microphones are assumed to be partly recyclable, since they partly consist of wiring and coils and no information is available on the other materials. The weather proof box can be made from a recyclable plastic.

**Table 14.1:** *Recyclability of all components*

| Component | Recyclable? | Total amount in system |
|---|---|---|
| **Emission drones** | | |
| CO-CX | No | 4 |
| NO-B4 | No | 4 |
| SO2-A4 | No | 4 |
| O3-AH | No | 4 |
| OPC-R2 | No | 4 |
| NO2-AE | No | 4 |
| MQ138 | No | 4 |
| Wind tunnel [3] | Yes | 4 |
| Main Structure [77] | Yes | 4 |
| Motors [4] | Yes | 16 |
| Esc's | Yes | 16 |
| Propellers [5] [6] | Yes | 16 |
| Flight Controllers | Yes | 4 |
| GPS module | Yes | 4 |
| Arduino | Yes | 4 |

[1] https://www.nature.com/articles/s41598-019-54045-w#:~:text=The%20most%20critical%20step%20in,resin%20for%20the%20further%20reuse. [Cited 13-06-2022]
[2] https://www.conserve-energy-future.com/can-you-recycle-electrical-wires.php [Cited 13-06-2022]
[3] https://www-tc.pbs.org/strangedays/pdf/StrangeDaysSmartPlasticsGuide.pdf [Cited 13-06-2022]
[4] https://intercotradingco.com/recycling-electric-motors/ [Cited 13-06-2022]
[5] https://www.apcprop.com/technical-information/manufacturing/ [Cited 13-06-2022]
[6] https://www.osti.gov/pages/servlets/purl/1485554 [Cited 13-06-2022]

| | | |
|---|---|---|
| Battery [7] | Yes | 8 |
| Raspberry Pi [8] | Yes | 4 |
| Intel camera [9] | Yes | 4 |
| Raspberry Pi camera [10] | Yes | 4 |
| Wind Tunnel Fan [11] [12] | Yes | 4 |
| SiK Telemetry Radio V3 | Yes | 4 |
| Transceiver | Yes | 4 |
| Wiring | Yes | 4 |
| SD card | Yes | 12 |
| Sensor support circuits | Yes | 28 |
| **Noise drones** | | |
| Ground-effect reducing plate [13] | Partly | 2 |
| Microphones | Partly | 2 |
| Sound card [14] | Yes | 2 |
| Main Structure [77] | Yes | 2 |
| Motors [15] | Yes | 8 |
| Esc's | Yes | 8 |
| Propellers [16] [17] | Yes | 8 |
| Flight Controllers | Yes | 2 |
| GPS module | Yes | 2 |
| Arduino | Yes | 2 |
| Battery [18] | Yes | 4 |
| Raspberry Pi | Yes | 2 |
| Intel camera [19] | Yes | 2 |
| Raspberry Pi camera [20] | Yes | 2 |
| SiK Telemetry Radio V3 | Yes | 2 |
| Transceiver | Yes | 2 |
| Wiring | Yes | 2 |
| SD Card | Yes | 6 |
| **GLS kits** | | |
| Raspberry Pi [21] | Yes | 40 |
| SanDisk 64GB SD card [22] | Yes | 40 |
| Huawei E3531 3G dongle | Yes | 40 |

[7] https://csm.umicore.com/en/battery-recycling/ [Cited 13-06-2022]
[8] https://www.raspberrypi.com/news/recycle-your-old-raspberry-pi-boards-with-okdo/ [Cited 13-06-2022]
[9] https://allgreenrecycling.com/camera-recycling/ [Cited 13-06-2022]
[10] https://allgreenrecycling.com/camera-recycling/ [Cited 13-06-2022]
[11] https://www.amazon.com/GDSTIME-60mm-Bearings-Brushless-Cooling/dp/B07THX713H [Cited 13-06-2022]
[12] https://www.mdpi.com/2313-4321/2/2/9 [Cited 13-06-2022]
[13] https://shop1.r-g.de/en/art/650800AX [Cited 13-06-2022]
[14] https://www.hollandrecycling.nl/producten/36450-insteekkaart-vergulde-kam-zonder-aanhechting/ [Cited 13-06-2022]
[15] https://intercotradingco.com/recycling-electric-motors/ [Cited 13-06-2022]
[16] https://www.apcprop.com/technical-information/manufacturing/ [Cited 13-06-2022]
[17] https://www.osti.gov/pages/servlets/purl/1485554 [Cited 13-06-2022]
[18] https://csm.umicore.com/en/battery-recycling/ [Cited 13-06-2022]
[19] https://allgreenrecycling.com/camera-recycling/ [Cited 13-06-2022]
[20] https://allgreenrecycling.com/camera-recycling/ [Cited 13-06-2022]
[21] https://www.raspberrypi.com/news/recycle-your-old-raspberry-pi-boards-with-okdo/ [Cited 13-06-2022]
[22] https://sendanddestroy.co.uk/product/memory-sd-card-destruction/ [Cited 13-06-2022]

| | | |
|---|---|---|
| weatherproof box | Yes | 40 |
| 12V to 5V DC step down converter | Yes | 40 |
| 12V 10Ah AGM deep-cycle battery[23] | Yes | 40 |
| Solar charge controller | Yes | 40 |
| 30W solar panel [24] | Yes | 40 |
| Ugreen USB audio card [25] | Yes | 40 |
| Rode SmartLav + electret microphone | Partly | 40 |
| GPS | Yes | 40 |
| Solar Panel connector | Yes | 40 |
| **Ground Station** | | |
| Spare Battery per emission drone | Yes | 8 |
| HOTA D6 Pro per emission drone [26] [27] | Yes | 8 |
| LTO platform per drone | Yes | 6 |
| Lenovo Thinkpad [28] | Yes | 1 |
| USB 10 ports | Yes | 1 |
| 10 outlet power strip | Yes | 1 |
| Leslaur Lipo safe bag | No | 8 |

| | |
|---|---|
| **Total Percentage of components recyclable** | 89.5 |

The total recyclable percentage of components in amounts, not counting the partly recyclable components, is 89,5 percent. A more meaningful number would be the percentage of mass recyclable. This can only be done for the emission drones, which were designed in detail. The only components that are not recyclable in the emission drones are the sensors. The total weight of the sensors of one emission drone is 88 grams. The total weight of an emission drone is 3041 grams. This means 97 percent of the mass of an emission drone is recyclable. This number does however assume that companies providing recycling options for components fully recycle everything, which might not be the case. The real number might therefore be lower, but it is still comfortably above the requirement of 70 percent.

### 14.2.2. Sustainability of Main Materials

The main materials used for the structure of the emission drones are chopped carbon fibre reinforced nylon (nylon chopped CF15) for the main structure and high-density polyethylene for the wind tunnel. The noise drones use the same main structure, the only difference is in the plate added on top of the drones. This top plate is made of a carbon fibre sandwich sheet. The supports for this plate are made from aluminium.

#### Nylon chopped CF15

Another consideration which could be classified as social sustainability is whether the material contain hazardous substances. The material is classified as not hazardous according to the European legislation [29]. For economic sustainability it is important to check whether the material uses non-

[23] https://ecocycle.com.au/batteries/how-to-recycle-a-lead-acid-battery/ [Cited 13-06-2022]
[24] https://www.epa.gov/hw/solar-panel-recycling [Cited 13-06-2022]
[25] https://www.hollandrecycling.nl/producten/36450-insteekkaart-vergulde-kam-zonder-aanhechting/ [Cited 13-06-2022]
[26] https://www.amazon.co.uk/HOTA-Balance-Powerful-Discharger-100-240V/dp/B07Q4SJPHY [Cited 13-06-2022]
[27] https://www.plasticcollectors.com/blog/what-is-abs-plastic/ [Cited 13-06-2022]
[28] https://www.hollandrecycling.com/products/31280-laptop-complete-with-battery/ [Cited 13-06-2022]
[29] http://www.fillamentumautomotive.com/wp-content/uploads/2020/10/SDS_Nylon-CF15-Carbon_EN.pdf [Cited 14-06-2022]

renewable resources. This is not the case for chopped carbon fibre reinforced nylon. Chopped carbon fibre is a recycled material from carbon fibres and can also be recycled again [78], this is even proven for carbon fibre in a composite with nylon [79]. Nylon is also a fully recyclable material [80]. Using a recycled carbon fibre composite also reduces the life cycle emissions of the carbon fibre [78], and therefore using this material instead of a material made from virgin materials positively impacts the environmental sustainability.

**High-Density Polyethylene**
The material used for the wind tunnel is high-density polyethylene. This material is fully recyclable and if the recycling process is conducted in a 'low residence time' apparatus the material properties change very little due to the recycling process [81]. To estimate the impact of this material on environmental sustainability, the carbon footprint was investigated. If a recycled HDPE is used the carbon footprint is 1.62 to 2.51 kg of $CO_2$ per kg HDPE us the circular footprint formula [81]. This is quite a low value, meaning the negative impact on environmental sustainability is small. The impact of the material on economic sustainability is heavily influenced by the depletion of fossil resources it causes. Recycled HDPE causes the depletion of 3.97 MJ per kg of material, which again is quite a low number. This material is also classified as a not dangerous according to European legislation [30]. This means it does not have a negative impact on social sustainability in this aspect.

**Sandwich sheet**
The plate for the noise drone is made of a carbon fibre sandwich sheet with a foam core. This foam core is made of a recyclable material [31]. The carbon fibre layers can be downcycled to chopped carbon fibre [78]. This means the material is not fully recyclable and therefore has a small negative impact on economic sustainability. It also means new carbon fibre has to be produced for the material, which costs energy. Therefore, it also has a small negative impact on environmental sustainability. The material is not hazardous [32], which means it does not have a negative impact on social sustainability in this aspect.

**Aluminium**
The supports of the plate for the noise drone is made of aluminium. Recycled aluminium can be used for this. Aluminium is one of the most recyclable materials used for engineering, and can be recycled almost an unlimited amount of times [33]. Because of this, the impact of aluminium on economic sustainability is very low. The impact of recycled aluminium on environmental sustainability is mostly defined by the carbon footprint, which is 0.5 kg of $CO_2$ per kg of recycled aluminium [34]. Furthermore, as with the other materials, aluminium is not a hazardous material either.

### 14.2.3. Carbon Dioxide Footprint of Operations
During one day of operation the amount of power used by the drones in total is around 7500 watt hours. This was calculated assuming 85 percent of the battery capacity of the drones is depleted for each flight, which is a slight overestimation, since safety factors were taken into account when designing the batteries. As described in Section 4.10 three emission drone are always flying during an eight hour working day, and the noise drones do one flight per day. Assuming the $CO_2$ emissions for energy production in the Netherlands, 325 grams of $CO_2$ is emitted per $kWh$. The means the operations of the drones cause 2.44 kg of $CO_2$ per day.

[30] https://silo.tips/download/material-safety-data-sheet-high-density-polyethylene [Cited 14-06-2022]
[31] https://www.r-g.de/en/art/650800AX [Cited 14-06-2022]
[32] http://www.ezentrumbilder.de/rg/pdf/si_en_AIREX_T90_T92.pdf [Cited 14-06-2022]
[33] https://www.aluminum.org/Recycling [Cited 14-06-2022]
[34] https://www.climateaction.org/news/carbon-footprint-of-recycled-aluminium [Cited 14-06-2022]

## 14.3. End-of-life Plan

The end-of-life moment for the different subsystems will be determined separately. After each mission every drone and GLS kit will be assessed as to whether they can be used for another mission, or whether the end-of-life procedure needs to be started for that subsystem. If only a part of a subsystem is not usable anymore, this part is replaced and the end-off-life procedure is applied to this part, while the rest of the system is used again.

### 14.3.1. General Procedure

The first step in the end-of-life procedure is to the disassemble the subsystem into its separate components. Each component is then assessed to see if they are still usable. The custom made components, namely the drone structures and the noise drone top plate, can only be reused in the ALEC system. If no new drones are being produced for the system when they could be reused, they will be recycled. The recycling procedure for these components is further explained in Subsection 14.3.2. The reusable off-the-shelf components can either be reused in the ALEC system, or when this is not possible by another user. If the component will be reused by another user it can be sold, or when it can not be sold it will be donated to any university or researcher that wants it, or to the manufacturer of the component. If the off-the-shelf component can not be reused, it will be recycled if possible. The components that are not recyclable should be disposed of in the manner the manufacturer specifies in the user manual or safety data sheet. The recyclable components have various different recycling procedures. For some components companies or programs exist for that specific type of component such as the cameras [35] and the Raspberry Pi [36]. Other electrical components can be brought to dedicated electrical component recycling companies such as 'Holland Recycling' [37]. The recycling of the batteries is explained further in Subsection 14.3.2. For other components, such as the propeller and the solar panels, recycling processes are known [38] [39]. Specific companies will have to be found by contacting companies that recycle the material and asking whether they can recycle the specific component.

### 14.3.2. Recycling of Main Components

**Main structure**

The main structure is recycled using a recycling process for chopped carbon fibre reinforced nylon. A summary of the recycling process, researched by R.J. Tapper et al. [77], of chopped carbon fibre reinforced nylon is shown in Figure 14.1. First dissolution takes place using a solvent, for example benzyl alcohol. The nylon polymer and fibres are then separated. The nylon polymer is then changed back into a solid and reduced in size. The fibres are separated and realigned. After that, the composite material can be made again.

[35] https://allgreenrecycling.com/camera-recycling/ [Cited 14-06-2022]
[36] https://www.raspberrypi.com/news/recycle-your-old-raspberry-pi-boards-with-okdo/ [Cited 14-06-2022]
[37] https://www.hollandrecycling.nl/recycling/elektronica-recycling/ [Cited 14-06-2022]
[38] https://www.osti.gov/pages/servlets/purl/1485554 [Cited 14-06-2022]
[39] https://www.epa.gov/hw/solar-panel-recycling [Cited 14-06-2022]

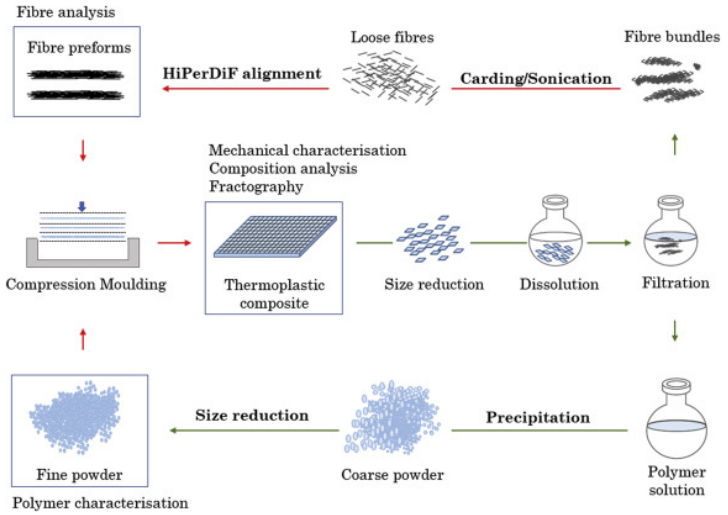


**Figure 14.1:** *Recycling process of chopped carbon fibre reinforced nylon [77]*

This recycling does reduce the mechanical properties of the material. When recycled two times, the strength and stiffness decrease with around 40 percent [77]. This recycling process will be outsourced to specialised composite recycling companies such as 'Composite Recycling' [40] or 'Gen2Carbon' [41].

**Batteries**

The batteries used in the system are lithium-ion polymer (LiPo) batteries. The recycling of the batteries will be outsourced to 'Umicore' [42]. The recycling process consists of two phases. First, the batteries are converted into an alloy containing useful metals that will be used for new batteries, and a slag fraction. The slag fraction is used for other purposes for metals, or can be processed again for metal recovery. Air is also released during the process. The process used in this phase is called 'Pyro-metallurgical treatment'. [43]. The second phase uses a 'Hydro-metallurgical process' and uses the alloy to make new batteries.

**Noise interference reducing plates**

The interference reducing plates on the noise drones are made of carbon fibre sandwich sheet with a PET foam core. According to research, recycled carbon fibre and recycled PET foam can be used to make new sandwich sheet composites [82]. To recycle the sheets, the carbon fibre layers first have to be separated from the foam core. Afterwards, both components can be recycled. The recycling of the carbon fibre will be outsourced to 'Gen2Carbon' [44]. The recycling of the foam core can be done by '3A Composites Core Material' [45], who are the manufacturers of the foam core material in the sheets used for the noise reducing plates.

To conclude this chapter; A sustainable development strategy was used in the design process. Using this strategy has resulted in the system being composed of mostly recyclable products, and the system adheres to the requirement of being 70 percent recyclable. The operation of the system causes the indirect emission of around 2.44 kg $CO_2$ per day, and an end-of-life plan has been constructed to make sure everything that can be recycled, is recycled.

[40] https://composite-recycling.ch [Cited 14-06-2022]
[41] https://www.gen2carbon.com/ [Cited 14-06-2022]
[42] https://csm.umicore.com/en/battery-recycling/ [Cited 14-06-2022]
[43] https://csm.umicore.com/en/battery-recycling/our-recycling-process#tabs [Cited 14-06-2022]
[44] https://www.gen2carbon.com/ [Cited 14-06-2022]
[45] https://www.3accorematerials.com/en/ [Cited 14-06-2022]

# 15

# Project Design and Development Logic

After the detailed design has been approved by the clients, several steps will have to be completed before it can be brought to the market. This development phase, after the detailed design is done and before it is brought to market, is called phase V. This chapter discusses the order of activities/steps that need to be taken after the DSE. The Gantt chart presenting the tasks of phase V is presented below in Figure 15.1. The duration of phase V will be around 290 days, although it has to be admitted that it is a very crude estimation with a lot of uncertainty.

During the start of the prototyping phase, sufficient financial resources need to be available to create such a prototype. Hence, the first step after the detailed design is finished would be to perform a financial analysis to find potential investors and do a scalability analysis. Investors could be for example airports, governments, near-airport communities and researchers. After sufficient funding has been found, the next step will be to start manufacturing a prototype starting with the buying of (non-)off-the-shelf prototype components. Thereafter, the individual components of the prototype should be tested with verification and validation. By testing the individual components first, one ensures that the prototype is built with working components and hence reduces the risk that the prototype does not work due to a malfunctioning component. A point of attention is the software as this is an essential part of the project, because it will be a mostly autonomous functioning system.

Thereafter, the subsystems can be assembled using the necessary components. Subsequently, subsystem level prototype testing will be performed. Subsystem level testing includes testing the ground level sensors, ground station, noise drone and emission drone. Subsequently, the tests of the individual subsystems should be analyzed. Based on this analysis the subsystem design might require improvement and iteration. The duration of the subsystem design is uncertain as it is heavily dependent on whether the subsystem design needs to be improved and if so, to what extent this needs to be done. A buffer is included at the end to account for these kinds of uncertainties. At this point in time, the certification procedure should have started as the government could potentially be reluctant about the ALEC system. It would be needed to show the government that the autonomously operating drone do not form a safety concern to the airport environment. It is of upmost importance that the V&V and testing is done correctly and corresponded correctly to the authorities. It needs to be proven that ALEC will never cause any kind of airplane accident or even fatal crash.

Then the system level prototype tests should be prepared and performed. This consists of multiple sub-tasks, namely testing the communication between systems, checking whether the system complies with the requirements, software testing and safety V&V. The latter two are deemed really important and vital to the project, so a relatively long time is allocated to these tasks. Especially the drones will require strict certification before they can be deployed close to runways of an airport. The duration of obtaining certification is uncertain, as it depends on the authorities assessing the system. The results of the prototype tests should be communicated to the investors. Thereafter, the team should consider finding additional scale-up partners. This consists of the sub-tasks of finding additional clients/investors and finding industry partners for, for example, buying off-the-shelf components in bulk. Once that task has been completed personnel should be trained to operate, service and maintain the system.

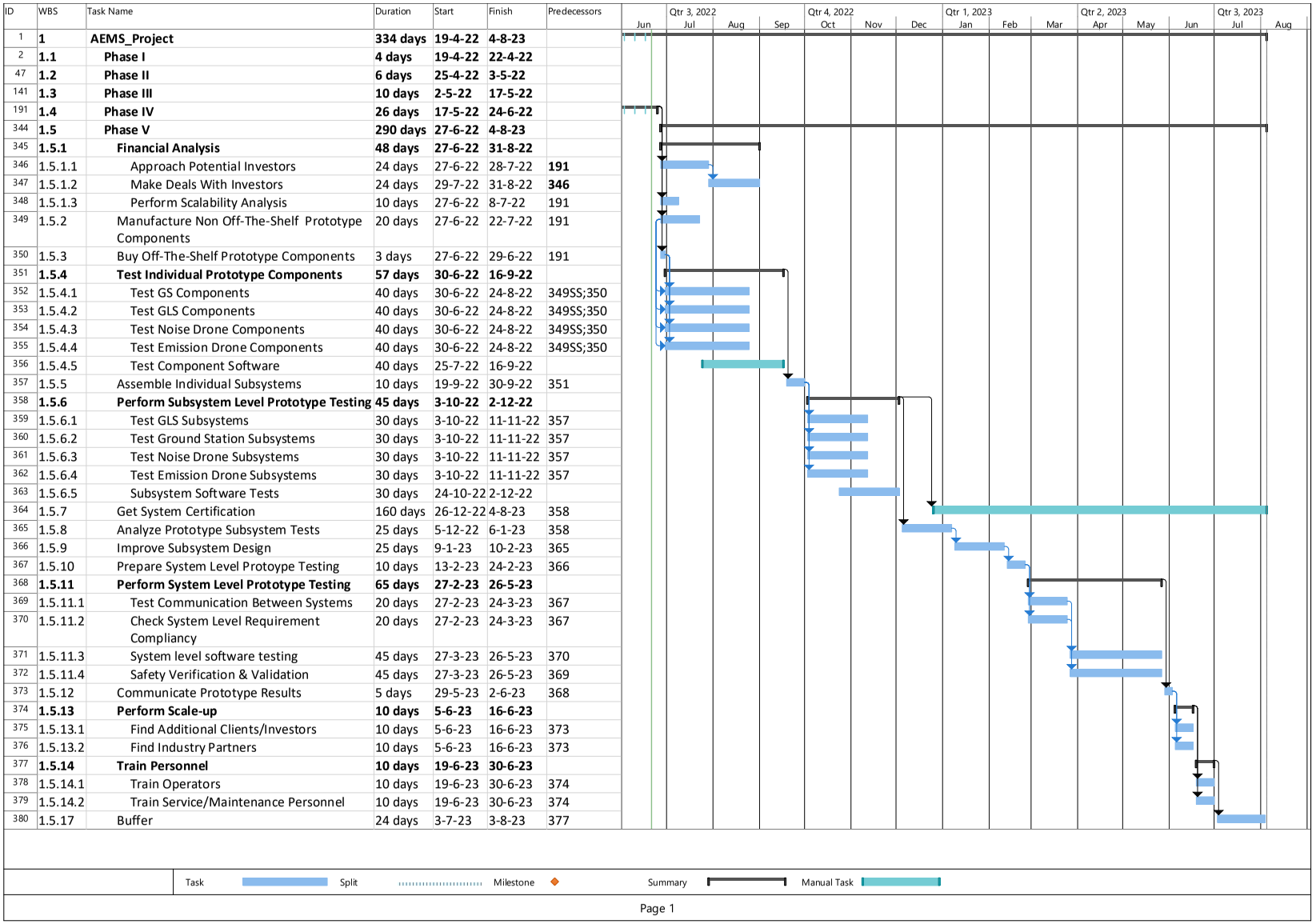


| ID | WBS | Task Name | Duration | Start | Finish | Predecessors |
|---|---|---|---|---|---|---|
| 1 | **1** | **AEMS_Project** | **334 days** | **19-4-22** | **4-8-23** | |
| 2 | **1.1** | **Phase I** | **4 days** | **19-4-22** | **22-4-22** | |
| 47 | **1.2** | **Phase II** | **6 days** | **25-4-22** | **3-5-22** | |
| 141 | **1.3** | **Phase III** | **10 days** | **2-5-22** | **17-5-22** | |
| 191 | **1.4** | **Phase IV** | **26 days** | **17-5-22** | **24-6-22** | |
| 344 | **1.5** | **Phase V** | **290 days** | **27-6-22** | **4-8-23** | |
| 345 | **1.5.1** | **Financial Analysis** | **48 days** | **27-6-22** | **31-8-22** | |
| 346 | 1.5.1.1 | Approach Potential Investors | 24 days | 27-6-22 | 28-7-22 | **191** |
| 347 | 1.5.1.2 | Make Deals With Investors | 24 days | 29-7-22 | 31-8-22 | **346** |
| 348 | 1.5.1.3 | Perform Scalability Analysis | 10 days | 27-6-22 | 8-7-22 | 191 |
| 349 | 1.5.2 | Manufacture Non Off-The-Shelf Prototype Components | 20 days | 27-6-22 | 22-7-22 | 191 |
| 350 | 1.5.3 | Buy Off-The-Shelf Prototype Components | 3 days | 27-6-22 | 29-6-22 | 191 |
| 351 | **1.5.4** | **Test Individual Prototype Components** | **57 days** | **30-6-22** | **16-9-22** | |
| 352 | 1.5.4.1 | Test GS Components | 40 days | 30-6-22 | 24-8-22 | 349SS;350 |
| 353 | 1.5.4.2 | Test GLS Components | 40 days | 30-6-22 | 24-8-22 | 349SS;350 |
| 354 | 1.5.4.3 | Test Noise Drone Components | 40 days | 30-6-22 | 24-8-22 | 349SS;350 |
| 355 | 1.5.4.4 | Test Emission Drone Components | 40 days | 30-6-22 | 24-8-22 | 349SS;350 |
| 356 | 1.5.4.5 | Test Component Software | 40 days | 25-7-22 | 16-9-22 | |
| 357 | 1.5.5 | Assemble Individual Subsystems | 10 days | 19-9-22 | 30-9-22 | 351 |
| 358 | **1.5.6** | **Perform Subsystem Level Prototype Testing** | **45 days** | **3-10-22** | **2-12-22** | |
| 359 | 1.5.6.1 | Test GLS Subsystems | 30 days | 3-10-22 | 11-11-22 | 357 |
| 360 | 1.5.6.2 | Test Ground Station Subsystems | 30 days | 3-10-22 | 11-11-22 | 357 |
| 361 | 1.5.6.3 | Test Noise Drone Subsystems | 30 days | 3-10-22 | 11-11-22 | 357 |
| 362 | 1.5.6.4 | Test Emission Drone Subsystems | 30 days | 3-10-22 | 11-11-22 | 357 |
| 363 | 1.5.6.5 | Subsystem Software Tests | 30 days | 24-10-22 | 2-12-22 | |
| 364 | 1.5.7 | Get System Certification | 160 days | 26-12-22 | 4-8-23 | 358 |
| 365 | 1.5.8 | Analyze Prototype Subsystem Tests | 25 days | 5-12-22 | 6-1-23 | 358 |
| 366 | 1.5.9 | Improve Subsystem Design | 25 days | 9-1-23 | 10-2-23 | 365 |
| 367 | 1.5.10 | Prepare System Level Protoype Testing | 10 days | 13-2-23 | 24-2-23 | 366 |
| 368 | **1.5.11** | **Perform System Level Prototype Testing** | **65 days** | **27-2-23** | **26-5-23** | |
| 369 | 1.5.11.1 | Test Communication Between Systems | 20 days | 27-2-23 | 24-3-23 | 367 |
| 370 | 1.5.11.2 | Check System Level Requirement Compliancy | 20 days | 27-2-23 | 24-3-23 | 367 |
| 371 | 1.5.11.3 | System level software testing | 45 days | 27-3-23 | 26-5-23 | 370 |
| 372 | 1.5.11.4 | Safety Verification & Validation | 45 days | 27-3-23 | 26-5-23 | 369 |
| 373 | 1.5.12 | Communicate Prototype Results | 5 days | 29-5-23 | 2-6-23 | 368 |
| 374 | **1.5.13** | **Perform Scale-up** | **10 days** | **5-6-23** | **16-6-23** | |
| 375 | 1.5.13.1 | Find Additional Clients/Investors | 10 days | 5-6-23 | 16-6-23 | 373 |
| 376 | 1.5.13.2 | Find Industry Partners | 10 days | 5-6-23 | 16-6-23 | 373 |
| 377 | **1.5.14** | **Train Personnel** | **10 days** | **19-6-23** | **30-6-23** | |
| 378 | 1.5.14.1 | Train Operators | 10 days | 19-6-23 | 30-6-23 | 374 |
| 379 | 1.5.14.2 | Train Service/Maintenance Personnel | 10 days | 19-6-23 | 30-6-23 | 374 |
| 380 | 1.5.17 | Buffer | 24 days | 3-7-23 | 3-8-23 | 377 |

**Figure 15.1:** *Gantt chart of the phase V*

# 16

# Conclusions and Recommendations

This chapter reflects on the final report and the DSE project as a whole and provides a conclusion in Section 16.1. Recommendations for future design and development of the system is provided in Section 16.2.

## 16.1. Conclusions

ALEC is a system composed of four types of sub-systems, namely four drones measuring emissions (emissions drones), two drones measuring noise (noise drones), 40 ground level sensors, and one ground station. It as two main goals: the first of creating a total environmental footprint metric produced by the system that combines all noise and emission measurements into a single score for an aircraft event. The second goal is to to provide accurate noise and emissions data that can be used by researchers to improve models. Subsequently, policy makers can make implement effective mitigation measures reducing the impact of noise and emissions created by aircraft on communities living in close proximity to airports.

The project can be divided into two measurement locations, namely near the runway at the airport and near communities most impacted by the aircraft flying over at a low altitude. For the measurements near the runway two types of flying vehicles were used: the emission drones and noise drones. During the operation of the mission, the emission drones will move to the area of interest and after each aircraft event, they will be assigned a new location to measure and hover. The noise drone, on the other hand, will select a sample location at the beginning of each operational day and begin measuring. Furthermore, the operations of the noise drone are assisted by the ground station, which provides an interface for the operators, an area to charge the drone batteries, and a location to process the data to create a total environmental metric. In addition, the ground station includes a model generation system using Gaussian Processes to create a dynamic estimation system to model aircraft plume and the noise experienced by local communities during a specific aircraft event. Furthermore, the ground station uses Bayesian Optimisation, a machine learning technique to select the optimal location for each drone to measure the aircraft event. On the near-airport community level, ground level sensors are included to actively track the noise truly experienced by local residents. The measurements are sent to the ground station to process through an FTP server using encrypted data compliant to GDPR regulation to ensure privacy to local communities.

The system aims to provide the measured data on a website. This data displays a total environmental footprint metric for each aircraft event, relative to the average of measured events. The environmental footprint metric is a function of the emissions measured and modeled near the runway, together with the noise measured and modeled using the noise drones and ground level sensors. Furthermore, an option has been designed to make the environmental footprint a function of the population density, distance traveled by the aircraft, and the amount of cargo and passengers carried by the aircraft. A goal is to also provide the possibility of downloading the raw data measured by various subsystems, such as concentration levels of the seven emission species, frequency spectra as measured by the ground level sensors and noise drones and ADS-B data. With the ADS-B data it is possible to link measurements to a certain aircraft event. This option is meant for researchers to analyse the data and improve their own models. In conclusion, ALEC as system aims to help airport stakeholders implement effective mitigation measures to reduce the impact of aviation on near-airport communities.

## 16.2. Recommendations

This DSE project resulted in a detailed design of ALEC. However, further research should be performed in later phases to improve the design. This section provides recommendations for such further research.

During the performance analysis of the emission drone a maximum velocity was determined. However, based on engineering knowledge, the maximum velocity seemed high. A possible reason for this high maximum velocity could be that the drag coefficients used in the analysis were not correct. During the calculations, the drag coefficients used were from a quad-copter with a similar shape on which CFD analysis was performed. However, the design team is unsure to what extent these drag coefficients are representative of the emissions drone in ALEC. Therefore, further research could focus on obtaining more accurate drag coefficients, for example by performing CFD analysis on the design. If the maximum velocity does prove to be correct, it could be the case that the propulsion system is over-designed. A smaller propulsion system could lead to lower weight, larger endurance, and lower cost. Whether the propulsion system is indeed over-designed or whether there are mistakes in the maximum velocity calculation should be investigated during further design of ALEC.

Furthermore, the total environmental footprint metric should be further discussed. The equation for the environmental footprint metric uses the noise and emission pollution emitted in an area of 20 km by 20 km. The data is obtained using ground level sensor, emissions drone, and noise drone measurements together with the noise and emissions models. However, further research should focus on the area of 20 km by 20 km. It should be investigated whether this is indeed the best area to represent the impact of aviation pollution on near-airport communities, or whether areas with other dimensions would be more suitable.

For the emissions drone, the sensor payload design should be revisited. Ideally in cooperation with the sensor manufacturer, a new sensor chamber should be designed as to truly maximise the performance of the sensors, since the current instructions provided by the company do not clarify certain requirements on airflow. The design could be reduced in size if exact information on the needs of the sensors would be provided.

Regarding the sampling and modelling algorithm, significant work has to be done to bring the system in a ready to deploy state. The software implemented was mainly used to prototype and prove the concept, whereas the detailed implementation still needs to be done. Several details, such as choosing a more precise performance metric or implementing sparse techniques for the Gaussian Processes would improve the quality of the model significantly. Moreover, developing an even more sophisticated model for the a priori kernel would help the model converge faster, and research in the direction of parallelising the acquisition function algorithm would render more efficient solutions.

The structure of the drone should be tested and the design iterated upon. As it is now, the structure is over-designed, because the tools to properly simulate the performance of composite materials, especially those which are 3D printed, are limited. The basic structure should be printed and thoroughly tested, and if possible adjusted to decrease weight. Overall, this could lead to significant reduction in cost as the weight of the structure will have a snowball effect on the remainder of components of both drones.

Lastly, there are several design options that should be considered regarding the ground level sensors. Some research projects use cheaper processing units, much cheaper than the 50,- EUR for the Raspberry Pi. It should be analysed whether cheaper processing units are implementable in the ground level sensor design. A temperature and humidity sensor could be added to the GLS to gain further knowledge of the effect of weather conditions on noise measured by the microphones.

# Bibliography


[1] D. S. Lee, D. Fahey, A. Skowron, M. Allen, U. Burkhardt, Q. Chen, S. Doherty, S. Freeman, P. Forster, J. Fuglestvedt, *et al.*, "The contribution of global aviation to anthropogenic climate forcing for 2000 to 2018," *Atmospheric Environment*, vol. 244, p. 117834, 2021.

[2] S. H. Yim, G. L. Lee, I. H. Lee, F. Allroggen, A. Ashok, F. Caiazzo, S. D. Eastham, R. Malina, and S. R. Barrett, "Global, regional and local health impacts of civil aviation emissions," *Environmental research letters*, vol. 10, no. 3, p. 034001, 2015.

[3] S. Lin, J. Munsie, M. Herdt-Losavio, S. Hwang, K. Civerolo, K. McGarry, and T. Gentile, "Residential proximity to large airports and potential health impacts in new york state," *International archives of occupational and environmental health*, vol. 81, no. 7, pp. 797–804, 2008.

[4] A. L. Hansell, M. Blangiardo, L. Fortunato, S. Floud, K. De Hoogh, D. Fecht, R. E. Ghosh, H. E. Laszlo, C. Pearson, L. Beale, *et al.*, "Aircraft noise and cardiovascular disease near heathrow airport in london: small area study," *Bmj*, vol. 347, 2013.

[5] A. Casablanca, M. Constantinov, B. Khan, S. Köbben, A. Kubba, E. Lucassen, V. Marek, Y. Oei, A. Pietersz, and J. Simons, "Autonomous environmental sensing midterm report," 2022.

[6] P. J. Wolfe, S. H. Yim, G. Lee, A. Ashok, S. R. Barrett, and I. A. Waitz, "Near-airport distribution of the environmental costs of aviation," *Transport Policy*, vol. 34, pp. 102–108, 2014.

[7] C. Grobler, P. J. Wolfe, K. Dasadhikari, I. C. Dedoussi, F. Allroggen, R. L. Speth, S. D. Eastham, A. Agarwal, M. D. Staples, J. Sabnis, and S. R. H. Barrett, "Marginal climate and air quality costs of aviation emissions," *Environmental Research Letters*, vol. 14, no. 11, p. 114031, 2019.

[8] T. Mokalled, S. Le Calvé, N. Badaro-Saliba, M. Abboud, R. Zaarour, W. Farah, and J. Adjizian-Gérard, "Identifying the impact of beirut airport's activities on local air quality-part i: Emissions inventory of no2 and vocs," *Atmospheric Environment*, vol. 187, pp. 435–444, 2018.

[9] A. Mahashabde, P. Wolfe, A. Ashok, C. Dorbian, Q. He, A. Fan, S. Lukachko, A. Mozdzanowska, C. Wollersheim, S. R. Barrett, M. Locke, and I. A. Waitz, "Assessing the environmental impacts of aircraft noise and emissions," *Progress in Aerospace Sciences*, vol. 47, no. 1, pp. 15–52, 2011.

[10] I. Víden, *Chemie Ovzduší*. Praha: Vydavatelsví VŠCHT Praha, 1 ed., 2005.

[11] O. of Research and D. N. C. for Environmental Assessment, "Integrated science assessment for oxides of nitrogen - health criteria," Tech. Rep. EPA/600/R-15/068, United States Environmental Protection Agency, Research triangle Park, NC, Jan 2016.

[12] O. of Research and D. N. C. for Environmental Assessment, "Integrated science assessment for ozone and related photochemical oxidants," Tech. Rep. EPA/600/R-20/012, United States Environmental Protection Agency, Research triangle Park, NC, Apr 2020.

[13] O. of Research and D. N. C. for Environmental Assessment, "Integrated science assessment for carbon monoxide," Tech. Rep. EPA/600/R-09/019F, United States Environmental Protection Agency, Research triangle Park, NC, Jan 2010.

[14] O. of Research and D. N. C. for Environmental Assessment, "Integrated science assessment for sulfur oxides - health criteria," Tech. Rep. EPA/600/R-17/451, United States Environmental Protection Agency, Research triangle Park, NC, Dec 2017.

[15] O. of Research and D. N. C. for Environmental Assessment, "Integrated science assessment for particulate matter," Tech. Rep. EPA/600/R-19/188, United States Environmental Protection Agency, Research triangle Park, NC, Dec 2019.

[16] F. Simões and M. Xavier, "6 - electrochemical sensors," in *Nanoscience and its Applications* (A. L. Da Róz, M. Ferreira, F. de Lima Leite, and O. N. Oliveira, eds.), Micro and Nano Technologies, pp. 155–178, William Andrew Publishing, 2017.

[17] O. of Research and D. N. E. R. Laboratory, "Air sensor guidebook," Tech. Rep. EPA/600/R-14/159, United States Environmental Protection Agency, Research triangle Park, NC, Jun 2014.

[18] M. Hossain, J. Saffell, and R. Baron, "Differentiating no2 and o3 at low cost air quality amperometric gas sensors," *ACS Sensors*, vol. 1, 10 2016.

[19] P. Ventura Diaz and S. Yoon, "High-fidelity computational aerodynamics of multi-rotor unmanned aerial vehicles," in *2018 AIAA Aerospace Sciences Meeting*, p. 1266, 2018.

[20] S. Yoon, P. V. Diaz, D. D. Boyd Jr, W. M. Chan, and C. R. Theodore, "Computational aerodynamic modeling of small quadcopter vehicles," in *American Helicopter Society (AHS) 73rd Annual Forum Fort Worth, Texas*, 2017.

[21] A. Casablanca, M. Constantinov, B. Khan, S. Köbben, A. Kubba, E. Lucassen, V. Marek, Y. Oei, A. Pietersz, and J. Simons, "Autonomous environmental sensing baseline report," 2022.

[22] M. Simma, H. Mjøen, and T. Boström, "Measuring wind speed using the internal stabilization system of a quadrotor drone," *Drones*, vol. 4, no. 2, p. 23, 2020.

[23] M. Demirhan and C. Premachandra, "Development of an automated camera-based drone landing system," *IEEE Access*, vol. 8, pp. 202111–202121, 2020.

[24] B. Jähne, *Digitale bildverarbeitung: und bildgewinnung*. Springer-Verlag, 2012.

[25] Q. Quan, *Introduction to multicopter design and control*. Springer, 2017.

[26] R. Felismina, M. Silva, A. Mateus, and C. Malça, "Study on the aerodynamic behavior of a uav with an applied seeder for agricultural practices," in *AIP Conference Proceedings*, vol. 1836, p. 020049, AIP Publishing LLC, 2017.

[27] U. S. N. Oceanic, A. Administration, and U. S. A. Force, *US Standard Atmosphere, 1976*, vol. 76. National Oceanic and Atmospheric Administration, 1976.

[28] D. G. Simons, *Course AE4431: Aircraft Noise and Emissions*. TU Delft, 2019.

[29] M. Albert, P. Bousquet, and D. Lizarazu, "Ground effects for aircraft noise certification," *23rd AIAA/CEAS Aeroacoustics Conference*, 2017.

[30] J. Cooley, P. Lewis, and P. Welch, "Historical notes on the fast fourier transform," *Proceedings of the IEEE*, vol. 55, no. 10, pp. 1675–1677, 1967.

[31] C. Rivero and P. Mishra, "Lossles audio compression: A case study," tech. rep., Technical Report 08-415, Department of computer and information Science and . . . , 2008.

[32] Y. Karnavas, I. Chasiotis, and D. Stravoulellis, "A practical bldc motor design procedure for diver propulsion vehicle applications," 09 2018.

[33] "Chapter 9 - emergency supply equipment," in *Electrical Systems and Equipment (Third Edition)*, British Electricity International, pp. 748–798, Oxford: Pergamon, third edition ed., 1992.

[34] S. Nvss, B. Esakki, L.-J. Yang, C. Udayagiri, and K. S. Vepa, "Design and development of unibody quadcopter structure using optimization and additive manufacturing techniques," *Designs*, vol. 6, no. 1, 2022.

[35] B. Theys and J. Schutter, "Forward flight tests of a quadcopter unmanned aerial vehicle with various spherical body diameters," *International Journal of Micro Air Vehicles*, vol. 12, p. 175682932092356, 01 2020.

[36] S. S. Sethi, R. M. Ewers, N. S. Jones, A. Signorelli, L. Picinali, and C. D. L. Orme, "Safe acoustics: An open-source, real-time eco-acoustic monitoring network in the tropical rainforests of borneo," *Methods in Ecology and Evolution*, vol. 11, no. 10, pp. 1182–1185, 2020.

[37] J. P. Bello, C. Silva, O. Nov, R. L. Dubois, A. Arora, J. Salamon, C. Mydlarz, and H. Doraiswamy, "Sonyc: A system for monitoring, analyzing, and mitigating urban noise pollution," *Communications of the ACM*, vol. 62, no. 2, pp. 68–77, 2019.

[38] V. Lostanlen, A. Bernabeu, J.-L. Béchennec, M. Briday, S. Faucou, and M. Lagrange, *Energy Efficiency is Not Enough:Towards a Batteryless Internet of Sounds*, p. 147–155. New York, NY, USA: Association for Computing Machinery, 2021.

[39] F. Mietlicki, C. Mietlicki, and M. Sineau, "An innovative approach for long term environmental noise measurement: Rumeur network in the paris region," in *Proceedings of the EuroNoise*, 2015.

[40] C. Bartalucci, F. Borchi, and M. Carfagni, "Noise monitoring in monza (italy) during covid-19 pandemic by means of the smart network of sensors developed in the life monza project," *Noise Mapping*, vol. 7, no. 1, pp. 199–211, 2020.

[41] X. Sevillano, J. C. Carrié, F. Alías, P. Bellucci, L. Peruzzi, S. Radaelli, P. Coppi, L. Nencini, A. Cerniglia, A. Bisceglie, R. Benocci, and G. Zambon, "Dynamap – development of low cost sensors networks for real time noise mapping," *Noise Mapping*, vol. 3, 01 2016.

[42] Sarab Sethi, "rpi-eco-monitoring," 2022.

[43] P. Maijala, Z. Shuyang, T. Heittola, and T. Virtanen, "Environmental noise monitoring using source classification in sensors," *Applied Acoustics*, vol. 129, pp. 258–267, 2018.

[44] C. Mydlarz, J. Salamon, and J. P. Bello, "The implementation of low-cost urban acoustic monitoring devices," *Applied Acoustics*, vol. 117, pp. 207–218, 2017. Acoustics in Smart Cities.

[45] V. Risojević, R. Rozman, R. Pilipović, R. Češnovar, and P. Bulić, "Accurate indoor sound level measurement on a low-power and low-cost wireless sensor node," *Sensors*, vol. 18, no. 7, 2018.

[46] S. S. Sethi, R. M. Ewers, N. S. Jones, C. D. L. Orme, and L. Picinali, "Robust, real-time and autonomous monitoring of ecosystems with an open, low-cost, networked device," *Methods in Ecology and Evolution*, vol. 9, no. 12, pp. 2383–2387.

[47] Rode Microphones, "smartlav+ professional lapel microphone datasheet," 2022.

[48] T. Van Renterghem, P. Thomas, F. Dominguez, S. Dauwe, A. Touhafi, B. Dhoedt, and D. Botteldooren, "On the ability of consumer electronics microphones for environmental noise monitoring," *J. Environ. Monit.*, vol. 13, pp. 544–552, 2011.

[49] V. Risojević, R. Rozman, R. Pilipović, R. Češnovar, and P. Bulić, "Accurate indoor sound level measurement on a low-power and low-cost wireless sensor node," *Sensors*, vol. 18, no. 7, 2018.

[50] M. Seeger, "Gaussian processes for machine learning," *International journal of neural systems*, vol. 14, no. 02, pp. 69–106, 2004.

[51] P. I. Frazier, "A tutorial on bayesian optimization," *arXiv preprint arXiv:1807.02811*, 2018.

[52] D. J. MacKay *et al.*, "Introduction to gaussian processes," *NATO ASI series F computer and systems sciences*, vol. 168, pp. 133–166, 1998.

[53] M. Xu, M. Tian, E. Modiano, and S. Subramaniam, "Rhoda topology configuration using bayesian optimization," in *International IFIP Conference on Optical Network Design and Modeling*, pp. 130–141, Springer, 2019.

[54] J. Snoek, H. Larochelle, and R. P. Adams, "Practical bayesian optimization of machine learning algorithms," *Advances in neural information processing systems*, vol. 25, 2012.

[55] R. Marchant and F. Ramos, "Bayesian optimisation for intelligent environmental monitoring," in *2012 IEEE/RSJ international conference on intelligent robots and systems*, pp. 2242–2249, IEEE, 2012.

[56] G. De Ath, R. M. Everson, A. A. Rahat, and J. E. Fieldsend, "Greed is good: Exploration and exploitation trade-offs in bayesian optimisation," *ACM Transactions on Evolutionary Learning and Optimization*, vol. 1, no. 1, pp. 1–22, 2021.

[57] R. Marchant and F. Ramos, "Bayesian optimisation for informative continuous path planning," in *2014 IEEE International Conference on Robotics and Automation (ICRA)*, pp. 6136–6143, IEEE, 2014.

[58] D. R. Jones, "A taxonomy of global optimization methods based on response surfaces," *Journal of global optimization*, vol. 21, no. 4, pp. 345–383, 2001.

[59] J. Wang, S. C. Clark, E. Liu, and P. I. Frazier, "Parallel bayesian global optimization of expensive functions," *Operations Research*, vol. 68, no. 6, pp. 1850–1865, 2020.

[60] K. Kandasamy, A. Krishnamurthy, J. Schneider, and B. Póczos, "Parallelised bayesian optimisation via thompson sampling," in *International Conference on Artificial Intelligence and Statistics*, pp. 133–142, PMLR, 2018.

[61] K. Synylo, A. Krupko, O. Zaporozhets, and R. Makarenko, "Cfd simulation of exhaust gases jet from aircraft engine," *Energy*, vol. 213, p. 118610, 2020.

[62] C. M. Bishop and N. M. Nasrabadi, *Pattern recognition and machine learning*, vol. 4. Springer, 2006.

[63] N. K. Arystanbekova, "Application of gaussian plume models for air pollution simulation at instantaneous emissions," *Mathematics and Computers in Simulation*, vol. 67, no. 4-5, pp. 451–458, 2004.

[64] A. De Visscher, *Air dispersion modeling: foundations and applications*. John Wiley & Sons, 2013.

[65] G. I. Kuś, S. van der Zwaag, and M. A. Bessa, "Sparse quantum gaussian processes to counter the curse of dimensionality," *Quantum Machine Intelligence*, vol. 3, no. 1, pp. 1–12, 2021.

[66] D. Duvenaud, *Automatic model construction with Gaussian processes*. PhD thesis, University of Cambridge, 2014.

[67] R. Merino-Martínez, S. J. Heblij, D. H. Bergmans, M. Snellen, and D. G. Simons, "Improving aircraft noise predictions consideringfan rotational speed," *Journal of Aircraft*, vol. 56, no. 1, pp. 284–294, 2019.

[68] J. L. Loeppky, J. Sacks, and W. J. Welch, "Choosing the sample size of a computer experiment: A practical guide," *Technometrics*, vol. 51, no. 4, pp. 366–376, 2009.

[69] N. A. Braathen, "Valuing mortality risk reductions in regulatory analysis of environmental, health and transport policies: Policy implications,"

[70] M. Lijesen, W. van der Straaten, J. Dekkers, and R. van Elk, "Geluidsnormen voor schiphol," 2006.

[71] T. R. Miller, "Variations between countries in values of statistical life," *Journal of transport economics and policy*, pp. 169–188, 2000.

[72] L. Prieto and J. A. Sacristán, "Problems and solutions in calculating quality-adjusted life years (qalys)," *Health and quality of life outcomes*, vol. 1, no. 1, pp. 1–8, 2003.

[73] United Nations World Commission and Development, "Our common future (brundtland report)," tech. rep., 1987.

[74] Professional Engineers and Geoscientists of BC, "Sustainability apegbc professional practice guidelines," 2016.

[75] A. Casablanca, M. Constantinov, B. Khan, S. Köbben, A. Kubba, E. Lucassen, V. Marek, Y. Oei, A. Pietersz, and J. Simons, "Autonomous environmental sensing project plan," 2022.

[76] United Nations Environment Programme, "Design for sustainability: A step-by-step approach," 2009.

[77] R. J. Tapper, M. L. Longana, I. Hamerton, and K. D. Potter, "A closed-loop recycling process for discontinuous carbon fibre polyamide 6 composites," *Composites Part B: Engineering*, vol. 179, p. 107418, 2019.

[78] F. Meng, J. McKechnie, T. Turner, and S. Pickering, "Energy and environmental assessment and reuse of fluidised bed recycled carbon fibres," *Composites Part A: Applied Science and Manufacturing*, vol. 100, pp. 206–214, 2017.

[79] L. Jiang, C. A. Ulven, D. Gutschmidt, M. Anderson, S. Balo, M. Lee, and J. Vigness, "Recycling carbon fiber composites using microwave irradiation: Reinforcement study of the recycled fiber in new composites," *Journal of Applied Polymer Science*, vol. 132, no. 41, 2015.

[80] S. Ding, B. Zou, P. Wang, C. Huang, J. Liu, and L. Li, "Geometric modeling and recycling of 3d printed fiber reinforced thermoplastic composite plain weft knitted structures," *Composites Part A: Applied Science and Manufacturing*, vol. 149, p. 106528, 2021.

[81] M. Loultcheva, M. Proietto, N. Jilov, and F. La Mantia, "Recycling of high density polyethylene containers," *Polymer Degradation and Stability*, vol. 57, no. 1, pp. 77–81, 1997.

[82] Q. Jiang, G. Chen, A. Kumar, K. Jani, V. Rajamohan, V. Barathan, and S. Rahatekar, "Sustainable sandwich composites manufactured from recycled carbon fibers, flax fibers/pp skins, and recycled pet core," *Journal of Composites Science*, vol. 5, 12 2020.

# A

## Software diagram

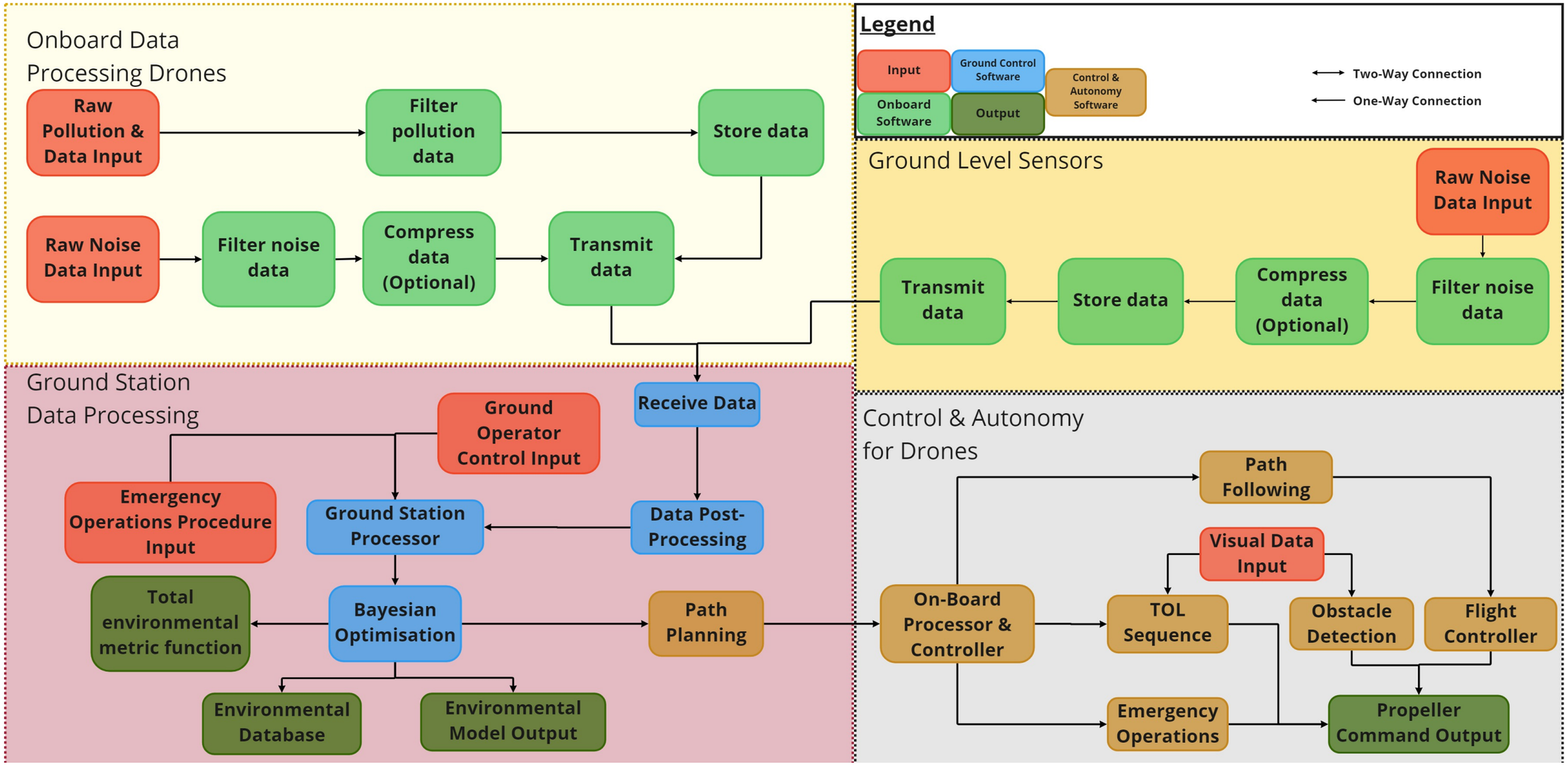


**Figure A.1:** *Software diagram of ALEC system*

# B

# Functional Flow Diagram

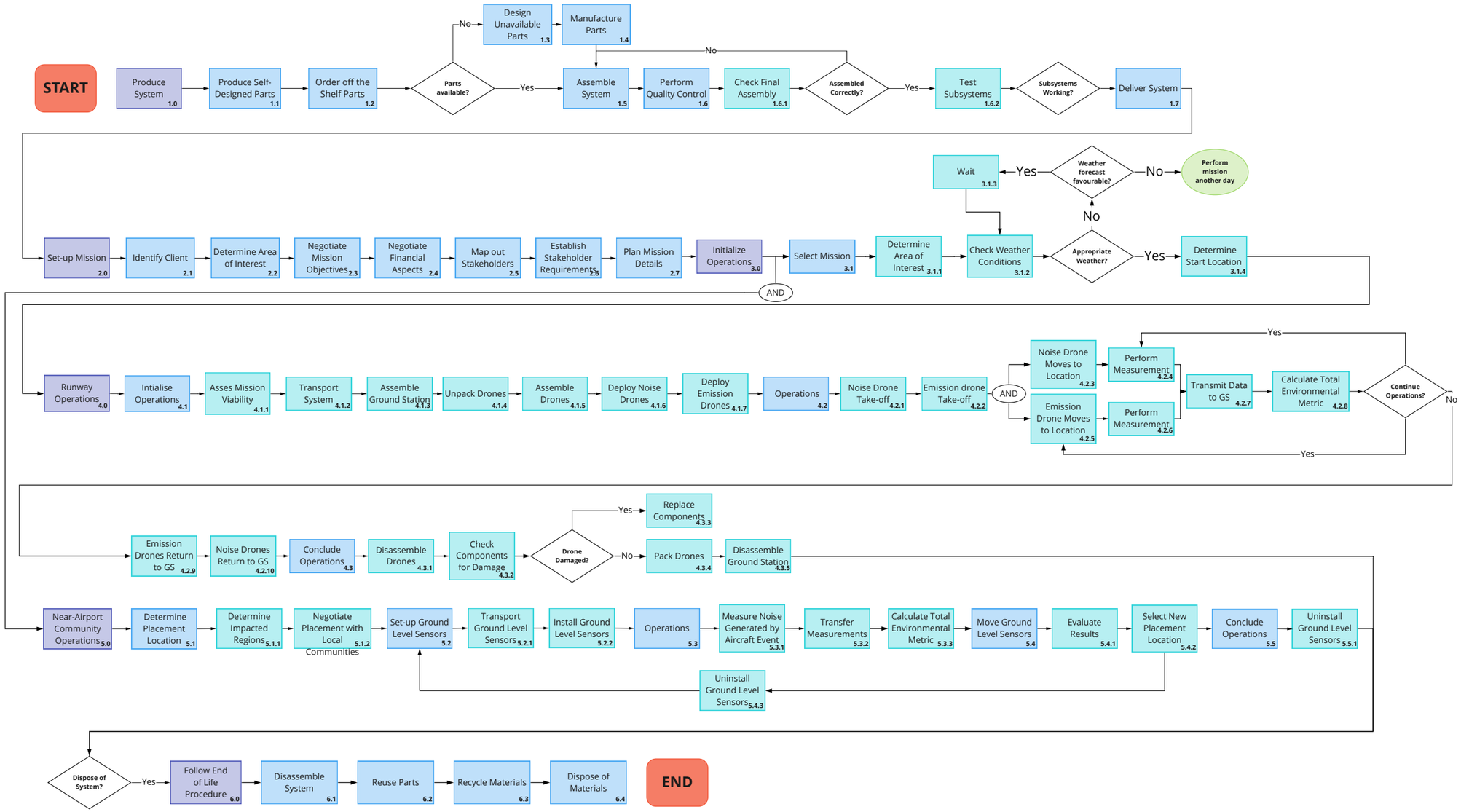


**Figure B.1:** *Functional flow diagram of ALEC*

# C

# Functional Breakdown Structure

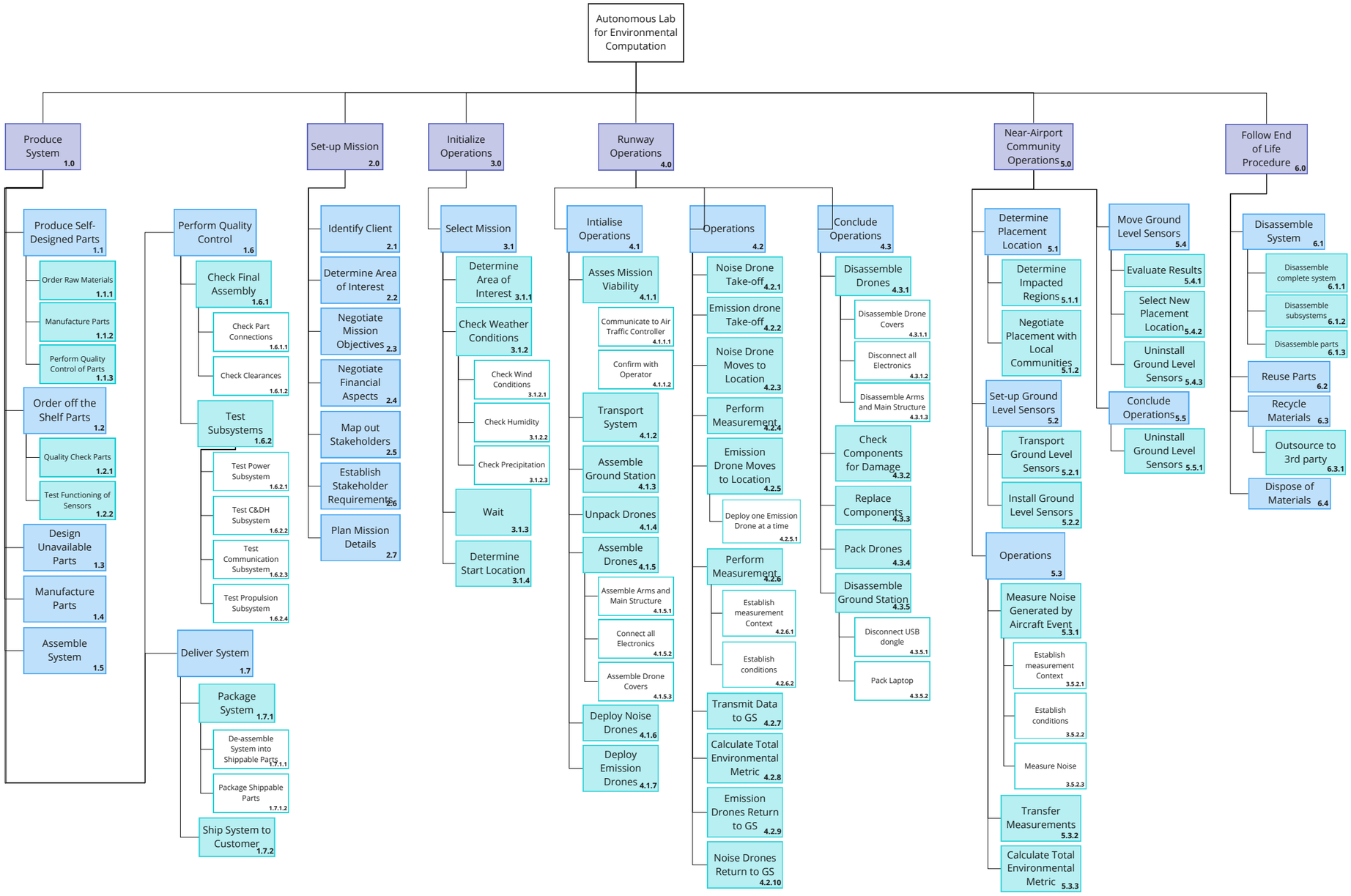


**Figure C.1:** *Functional breakdown structure of ALEC*

# D

# Drone Configuration

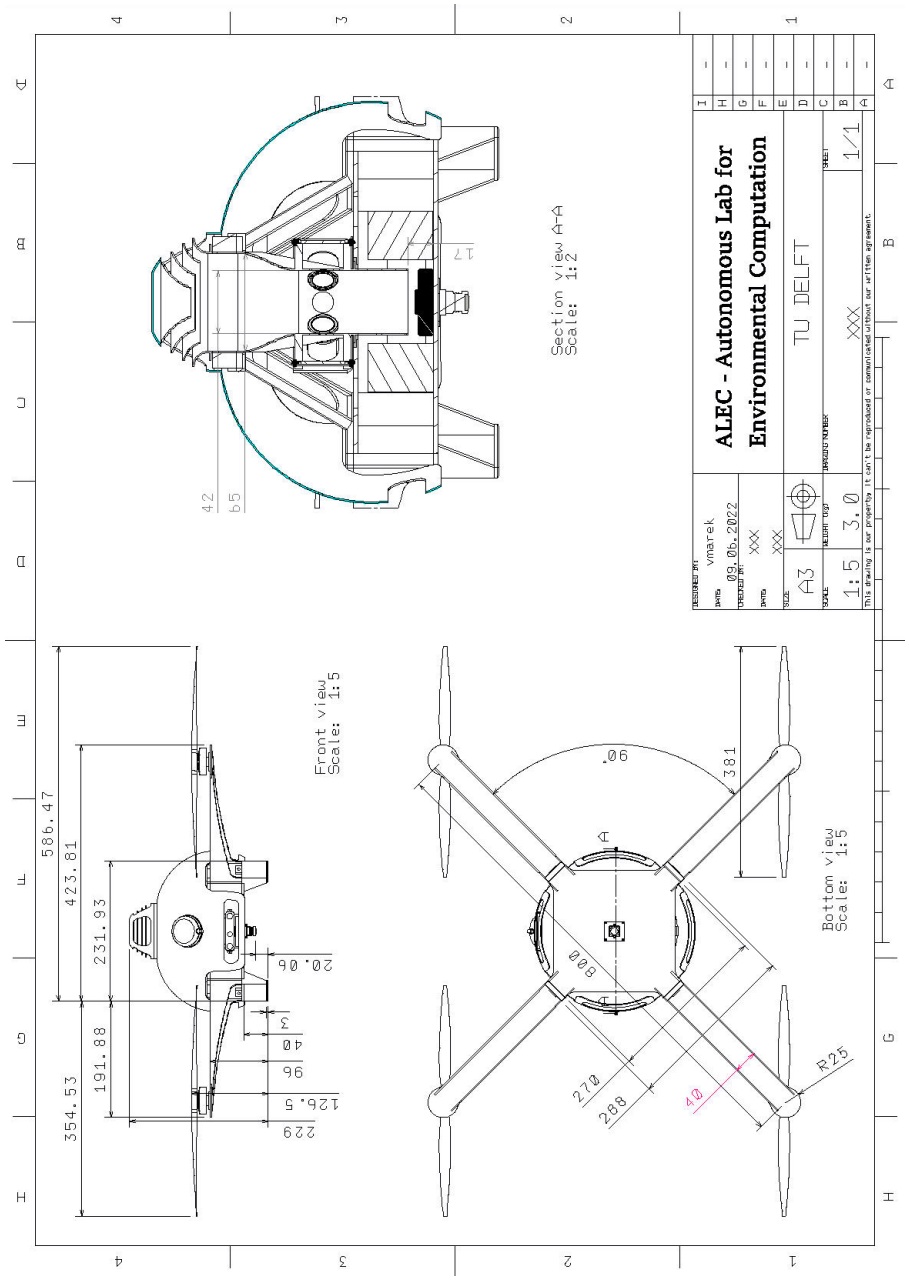


**Figure D.1:** *Detailed technical drawing of the ALEC emission drone*